

Investigating the Crosstalk between Small Extracellular vesicles and RNA granules in Huntington's Disease

DISSERTATION

zur Erlangung des Grades
eines Doktors der Naturwissenschaften
im Promotionsfach Biologie

vorgelegt von

M.Sc. Deepti Kailash Nabariya

eingereicht bei der Naturwissenschaftlich-Technischen Fakultät

der Universität Siegen

Siegen 2024

Doktormutter und erstgutachter

Prof. Dr. Sybille Krauss

Universität Siegen

Zweiter Gutachter

Prof. Dr. Hans-Michael Merzendorfer

Universität Siegen

Tag der mündlichen Prüfung

11.03.2025

Table of contents

CONTENTS

Acknowledgements.....	4
Abbreviations and Annotations	7
List of Tables	11
List of Figures.....	12
List of Appendices.....	14
Abstract.....	15
Zusammenfassung.....	17
Introduction.....	19
1. RNA Granules	21
1.1. RNA granule biogenesis: Liquid- Liquid Phase Separation (LLPS)	22
1.2. Cytoplasmic RNA granules	27
1.2.1. Stress Granules (SGs).....	27
1.2.1.1. SG composition and formation	28
1.2.1.2. Stress granule (SG) disassembly.....	32
1.2.2. Processing bodies (P-bodies).....	33
1.2.2.1. P-bodies composition, assembly and disassembly	34
2. Extracellular Vesicles.....	37
3. Huntington’s Disease	42
3.1 The biology and function of Huntingtin	43
3.2 The etiology of <i>Huntingtin</i>	46
3.3 Diagnosis, prognosis and therapy.....	48
3.4 RNA granules and HD	50
3.5 sEVs in HD.....	51
Rationale of the Project	53
Materials and Methods.....	56
MATERIALS	57
1. Instruments and Devices.....	57
2. Laboratory consumables.....	57
3. Chemicals and reagents	58
4. Kits	59
5. Antibodies	59
6. Cell lines.....	60

7.	Buffers, solutions and media	60
8.	Primers	61
9.	Probes	61
	METHODS	63
1.	Cell culture.....	63
1.1	Thawing of cells.....	63
1.2	Passaging of cells.....	64
1.3	Seeding the cells.....	64
1.4	Treatment of cell line.....	64
1.5	Isolation of sEVs and total cytoplasmic RNA granules from HEK Q83 cell line	65
1.5.1	Isolation of sEVs and RNA granules	65
2.	Validation and characterization of the isolated sEVs and cytoplasmic RNA granules	66
2.1	Western blot.....	66
2.1.1	Sample preparation	67
2.1.2	Sodium dodecyl sulphate-polyacrylamide gel electrophoresis (SDS-PAGE) and western blot..	67
2.1.3	Nanoparticle tracking analysis (NTA)	70
2.1.4	Scanning electron microscopy (SEM)	70
3.	RNA isolation.....	71
4.	RNA sequencing	71
4.1	RNA Concentration and Purity Measurement	71
4.2	RNA sequencing and quality control	71
4.3	Transcript mapping quantification	72
4.4	Differential gene expression analysis	73
5.	Mass spectroscopic analysis	75
5.1	Sample preparation for mass spectrometry	75
5.2	Mass spectrometry	75
5.3	Data analysis for mass spectrometry	76
5.4	Bioinformatic analysis of the mass spectroscopic data	76
5.4.1	KEGG mapper analysis.....	76
5.4.2	Enrichment analysis.....	77
5.4.3	STRING	78
5.4.4	Statistical Tests in Data Analysis	79
	Results	82
1.	Isolation of sEVs and RNA granules	83
2.	Transcriptomic analysis of sEVs and RNA granules.....	85
3.	Analysis of commonly detected genes in control and HD sample.....	92

4.	Comparative Analysis of Gene Expression Profiles in Control and HD Conditions Using Presence-Absence and Differential Expression Approaches.....	94
5.	Validation of HD Marker Gene Abundance Using qRT-PCR Analysis	99
6.	Validation of HD Marker Transcripts in YB1-Positive RNA Granules Using RNA-FISH	100
7.	Identification of REST-Regulated genes in RNA Granule and sEV samples using the TFLink database.....	109
8.	Comparison of the control and HD RNA granule and sEVs marker genes with data from HD patients.....	111
9.	Mass spectroscopic data revealed gene sets present in sEVs and RNA granules	112
10.	sEVs and RNA granules share content in both control and HD samples	113
11.	Interactions network predictions between proteins of the sEV and RNA granule dataset.....	114
12.	Pathway and Interaction Network Analysis of sEV and RNA Granule Proteomes in HD	117
13.	Functional Enrichment Analysis Revealed RNA Granule-Related GO Terms in sEV Dataset and sEV-Related GO Terms in RNA Granule Dataset.....	122
14.	Distinct Protein Associations in Shared Signaling Pathways of sEVs and RNA Granules.....	124
15.	Proteins present in HD RNA granules and sEVs also bind to mutant <i>HTT-RNA</i>	127
	DISCUSSION	129
1.	LncRNAs and REST	131
2.	Shared transcriptomic and proteomic cargo of sEVs and RNA granules	135
3.	Crosstalk Between sEVs and RNA Granules in HD: Pathway Disruption and Mitochondrial Dysfunction.....	140
4.	Differential RNA Sorting and Early Biomarkers in HD sEVs and RNA Granules	145
5.	Conclusions.....	146
	BIBLIOGRAPHY.....	148
	APPENDIX.....	168

ACKNOWLEDGEMENTS

A PhD is never a solitary endeavor; it is a collective journey built on the support, encouragement, and inspiration of countless remarkable individuals. These are the people who listen to you, console you during moments of doubt, motivate you to persevere, and celebrate your achievements as their own. I am profoundly grateful to each of them.

First and foremost, my heartfelt gratitude goes to my supervisor, **Prof. Sybille Krauss**, whose unwavering belief in my potential has been the cornerstone of my journey. Her warmth, understanding, and steadfast support during even the most challenging times gave me the strength to keep going. She welcomed me with open arms, inspired me with her integrity and dedication, and taught me invaluable lessons that extend far beyond academia. I will forever cherish the wisdom and kindness I have gained from her mentorship.

I also extend my sincere thanks to **Prof. Hans Merzendorfer**, **Prof. Maria A. Brehm**, **Prof. Manuela Killian**, **Prof. Ina Maja Vorberg** (DZNE, Bonn) and **Prof. Florian Centler**, whose valuable suggestions and access to lab resources greatly enriched my research. I am deeply grateful to my mentor, **Prof. Ravindran Nambiar**, whose passion for science inspired my own and whose unwavering support and guidance have been instrumental in shaping my career. I would also like to express my gratitude to the **University of Siegen** for providing translational funding, which was pivotal for the successful completion of my doctoral thesis.

A special thank you to **Lisa Knüpfer-Maria**, who has been more than a colleague; she has been a true friend. From assisting with experiments to being a pillar of motivation and a patient listener, her empathy and support have been a source of immense comfort. My gratitude also extends to **Annika Reisbitzer**, **Sabrina Derksen**, and **Patrick Hartwich**, whose thoughtful feedback and constant encouragement have significantly shaped my work. I am deeply grateful to **Ingeborg Baldus**, **Kirsten Jenke**, and **Katrin Haub** for their exceptional administrative support, helping me navigate paperwork and processes with ease.

To my dear friends—**Eva Shirley**, **Hardik Zalavadiya**, **Dr. Sriram Garg**, **Esther Van Bree**, **Christina Böhringer**, **Mark Hase**, **Ish Raorane**, **Chirag Shah**, **Shrey Sharma**, **Neha Quadri**, **Neeraj Raj**, **Major. Gurpreet Singh Virk**, **Annet Mary Sam**, **Chantal Elisabeth Hohe**, **Julia Nikulski**, **Maria Gabriela Lopez Garro**, **Chirag Palekar** and **Adriana Geraci**—thank you for being my unwavering support system. The memories we have created are among the most

Acknowledgements

precious treasures of my PhD journey. From listening to my endless rants to celebrating my milestones, you have all been there through thick and thin. A very special thank you goes to **Hardik Zalavadiya**, whose extraordinary support during the busiest periods of my thesis truly meant the world to me. You reminded me to find balance and brought comfort and friendship that will always remain close to my heart.

I also want to express my immense gratitude to the **CrossFit Siegen community**, my family away from home. You taught me to embrace challenges, to push myself beyond my limits, and to celebrate the journey itself. You helped me grow stronger every day—not just physically, but mentally and emotionally. Thank you for being my safe space in Siegen, for the warmth and camaraderie, and for the blood, sweat, and laughter we shared—quite literally! I am so proud to have been part of such a wonderful community. Cheers to us and the memories we created together!

I owe my deepest gratitude to my family. To my mother, **Vandana Nabariya**, who believed in me even when I doubted myself and stood beside me, overcoming every obstacle to support my dreams—I owe everything to you. To my father, **Kailash Nabariya**, and my grandfather, **Vishnudas Nabariya**, your unwavering belief in my dreams gave me courage and stability. To my siblings, **Vivek and Vaishnavi Nabariya**, thank you for prioritizing my aspirations and supporting our family with grace and strength, allowing me to focus on my work without worry. I am so proud of both of you and deeply grateful for your love and sacrifices. To my late grandparents **Ramgopal Vyas** and **Kamala Nabariya**, your appreciation, love and pride in me have been my inspiration.

Finally, my biggest thanks go to my husband, **Dr. Dinesh Tiwari**. I wouldn't be where I am without your constant encouragement and guidance. From helping me prepare for my interview presentation to navigating the maze of paperwork and standing by my side through every challenge, your support has been my anchor. You have been my rock, my partner, and my greatest cheerleader. Thank you for inspiring me, believing in me, and walking this path with me every step of the way. I love you, and I am endlessly grateful.

Dedicated to my beloved parents-

Vandana and Kailash

ABBREVIATIONS AND ANNOTATIONS

ATP: Adenosine Triphosphate

APS: Ammonium Persulphate

BSA: Bovine Serum Albumin

CAG: Cytosine Adenine Guanine (Trinucleotide Repeats)

CFLs: Cofilins

CPEB: Cytoplasmic Polyadenylation Element-Binding Protein

CHMP: Charged Multivesicular Body Proteins

CO₂: Carbondioxide

CSF: cerebrospinal fluid

DMEM: Dulbecco's Modified Eagle's Medium

DMSO: Dimethyl sulfoxide

EDTA: Ethylenediaminetetraacetic Acid

EGFR: Epidermal Growth Factor Receptor

eIF: Eukaryotic Initiation Factors

ESCRT: Endosomal Sorting Complexes Required for Transport

EXOC1: Exocyst Complex Component 1

FCS: Fetal Calf Serum

FMRP: Fragile X Mental Retardation Protein

FXR1: Fragile X Mental Retardation-Related Protein 1

G3BP1: Ras GTPase-Activating Protein-Binding Protein 1

G418: Geneticin

GAPDH: Glyceraldehyde-3-Phosphate Dehydrogenase

GCN2: General Control Non-Derepressible 2 Kinase

GO: Gene Ontology

HAR1: Human Accelerated Region 1

HDAC6: Histone Deacetylase 6

HEK293T: Human Embryonic Kidney Cells SV40 T-Antigen

HSP70: Heat-Shock Protein 70

HD: Huntington's Disease

HTT: Huntingtin gene

HTT: Huntingtin Protein

IDDs: Intrinsically Disordered Domains

IDRs: Intrinsically Disordered Regions

ISEVs: International Society for Extracellular Vesicles

ILVs: Intraluminal Vesicles

KEGG: Kyoto Encyclopedia of Genes and Genomes

LEVs: Large Extracellular vesicles

LncRNAs: long non-coding RNAs

LCDs: Low Complexity Domains

LLPS: Liquid-Liquid Phase Separation

MHC: Major Histocompatibility Complexes

MISEV: Minimal Information for Studies of Extracellular Vesicles

MgCl₂: Magnesium Chloride

mHTT: Mutant HTT

mRNA: Messenger RNA

miRNAs: micro RNAs

MSCs: Mesenchymal Stem Cells

MVBs: Multivesicular Bodies

MW: Molecular weight

NaCl: Sodium Chloride

ncRNAs: non-coding RNAs

NES: nuclear export signal

NEAT1: Nuclear Paraspeckle Assembly Transcript 1

NMD: Nonsense-Mediated Decay

NTA: Nanoparticle Tracking Analysis

NRSE: Neuron-Restrictive Silencer Element

P-bodies: Processing Bodies

PABP1: Polyadenylate-Binding Protein 1

PKR: Double-Stranded RNA-Dependent Protein Kinase

PERK: PKR-Like Endoplasmic Reticulum Kinase

PI3P: Phosphatidylinositol-3-Phosphate

PCA: Principal Component Analysis

PPI: Protein–Protein Interaction

RE1: Repressor Element 1

rRNA: Ribosomal RNA

RBP: RNA binding proteins

REST: Repressor Element 1 Silencing Transcription Factor

RIN: RNA Integrity Number

RNP: Ribonucleoprotein

RNAi: RNA Interference

RNA-FISH: RNA-Fluorescence *In situ* Hybridization

SDS-PAGE: Sodium Dodecyl Sulphate-Polyacrylamide Gel Electrophoresis

sEVs: Small Extracellular Vesicles

SEM: Scanning Electron Microscopy

SGs: Stress Granules

siRNAs: Small Interfering RNAs

shRNAs: Small Hairpin RNAs

TIA-1: T- Cell Intracellular Antigen-1

TBS: Tris-Buffered Saline

TBST: Tris-Buffered Saline with Tween 20

TEMED: N,N,N',N' -Tetramethylethylenediamine

TTP: Tristetraprolin

TNTs: Tunnelling Nanotubes

tRNA: Transfer RNA

UTRs: 3' untranslated regions

WDR1: WD Repeat-Containing Protein 1

YB1: Y Box Binding Protein 1

ZNFs: Zinc Finger Protein

LIST OF TABLES

Table 1. Recipe for SDS-PAGE gel.

Table 2. Markers for sEVs and RNA granules.

Table 3. Components for the cDNA synthesis reaction (left) and qRT-PCR reaction (right).

Table 4. RNA concentration of the replicates.

Table 5. RIN scores, RNA concentrations and 28S/18S Ratio of control and HD sEVs and RNA granules.

Table 6. Gene distribution across sEV and RNA granule samples.

Table 7. differential gene expression data for control and HD conditions across sEVs and RNA granules.

Table 8. Marker genes for control sEVs and RNA granules.

Table 9. Marker genes for HD sEVs and RNA granules.

Table 10. Coefficients of correlation in stressed control and HD cells.

Table 11.1. REST regulated genes.

Table 11.2 REST regulated genes in HD samples.

Table 12. Pathway Proteins in Control and HD sEVs.

Table 13. Pathway Proteins in Control and HD RNA granules.

LIST OF FIGURES

Figure 1. Schematic diagram representing different types of inter and intracellular RNA granules in the neuronal cell.

Figure 2. Schematic diagram depicting life cycle of the mRNA.

Figure 3. Depiction of two different types of phases in the cell.

Figure 4. SG formation.

Figure 5. Preparation of blotting stack for Western blotting.

Figure 6. Western blot analysis of RNA granules and sEVs.

Figure 7. NTA analysis of sEVs.

Figure 8. Characterization of sEV morphology by SEM.

Figure 9.1. Virtual gel image of RNA integrity.

Figure 9.2. Electrophoregram analysis of RNA from different samples.

Figure 10. Principal Component Analysis (PCA) plot.

Figure 11. RNA composition in samples.

Figure 12. Consistently detected genes.

Figure 13. RNA composition in samples.

Figure 14. Approach 1.

Figure 15. Approach 2.

Figure 16. Biotypes of marker transcripts.

Figure 17. Validation of HD marker genes by qRT-PCR.

Figure 18. Controls for RNA-FISH

Figure 19.1. No probe controls for Lnc-DUXA1.

Figure 19.2. No probe controls for Lnc-LHR1.

Figure 19.3. No probe controls for SNHG7

Figure 20.1. RNA-FISH analysis of Lnc-DUXA1.

Figure 20.2. RNA-FISH analysis OF Lnc-LHR1.

Figure 20.3. RNA-FISH analysis OF SNHG7.

Figure 21. Comparing log₂ fold changes of patient data with HD sEVs dataset.

Figure 22. Comparison of proteomic content from sEVs and RNA granules.

Figure 23. STRING analysis of control RNA granule proteins.

Figure 24. STRING analysis of HD RNA granule proteins.

Figure 25: STRING analysis of Control sEVs.

Figure 26: STRING analysis of HD sEVs.

Figure 27: STRING analysis.

Figure 28. Venn diagram representing the overlapping between HD sEVs, RNA granules and proteins that bind to mutant HTT - RNA.

Figure 29. Hypothetical model of cellular adaptations to manage mHTT pathology in HD cells.

Figure 30. Schematic representation of JAK/STAT dysregulation and its cellular handling in HD cells.

LIST OF APPENDICES

Appendix 1. List of Marker Genes for control sEVs and RNA granules.

Appendix 2. List of Marker Genes for HD sEVs and RNA granules

Appendix 3. List of proteins exclusively present in control sEVs.

Appendix 4. List of proteins significantly overrepresented in control sEVs when compared to HD sEVs.

Appendix 5. List of proteins exclusively present in HD sEVs.

Appendix 6. List of proteins significantly overrepresented in HD sEVs when compared to control sEVs.

Appendix 7. List of proteins exclusively present in control RNA granules.

Appendix 8. List of proteins significantly overrepresented in control RNA granules when compared to HD RNA granules.

Appendix 9. List of proteins exclusively present in HD RNA granules.

Appendix 10. List of proteins overrepresented in HD RNA granules when compared to control RNA granules.

Appendix 11. List of HD sEV Proteins Associated with Neurodegenerative Disorders.

Appendix 12. List of HD RNA granules Proteins Associated with Neurodegenerative Disorders

Appendix 13. List of control sEV Proteins Associated with Neurodegenerative Disorders.

Appendix 14. Functional enrichment analysis of control RNA granules.

Appendix 15. Functional enrichment analysis of control sEVs.

Appendix 16. Functional enrichment analysis of HD sEVs.

Appendix 17. Functional enrichment analysis of HD RNA granules.

ABSTRACT

Huntington's disease (HD) is a neurodegenerative disorder marked by progressive neuronal degeneration, with no current cure. Recent research suggests that RNA granules (such as stress granules and p-bodies) and small extracellular vesicles (sEVs) play critical roles in cellular dysfunction in HD. Both compartments share features like liquid-liquid phase separation (LLPS) and RNA-binding proteins, but the relationship between mutant huntingtin (mHTT) and their shared content remains unexplored.

In this study, we analyze the transcriptomic and proteomic profiles of sEVs and RNA granules in a model expressing mHTT to understand their molecular interactions in HD. Our results show significant changes in gene expression in both sEVs and RNA granules, with a notable decrease in sEVs. Long non-coding RNAs (lncRNAs) were abundant in both compartments, and their expression shifted in HD, suggesting their involvement in disease progression. Additionally, 139 genes in our marker list are regulated by the Repressor Element 1 Silencing Transcription Factor (REST), which is disrupted in HD. Three marker genes (SNHG7, LHR1-LNC1610-1, and lnc-DUXA-1) were validated in RNA granules using RNA-FISH, showing partial co-localization with YB1-positive stress granules. qRT-PCR confirmed increased expression of all five marker genes (lnc-SLC30A5-6, SNHG7, SNHG12, LHR1-LNC1610-1, and lnc-DUXA-1) in HD RNA granules, with three markers showing increased expression in sEVs, though two exhibited high variability.

To validate the relevance of our findings, we compared the expression patterns of HD sEV marker genes with a recently published RNA sequencing dataset of plasma EVs from HD patients. Our results show a stronger correlation between the pre-HD group in the patient dataset and our cell model, suggesting that our model better reflects the early stages of HD progression.

We also identified distinct protein profiles in HD sEVs and RNA granules, with 13 shared proteins, highlighting a unique molecular signature for HD. STRING and KEGG pathway analyses revealed enriched pathways related to neurodegenerative diseases, suggesting broader impacts on neurodegenerative processes. Overlapping GO terms between RNA granules and sEVs point to functional interactions, particularly in RNA transport and metabolism. Notably, WDR1, a protein associated with mHTT-RNA complexes, was identified

in both HD sEVs and RNA granules, suggesting its role in HD pathogenesis by influencing RNA granule formation and facilitating intercellular communication via sEVs. Our findings demonstrate that mHTT alters the composition of sEVs and RNA granules in HD. The detection of miRNAs, zinc finger proteins (ZNFs), and lncRNAs in sEVs suggests that HD cells may attempt to manage stress and intercellular signaling. The identification of overlapping proteins like WDR1, RANBP6, and ITGAV offers potential biomarkers and therapeutic targets. This study enhances our understanding of HD pathology by revealing the differential sorting of RNA and proteins in HD, with implications for early diagnosis and targeted therapies.

ZUSAMMENFASSUNG

Die Huntington-Krankheit (HD) ist eine neurodegenerative Erkrankung, die durch progressive neuronale Degeneration charakterisiert ist und für die es derzeit keine Therapie gibt. Aktuelle Forschungsergebnisse deuten darauf hin, dass RNA-Granula (wie Stress-Granula und P-Bodies) und kleine extrazelluläre Vesikel (sEVs) eine entscheidende Rolle bei der zellulären Dysfunktion bei HD spielen. Beide Kompartimente teilen Merkmale wie ihre Verbindung zum Prozess der liquid-liquid phase separation (LLPS) und in beiden Kompartimenten vorkommende RNA-bindende Proteine. Die Beziehung zwischen mutiertem Huntingtin (mHTT) und ihrem gemeinsamen Inhalt ist bislang jedoch nicht vollständig erforscht.

In der vorliegenden Arbeit wurden die transkriptomischen und proteomischen Profile von sEVs und RNA-Granula in einem Modell, das mHTT exprimiert, untersucht um ihre molekularen Interaktionen bei HD zu verstehen. Unsere Ergebnisse zeigen signifikante Veränderungen in der Genexpression sowohl in sEVs als auch in RNA-Granula. Long non-coding RNAs (lncRNAs) waren in beiden Kompartimenten reichlich vorhanden, und ihre Expression verschob sich bei HD, was auf ihre Beteiligung an der Krankheitsprogression schließen lässt. Die Analyse der differentiellen Genexpression, insbesondere der lncRNAs, stimmt mit den RNA-Sequenzierungsdaten aus den EVs von HD-Patientenplasma überein. Darüber hinaus werden 139 Gene in unserer Markerliste durch den Repressor Element 1 Silencing Transcription Factor (REST) reguliert, der bei HD unterbrochen ist. Drei Markergene (SNHG7, lnc-LHR1 und lnc-DUXA-1) wurden mittels RNA-FISH in RNA-Granula validiert und zeigten eine teilweise Ko-Lokalisierung mit YB1-positiven Stress-Granula. Die qRT-PCR bestätigte eine erhöhte Expression aller fünf Markergene (lnc-SLC30A5-6, SNHG7, SNHG12, lnc-LHR1, and lnc-DUXA-1) in HD-RNA-Granula. Dieser Marker zeigten auch in sEVs eine erhöhte Expression während die anderen zwei Variabilität zeigten.

Um die Relevanz unserer Ergebnisse zu überprüfen, haben wir die Expressionsmuster von HD sEV-Markergenen mit einem kürzlich veröffentlichten RNA-Sequenzierungsdatensatz von Plasma-EVs von HD-Patienten verglichen. Unsere Ergebnisse zeigen eine stärkere Korrelation zwischen der Prä-HD-Gruppe und unserem Zellmodell, was darauf hindeutet, dass unser Modell die frühen Stadien der HD-Progression besser wiedergibt.

Wir haben auch unterschiedliche Proteinprofile in HD sEVs und RNA-Granula identifiziert, mit 13 gemeinsamen Proteinen, was eine einzigartige molekulare Signatur für HD hervorhebt. STRING- und KEGG-Analysen ergaben eine Anreicherung von Signalwegen, die mit neurodegenerativen Erkrankungen in Verbindung stehen. Sich überschneidende GO-Terme zwischen RNA-Granula und sEVs deuten auf funktionelle Interaktionen hin, insbesondere beim RNA-Transport und -Stoffwechsel. Insbesondere WDR1, ein Protein, das mit mHTT-RNA-Komplexen assoziiert ist, wurde sowohl in HD sEVs als auch in RNA-Granula identifiziert, was auf seine Rolle in der HD-Pathogenese hinweist, indem es die Bildung von RNA-Granula beeinflusst und die interzelluläre Kommunikation über sEVs erleichtert.

Unsere Ergebnisse zeigen, dass mHTT die Zusammensetzung von sEVs und RNA-Granula bei HD verändert. Der Nachweis von miRNAs, Zinkfingerproteinen (ZNFs) und lncRNAs in sEVs deutet darauf hin, dass HD-Zellen versuchen könnten, Stress und interzelluläre Signalwege verändert zu regulieren. Die Identifizierung von sich überlappenden Proteinen wie WDR1, RANBP6 und ITGAV zeigt potenzielle Biomarker und therapeutische Ziele auf. Diese Studie erweitert unser Verständnis der HD-Pathologie, indem sie die unterschiedliche Sortierung von RNA und Proteinen bei HD aufklärt, was für die Frühdiagnose und gezielte Therapien nützlich sein kann.

INTRODUCTION

Compartmentalisation in biological systems like eukaryotic cells is a prerequisite for spatiotemporal control of thousands of simultaneous biomolecular reactions, which must be synchronised for running accurate operations. To attain this level of intricate organisation, the cellular inland is organized into different organelles. The term organelle describes a diverse group of organized and specialized structures within the cell.

Two properties are essential for an organelle in a biological system: separation and liberty for components to diffuse freely so that a reaction can take place. Organelles can be membrane-less or membrane-bound. They are dynamic and distinctly structured compartments that can either be permanent residents of the cell or can be released into the extracellular space [1, 2]. There are dozens of intracellular organelles that have properly defined membrane boundaries. Examples include mitochondria, that are the sites ATP generation [3], the nucleus, that physically separates transcription from translation, thereby providing post transcriptional control and regulation [4], or lysosomes, which are empowered with degradation abilities [5]. Some membrane-bound organelles that are released into the extracellular environment include extracellular vesicles like exosomes (sEVs) (**Figure 1**), microvesicles and apoptotic bodies [6].

Non-membrane-bound organelles can be divided by their subcellular localization into nuclear bodies and cytosolic granules. Nuclear bodies include the nucleoli (ribosome production in nucleus) [7], Paraspeckles (retains RNA in the nucleus to control gene expression) [8], splicing speckles (rich in splicing machinery) [9], Cajal Bodies (aids transcription and processing of RNA) [10], Gems (Gemini of Cajal bodies) (involved in spliceosomal snRNP biogenesis, transcription, and translation) [11], and nuclear stress granules (form in response to stress stimuli) [12]. Non-membrane-bound organelles that exist in the cytoplasm include stress granules (SGs), processing bodies (p-bodies), and neuronal transport granules (**Figure 1**) [13]. All the above mentioned nuclear and cytoplasmic organelles are largely made up of RNA and its binding proteins, and thus they are also referred to as RNA granules. Other non-membrane-bound organelles found in the cell include centrosomes [14], glycogen granules [15], and signalling complexes on the inner side of the membrane [16, 17].

Cytoplasmic RNA granules can be divided into germ cell granules (germinal, polar and P granules), somatic granules (SGs and p-bodies) and neuronal granules (neuronal transport RNA granules) [13]. The earliest literature on cytoplasmic RNA granules dates back to 1865,

wherein dark staining polar granules were described by Metschnikoff in the larvae of *Miastor metraloas*; a fly [18, 19]. Parallely, similar structures called germinal granules were found in *Xenopus laevis* and P granules were found in *Caenorhabditis elegans* [20, 21]. Germ cell granules promote germ cell development in embryos. They spatiotemporally control maternal mRNA translation, contain proteins that help in the regulation of translation initiation, translation control and decay processes [20, 22]. Cytoplasmic RNA granules like SGs and p-bodies work in a similar fashion.

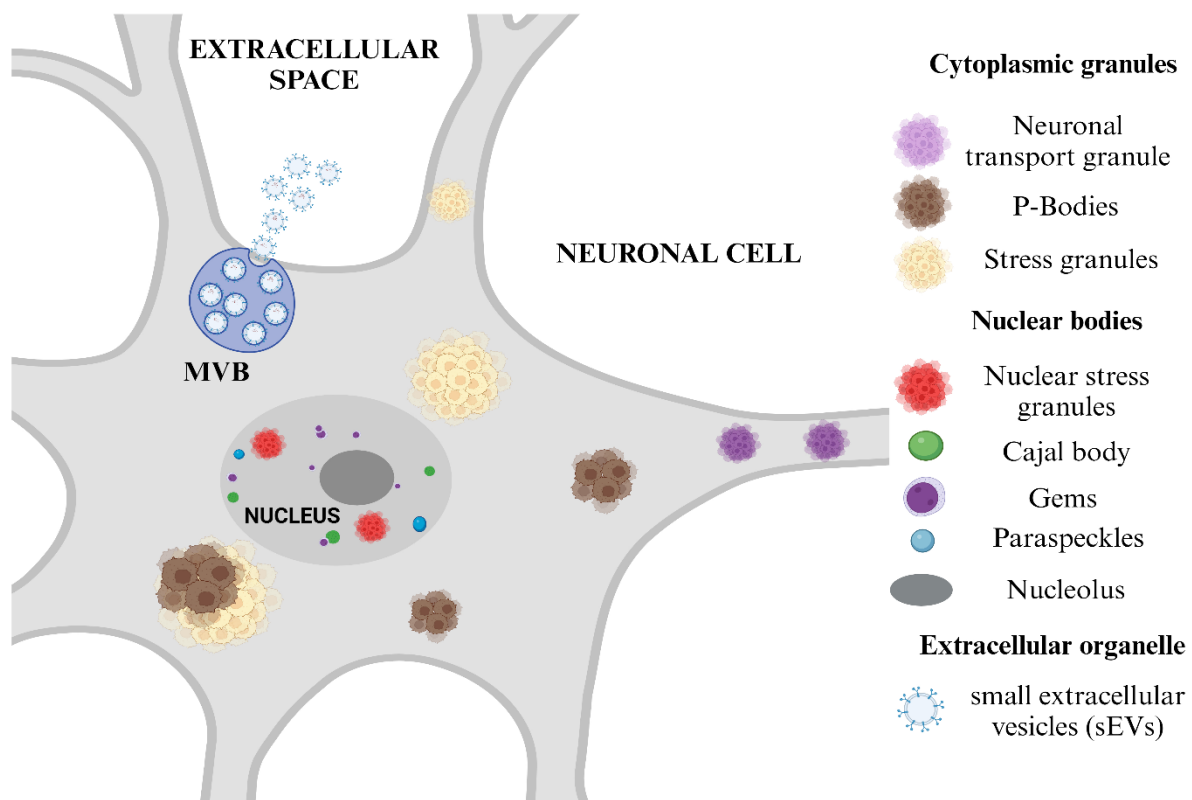


Figure 1. Schematic diagram representing different types of inter and intracellular RNA granules in the neuronal cell. Intercellular organelle includes small extracellular vesicles (sEVs) originating from multivesicular bodies (MVBs). Intracellular RNA organelles include organelles both from the cytoplasm and the nucleus. The panel on the right shows what each depiction represents in the neuronal cells. (Created with Biorender)

This thesis focusses on the cytoplasmic somatic RNA granules (SGs and p-bodies).

1. RNA Granules

Of all cellular components, mRNAs (messenger RNA) have quite a manoeuvring life history. From its genesis to its decease, mRNAs are seldom left unaccompanied. From the moment an mRNA is transcribed, a complex cascade of associations with various RNA binding proteins (RBP) is initiated. After the process of transcription in the nucleus, the pre-mRNA is

extensively processed by several RBPs before it is sent to its actual workplace, the cytoplasm, where it is translated into proteins [23, 24]. Apart from pre-mRNA processing, RBPs also indulge in mRNA localization, translation, degradation, and stability (**Figure 2**) [25-31]. When RBPs bind to their target mRNAs, they form Ribonucleoprotein (RNP) complexes by RNA-protein, protein-protein and RNA-RNA interactions [32-34]. These RNA-protein clusters can coalesce into non-membrane-bound, spherical RNA granules [35]. RNA granules play a pivotal role in regulating the fate of the mRNA. They are extremely dynamic, contain translationally repressed RNA and exhibit functional plasticity. They help in the spatiotemporal fine tuning of protein expression, thereby affecting several cellular mechanisms requiring complex distribution of proteins.

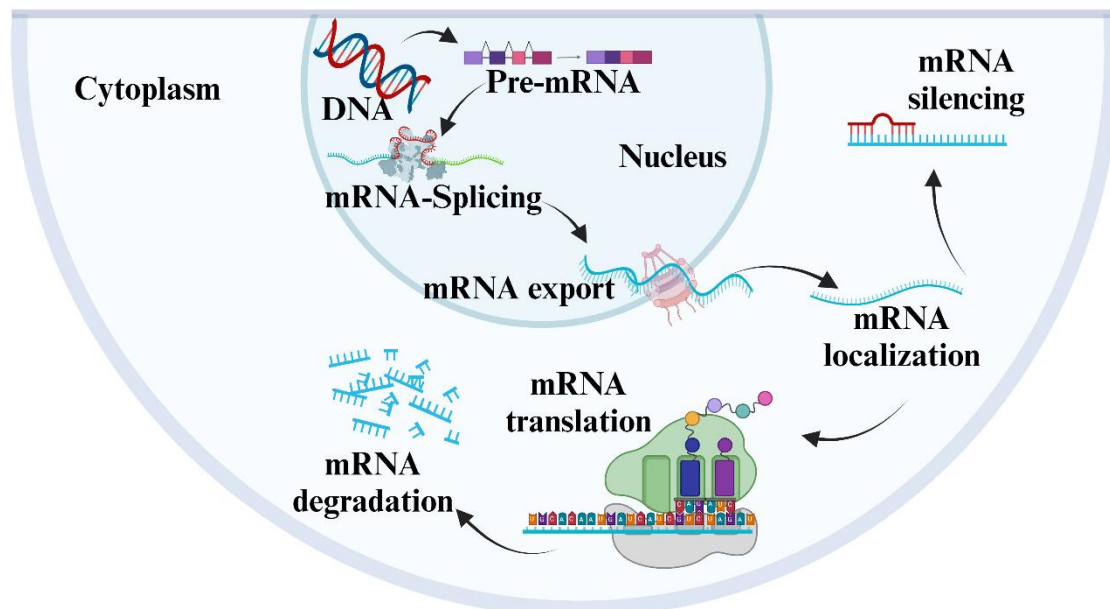


Figure 2. Schematic diagram depicting life cycle of the mRNA. DNA transcribes into RNA in the nucleus [36]. The pre-mRNA is formed which is then capped (methylated 5' end that helps in protection of the RNA from degradation, recruitment of RBPs for RNA processing, export into cytoplasm and translation) [37] and tailed (Polyadenylated tail is added to facilitate nuclear export and stability of the RNA) [38]. It is followed by splicing (helps in the formation of many functional mRNAs to be formed from a single transcript)[36]. After splicing, the RNA is exported into the cytoplasm where it is localized and either translated or silenced to control gene expression. The lifecycle of the mRNA ends with its degradation . (Created with Biorender)

1.1. RNA granule biogenesis: Liquid- Liquid Phase Separation (LLPS)

RNA granules have stable, solid-like cores and dynamic, liquid-like unstable outer shells. In the process of granule formation, the core formation precedes the shell formation. Also, the RNA granule scaffold proteins can be distinguished into solid (core) and liquid (shell) types which induces the formation of distinct substructures that differentially affect each other (Figure 3)

[39, 40]. The process of liquid-liquid phase separation (LLPS) primarily drives the formation of RNA granules. One of the earliest examples of an RNA granule having liquid like properties was of p-bodies from the embryos of *Caenorhabditis elegans* [41]. Further observations recorded different properties of P bodies like fusion, exchange of biomolecules with cytoplasm and honey like viscosity [42], clearly suggesting their liquid state. Further studies recorded the viscosity of nucleoli (nuclear RNA granule) to be 50 times more than P bodies confirming the liquid-like property of RNA granules [43].

To understand the process of LLPS, it is important to understand liquids and their properties. Liquid molecules have the ability to rearrange. Their shape either depends on the container or on surface tension. Surface tension is the mechanical tension in between two phases. It lowers the area of interface to the lowest possible which is a drop. Since drop is spherical, surface tension carves liquid drops to be spherical. In liquids, molecules can move quickly and are easy to mix. This leads to stochastic collision of reactants enabling biochemical reactions in liquids.

Two miscible liquids mix because the entropy is higher in a mixed state and thermodynamic systems evolve at higher entropy levels. Molecular rearrangements in liquids exhibit diffusion that aids equal mixing [44]. For example, when we add dye to water, the local concentration of the dye is very high, the molecules diffuse, and the net flux of molecules is from high to low concentration of dye. This happens until the concentration of the dye is equal and the entropy of the system is maximum. This gradient-driven transport is called diffusive flux. In a chemical reaction, mixing is an important phenomenon by which different molecules meet randomly. Diffusion not only aids this process but also allows transport of biomolecules independent of the concentration gradient. Thus, mixing and diffusion balance local concentrations of biomolecules. But liquids can also demix into two distinct phases due to physical interactions between different molecules. In this case, two neighbouring molecules will have lower energy in the system than two molecules of different types. Some biomolecules have greater affinity towards each other than with other biomolecules. These affinity differences can lead to phase separation [44-47].

Viscosity is the property of liquids that describes their resistance to flow. When a liquid is flowing in a pipe driven by pressure, the rate of flow relies on its viscosity[48]. Complex fluids are mixtures that have a coexistence between two phases like liquid-liquid. Liquid- liquid

phase transition describes the process of separating an untangled, low-density liquid from an entangled, high-density liquid. For compartmentalization within a cell, phase separation helps in concentrating biomolecules at one place. For example, in p-bodies, a subset of biomolecules segregates from the cytoplasm and coexist as two phases: the cytoplasm and the P-body (Figure 3).

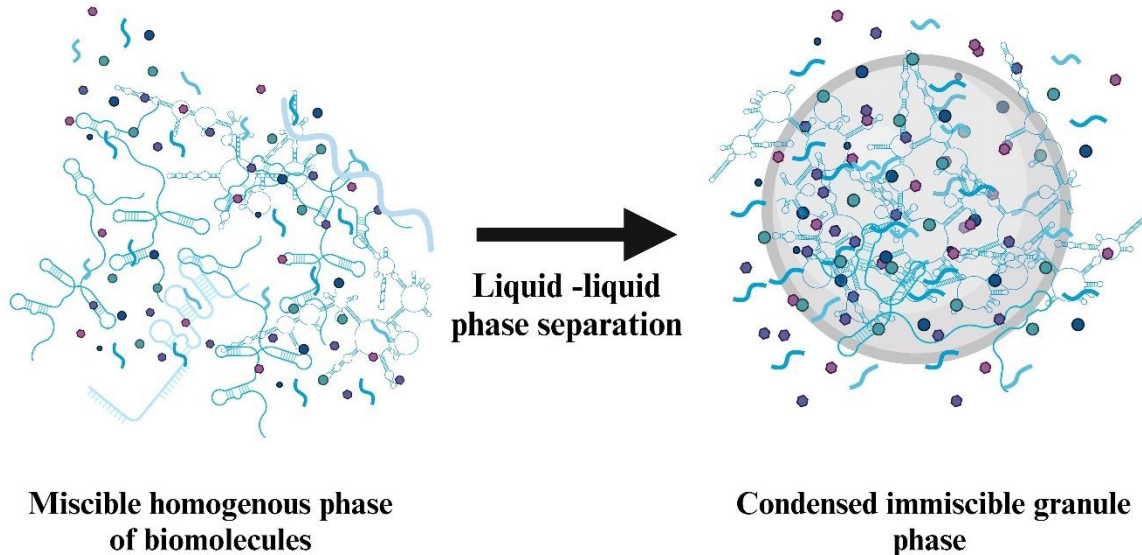


Figure 3. Depiction of two different types of phases in the cell. In the cytoplasm biomolecules are generally present in the miscible homogenous form. Upon liquid-liquid phase separation, the biomolecules take an immiscible form that we call RNA granules. It has a tight bound inner shell and a loose outer core that generally aids in molecular exchange. (Created with Biorender, inspired by Majumdar et al.,2019 [49])

One of the key forces involved in the formation of these organelles are multivalent protein-RNA, RNA-RNA and protein-protein interactions. Proteomic and genetic studies have shown that the defining feature of proteins and RNA molecules driving phase separation include multivalent nature of adhesive domains and/or linear motifs [50-53]. Multivalency can be a consequence of

1. folded proteins with precise surfaces for interaction. This can lead to the formation of oligomers that create multivalency for other associative molecules that interact stereospecifically.
2. folded domains. They can be sewed together with the help of linkers forming multivalent linear proteins and
3. intrinsically disordered regions (IDRs). Multiple short linear protein motifs can be scaffolded by IDRs.

Evidently, multivalency can occur by the combination of these three or by structure formation inside IDRs.

IDRs are found in proteins that drive phase transitions. IDRs are regions that do not fold into a fixed 3-dimensional structure but exist in heterogeneous conformations [54]. Many IDRs have different amino acid compositions and repetitive sequences. Low complexity domains (LCDs) are a subset of IDRs are formed by only a small subset of amino acids [50, 54-56]. Studies with cryo-electron microscopy showed that stacking of LCDs facilitated assembly of proteins which can lead to phase transition from a liquid to a gel like state or a gel like state to an aggregated insoluble state. Instead of containing a balanced distribution of the 20 amino acids typically resulting in a specific three-dimensional protein structure, LCDs are often composed of a limited number of amino acids. LCDs have a protein sequence containing stickers (low complexity clusters) separated by spacers or linkers [57]. Spacers are high in glycine and glutamine. Glycine makes the LCDs more dynamic by promoting the liquidity of the droplet thereby facilitating exchange biomolecules and disassembly. On the other hand, glutamine decreases the dynamicity of the LCDs by hardening the droplet [58]. When stickers are in close proximity, low affinity interactions between LCDs of homologous RBPs are supported. This intermolecular binding via LCDs helps to form liquid droplets in aqueous environment.

There are RNA recognition motifs in RBPs, which drive phase transition by providing a scaffold for RBPs to bind in a very close proximity [59, 60] and thus, membrane-less organelles often contain RNA. RNA promotes phase separation of many RBPs and regulates spatiotemporal distribution and nucleation of membrane-less organelles [61]. Nucleation is the process by which the initiation of droplet formation of RNA granule occurs. Homogenous nucleation described a process in which molecules randomly come together to start a droplet formation. However, this process is rather a rare event [62]. In heterogeneous nucleation, droplets can initiate to form at a pre-existing site [63]. Examples include preassembly of certain molecules or use of special structures like a centriole for centrosomes [64] and chromatin in case of a spindle [65].

The size of these membrane-less compartments can be controlled in several ways:

1. By stopping the fusion process.
2. By components which can only dissolve in the droplets.

3. By chemical reactions that can stabilize the droplets from the process of Ostwald ripening [66].
4. By the number of molecules to build the phase [67-69].

Ostwald ripening is a phenomenon in solid or liquid solutions that describes the change of a homogeneous structure over time, a process by which biomolecules can diffuse from small droplets to the larger droplets [66]. Even if there are strong interactions between the biomolecules in a droplet, chemical processes like ATP hydrolysis can counteract Ostwald ripening. ATP hydrolysis can be used to break and form bonds between molecules within droplets. Moreover, active transport processes can be driven by ATP hydrolysis which can promote phase separation [70, 71].

While the process of LLPS is quite fascinating and ensures systematic function of the cell, it comes with its consequences. Upon higher protein concentrations, the LLPS could turn sideways and cause aggregation leading to liquid-solid phase transition into gels or crystals [43, 72, 73]. Cells use deaggregases to distort aggregates and maintain the intracellular dynamics [74-77]. In pathological conditions aberrant RNA-protein complexes tend to form aggregates and deaggregases fail to function [78]. For instance, overexpression of stress granule markers is seen in HD mouse models and patients [79].

The composition of RNA granules depends on the current situation of the cell, for example its translational activity. Therefore, changing cellular demands leads to dynamic assembly and disassembly of these granules resulting in a compositional change within. While each granule has its own set of signature molecules, there is a subset of proteins and RNAs that they share with each other in order to form a collaborative system. This system can be adjusted to satiate and support various stages of different cellular states by tweaking the destination of the biomolecule: be it stress, a transport mechanism, a developmental stage, decay processes or any other specialised function [80]. Time lapse video of microscopic analysis further reveals that the interaction between different RNA granules occurs via docking [81-83]. Further, the non-membranous model of the granules supports the exchange between granules [84]. Therefore, different kinds of RNA granules act as a network system and not as independent entities.

1.2. Cytoplasmic RNA granules

1.2.1. Stress Granules (SGs)

After over a century of germ cell granule discovery, another type of RNA granule was observed in the cytoplasm of heat shock exposed tomatoes [85]. Structurally and compositionally analogous granules were later observed in mammalian cells when exposed to environmental stresses like hypoxia, heat, UV radiation and oxidative stress and were called SGs [86].

Cells are surrounded by a number of stress-inducing stimuli ranging from changes in PH to lack of metabolites, a viral or bacterial invasion, or other pathological conditions. These stimuli can derail cellular homeostasis. The cellular ribostasis and proteostasis is disrupted and if left unattended can even lead to organismal decease [87]. Cells handle such detrimental challenges by going on survival mode. They shut down global translation and prioritize the production of biomolecules needed to eliminate stress. These mechanisms are supported by the formation of SGs. SGs are irregularly shaped, micron sized, transient, fibrillo-granular, electron dense compartments that accumulate, store and protect untranslated mRNAs and components of translational machinery [88-90]. Their size depends on the time and type of stress and can range from 0.1-4 μm in size [91, 92]. They preserve transcripts until the stress subsides and separate them from transcripts that are to be degraded [88]. The hypothesis behind this storage of mRNA instead of its degradation is that the process can aid in rapid reinitiation of translation after the SG disassembly without any ATP expensive resynthesizing costs [86].

Both exogenous and endogenous stress stimulate the assembly of SGs. The formation of SGs is dependent on the type of stress and the signalling pathways the stress triggers [93]. SGs have a dynamic outer shell that can easily disassemble and a more stable inner core. The multistep process of SG assembly begins with translational arrest and polysome dissociation (translation initiation complexes separate from the mRNA) followed by the formation of the inner core by the oligomerization of RNA-protein complexes via LLPS. Aggregating proteins can trigger an abnormal liquid-to-solid phase transition within SGs, a process that should not occur under normal conditions. Typically, the shell and core of SGs form independently before eventually fusing. Intrinsically disordered domains (IDDs)—specific regions within IDRs that serve distinct functional roles—of core proteins facilitate the formation of the dynamic outer shell. This outer shell expands through the fusion of smaller granules by establishing weak,

transient interactions[40, 50, 60, 94]. This dynamic shell modulates rapid exchange of biomolecules with the cytoplasm in an ATP driven process. Several proteins like fragile X mental retardation protein (FMRP), Ras GTPase-activating protein-binding protein 1 (G3BP1), T- cell intracellular antigen-1 (TIA-1) and tristetraprolin (TTP) can promote SG formation by providing a scaffold for other biomolecules to bind [95, 96]. Interestingly, even in the absence of stress, their overexpression can lead to SG assembly [96-100].

1.2.1.1. SG composition and formation

It is estimated that the inner core of the SGs consists of around 42,000 RNAs within which 80% are mRNAs [101]. Besides polyadenylated mRNAs, SGs contain several, micro RNAs (miRNAs), non-coding RNAs (ncRNAs), ribosomal subunit machineries, translation initiation factors, proteins involved in mRNA processing, stability, silencing and transport, ubiquitin, signalling molecules, poly ADP ribose and nuclear transport factors [102-107]. The most important constituents of SGs include can be divided into four categories:

1. Silenced translation initiation complexes that are bound to mRNA and can be trusted as SG markers. They include mRNA transcripts, small ribosomal subunits, PABP1, eIF3, eIF4E, eIF4A, eIF4G and eIF4B [86, 108].
2. mRBPs that are involved in either RNA stability or silencing. The translation silencing factors include FMRP [99], FAST [109], Argonaute, ataxin-2 [110], TIA1, TIA-1-related (TIAR)[111], fragile X mental retardation-related protein 1 (FXR1) [99], cytoplasmic polyadenylation element-binding protein (CPEB) [112], RNA-associated protein 55 (Rap55, Lsm14) [113], pumilio [114] and smaug [115]. The decay supporting machinery includes TPP, RNA helicase RCK (p54), endonuclease polysome-associated RNase 1 (PMR1), zipcode binding protein 1 (ZBP1) and BRF1 [100, 112, 116, 117]. While some proteins, such as PMR1, RCK, RISCs, and FXR1, are components of polysomes, others, like TIA1 and TIAR, are not involved in polysomal assembly and are likely active translational repressors[116], [118, 119] [108]. By binding to mRNA, TIA1 and TIAR can inhibit translation and promote the formation of SGs. In contrast, proteins like Argonaute, RCK, and FXR1, which are associated with actively translating polysomes, regulate translation in a different manner. In their inactive state, these proteins support translation. However, upon activation or overexpression, they shift to repress translation, disassemble polysomes, and facilitate SG formation.

3. Proteins of cellular metabolism like splicing, RNA localization and RNA editing. These proteins nucleate SGs upon overexpression. These include G3BP1 (SH3-domain-binding protein)[97], Caprin [120], Survival of motor neurons (SMNs) [121], FAST [109] and the long interspersed nuclear element 1 transposon open reading frame 1 (LINE 1- ORF1p) [122]. Some other proteins that fall into this category include apolipoprotein B mRNA-editing enzyme catalytic polypeptide-like 3G (APOBEC3G)[123], Staufen [124] and ZBP1 [117].
4. Proteins that are present in SGs due to their interactions with the core SG biomolecules. An example of such a piggyback interaction is the binding of FAST [125], steroid coactivator 3 (SRC3) [126], FUSE-binding protein or KH-type splicing regulatory protein (FBP/KSRP) [127] and PMR1 [116] to TIA-1, which recruits these proteins to SGs. Proteins like tumor necrosis factor receptor-associated factor 2 (TRAF2), Disrupted-in-Schizophrenia (DIS1), plakophilin 1 and plakophilin 3 are another set of proteins that do not play any role in RNA metabolism and yet end up in SGs because of the piggyback interactions. For instance, plakophilin 3 binds with G3BP and PABP-1 and TRAF binds to eIF4G [128, 129].

The recruitment of mRNA into SGs is highly selective. Although only 50% of the poly A transcripts and its binding proteins are found in SGs, almost 90% of the total TIA-1 is found in the SGs [86]. Some of the SG residents are mRNAs encoding insulin-like growth factor II (IGF-II), β -actin, c-MYC and glyceraldehyde-3-phosphate dehydrogenase (GAPDH). Other mRNAs encoding proteins like heat-shock protein 70 (HSP70) and heat-shock protein 90 (HSP90) are not found in SGs [117, 130]. However, the mechanism behind this selective recruitment remains elusive.

One hypothesis explaining this selection is that mRNA localization to specific SGs is highly influenced by the post-transcriptional modifications of the RNA. SG markers like G3BP1 and FMR1 interact differently with transcripts harboring N6-methyladenosine (m6A) modifications. While G3BP1 preferentially binds to m6A-modified RNAs, suggesting a possible enrichment of m6A in G3BP1-positive granules, FMR1 repels these methylated transcripts [131]. However, in some cases G3BP1 and FMR1 join to form a complex [132].

m6A modifications are prevalent in the brain and increase with neuronal maturation. This observation suggests that mRNA targets of G3BP1 and FMR1 may be differentially regulated with age, potentially influencing neurodegenerative disease mechanisms [131, 133].

Further, SG core transcripts have lower GC content, shorter half-lives, long coding and UTR regions, lower translational efficacies and are scarce in the cell. 7.1 kb is the average length of the SG transcript which is longer than the other non-enriched transcripts [101]. Since longer RNAs have more sites of intermolecular interactions, this length may impart greater opportunities for RNA-RNA and RNA-protein interactions thereby facilitating condensation and phase separation [34, 101].

Apart from post transcriptional RNA modifications, post translational modifications of SG proteins also affect SG assembly, fusion and disassembly. Methylation, deacetylation, dephosphorylation and O-GlcNAcylation play an important role in the formation of SGs [134, 135]. Methylation increases the hnRNPA1, FUS and FMRP's interactions with SGs [136, 137]. However, G3BP1, when methylated can inhibit SG formation. G3BP1, TPP or FUS phosphorylation inhibits SG assembly. Furthermore, phosphorylation of FUS or TDP-43 prevents these proteins from being incorporated into SGs, disrupting their ability to localize and participate in the granule formation process [97, 138].

The canonical formation of SGs relies on the phosphorylation of eIF2 α at serine 51. This phosphorylation inhibits the exchange of GTP/GDP on the eIF2-GTP-tRNAMet complex, which is crucial for the addition of methionine at elongating AUG codons during translation. As a result, the formation of the 43S pre-initiation complex is blocked, leading to a halt in cap-dependent translation and triggering SG formation which further stops the formation of 43S pre-initiation complex, and cap dependent translation is obstructed. This leads to the formation of SGs [89, 139].

Four upstream kinases are responsible for phosphorylating eIF2 α in response to different types of stress:

- **PKR (double-stranded RNA-dependent protein kinase)**, which responds to viral infections,
- **PERK (PKR-like endoplasmic reticulum kinase)**, which reacts to ER stress,
- **GCN2 (general control non-derepressible 2 kinase)**, which is activated by amino acid deficiency,

- **HRI (heme-regulated inhibitor kinase)**, which responds to osmotic and oxidative stress.

Although each kinase is activated by distinct stress signals, they can all converge on eIF2 α phosphorylation to induce SG formation. Moreover, there is crosstalk between these kinases, allowing multiple kinases to phosphorylate eIF2 α under certain conditions (Figure 4)[87, 139-142].

In addition to canonical pathways, SGs can also form through non-canonical mechanisms, independent of eIF2 α phosphorylation. In this case, the initiation of SG formation occurs through the disruption of the eIF4F cap-binding complex, which is responsible for regulating translation initiation. The eIF4F complex is composed of eIF4A, eIF4E, and eIF4G, and any interference with the function or assembly of this complex can inhibit translation, leading to SG formation without eIF2 α phosphorylation (**Figure 4**).

For example, non-canonical SGs can form by inhibiting eIF4A helicase activity using silvestrol [143], or by modulating eIF4E through hydrogen peroxide or selenite. Viral cleavage of eIF4G also triggers non-canonical SG formation. Additionally, SGs can form by preventing the interaction between eIF4A and eIF4G using anti-inflammatory lipids like 15-deoxy- Δ -12,14-prostaglandin J2 and prostaglandin A1 [103, 144-150].

While SG production is enhanced by polysome destabilization with puromycin, SG production is stalled and SGs are dissolved upon polysome stabilization with emetine or cycloheximide [98, 151, 152]. eIF2 α -dependent SGs can be disassembled by the integrated stress response inhibitor (ISRIB). ISRIB can also restore translation initiation [153].

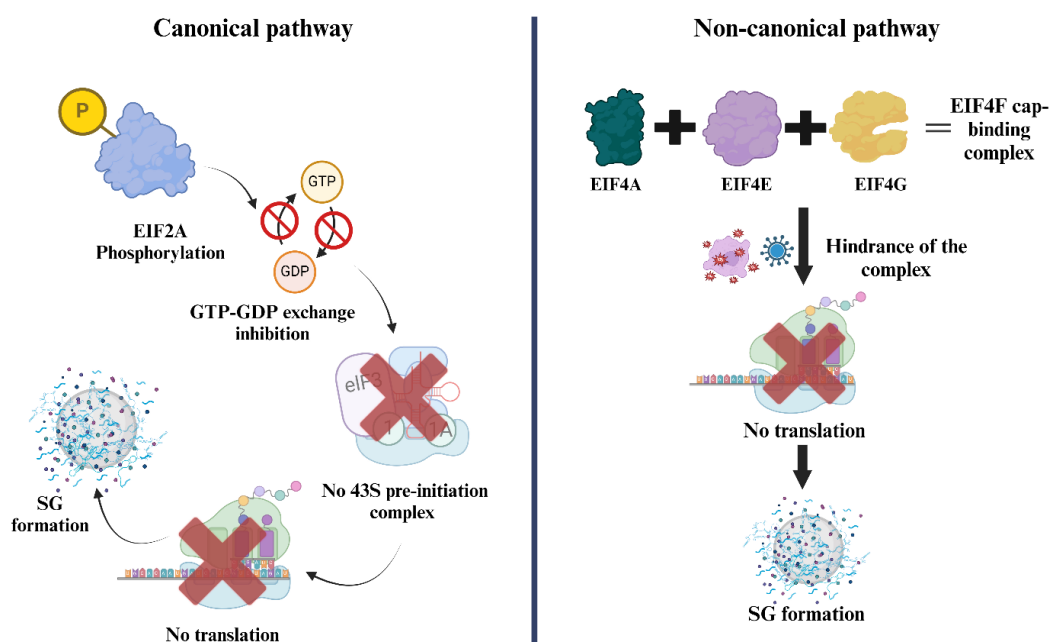


Figure 4. SG formation. SGs form either canonically or non-canonically. The canonical formation of SGs is triggered by the phosphorylation of eIF2 α at serine 51, which blocks GTP/GDP exchange in the eIF2-GTP-tRNAMet complex, halting the 43S pre-initiation complex and cap-dependent translation. This phosphorylation is mediated by four kinases—PKR, PERK, GCN2, and HRI—in response to various stresses like viral infections, ER stress, amino acid deficiency, and oxidative stress. Multiple kinases can sometimes collaborate to phosphorylate eIF2 α . SGs can also form non-canonically without eIF2 α phosphorylation by disrupting the eIF4F cap-binding complex (via oxidative stress, viruses etc.), which regulates translation initiation.

SG formation is often triggered by impaired translation initiation, but SGs can also form independently of both eIF2 α phosphorylation and stalled translation initiation. For instance, UV radiation or the overexpression of SG proteins such as FMRP, G3BP1, and TIA-1 [96, 97, 99, 154]. While the mechanisms behind SG formation in response to UV radiation require further investigation, the effects of SG protein overexpression are better understood. When SG proteins accumulate at high concentrations, their low-complexity domains drive intermolecular interactions, leading to protein aggregation and SG formation through oligomerization (e.g., G3BP1) and the recruitment of RNA into granules [96, 97, 103].

1.2.1.2. Stress granule (SG) disassembly

SGs are transient formations. They disassemble once the stress is abolished from the system. Their disassembly leads to the release of mRNA and ribosomal subunits, as well as signalling molecules that were trapped in the SGs, which are then available for *de novo* synthesis of proteins [155]. Though the exact mechanism behind the SG disassembly remains a subject of interest, studies suggest that there are two possible mechanisms of SG clearance: by granulophagy and by chaperone-mediated disaggregation [103].

The process of SG disassembly by granulophagy is a two-step process. It includes the breakdown of the outer shell followed by core clearance via autophagy. The shell dissolution releases mRNAs and other biomolecules into the cytosol thereby reinitiating their translation. Once, the outer shell is dismantled it is easy for the degradation machinery to attack the SG cores and engulf them. Another way of the core clearance may be that degradation factors packed inside the core are activated upon stress release and dissolve the core [156]. Granulophagy requires several factors that are a part of the autophagic and proteasomal system. Some of the examples include an ATPase called valosin-containing protein (VCP/p97), Histone deacetylase 6 (HDAC6) and Spleen Tyrosine Kinase (SYK) that are localized within the

SGs [156-158]. The pro-inflammatory SYK phosphorylates SG proteins, thereby aiding SG clearance by autophagy [159].

The second mechanism for SG clearance involves chaperone-mediated disaggregation [95]. Multiple studies highlight the role of HSP70 in SG dissolution. While overexpression of HSP70 prevents SG formation, the absence of HSP70 results in failed SG disassembly and impaired translational recovery. HSP70 overexpression specifically interferes with the aggregation of TIA-1, a key SG nucleating protein, thereby promoting SG disassembly. Additionally, SG clearance is supported by the HSPB8-BAG3-HSP70 complex. HSP40 co-chaperones also play a critical role in determining the pathway for SG dissolution studies show the role of HSP70 in the dissolution of SGs [96, 160-162].

Similar to SG formation, its disassociation is a multistep process too. It can have initial steps like formation of smaller cores from the SG core to be dissociated, which could be subsequently removed either by granulophagy or via chaperone-mediated processes [40]. The identified pathways involved in SG removal include degradation of mRNAs by p-bodies and other scaffold proteins by proteasomes [95]. One way in which SG formation and proteasome inhibitors are linked is by the phosphorylation of eIF2 α . Proteasome inhibitors stimulate modifications in eIF2 α via different kinases like HRI and PERK. Also, proteasome inhibitors can trigger various stresses including oxidative and ER stress ensuring that eIF2 α phosphorylation subsequently triggers SG formation [163]. In conclusion, proteasomes, granulophagy and chaperones either individually, collectively or in combination disintegrate SGs.

1.2.2. Processing bodies (P-bodies)

After transcription, an mRNA undergoes multiple fidelity and quality checks both in the nucleus and in the cytoplasm before it is translated into a protein. While some mRNAs are given a green signal for translation, others are maintained in a translationally repressed state so that they can be spatiotemporally activated. Other mRNAs are enrouted towards decay or translational quiescence [164]. There are hundreds of RBPs and regulatory RNAs involved in this system, a subset of which compartmentalize in the cytoplasm forming uniform, spheroid, non-membrane-bound organelles called p-bodies [164, 165]. However, how these biomolecules are recruited into p-bodies remains a mystery.

P-bodies are 100- 300 μm in size, but upon stress, p-bodies are much bigger and are present in higher concentrations when compared to the normal conditions [112, 166, 167]. They contain several components of 5'–3' mRNA decay machinery, the nonsense-mediated decay pathway, posttranscriptional processes, translation repression, and the RNA-induced silencing complex [109, 168]. However, these pathways are active even when cells lack detectable levels of p-bodies indicating that p-bodies are not required for silencing. Studies show that blocking the silencing pathways stops p-body formation and therefore inferred that p-bodies are formed as a consequence of silencing. Further studies proved that mRNAs must enter decapping and/or silencing pathways to nucleate p-bodies [166].

P-bodies are not only the site of degradation, but also an mRNA storage unit. The fate of the mRNAs in p-bodies varies, while some are degraded, others remain enriched [169]. Cells use p-bodies as a place to store mRNA-protein complexes when they want to shut down certain pathways [170]. Microscopic studies have revealed an interesting docking phenomenon between SGs and p-bodies where they are found juxta-positioned on one another. It is hypothesized that this docking process enables the transfer of biomolecules from SGs to p-bodies for degradation [109, 171]. In cell types like neurons with long protrusions like axons, p-bodies act as sites of local degradation or storage for translationally repressed RNAs. However, it remains unresolved whether p-body assembly takes place in the neurite or in the soma [82].

1.2.2.1. P-bodies composition, assembly and disassembly

Proteins involved in the degradation of bulk mRNA were among the first proteins detected in p-bodies [13, 165]. In eukaryotes, this process includes:

- Removal of the poly A tail by deadenylases [172].
- Digestion of mRNAs from their 3' end [173] or alternatively
- Removal of the cap structure by the decapping enzyme DCP2, thereby making the mRNA degradation prone by exonuclease XRN1 [174].

Therefore, decapping enzymes and its complexes (DCP1/2, Hedls, hEdc3, and p54/RCK), coactivators and XRN1 are found in p-bodies [175, 176]. Apart from these proteins, LSM1-7 (regulates RNP assembly) [177], RAP55/LSM14 (mediates translational regulation)[167, 178], GW182 (part of miRNA pathway)[179], SMG5, SMG7, and UPF1 (part of nonsense-mediated

decay pathway)[180, 181] were also found. Other biomolecules that known to localize in the p-bodies comprise of

- Argonaute proteins and miRNA which support RNA interference (RNAi) and miRNA-mediated gene silencing [182, 183].
- Proteins that facilitate AU-rich element (ARE)-mediated mRNA decay which is a pathway that degrades AU-rich mRNAs at their 3' untranslated regions (UTRs) [109, 184].
- Translational repressors like eIF4E-transporter (eIF4E-T)[185].
- RNA-binding proteins that are involved in translation/decay pathways like BRF1, TTP, CPEB and Smaug[13].

P-bodies can assemble or disassemble in response to various cellular stimuli. Their non-membranous structure allows rigorous exchange of RNAs and proteins in response these cues [186]. Further, several decapping activators and post-translational protein modifications like ubiquitination and phosphorylation are responsible for p-bodies assembly [187, 188]. K63-ubiquitylation regulates DCP1a phosphorylation and p-body formation. Tenekeci et., 2016 showed that mutations of ubiquitinated lysines to arginine at the C-terminal region of DCP1A is associated with altered P-body sizes, DCP2 binding and decapping activities. Additionally, complete loss of p-bodies was observed upon expression of ubiquitin mutant indicating the importance of ubiquitin in P-body formation, either separately or by modulating other post-translational protein modifications like phosphorylation [189]. Arginine demethylation in the C-terminal R/G-rich domain of Lsm4 was found important for P-body formation as its absence resulted in P-body deficiency [190, 191].

The maintenance of p-bodies depends on many of its resident proteins like Edc3, Lsm4 and DDX6. The specific domains of these proteins contain RNA-binding sites with low-complexity sequences that are associated with LLPS, indicating the importance of this process in the formation and maintenance of p-bodies [192-196]. Its maintenance also depends upon translationally repressed mRNA. The entrapment of mRNA in polysomes by cycloheximide causes P-body loss and DCP1, DCP2 and XRN1 depletion leads to increased P-body assembly. This could be due to the aggregation of mRNA decay intermediates [167, 197, 198]. Studies have also reported the significance of ATPase activity in maintaining integrity of the p-bodies. The fluidity of the p-bodies is likely to be an energy consuming process. However, the process

needs to be highly regulated since ATPase hyperactivity could lead to dissociation of p-bodies [199, 200]. It was also shown that phase separated liquid droplets could mature into amyloid-like aggregates. This may be coherent with the role of energy-dependent process in the preservation of P-body liquidity and inhibition of toxic aggregate formation [32].

Interestingly, microtubular disassembly leads to an increase in P-body formation. Under normal conditions only a few p-bodies assemble in a particular cytoplasmic region of the cell and remain there for most of the cell cycle suggesting that the formation of p-bodies is tightly controlled, and p-body components are diffusely distributed and do not assemble. Upon drug-induced microtubule disassembly, the number of p-bodies increases, which does not hinder mRNA metabolism, indicating that P-body aggregation is independent of mRNA decay or mRNA translation modifications [201].

P-bodies move directionally along microtubules, a cytoskeletal network that also facilitates the transport of certain localized RNAs after their export from the nucleus. Unlike p-bodies, which use microtubules for active movement, these RNAs hitch a ride on the microtubule network to reach specific cellular destinations. Additionally, mRNAs are often found associated with mitotic microtubules, suggesting that p-bodies might be anchored to the microtubule network. This anchoring could increase the likelihood of encounters between p-bodies and mRNAs, facilitating mRNA processing or decay. This idea is supported by the observation that the movement of p-bodies becomes significantly less efficient when microtubules are disrupted, leading to reduced directional transport and reliance on slower, passive diffusion in the cytoplasm. It remains unclear, however, whether all mRNAs that come into contact with p-bodies actually interact with them. Interestingly, some p-bodies move around the nucleus, hinting at a possible "patrolling" function, where they scan for freshly transcribed RNAs. Nonsense-mediated decay (NMD)-targeted mRNAs are recognized as they emerge from the nucleus, and it is possible that p-bodies pick up NMD-related factors during this patrolling, given that p-bodies contain key components of the NMD pathway. This suggests a dynamic and coordinated role for p-bodies in regulating mRNA decay and quality control within the cell [202-205].

Cells have an impeccable communication and networking system, be it within the cell (intracellular) or in between the cells (intercellular). An excellent example of intracellular communication are the RNA granules. While each granule has its own set of signature

molecules, there is a subset of proteins and RNAs that they share with each other to form a collaborative system. Microscopic studies have revealed an interesting docking phenomenon between SGs and p-bodies that enables the transfer of biomolecules from SGs to p-bodies for degradation [109, 171]. Their non-membranous model compliments this molecular exchange and establishes a strong networking system [84].

Intercellular communication can be either facilitated by systems like gap junctions, tunnelling nanotubes (TNTs) or via hormones. Apart from these canonical systems, cells also use exosomes/small extracellular vesicles (sEVs) that are secreted out of the cells as a non-canonical mechanism of intercellular communication [206, 207]. Apart from non-membrane bound RNA organelles SGs and p-bodies, in this study we also focus on membrane-bound RNA organelle, sEVs.

2. Extracellular Vesicles

Extracellular Vesicles (EVs) is a generic term that includes all vesicles that are secreted by cells into the extracellular Space. EVs are micro- to nanosized, spherical, lipid bilayer membrane-delimited particles that cannot multiply on their own and are found in biofluids like blood-plasma, cerebrospinal fluid (CSF), tears, bile juice, synovial fluid, saliva and breast milk. They can be further divided into small EVs (sEVs) which are < 200 nm in size (e.g., exosomes) and large EVs (IEVs) which are > 200 nm in size (e.g., microvesicles (100–1,000 nm) and apoptotic bodies (1–5 μ M)) [208, 209]. sEVs are composed of several biomolecules including DNA, RNAs (mRNA and ncRNAs like transfer RNAs (tRNAs), ribosomal RNAs (rRNAs), microRNAs (miRNAs)), membrane-, transmembrane-, and soluble proteins, as well as a wide range of peptides, lipids, and their derivatives [210-212]. The membrane of sEVs is cholesterol and sphingomyelin-enriched which is essential for formation of lipid rafts [213]. sEVs have a density of about \sim 1.1–1.2 g/mL. However, their density is affected by several factors including protein:lipid ratio and the action of sEV metabolic pathways. The size, shape, and density of sEVs are determined by its cargo. Therefore, sEVs are vastly variable. They contain a broad variety of membrane proteins, transmembrane proteins, soluble proteins and a wide range of enzymes. They also contain glycoconjugates and lipids such as phosphatidylcholine (PC), phosphatidylserine (PS) and phosphatidylethanolamine (PE) [214].

sEVs aid intercellular communication, biomolecule shuttling and removal of redundant biomolecules from the cells. Since they mimic the physiological cargo of their mother cell, they

can act as biomarkers for the diagnosis of several pathological conditions or to check the effectiveness of the treatment in patients with minimum invasion. Furthermore, sEVs are strong candidates as target-specific delivery systems. They have a lipid bilayer that protects the inner biomolecules. They contain receptors on this lipid bilayer that enable precise delivery of sEVs to their target site. sEVs can be easily engineered, and they can cross the blood-brain barrier [212, 215, 216].

Although focused research on extracellular vesicles (EVs) only began in the late 1980s and 1990s, early observations date back to the 1940s when Chargaff studied blood coagulation and identified particulate structures, which we now believe were EVs. In 1967, Peter Wolf described these particles as “platelet dust,” distinguishable from platelets and sedimentable by high-speed centrifugation. This was followed by significant findings in the 1970s and 1980s, including the proposal by Nunez et al. that vesicles are released through fusion with the plasma membrane, a process now understood as exosome secretion. The landmark studies by Johnstone and Harding in 1983 confirmed the release of these vesicles from MVBs, marking the beginning of modern EV biology. As the field expanded, the International Society for Extracellular Vesicles (ISEV) established the MISEV guidelines in 2014, with updates in 2018 and 2024, to standardize EV research. These guidelines discourage the use of the term “exosomes” due to the difficulty in isolating MVB-specific vesicles, encouraging the term “small extracellular vesicles” (sEVs) to ensure clarity and reproducibility in the field. Therefore, in our study we use the term small extracellular vesicles (sEVs) [209, 217-224].

2.1 sEV biogenesis and composition

sEVs are formed by the process of inward budding of the early endosomal membrane, which mature into MVBs. MVBs and late endosomes are a part of specialized endosomal compartments that comprise of several intraluminal vesicles (ILVs) that encapsulate several biomolecules upon specific sorting [222]. Cytoskeletal and microtubule networks transport MVBs to the plasma membrane, where they fuse with the cell surface and undergo exocytosis leading to the secretion of ILVs into the extracellular space. These ILVs, once released, are called exosomes/sEVs [225]. MVBs that do not fuse with the plasma membrane to release sEVs are instead directed towards degradation. They either fuse directly with lysosomes or first merge with autophagosomes, which then fuse with lysosomes, leading to the breakdown of their contents. [226].

To date, several mechanisms involved in the biogenesis of sEVs have been discovered. The endosomal sorting complexes required for transport (ESCRT) machinery along with SNARE complexes, tetraspanin and lipid-dependent mechanisms play a vital role in the biogenesis and secretion of sEVs [214, 227]. The ESCRT machinery deforms, repairs, and seals the membrane during several processes that include MVB biogenesis, sealing of the nuclear envelope and plasma membrane repair [228, 229]. The ESCRT machinery is a multi-subunit system in the cytoplasm which facilitates cargo sorting and vesicle budding in MVBs. There are 5 ESCRT complexes, namely, ESCRT-0, -I, -II, -III and Vps4 [230]. Hepatocyte growth factor-regulated tyrosine kinase substrate (Hrs) of ESCRT-0 recognises and sorts ubiquitinated cargo to endosomal compartments rich in phosphatidylinositol-3-phosphate (PI3P), a phospholipid found in early and late endosomes. It regulates membrane-trafficking and cell signalling. The main role of PI3P in the ESCRT pathway is to facilitate organisation of cargo by interacting with Hrs [230]. Next, ESCRT-1 is recruited by ESCRT-0 by interacting with tumor susceptibility gene 101 (Tsg101), an ESCRT subunit. ESCRT-I and ESCRT-II promote the inward budding of the endosomal membrane around assembled ubiquitinated proteins. Subsequently, a subunit from ESCRT-III called the charged multivesicular body protein-6 (CHMP6) binds with to ESCRT-II to recruit CHMP4. CHMP4 then polymerizes around the neck of ILV pouch (in budding state) like a coil. CHMP3 activates next, the bud is cleaved, ILVs are formed, and ESCRT-III is disassembled in an energy consuming process catalysed by Vps4 [230]. TSG101 and ALIX are the most common sEV components. ALIX binds to the subunits of ESCRT-III and helps in the budding and cleaving processes during the formation of ILVs. Syndecan heparan sulfate proteoglycan, through its cytoplasmic adaptor, syntenin interacts with ALIX to aid the formation of ILVs and thereby in the production of sEVs [231]. ALIX recruits ESCRT-III to late endosomes facilitating the incorporation of tetraspanins into the membrane of sEVs [232]. The role of ubiquitination in sEV cargo sorting remains unresolved. However, the ESCRT pathway is ubiquitination-dependent and proteins like TSG101, Hrs and STAM1 bind to ubiquitin and play an important role in sEV formation and biogenesis. Although, sEVs are enriched with ubiquitinated cargo and ubiquitinated sequences of Major Histocompatibility Complex (MHC)-II increases their incorporation into the cargo, sEVs still have non-ubiquitinated MHC-II's in their cargo signifying a ubiquitination-independent sEV loading [233-235]. Apart from the ESCRT pathway, lipids like ceramide form raft-like structures that support inward budding in ILVs [236] **(Figure 5)**.

Both the ESCRT and lipid-mediated pathways operate simultaneously during sEV biogenesis, although the lipid-dependent mechanism varies by cell type. For instance, inhibiting ceramide production in melanoma cells does not affect sEV production. Tetraspanins, such as CD81, CD63, and CD9, play crucial roles in membrane scaffolding and are key biomarkers for sEVs. They also participate in sEV formation: CD63 assists with loading cargo into sEVs, CD9 interacts with CD10 to enhance its loading, and CD81 is involved in cargo sorting. However, tetraspanin-6 negatively regulates sEV production by interacting with syntenin and disrupting the ALIX-syntenin complex, directing MVBs toward lysosomal degradation instead of sEV release [237-242].

Taken together, the biogenesis of sEVs is a fine-tuned, strictly- controlled, multi-layered pathway, whose mechanisms of origin and secretion are controlled by the ESCRT pathway and other molecular players that involve tetraspanins, Rab and Ral proteins. Since sEV formation and secretion are largely dependent on these proteins, their presence in the molecular cargo is invariable and are hence used as molecular markers for sEVs. In addition, the involvement of autophagy-related proteins indicates the dual nature of sEVs: as an effective communication system and a robust cellular waste management system possibly during stress.

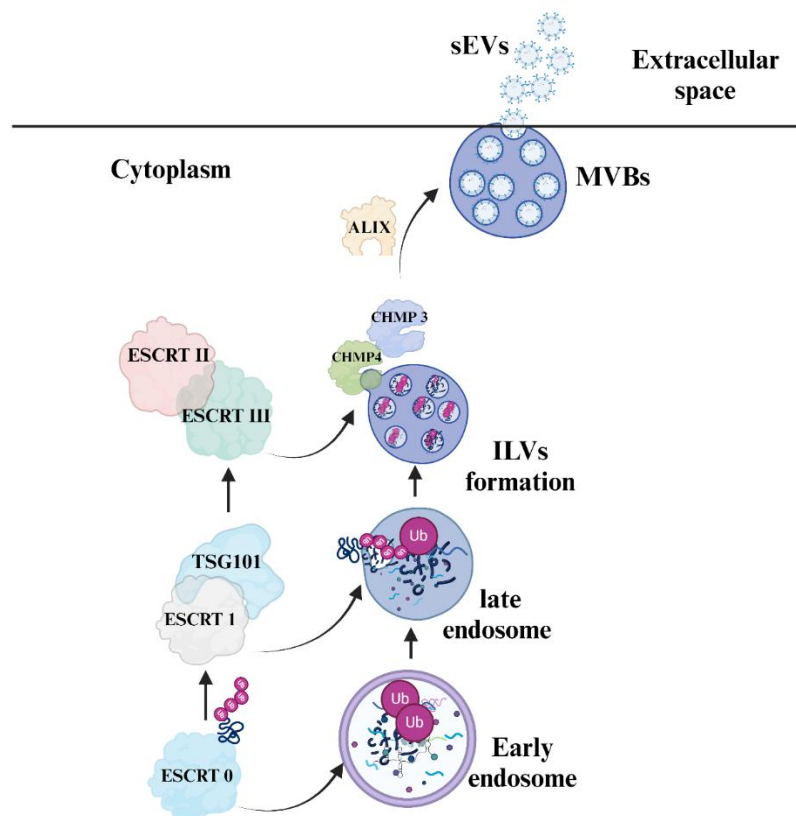


Figure 5. Biogenesis of sEVs. Hepatocyte growth factor-regulated tyrosine kinase substrate (Hrs) in the ESCRT-0 complex recognizes ubiquitinated cargo and directs it to PI3P-rich endosomal compartments. ESCRT-I is recruited via Tsg101 and, along with ESCRT-II, promotes inward budding of the endosomal membrane. ESCRT-III subunits, such as CHMP6 and CHMP4, polymerize around the neck of the budding vesicle, and Vps4 mediates vesicle scission in an ATP-dependent process. ALIX and syndecan-syntenin interactions further aid ILV and sEV formation, while ceramide also supports budding through raft-like structures, indicating both ESCRT-dependent and -independent pathways in sEV biogenesis. (Created with Biorender)

2.2 sEVs function

sEVs are intercellular communication systems carrying signals that are required for maintaining homeostasis of several pathways within the cellular system [243]. The crosstalk between cells via sEVs can be unidirectional, bidirectional or systemic: that is, the message sent to one cell by another may or may not be reciprocated or reciprocated by trafficking sEVs to different cells, tissues and organs. These interactions are not limited to release and delivery of biomolecules, but also linked with modulation of target-cell by for example, activating histocompatibility complex interactions, working as antigen-presenting vesicles and stimulating immune responses and promoting cell-surface interactions [244, 245]. The mechanism of sEV uptake into the recipient cells is still poorly understood. Different routes of uptake have been recorded that includes direct fusion, phagocytosis, micropinocytosis, receptor-mediated endocytosis, lipid raft and clathrin interactions [226]. Once taken up by the endosomes, the sEVs have to make their way into the cytoplasm. Endosomal escape means acidic compartments of the lysosomes that might potentially hinder the integrity of the sEV cargo. Although initially direct membrane fusion leading to direct delivery in the cytoplasm was postulated, we now know that the uptake of sEVs is a complex mechanism and in depth analysis based on high resolution microscopy and live cell reporters are required to deduce the pathways taken [246, 247].

The biological roles of sEVs are well understood. sEVs play an important role in tissue repair and regeneration, thereby promoting the formation of myelin, neuronal growth and survival. On the other hand, sEVs isolated from the central nervous system (CNS) have been found to contain pathogenic proteins and peptides like beta amyloid, alpha synuclein and superoxide dismutase aiding disease progression [248-255]. During oncogenesis, sEVs modulate the surroundings, involve in immune cell dysregulation, tumor proliferation and progression and their numbers are substantially increased [256]. sEVs carry viral proteins from the infected

cells. Resistance genes and virulence factors are transmitted using sEVs [257, 258]. sEVs play a complex role, acting as protectors, promoting disease progression, and adding layers of functionality that complicate their overall impact. Since sEVs carry cell-specific signatures and deliver precise, target-specific information, they hold great promise as both diagnostic markers and drug delivery systems. In animal models, sEVs have successfully delivered therapeutic cargo with minimal immune clearance, and nano-delivery systems using sEVs from mesenchymal stem cells (MSCs) are already in clinical trials [259]. For diagnostics, sEVs have been shown to carry disease-specific markers: for example, alpha-synuclein in Parkinson's disease is present in sEVs from both plasma and CSF, while kidney injury markers are found in sEVs from renal cells, and markers for pancreatic and lung cancer have also been identified in sEVs. These vesicles not only offer valuable biomarkers for disease diagnosis but can also be used to monitor treatment effectiveness [244, 245, 260-264].

Interestingly, sEVs share several similarities with SGs and p-bodies. Both originate from the cytoplasm and carry large cargos of RNA and proteins. Many RNA-binding proteins found in SGs and p-bodies are also involved in loading sEVs during their formation, showing significant overlap in their protein content. Evidence suggests that LLPS, which drives the formation of RNA granules, also aids in sorting biomolecules into sEVs [265-267]. Therefore, in this study, we are investigating the content and crosstalk between RNA granules and sEVs. This crosstalk was studied in a Huntington's disease model.

3. Huntington's Disease

Huntington's Disease (HD) is a rare genetic disorder that is inherited in an autosomal dominant way. It is caused by an expansion of a CAG trinucleotide repeat (encoding a polyglutamine motif) in exon 1 of the *Huntingtin* gene (*HTT*) on chromosome 4p16.3. 0.48 HD cases are found per 100,000 person-years with a higher incidence rate in Europe and north America compared to the Asian and African continents. The pooled prevalence of HD is 4.88 per 100,000 [285]. The normal CAG repeat length in the *HTT* gene is between 5-35 repeats. There is low penetrance of the disease in people with 35-39 repeats, while 40 or more repeats lead to HD conditions. There is an inverse correlation between the age of onset and the number of repeats. The mean age of onset is 40 years and juvenile cases account only 5% of all cases. This neurodegenerative condition has a wide neuropsychiatric clinical spectrum that may involve combinations of a triad of symptoms: motor, cognitive, and psychiatric. The disease

progression spans between 15-20 years. In the early years, choreiform movements with gait disturbances are observed followed by motor impairments like rigidity and bradykinesia. Approximately 50% of the patients show cognitive symptoms like depression years before HD is diagnosed. Suicide associated with depression is very high in HD patients [268-271]. The characteristic symptom of HD is chorea, which is derived from a Greek word χορεία, meaning, a circle dance. It describes the movement disorder characterized by loss of voluntary movements and replaced by involuntary actions due to neurodegeneration [272, 273]. Other symptoms like emotional deficits and psychiatric symptoms are also observed in early HD. Patients often show signs of apathy, dysphoria, agitation, social disinhibition, irritability, anxiety and impulsivity [274]. The rate of progression of the disease varies and is not connected with the development of other motor and cognitive symptoms like chorea [274]. Behavioural changes often precede cognitive impairment, but by the time the disease is diagnosed, most patients already suffer from significant cognitive impairment which progresses slowly, over years, finally leading to dementia. Alterations in the CNS drive pathogenesis in HD. Striatal neurons and neurons projecting from the cortex to the striatum are the most vulnerable to cell death. Moreover, thinning of the cortex and reduction of the striatum start in patients up to a decade before they start showing symptoms. Apart from these clinical and neuropsychiatric features, patients of HD also suffer from weight loss, skeletal-muscle wasting, osteoporosis, testicular atrophy, and metabolic and immune disturbances. Patients generally live for up to 20 years after the onset of the disease and fatal aspiration pneumonia is generally the cause of their death [275-278].

3.1 The biology and function of Huntingtin

The *HTT* gene is highly conserved across species, from flies to mammals, and consists of 67 exons. Upon transcription, it produces two mRNA transcripts: one is 10,366 bp, and the other is 13,711 bp. The latter is abundant in the brain [279-294]. Wild-type HTT binds with transcription factors like and the tumor suppressor protein 53 (p53), cAMP-response element (CREB)-binding protein (CBP) and the nuclear factor- κ B (NF- κ B). Moreover, HTT interacts with transcriptional activators and repressors like Gln-Ala repeat transcriptional activator CA150, the repressor element-1 transcription factor/neuron restrictive silencer factor (REST/NRSF) and the corepressor C-terminal-binding protein (CtBP) [295-299]. Through its various interactions, HTT influences several key cellular processes. For example, by interacting with

p53, HTT regulates genes involved in DNA repair, apoptosis, cell-cycle control, and responses to cellular stress. HTT also plays a role in regulating the transcription of repressor element 1 (RE1), also known as the neuron-restrictive silencer element (NRSE). RE1 is recognized by REST, a transcriptional silencer, suggesting that HTT helps regulate genes controlled by RE1, which are crucial for the development and protection of the nervous system. Additionally, HTT binds to REST/NRSF in the cytoplasm, preventing the formation of nuclear co-repressors. This action promotes the transcription of genes like brain-derived neurotrophic factor (BDNF), which contains an RE1 element on its promoter. BDNF is vital for neuronal development and survival, and *HTT's* role in sequestering REST ensures that BDNF and other RE1-regulated genes can be transcribed to support neural health [298, 300]. Apart from this, *HTT* also controls chromatin remodelling, helps in the embryogenesis and development of the nervous system, regulates tissue maintenance, supports organogenesis and formation of the tissue and have pro-survival and anti-apoptotic properties [301-304]. In primary neurons, wild-type *HTT* protects the cell from several death inducing stimuli, even against mutant HTT [305, 306]. The *HTT* gene is ubiquitously expressed throughout the body, however, the expression is higher in the nervous system. Its expression is observed throughout various regions of the nervous system, including areas of the brain where neurodegeneration is less prominent, such as neurons projecting from the striatum, interneurons, and regions like the cortex, cerebellum, and hippocampus. However, HD is increasingly recognized as a multisystem neurodegenerative disorder, affecting multiple regions and systems within the human brain.[307].

The expression of *HTT* is also abundant in dividing cells suggesting its crucial role in cell division and neurogenesis. During mitosis, it is localized at the spindle poles and interacts with dynein to promote NUMA accumulation, which functions through the process of phase separation and regulates assembly of mitotic spindles [308, 309]. Apart from this, HTT is also found in the neuronal cilia, photoreceptor cilia and other ciliated cells advocating the importance of HTT in ciliogenesis [310, 311].

The *HTT* gene product is approximately 348 kDa. It is larger in humans than in other species. The consequences of this variability in normal HTT function remain unresolved. However, deletion of the polyglutamine stretch located near the N-terminus of the protein enhances longevity and autophagy in mice. The N-terminal of HTT protein contains an amphipathic α -

helix structure, which functions as a nuclear export signal (NES) and undergoes post-translational modifications, such as phosphorylation at serines and ubiquitination, acetylation, and sumoylation at lysines. These modifications influence HTT's clearance and subcellular localization [279-284].

HTT is composed of several HEAT repeats, clustered into 3-5 α -rod domains with disordered regions, acting as scaffolds for different proteins mediating several inter- and intramolecular interactions. It has multiple proteolytic sites and is cleaved by proteases like MMP10, caspases, cathepsins, and calpains [280, 297, 312, 313].

HTT directly interacts with dynein or indirectly via Huntingtin-associated protein 1 (HAP1) along with the subunit of dynactin and KIF5 to facilitate anterograde and retrograde transport within neurons. It helps transport organelles like GABA-receptor vesicles, BDNF-containing vesicles, autophagosomes, endosomes, and lysosomes. It also binds to glyceraldehyde 3-phosphate dehydrogenase (GAPDH) on vesicles, increasing vesicular transport velocity along microtubules [314-320].

Interestingly, HTT also plays a role in endosomal trafficking and endocytosis. HTT interacts with HIP1 and HIP1R and support invagination and membrane coating in clathrin-mediated endocytosis. HTT N- and C-terminal domains interact with dynamin 1 suggesting its role in the activation of the protein [321-324]. HTT along with dynamin, amphiphysin, endophilin-A3 and endophilin-B1 forms a complex and aids vesicle recycling and endocytosis [325, 326]. It also interacts with GTPase Rab11 and activates it. Rab11 then participates in vesicle recycling [327]. Rab5 binds with HAP40 which is under the regulation of HTT to form a complex. This complex is then recruited to the early endosome. HTT with HAP40 allows endosomes to switch from microtubules to actin. HAP40 is upregulated in brain of HD patients [328].

HTT function is regulated by several post-translational modifications (PTMs), including palmitoylation, acetylation, sumoylation, phosphorylation, and ubiquitination, with most research focused on HD. For instance, acetylation of mutant HTT facilitates its clearance via the autophagy-lysosomal pathway, while phosphorylation reduces proteolysis and alleviates polyglutamine (polyQ)-mediated toxicity. Phosphorylation also affects HTT's localization within the nucleus and influences intracellular transport in both anterograde and retrograde directions [282, 315, 329-331].

HTT also functions as an autophagy-related protein. In its mutant form, HTT abnormally activates autophagy by inhibiting mammalian target of rapamycin (mTOR) kinase, resulting in an excessive formation of autophagosomes. However, these autophagosomes exhibit a loading defect, preventing the proper degradation of proteins and organelles. Additionally, HTT interacts with p62, aiding in the recognition of ubiquitinated proteins and promoting autophagosomal loading and the initiation of autophagy [332-335].

3.2 The etiology of *Huntingtin*

Mutant *HTT* (*mHTT*), like the wild type, is expressed throughout the body. However, the primary cause of morbidity and mortality in HD is its detrimental impact on the central nervous system (CNS). This is partly because neurons, unlike many other cell types with shorter lifespans, are terminally differentiated and live long enough to accumulate damage from *mHTT*. Nevertheless, this is not the sole explanation, as not all neurons are equally affected. Degeneration is particularly widespread in specific regions of the brain, including the cerebral cortex, brainstem, caudate, putamen (striatum), pallidum, and thalamus [336, 337].

While HD was traditionally thought to result from a toxic gain of function in *mHTT*, recent studies suggest that the condition may involve more complex mechanisms. For instance, experiments show that reducing *HTT* gene expression is lethal, but the introduction of *mHTT* initially alleviates this lethality, leading to an HD phenotype later in life. Additionally, growing evidence indicates that HD also affects peripheral tissues, and systemic signaling originating from these tissues can influence the progression of HD in the brain. This suggests a broader, systemic involvement of *mHTT* beyond the CNS [338-340].

The process of neurodegeneration in HD is linked to several molecular mechanisms that are triggered by products of the *mHTT* gene, both the RNA and the protein. In HD, the HTT protein misfolds and aggregates. Also, the mutant protein binds to other proteins aberrantly, hindering their spatiotemporal and physiological function. This misfolding and aggregation of the protein in the CNS is the pathological hallmark of the disease. There are several protein-mediated mechanisms that contribute towards the neurotoxicity including deregulated protein degradation, axonal transport defects, protein aggregation, mitochondrial dysfunction, transcriptional deregulation and transport defects in the axon of the neurons [339, 341, 342].

Several studies in the recent years have demonstrated RNA-mediated pathogenesis in HD [343-345]. RNA molecules fold and form either non-canonically paired or fully paired regions like hairpin loops, bulges, pseudoknots and multibranch loops to minimize their free energy. RNA-RNA and RNA-protein interactions are facilitated by these structural motifs that act as recognition sites. While this three-dimensional structure is important for supporting several cellular processes, mutations like in HD can lead to the formation of aberrantly folded RNA-hairpins that result in a toxic gain-of-function [346]. Watson–Crick base-pairing between G-C positions and wobble base pairing at the A–A mismatches form when the RNA folds with the opposing strands of CAG repeats. In normal *HTT* transcripts, the CAG repeats are interspersed with CCG pairs. However, in the diseased condition, the CAG repeat length increases leading to the formation of a hairpin loop of pure CAG repeats. The hairpin is divided into the base, the stem with the double-stranded CAG region and a terminal loop. The size of the loop varies according to the number of repeats, odd number of repeats lead to a loop of seven nucleotides and even number results in the loop of four. The number of repeats also determine the length and stability of the hairpin. The mutated CAG-hairpin structures aberrantly sequester RNA-binding proteins, disrupting their normal functions and interfering with essential cellular pathways. This misappropriation of RNA-binding proteins impairs critical processes, leading to cellular dysfunction and contributing to disease pathology [347, 348]. These disruptions contribute to neurodegeneration through several RNA-mediated mechanisms including :

1. siRNA machinery deregulation: The altered hairpin structure can affect RNA interference pathways by disrupting the recruitment of proteins involved in the siRNA machinery, leading to impaired gene silencing and contributing to toxic gene expression profiles [349].
2. Aberrant translation: In HD, both mutant *HTT* mRNA and mutant HTT protein disrupt the general translation machinery. The mutant *HTT* mRNA promotes its own translation, while the mutant HTT protein interferes with ribosomal function. This dual disruption causes widespread impairment of protein synthesis. Additionally, the sequestration of RNA-binding proteins by the mutant CAG-hairpin structures further affects normal translation, leading to the production of aberrant or misfolded proteins. These dysfunctional proteins exacerbate cellular stress and toxicity, contributing to the progression of neurodegeneration in HD [350].

3. Deregulated splicing: The sequestration of splicing factors by mutant CAG-repeat RNA disrupts the splicing of not only the mutant *HTT* transcript but also other crucial mRNAs. This misregulation of splicing is a major mechanism of RNA-mediated toxicity in HD, resulting in the production of dysfunctional protein products. The altered splicing patterns exacerbate neuronal damage, contributing to the progression of neurodegeneration [350].

The proteolysis of mutant HTT plays a critical role in HD pathogenesis as well. Increased proteolytic activity in the brains of HD patients results in the formation and aggregation of small HTT fragments containing the expanded CAG repeat, which can form inclusions in the cytoplasm or translocate to the nucleus. In the nucleus, HTT is capable of inducing neurodegeneration. Blocking its nuclear localization prevents the formation of nuclear inclusions and halts neurodegeneration. Interestingly, when inclusion formation is inhibited, cell death increases, suggesting that inclusions may serve as a protective mechanism against HTT-induced cytotoxicity [285-294].

3.3 Diagnosis, prognosis and therapy

The diagnosis for HD includes investigation of personal and family history, psychiatric and neurological examination and finally genetic testing[285, 293]. To date, there is no cure for HD and all the available treatments are palliative in nature. These treatments only partially relieve patients from the symptoms without addressing the cause of the disease. Genetic counselling is given to the families of the patients. Physiotherapy and speech therapy helps patients to manage involuntary movements and speech problems. Psychotherapies is given to soothe depression and anxiety. Tetrabenazine and Deutetrabenazine are commonly used to manage involuntary movements (chorea) in HD patients. Both drugs reduce dopamine levels in the brain by inhibiting vesicular monoamine transporter 2 (VMAT2), which is responsible for packaging dopamine into synaptic vesicles. By lowering dopamine activity, they help to control the excessive, erratic movements seen in HD. Valbenazine, currently under review for FDA approval to treat chorea in HD, operates through a similar mechanism, inhibiting VMAT2 to decrease dopamine signaling and reduce abnormal motor movements [287][351].

While achieving a cure or a symptom-free state in HD remains a challenging goal, ongoing research is focused on developing diagnostic tools to monitor disease progression and therapies to manage symptoms. Current trials, such as the AON trials, aim not only to slow

down the progression of the disease but also to potentially halt or even reverse its course. These efforts represent a significant step towards addressing the underlying causes of HD and improving patient outcomes. Therapeutic strategies at the post-transcriptional level are promising since targeting the RNA would consequently stop its translation to protein which would deprive most of the pathological mechanisms. One way of doing it is through antisense oligonucleotides (AONs) either by targeting one allele (only mutant) or both the alleles (normal and mutant). One example of AON's targeting both alleles was tominersen. In pre-clinical trials, the mutant HTT RNA was reduced by 80% upon treatment, and improvement in the symptoms was observed. In young animals motor deficit was completely eliminated. In the clinical trials, intrathecally administered tominersen showed reduced HTT protein levels in the CSF of early HD patients [352]. However, it was unclear if reduction in the levels of normal HTT had effects. To address this, phase 3 trials were done (GENERATION-HD; NCT03761849; sponsored by Hoffmann-La Roche), but were terminated due to poor tolerance of the maximum dose in patients indicating that lowering the levels of normal HTT below a certain point might not be tolerated long term and mutant allele specific approach might be more effective. Additionally, the trials indicated that outcomes were more promising in younger patients, suggesting that earlier intervention may yield better results [353][354]. This approach requires AONs to be designed against single nucleotide polymorphism (SNPs) on the mutant allele. There are many SNPs on the HTT sequence and with the help of special techniques, information on which allele carries what SNP can be determined in order to generate AONs that target only the mutant RNA. This approach was tested in clinical trials but was terminated due to lack of consistent reduction of mutant HTT. As a result, an alternative approach was made by Wave life sciences and is an improvement on the previous AONs. It is now in the clinical trial stage on a small group in Canada and Europe [355].

RNA interference (RNAi) therapies, akin to antisense oligonucleotides (AONs), aim to degrade mutant *HTT* RNA by binding to and silencing it. These therapies employ molecules such as miRNA, short hairpin RNA (shRNA), and small interfering RNA (siRNA) to target and diminish the expression of mutant *HTT*. Sanofi and Voyager Therapeutics are developing an shRNA-based drug delivered via adeno-associated virus (AAV) during brain surgery. UniQure is advancing AMT-130, an Adeno-Associated Virus-Mediated Gene Therapy, which also uses AAV to deliver shRNA directly to brain cells. Both drugs have demonstrated potential in preclinical

studies and are moving toward clinical trials. AMT-130 involves administering the AAV vector directly into the brain via a surgical procedure, aiming for targeted and localized expression of therapeutic shRNA in brain cells. This gene therapy model is designed for one-time treatment, with the AAV integrating into the genome to produce RNAi molecules that suppress mutant HTT production [355]. While the upfront cost of brain surgery might seem high, it's crucial to consider the long-term financial impact on caregivers over many years. Nonetheless, the invasive nature of brain surgery and associated risks are significant concerns. Therefore, developing cost-effective and less invasive treatment options is essential, given the extreme psychological, psychiatric, and financial strain that HD imposes on patients and their families.

3.4 RNA granules and HD

SG proteins, including G3BP1, interact with mutant HTT, influencing its cellular distribution and aggregation. In both mouse models and HD patients, SG proteins like G3BP1 are overexpressed, suggesting a link between SG dynamics and HD pathology. When G3BP1 is knocked down in patient-derived induced pluripotent stem cells (HD-iPSCs), mutant HTT levels increase, and the cells lose their ability to suppress HTT aggregation. Similarly, in a *C. elegans* model, the absence of G3BP1 leads to accelerated toxicity and aggregation of mutant HTT, highlighting G3BP1's protective role. Under non-stressed conditions, G3BP1 prevents mutant HTT aggregation and promotes its proteasomal degradation. However, during stress, G3BP1 relocates to SGs, where it loses its ability to interact with mutant HTT. This shift triggers the formation of HTT aggregates, which can persist even after the stress has been resolved. In fact, increasing G3BP1 levels has been shown to prevent aggregation and promote degradation of mutant HTT. However, once SGs are formed, G3BP1's ability to control mutant HTT aggregation becomes severely compromised, indicating that the formation of SGs and the sequestration of G3BP1 are key factors in HTT aggregation in HD [356].

Besides SGs, p-bodies are also affected in HD. Under normal conditions Argonaute (AGO2) and HTT protein are colocalized. AGO2 and HTT interaction leads to RNA-mediated gene silencing in p-bodies. In mutant HTT expressing mouse striatal cells, fewer p-bodies were observed [357]. AGO2 and HTT are also present in neural RNA transport granules and move along the microtubules. HTT localizes with microtubule proteins while transporting β -actin (ACTB) mRNA. Reduced HTT levels lead to reduction in the mRNA transport levels suggesting that

mutant HTT protein may interfere with the transport of RNA to neuronal extensions [358, 359].

In an intriguing study, CSF from HD patients was collected, and the miRNA composition within EVs was analyzed. The findings revealed that a subset of miRNAs, which target specific mRNAs, were differentially expressed in the prefrontal cortex of HD patients. Notably, these target mRNAs were enriched in those associated with SGs, including G3BP1. In HD mouse models and patients, the density of G3BP1 granules was found to be significantly increased in the brain. This study provided evidence that SG-related proteins, such as G3BP1, are present in EVs, highlighting a potential link between EVs and SG dynamics in HD [79].

The number of studies in RNA granules in context with HD is very limited and more studies to understand their importance in the pathology of the disease is the need of the hour.

3.5 sEVs in HD

In the context of HD, growing evidence suggests that sEVs transport and release disease-specific cargo, including *mHTT* RNA and protein. These sEVs can be secreted from cells affected by HD and then taken up by neighbouring cells, further contributing to the disease's spread within tissues. Several studies have demonstrated that mHTT protein can be secreted and subsequently internalized by other cells. For instance, Ren *et al.* (2009) showed both *in vivo* and *in vitro* uptake of polyglutamine peptides, which led to cytoplasmic aggregation in recipient cells [360]. Several other studies evidenced intercellular transmission of the mHTT protein [361-364]. In line, Cicchetti *et al.*, 2014 confirmed the propagation of the mHTT protein to the transplanted tissue in patients with HD, who underwent a striatal tissue transplantation [365]. While these studies confirm mHTT's intercellular propagation, their route of transmission was not identified. However, other studies have evidenced that *mHTT* RNA and protein can be transferred from one cell to another with the help of sEVs. An experiment showed that when medium from mHTT expressing HEK cells was added to SH-SY5Y cells, within 5 days of exposure, the mHTT was detectable in SH-SY5Y cells. Next, mHTT aggregates were detectable within 4 days upon co-culturing murine neuronal stem cells with sEVs. It was also shown that mHTT was detectable in mice that were injected with sEVs obtained from the fibroblasts of HD mice. They even showed HD phenotype [366]. Besides transmitting mHTT protein, sEVs also propagate *mHTT* RNA. sEVs containing *mHTT* RNA induce HD symptoms in mice [367-370]. The damage of mitochondrial and autophagic system is seen in patients with

manifest HD. The impairment of the autophagic process and damaged mitochondria accumulation leads to an increased section of sEVs [371]. Mitochondrial biomolecules including increased levels of mtDNA is found in HD sEVs [372, 373]. Interestingly, the cargo of healthy sEVs seems to have protective roles in HD. sEVs derived from human umbilical cord blood were injected in HD rats. The injection led to improved antioxidant activities, partially decreased neurodegeneration, enhanced motor and neuromuscular abilities and decreased gliosis [374]. Cortico-striatal stimulation and motor skill learn are known to reduce the neuropathology and attenuate cognitive functions. EVs are involved in training-mediated adaptation processes. To understand how motor skill training modulates EVs, mice with cognitive and motor deficits were trained and their striatal EVs were isolated. The mice showed alterations in their sEV population. The proteome of EVs resembled the deficiencies present in HD. Training led to restoration of the EV concentration and protein deficiencies related to neurodegeneration and metabolic pathways [375].

The potential of sEVs in diagnosis and therapy in HD has a wide scope and hence, investigations on the understanding of sEVs and their crosstalk is integral.

RATIONALE OF THE PROJECT

Rationale of the project

HD is a genetic neurodegenerative disorder with no cure. RNA granules like SGs and p-bodies are deregulated in HD. sEVs contribute to intercellular transmission of the HTT gene products leading to the progression of the disease. Moreover, sEVs carry the genetic and physiological cargo of its parent cell and could be exploited as biomarkers for tracking the progression of the disease. While on one hand, both RNA granules and sEVs can push neuronal cells towards degeneration, on the other hand, sEV's therapeutic and diagnostic capabilities are a topic that cannot be omitted.

While ongoing studies establish strong grounds for understanding the role of sEVs and RNA granules in HD, there are no studies that systematically assess the effect of mutant *HTT* on the shared content of sEVs and SGs. Interestingly, sEVs and RNA granules show a number of correspondences with each other: With respect to their biogenesis, their site of origin is the cytoplasm. They both are composed of different kinds of RNA and proteins. Loading of sEVs is promoted by RNA-binding proteins that are also present in SGs and p-bodies. A study of cerebrospinal fluid (CSF) from HD patients found that certain miRNAs in EVs targeted mRNAs that were differentially expressed in the prefrontal cortex. These mRNAs were notably enriched in stress granule components like G3BP1, suggesting a link between EVs and SG dynamics in HD. SGs, p-bodies and sEVs share proteins, 18.4% of P-body proteins, and 28.7% of SG proteins overlap with the proteome of sEVs. LLPS, the cause of RNA granule formation, also helps in sorting of biomolecules into sEVs. It was shown that in order to sort miRNAs into sEVs, condensation of YBX1 into p-bodies by the process of LLPS was integral [267, 376-380][79].

Therefore, in this study, we are investigating the content and crosstalk between RNA granules and sEVs upon the expression of *mHTT* gene. The disruption of RNA-protein interactions in these organelles in HD has led us to investigate whether these compartments share common content and how this content is influenced by *mHTT*. With this project, we aim to establish a foundation for diagnosing, treating, and monitoring the progression of HD by investigating the transcriptome and proteome of sEVs and RNA granules. Given the substantial biomolecular cargo within sEVs and RNA granules, our objectives are to 1) identify specific RNA or protein biomarkers for HD, 2) determine if silencing these biomarkers affects disease progression and 3) explore the crosstalk between sEVs and RNA granules in both normal and HD conditions. Based on the aforementioned knowledge and findings, isolation and characterization of

Rationale of the project

different kinds sEVs and RNA granules from an HEK293T cell line expressing mutant HTT with 83 CAG repeats under an Tet-off promoter was done the following questions were addressed:

- 1. Do the transcriptomic and proteomic content of sEVs overlap with RNA granules?**
- 2. Is there a difference between the proteomic and transcriptomic contents of sEVs and RNA granules upon expression of mHTT?**
- 3. Can we find a set of biomarker transcripts that are upregulated both in HD RNA granules and sEVs?**
- 4. Can we find differentially expressed proteins, which may play a role in HD?**

MATERIALS AND METHODS

MATERIALS

1. Instruments and Devices

Instruments and Devices	Company
Arctik ULTF 320 [®] -800C fridge	Arctik
Bandelin sonopuls sonicator	Bandelin
Cat RM 5K roller mixer	CAT (24VDC)
Eppendorf ThermoMixer [®] C	Eppendorf (5382000015)
FEI DualBeam Helios NanoLab 600 (FIB)	FEI
Fisherbrand Analytical measuring balance	Fischer scientific
Heracell™ 240i CO2 Incubator, 240L	Thermo Scientific (16416639)
Herasafe™ 2030i Biological Safety Cabinet	Thermo Scientific (15913130)
iBright FL1500 Imaging System	Invitrogen™ (A44241)
Inverted Microscope Primovert	Carl Zeiss (491206-0011-000)
Invitrogen™ Power Blotter System	Invitrogen™
LKexv 2600 MediLine Lab Refrigerator (40C)	Leibherr (9005382237458)
Micro 220 R centrifuge	Hettich Labs
Microwave	Exquisit (MW 802 G)
Mini Blot Mixer	VWR
Mini Gel Tank	Invitrogen™
NanoPhotometer [®] N50	Implen (N50)
Pioneer™ Precision measuring balance	Ohaus (PX323)
Q-Exactive HF mass spectrometer	Thermo Fisher Scientific
qTOWER ³ Series Real-Time PCR Thermal Cycler	Analytik Jena
Rotina 420 R	Hettich Labs
Shaking Water Bath, 18 L	VWR (10128-128)
SureCast™ Gel Handcast - Hardware and Reagents	Invitrogen™ (HC1000SR)
System VX-95 autoclave	System
Tisch-pH-Meter pH 50 ViLab Basic	ViLab, Dostmann
Ultimate 3000 RSLCnano LC system	Thermo Fisher Scientific
VIP Plus -150°C Cryogenic Freezer	PHcbi (MDF-C2156VANC-PA)
Vortex Mixers	VWR
Zeiss LSM 900 (Airyscan 2)	Zeiss
ZetaView [®]	Particle Metrix

2. Laboratory consumables

Laboratory consumables	Company
Acclaim PepMap RSLC column (15 cm × 75 μm, 2 μm, 100 Å)	Thermo Fisher Scientific
Cell scraper M	TPP (99003)
Cell culture flask, T-75, surface: Cell+, Filter cap	Sarstedt (83.3911.302)
cell culture chamber, 8 wells, on glass slide, removable frame	Sarstedt (94.6170.802)
Cell culture dish: 150 x 20 mm, surface: Cell+	Sarstedt (83.3903.300)
Disposal bag, 2 L: 300 x 200 mm	Sarstedt (86.1197)

Filter tips (0-200 µl)	Nerbeplus (06-662-5300)
Filter tips (100-1000 µl)	Nerbe plus (06-693-5300)
Filter tips, transparent, Biosphere® plus (1000 µl)	Sarstedt (70.3050.255)
Filtropur S 0,2 sterile filters	Sarstedt (83.1826.001)
Falcon tube, 50 ml, 114 x 28 mm, PP	Sarstedt (62.547.254)
Injekt® Solo Disposable Syringe (Luer) 10 ML	Braun (4606108V)
Multi-purpose beaker, 120 ml: 105 x 44 mm	Sarstedt (75.9922.420)
Nalgene® centrifuge tubes	Beckmann Coulter (T1043-10EA)
Pipette tip PP "classic" (0,1-20 µl)	Nerbe plus (07-112-0000)
Pipette tip PP "classic" (1-200 µl)	Nerbe plus (07-122-0073)
Pipette tip PP "classic" (100-1000 µl)	Nerbe plus (07-132-0095)
Protein LoBind Tubes	Eppendorf (0030108442)
Power Blotter Pre-cut Membranes and filters	Invitrogen (PB7320)
Screw tube, 15 ml, (LxØ): 120 x 17 mm, PP	Sarstedt (62.554.009)
Serological pipette (5 ml)	Sarstedt (86.1256.001)
Serological pipette (10 ml)	Sarstedt (86.1254.001)
Serological pipette (25 ml)	Sarstedt (86.1685.001)
serological pipette (50 ml)	Sarstedt (86.1253.001)
Sera-Mag SpeedBeads	GE Healthcare (45152105050250)
Sera-Mag SpeedBeads	GE Healthcare (65152105050250)
Slide-A-Lyzer™ MINI Dialysis Device, 2K MWCO, 0.1 MI	Thermo Fisher (69580)
SureCast™ Glass Plates	Invitrogen™ (HC1001)

3. Chemicals and reagents

Chemicals and Reagents	Company
Ammonium Persulfate (APS)	VWR (MG133-100G)
Bovine Serum Albumin (BSA)	Carl Roth (3854.2)
Bromphenol Blue sodium salt	Sigma Aldrich (B8026-25G)
β-Mercaptoethanol	VWR (0482-100ml)
Calcium chloride	Sigma (C1016-500G)
Chloroform 99,8%	Fischer Scientific (11352878)
cOmplete™ ULTRA Tablets, Protease Inhibitor Cocktail	Roche (05892970001)
Ethylenediaminetetraacetic acid (EDTA)	Sigma aldrich (106321-500G)
EGTA	Carl Roth (3054.1)
Ethanol absolute	VWR (20821.365)
Fluoroshield with DAPI histology mounting	Sigma (SIF6057-20ml)
Glacial Acetic acid	VWR (0714-500ml)
Glycine	VWR (M103-5KG)
Glycerin	Carl Roth (3783.1)
HPLC grade water	Carl Roth (A511.2)
Hygromycin B-Lösung	Carl Roth (CP12.2)
Lithium chloride	Sigma (L9650-100G)
L-Lysine	Sigma Aldrich (62840-100G-F)
Magnesium chloride	Sigma (M8266-1KG)
Milk powder	Carl Roth (T145.2)

Nonidet P40 Substitute	USB (19628)
Phenol crystalline	AppliChem Panreac (A1382.0250)
PhosSTOP™ (Phosphatase inhibitor tablets)	Roche (4906845001)
Pierce™ECL Western Blotting Substrate	Thermo Scientific™ (32109)
Potassium acetate	Sigma (32309-1KG)
Potassium chloride	Sigma (60130)
2-Propanol (Isopropanol)	Carl Roth (9866.1)
RiboLock RNase Inhibitor	Thermo Scientific™ (EO0381)
ROTI®Cell Trypsin/EDTA solution (10x)	Carl Roth (1Y19.1)
SDS Pellets	Carl Roth (CN30.3)
Sodium chloride	Carl Roth (3957.1)
Sodium hydroxide	Carl Roth (9356.1)
Spectra™ Multicolour Broad Range Protein Ladder	Thermo Fisher (PIER26634)
Sucrose	Sigma (S7903-1KG)
TEMED	Invitrogen™ (HC2006)
TRIS hydrochloride	Carl Roth (9090.2)
Triton X-100	Sigma (X100- 1L)
Trypan Blue	Carl Roth (CN76.1)
Tween 20	PanReac AppliChem (A4974.0100)

4. Kits

Kit	Company
mirVana™ miRNA Isolation Kit	Thermo Scientific™ (AM1561)
Pierce™ BCA Protein Assay Kit	Thermo Scientific™ (23225)
ViewRNA™ Cell Plus Assay Kit	Invitrogen™ (88-19000-99)
Monarch® Total RNA Miniprep Kit	NEB (T2010S)
TaqMan™ Reverse Transcription Reagents	Invitrogen™ (N8080234)

5. Antibodies

Antibody	Species	Dilution	Application	Company
Primary Antibodies:				
Anti-AIP/ Alix	Mouse	1:500	WB	BD Biosciences (611620)
Calnexin	Rabbit	1:1000	WB	Abcam (ab92573)
eIF4E	Rabbit	1:1000	WB	CST (2067S)
Flotillin	Rabbit	1:1000	WB	Abcam (ab133497)
FMRP	Rabbit	1:1000	WB	CST (4317S)
G3BP1	Mouse	1:100	WB	Santa Cruz (SC-365338)
Hsc70/Hsp70	Mouse	1:1000	WB	Enzo (ADI-SPA-820D)
MID1	Rabbit	1:1000	WB	Homemade
YB1	Rabbit	1:1000	WB/IS/FISH	Abcam (ab12148-100)
WDR1	Mouse	1:100	WB	Santa Cruz (sc-393159)
Phalloidin-FITC	-	1:1000	WB/IS	AAT Bioquest (23101)
Secondary antibodies:				
Alexa Flour 455	Mouse	1:1000	FISH/IS	ThermoFischer (A32723)
Alexa Flour 555	Rabbit	1:1000	FISH/IS	Abcam (ab150078)

Alexa Flour 647	Rabbit	1:1000	FISH/IS	Invitrogen (A-21244)
HRP-conjugated	Mouse	1:1000	WB	Santa Cruz (sc-2005)
HRP-conjugated	Rabbit	1:1000	WB	Santa Cruz (sc-2357)

6. Cell lines

Cell line	origin	Medium	provider
HEK Q83	Human	DMEM Low glucose medium 10% Tetracycline free FCS 1% 100mM Glutamine 150 µg/mL G418 120 µg/mL Hygromycin	Wanker Lab [381]
HELA	Human	DMEM Low glucose medium 10% Sterile filtered FCS 1% 100mM Glutamine	DSMZ (ACC 57)
HEK 293T	Human	DMEM Low glucose medium 10% Sterile filtered FCS 1% 100mM Glutamine	DSMZ (ACC 635)

7. Buffers, solutions and media

Buffer, solutions and media	Composition	Company
DMEM Low Glucose,W/O L-Glutamine		Capricorn Scientific (DMEM-LPXA)
Magic Mix (2X)	48% urea (w/v) 15mM Tris-HCL pH 7.5 8.7% glycerine (w/v) 1% SDS (w/v) 0,004% Bromophenol blue (w/v) 143mM Mercaptoethanol	Home-made
PEM Buffer	1 M PIPES 0,05 M EGTA 0,02 M MgCl ₂ , pH 7 The pH was adjusted using NaOH (5 M)	Home-made
Phosphate buffered saline (PBS)		Sigma (P4417-100TAB)
Power Blotter 1-Step™ Transfer Buffer (5X)		Invitrogen™ (15816172)
ROTI®Cell Glutamine solution		Carl Roth (9183.1)
RotiCell PBS/EDTA		Carl Roth (9152.1)
RNA granule lysis buffer	50 mM Tris pH 7.6 50 mM NaCl 5 mM MgCl ₂ 0.1% NP-40 (v/v) 1 mM β-mercaptoethanol, 1x EDTA-free protease inhibitor cocktail 0.4 U/mL RNase inhibitor	Home-made

RIPA Buffer	50mM TRIS HCL pH: 7,4 150mM NaCl 1% Triton X-100 (v/v) 0,5% sodium deoxycholate (w/v) 0,1% SDS (w/v) 1mM EDTA	Home-made
Sodium Arsenite Solution		Merck (1.06277.1000)
SureCast™ Acrylamide Solution		Invitrogen™ (HC2040)
SDS Buffer (1000 mL 10X solution)	Glycine (144 grams) Tris (30 grams) 20% SDS solution (w/v) (50 mL)	Home-made
Tetracycline free FCS		PAN-Biotech(P30-3602)

8. Primers

Transcript	Primer Sequence	provider
HSALNT0279541 (LHR1-LNC1610-1)	Forward Primer: CGTGAAGTCCGTGGAAGCCT Reverse Primer: CCCTTCACCATTTCCGACGG	ThermoFischer
Non-protein coding SNHG7:8	Forward Primer: AGCTTCGGGAAGCCTGGA Reverse Primer: TTGGAGGATTGACCCTGTTC	ThermoFischer
HSALNT0088996 (lnc-SLC30A5-6)	Forward Primer: AGTGAGAGGACTGTGGCAGG Reverse Primer: GGCTGTCCATCTGTCTCCA	ThermoFischer
HSALNT0398958 (lnc-DUXA-1)	Forward Primer: TACTGGGCTGAGCTGGCATG Reverse Primer: TTGGCCTGTAGTGTGGGGTG	ThermoFischer
non-coding RNA	Forward Primer: AGCCAGTCAGTGTAGCGCAT Reverse Primer: AGAGGGACAAGTGCGTTCA	ThermoFischer
SNHG12	Forward Primer: ACAGAGATCCCGCGTACTT Reverse Primer: GGCAATTCAGATCCCAGGGC	ThermoFischer
GAPDH	Forward Primer: ATGGAAATCCCATCACCATCTT Reverse Primer: CGCCCCACTTGATTTTGG	ThermoFischer
RLP22	Forward Primer: TGACATCCGAGGTGCCTTTC Reverse Primer: GTTAGCAACTACGCGCAACC	ThermoFischer

9. Probes

Full sequences of the oligo probes were not provided by the company due to the presence of confidential regions that bind to other molecules essential for the assay's function. However, specific parts of the oligos that bind to our targets were shared. There are two types of oligos used in the assay: Label oligos (ZZ oligos) (red), which are responsible for bridging the target transcript to the branched DNA (bDNA) and generating the signal, and Blocker oligos (green), which simply fill space and do not participate in the bridging or signal production.

For the LHRI_LNC1610_1 target (Accession ID MN298676, human), the probe set targets the region between 3976-4955, with 7 bDNA molecules involved. For SNHG7 (Accession ID NR_024542, human), the region targeted is 35-828, involving 15 bDNA molecules. Lastly, for URS000233D421/ Inc-DUXA1 (Accession ID GS12187, human), the probe set targets the region between 1085-2335, utilizing 20 bDNA molecules.

Probe	Sequence	Company
Inc-DUXA1 (Alexa Flour 647)	>GS12187 URS000233D421 cccaggctgatctcaaattcctggcctctggcaatcctcctcataggacttccaaatgctgggattata ggagtgagccactgacccggcctgtatacaattttaccatcaattcaaattacattaaaaaatttagt ataatgagagtaaagattaaatatacagacaaaccaggatatttaattagctatctcagtaatgat ttcaagaaggcaggatataacattggtaggttctattagattacacacataatggacaaactgagct gacagatacacaagaacgagatcagttgccaatgttttcttttagcacaactgagatttaaaa aactgacaatagttagtatacagaaaaactttaactttcatagataaaagagagaatacaatcagtg tagagatcaacaaaagatacctcaaactcctggcctcaagtgcctcttgcctcagcctccaaaatgt tgagattacaggcttgagccatcatgccagcctagatacctgatttcttttaattatgcttgaattcaa attcaaaatactaagtnnn nnnnnnnnaaattgaagattttttttgtaaataatgacaatacaatttcatagactttttatta gtagtatcatagggcagcttctgacaaataggaaaagtagatagggctgtccttagagtagtgcttg ggctgattacctaacttctctgacactcagcactgtcatcattacattgaaggggtccctacggctccta aagtgctcaagctctattaccacacattttgtcatttttaaatatcatagatattcaacctgaag tttactttactgcccacgtcatctcatatattctcatgagatgagttcatgaattctaagcagatc attaatgtatttttaaaaagatann nnn nnn ttaagaataacagtataccacttaataccaaaagcat ctctacagcattattcattatatacaatttttaaatcagccaaaatgcaaagctactattagtaatac attaaggtgtgaactatgaagaagtaaaatgagtaaggcaaaattctggatggcggctccttgaag gggaggatggaattggcaatctggcaggctcatgccggcatgctgattttgttctattata	Thermo Fischer (VPWCWJM)
SNHG7 (Alexa Flour 488)	> c NR_024542 Homo sapiens small nucleolar RNA host gene 7 (SNHG7), transcriptvariant 2, long non-coding RNA. [Homo sapiens] PRI 09-MAY- 2018 ctctgcgtgcccggaggctgcccgtggcgggtggccgcctgacttctctcccggccagttctcgagcg cctcaccgggctcgcctcgcagcctcgtctcgtgctgctgcgctgcgctgaggggactgggctgctggc ctccgggtgcgggtggggcaggctcgaacctggggcgtcctggcgcgagccgaggatggggg ccgggcccggaggagggcgcctggtgttcccttggtagagggcgctgcggcctgcgctggt tccagccaggaagcttcgggaagcctggacgtctcactggagatgacacgtgctggtgggtgttggc attctgttatttaacacgggaagggtgacttcgctgtgatggacttccagtgtgagcactggccag agtgaccaggctgaccagaccagccctgatccagatgcagaggccaggatgtgggcccagccctgtg ccaggaggctggctggaataaaggtaacagatagaggcctcaccctctgggacctggcactcagg gtgttgcagcctcagagcccactgccccagggccacagctgcatctcctgcccctgctgtcattacag ggatgggaggctggatgggggagcggctgcccctgctgggtgtgtgtgtattcctgccggccag gggcactgccaggaccgctccctttcatatcccattcttaagttctgctattgtggtattctgggtg gaaaaaagaaccgctggctgttttgaactgctggaacctaaagacctgaattttttcccccca aggggaaatctatggaaaacattatttttaaaatacaggatgaagtgaattaaagatttaaatgc acatttcttaaggataattttctgtgttggcaaaatttgagagtaaatggtcttgaatggaaaaaaa aaaaaaaaa	Thermo Fischer (VPU62YP)
Inc-LHR1 (Alexa Flour 546)	>MN298676 LHRI_LNC1610_1 agggagactcgaagtactctgaggctgttagagggtaaaatagagaccagtaaaattgtaataagc agtgcttgaattatttggttcggtgttttctattagactatggtgagctcaggtgattgatacctgatg cgagtaatacggatgtgttaggagtgaggactctaggggatttagcggggtatgctgttggggcca gtcctcctaattgggggnnn nnn nnn nnn	Thermo Fischer (VPTZ9ET)

10ng/mL of Doxycycline was added to keep the cells in a non-induced state. In order to maintain antibiotic pressure of the cloned cell line to avoid loss of the transfected gene, 150 µg/mL Hygromycin was added. The cells were then incubated at 37 ° C with 8% CO₂ in a humidified incubator. After 16-24 hours, the medium was changed so that residual DMSO and dead cells are removed.

1.2 Passaging of cells

Once the cells were 90-95% confluent, the medium was discarded, and the cells were washed with 2 mL ROTI®Cell PBS. 1 mL trypsin-EDTA solution (3 parts of ROTI®Cell Trypsin/EDTA solution (10x) was mixed in 7 parts ROTI®Cell PBS) was added to detach the cells from bottom of the flask and the flask was incubated at 37 ° C for 5 minutes to activate the enzyme. After ensuring the detachment of cells by the action of the enzyme, the reaction was stopped by adding 5-6 mL of fresh medium. The cells were then collected in a falcon tube and centrifuged at 500 X g for 5 minutes at room temperature. The supernatant was removed, and the pellet was resuspended in an appropriate amount of medium based on the size of the pellet.

1.3 Seeding the cells

10 µL of cells were taken and resuspended with an appropriate amount of 0.5% w/v Trypan blue dye to count the number of viable cells using Neubauer's chamber with a light microscope. Cells were then seeded according to the size of the flask/culture dish and growth rate (1.0-1.5 x 10⁵ cells per 9.6 cm²).

1.4 Treatment of cell line

In the HEK Q83 cell line, which uses an inducible Tet-off system to express FLAG-tagged *HTT* exon 1 containing 83 CAG repeats, the expression of *HTT* exon 1 is triggered by removing doxycycline. This is achieved by washing the cell pellet twice with 5 mL of cell culture-grade PBS. Following the washes, the cells were seeded and incubated for 72 hours to allow *HTT* exon 1 expression. After this incubation period, the cells are exposed to 0.5 mM arsenite for 55 minutes at 37°C in a humidified incubator with 8% CO₂ to induce cellular stress before harvesting.

1.5 Isolation of sEVs and total cytoplasmic RNA granules from HEK Q83 cell line

To isolate sEVs and RNA granules, approximately 3×10^6 cells were seeded in 147 cm² plates (eight plates each for control (non-stressed, non-induced, with doxycycline) and HD (stressed, induced for *HTT* expression, without doxycycline) samples) in 18 mL EV-depleted medium and incubated at 37 °C with 8% CO₂ in a humidified incubator for 72 hours. To prepare EV depleted medium, Tetracycline-free FCS was centrifuged at 100,000 X g for 16 hours at 4 °C and filtered with 0.22-micron filters. Then, DMEM low glucose medium was supplemented with 10% of this EV-depleted FCS instead of the normal Tetracycline-free FCS, 1 mM Glutamine and 120 µg/mL G418. After 72 hours, the medium was collected from both the sample sets and fresh 18 mL medium with 0.5 mM Arsenite was added to the stressed samples. In control samples, normal medium with Doxycycline was added and both were incubated at 37 °C with 8% CO₂ in a humidified incubator for 55 minutes. After 55 minutes, the medium was removed, the cells were washed with 3 mL PBS and harvested in 2-3 mL PBS by using a cell scraper. The cells were then centrifuged at 500 X g for 5 minutes. The supernatant was discarded, and the pellet was stored in -80 °C until isolation of RNA granules was performed.

1.5.1 Isolation of sEVs and RNA granules

sEVs were isolated from the culture medium by using the classical differential ultracentrifugation method. The protocol was a slightly modified version of the isolation technique described in Raposo *et al.*, 1996 [387]. Briefly, the collected culture medium was centrifuged at 300 X g for 10 minutes at 4 °C to remove cells and cell debris. The supernatant was collected and centrifuged at 2000 X g for 20 minutes at 4 °C to pellet high molecular weight proteins. The supernatant was spun at 16,000 X g for 30 minutes to remove larger vesicles like apoptotic bodies. After this, the supernatant was ultracentrifuged at 100,000 X g for 1 hour 10 minutes at 4 °C to obtain the sEV pellet. The supernatant was discarded, and the pellets from the 8 plates were resuspended in 2-3 mL PBS and pooled in one tube. These samples were then ultracentrifuged again at 100,000 X g for 1 hour 10 minutes at 4 °C to obtain the sEV pellet. Finally, the supernatant was removed, the sEV pellet was resuspended in 300 µL PBS and stored at -80 °C until further use.

Cytoplasmic RNA granules were isolated from the cells using a slightly modified version of the isolation procedure described by Namkoong *et al.*, 2018 [388]. The frozen pellets were thawed

on ice and resuspended in 5 mL ice cold RNA granule lysis buffer (50 mM Tris pH 7.6, 50 mM NaCl, 5 mM MgCl₂, 0.1% NP-40, 1 mM β-mercaptoethanol, 1x EDTA-free protease inhibitor cocktail, 0.4 U/mL RNase inhibitor). The cells were then lysed using a Dounce homogenizer (30 strokes per mL). After that, the cells were centrifuged at 2000 X g for 2 minutes to remove cell debris, and the supernatant was collected. A 500 μL of this supernatant was kept as a control sample for the Western blot analysis (total protein lysates). The rest of the supernatant was centrifuged at 10,000 X g for 10 minutes to separate the soluble fraction of proteins from the insoluble RNA granules/pellet fraction. The obtained fragment was resuspended in 350 μL HPLC grade water and stored at -20 °C until further use.

2. Validation and characterization of the isolated sEVs and cytoplasmic RNA granules

The isolated cytoplasmic RNA granules were validated by detecting various RNA granule markers via western blot analysis. Validation of the sEVs was done according to the minimal information for studies of extracellular vesicles (MISEV) guidelines. MISEV is an initiative by the International Society for Extracellular Vesicles (ISEV) to standardize, promote and advance extracellular sciences at a global level. These guidelines established a standard experimental and reporting requirements with respect to exosomal sciences. According to these guidelines, the following validations are mandatory:

- 1) A minimum of three protein markers of EVs must be visualized. These proteins should include a cytosolic protein and a transmembrane/lipid-bound protein. At least one negative marker must be shown.
- 2) Characterization of EVs must be done by two different techniques. Like for example, electron microscopy (both close-up and wide-field images) and single particle analysis (not microscope based) [389].

sEVs were characterized by detecting various positive and negative markers by western blot analysis, the vesicular size was determined using nanoparticle tracking analysis (NTA) and scanning electron microscopy (SEM).

2.1 Western blot

To visualize RNA granule and exosome markers, a western blot analysis was done.

2.1.1 Sample preparation

sEVs: The sEV samples were thawed on ice and diluted with equal volumes of RIPA buffer. Protease inhibitors were added to inactivate and block proteolytic enzymes that are released from the cells upon their lysis, which would otherwise degrade our protein of interest. The samples were vortexed and incubated on ice for 30 minutes with frequent short vortexes in between. After incubation, the samples were centrifuged at 10,000 RPM for 10 minutes at 40 C and the supernatant was obtained. Sonification was done at 50% intensity for 15-17 seconds and the sample was kept on ice until the foam settled down. sonication was used to disrupt sEV membranes, allowing for the effective release and solubilization of proteins for accurate detection and quantification during western blotting.

RNA Granules: The RNA granule samples were thawed on ice and then treated with Benzonase (50 U per 100 μ L of cell lysate). The samples were then incubated for 30 minutes on ice before proceeding further. Benzonase endonuclease breaks down all DNA and RNA in a sample, which helps improve the clarity and accuracy of western blots by preventing band shifts. When nucleic acids are left intact, they can form complexes with proteins, increasing the apparent molecular weight of the proteins. This leads to the proteins migrating to incorrect positions during gel electrophoresis, which complicates the analysis and interpretation of the results. By degrading the nucleic acids, Benzonase ensures proteins migrate correctly, resulting in more reliable and high-quality blots.

2.1.2 Sodium dodecyl sulphate-polyacrylamide gel electrophoresis (SDS-PAGE) and western blot

SDS-PAGE is a method used to separate proteins based on their molecular weight. In this process, proteins are treated with the anionic detergent SDS both before and during electrophoresis. SDS binds to positively charged and hydrophobic regions of proteins, giving them a uniform negative charge. Additionally, SDS denatures the proteins, causing the polypeptide chains to unfold into extended conformations. To further assist in this, samples are treated with β -mercaptoethanol, which reduces disulfide bonds, fully linearizing the proteins. To enhance protein denaturation and improve separation, urea is added. Other components include glycerol, which increases the sample density, and bromophenol blue, a dye that helps track sample migration during electrophoresis. This mixture, referred to as the "magic mix," was prepared in 2X concentration and mixed with 20 μ L of protein samples. The

samples were then boiled for 5-7 minutes at 95°C to ensure complete denaturation before electrophoresis. For preparing discontinuous gels, the casting plates were assembled with spacers into a casting frame and the gels were poured according to the **table 1**. The polymerized gels were then assembled into an electrophoretic unit filled with SDS buffer. The the samples were loaded along with a molecular marker (10- 270 kDa) (Spectra™ Multicolour Broad Range Protein Ladder). The gel was run initially at 80-90 V until the marker separation is visible. This low voltage gives more time for protein to separate and therefore better resolution. Then the voltage was increased to 110 V until the blue dye front was visible at the end of the gel. After the gel run was completed, the gels were carefully removed and incubated in transfer buffer for 10 minutes before proceeding to western blot.

For western blotting, a semi-dry blotting system (Invitrogen Power Blotter–Semi-dry Transfer System) was used. Briefly, pre-cut nitrocellulose membranes and filter papers (Invitrogen Nitrocellulose/Filterpaper Sandwich (0.2 µm pore size, 8.3 x 7.3 cm)) were soaked in 1-Step Transfer Buffer (Invitrogen Power Blotter 1-Step™ Transfer Buffer (5X)) for 15 minutes. The blotting stack, including the gel, was assembled as per the protocol shown in Figure 5. Based on the molecular weight range of interest—Low MW (<25 kDa), Mixed-range MW (25-150 kDa), or High MW (>150 kDa)—a pre-programmed method was selected, and blotting was carried out accordingly (**Figure 5**).

Following the transfer, the membrane was blocked in 5% bovine serum albumin (BSA) in TBS-T for 1 hour. The membranes were then incubated overnight at 4°C with primary antibodies (**Table 2**). The next day, the membranes were washed three times with TBS-T for 5 minutes each and then incubated with their respective secondary antibodies for 2 hours at room temperature. After incubation, the antibodies were removed, and the blots were washed three times with TBS-T before visualization using the iBright Imaging System (Invitrogen iBright FL1500 Imaging System).

Table 1. Recipe for SDS-PAGE gel. Quantities of reagents for preparing an SDS-PAGE gel, with component ratios based on the gel's desired properties.

Resolving gel solution	Gel %				Stacking gel solution	Gel %
	8%	10%	12%	16%		4%
Acrylamide solution (40%)	1.6 mL	2.0 mL	2.4 mL	3.3 mL	Acrylamide solution (40%)	300 mL
Resolving buffer	2.0 mL	2.0 mL	2.0 mL	2.0 mL	Stacking buffer	750 mL

Distilled water	4.3 mL	3.9 mL	3.5 mL	2.7 mL	Distilled water	1.92 mL
10% APS	80 µL	80 µL	80 µL	80 µL	10% APS	30 µL
TEMED	8 µL	8 µL	8 µL	8 µL	TEMED	3 µL

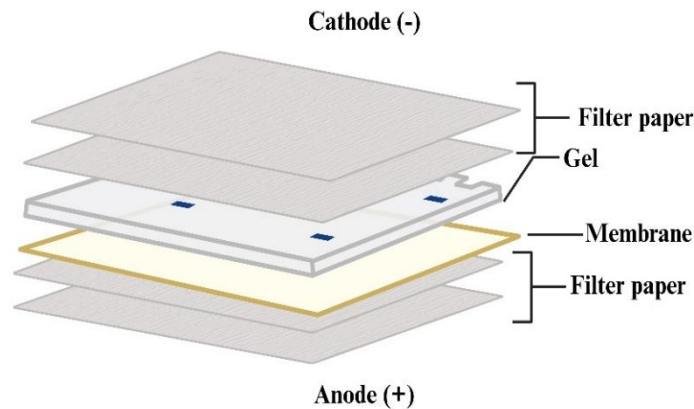


Figure 5. Preparation of blotting stack for Western blotting. The Invitrogen™ Nitrocellulose/Filter paper Sandwich (0.2 µm pore size, 8.3 x 7.3 cm) was used for western blotting. In the assembly, the nitrocellulose membrane was placed on the anode side, followed by the SDS-PAGE gel and filter papers. This setup ensures effective protein transfer, as negatively charged, SDS-coated proteins migrate towards the positively charged anode during electrophoresis. SDS coats proteins uniformly with a negative charge, denaturing them and unfolding their polypeptide chains. As an electric current is applied, these negatively charged proteins travel from the gel (on the cathode side) towards the nitrocellulose membrane (on the anode side), where they are captured. This method ensures that proteins are efficiently transferred from the gel to the membrane, providing a solid platform for accurate detection and analysis of specific proteins in western blotting (Created with biorender).

Table 2. Markers for sEVs and RNA granules. A list of marker proteins is essential for validating the presence of sEVs and RNA granules in samples. These marker proteins are critical for confirming the identity and purity of the sEVs and RNA granules, ensuring the accuracy and reliability of experimental results.

Marker Type	Antibody	Mol. wt	Company	Dilution
Positive markers for sEVs	HSP70	70 kDa	Enzo	1:1000
	AIP1/ALIX	105 kDa	BD Biosciences	1:500
	Flotillin	48 kDa	Abcam	1:1000
Negative markers for sEVs	Calnexin	90 kDa	Abcam	1:1000
Positive markers for RNA granules	G3BP1	68 kDa	Santa Cruz	1:100
	EIF4E	25 kDa	Santa Cruz	1:1000
	FMRP	80 kDa	CST	1:1000
	YB1	36 kDa	Abcam	1:1000
Negative markers for RNA granules	Calnexin	90 kDa	Abcam	1:1000

	Lamin A/C	69 kDa	Santa Cruz	1:200
--	-----------	--------	------------	-------

2.1.3 Nanoparticle tracking analysis (NTA)

Nanoparticle tracking analysis (NTA) is used to measure the nanoparticle size distribution in samples. It works on the properties of Brownian motion and light scattering. When particles are loaded in a liquid suspension into the sample chamber illuminated by a specially shaped laser beam, the particles that encounter the beam scatter the laser light, which is captured by the microscope and viewed with a camera. The NTA software analysis measures many particles both individually and simultaneously and uses the Stokes Einstein equation for calculating their hydrodynamic diameters. NTA was done using the ZetaView[®] particle analyser (AG Vorberg, DZNE Bonn). Briefly, the sEVs were diluted in the ratio 1:100,000 in sterile PBS. The sample chamber was flooded with PBS until no particles were seen. The particle drift was checked, and the 1 mL sample was loaded into the chamber with a syringe. The samples were then measured at 11 positions and the size distribution was obtained.

2.1.4 Scanning electron microscopy (SEM)

The scanning electron microscopy (SEM) is a technique used to analyse the microstructure morphology of particles. It uses a focused electron beam to scan across the sample systematically, producing electron signals that are then converted into visual signals on the cathode ray tube (CRT).

For size characterization of the sEVs, SEM (FEI DualBeam Helios NanoLab 600 (FIB)) was used. The sEVs (see section xxx) were dialysed to remove salts (Slide-A-Lyzer[™] MINI Dialysis Device, 2K MWCO, 0.1 mL). Briefly, the sEVs were thawed to room temperature and the membranes of the dialysis device were hydrated for 2 minutes. The samples were loaded in the dialysis device and then incubated in 500 mL sterile water for 2 hours at room temperature. The silicon chips were first sonicated for 5 minutes each in acetone, ethanol, and distilled water, then rinsed with water and blow-dried. After preparation, 0.5 µl of the 1:1000 diluted samples were applied to the cleaned and dried chips. The samples were then allowed to air-dry under a sterile hood for 10-15 minutes.

To make surface conductive, a coating of 2–5 nm gold was applied by sputtering (SPI-Module Sputtering, Argon as gas for plasma) before imaging by scanning electron microscope. Samples

on silicon chips were mounted on a SEM stage by carbon paste and both close-up and wide-field images were taken at 10 KV.

3. RNA isolation

For the isolation of total RNA from sEVs and cytoplasmic RNA granule cores, mirVana™ miRNA Isolation Kit (Invitrogen) was used following the manufacturer's instructions.

4. RNA sequencing

4.1 RNA Concentration and Purity Measurement

For the isolation of total RNA from sEVs and cytoplasmic RNA granule cores, mirVana™ miRNA Isolation Kit (Invitrogen) was used. The protocol used was previously described in section 3. The RNA concentrations in the samples were determined using the Qubit™ RNA Assay Kit (Q32855). The procedure involved diluting the Qubit RNA reagent 1:200 in Qubit RNA buffer, with 200 µL of this working solution prepared for each sample and standard. For the standards, 190 µL of the working solution was combined with 10 µL of the corresponding RNA standard in two separate tubes (Standard 1 and Standard 2). For the samples, 199 µL of the working solution was mixed with 1 µL of each RNA sample in individual assay tubes. After gently mixing, all tubes were incubated for 2 minutes at room temperature. The RNA concentrations were then measured using the Qubit Fluorometer, following the manufacturer's guidelines, ensuring accurate quantification.

4.2 RNA sequencing and quality control

For both sEVs and RNA granules, five biological replicates were performed for each condition: HD and control, resulting in a total of 20 RNA sequencing samples. NGS analyses were carried out at the Competence Centre for Genomic Analysis (Kiel). The Illumina Stranded Total RNA Library Preparation Kit was used to prepare the samples for whole-transcriptome sequencing. Sequencing was conducted on the Illumina NovaSeq platform with S1 flow cells, using 2x100 bp paired end reads. One HD sEV sample yielded only a few thousand reads and was excluded from further analysis. On average, sEV samples generated 14.4 million reads, while RNA granule samples produced 45.3 million reads.

FastQC (version 0.12.1) was used to assess read quality. Quality trimming and filtering were done in two steps: first, Trimmomatic removed adapter sequences and low-quality bases

(below 20) from both ends of the reads [390, 391]. Then, cutadapt [392] was used to remove the first three bases, correct high-quality but incorrect "G" calls at the 3' end of the reads (using the option `--nextseq-trim=20`), trim poly-A and poly-T tails, and clip sequences with 10 or more consecutive "G"s from read ends. Read pairs with one read shorter than 10 bp were discarded. On average, 85.8% of the sEV reads and 99.3% of the RNA granule reads passed quality filtering. Unpaired reads after filtering were discarded.

4.3 Transcript mapping quantification

For read alignment and quantification, Salmon (version 1.10.2) was used in mapping-based mode, employing the pseudoalignment strategy. The reference database was created by non-redundantly combining GENCODE transcript sequences (Release 44, GRCh38.p14) with RNACentral sequences (Release 22) annotated as "Homo sapiens," resulting in a total of 921,552 unique sequences. The index was built with a k-mer length of 13 (option `"-k 13"`), using the entire genome as a decoy sequence. Mapping and quantification of sample reads were performed with the library type set to IU and the options `"--numBootstraps 100 --seqBias --gcBias."` The average mapping rate across all samples was 72.3%.

The Salmon transcript outputs were processed in R using tximport (version 1.26.1) and aggregated to the gene level. However, non-coding RNA transcripts from the RNACentral database were incorrectly classified as 'genes' in downstream analysis. As a result, any reference to 'genes' also includes ncRNAs. To identify condition-specific genes, only those consistently detected within at least one of the four conditions (sEVs/RNA granules, induced (HD), and non-induced (control)) were considered. These "consistent genes" needed to have an abundance of ≥ 10 counts in all samples for the respective condition, allowing for one mismatch.

To compare our cell line results with patient data, we obtained raw sequencing data from a study focused on plasma extracellular vesicles[393]. This dataset included 59 samples across three patient groups: 21 healthy controls, 19 pre-HD individuals (without clinical signs), and 19 early-HD patients (with early clinical signs). The sequencing data was processed similarly to our samples, except trimming ten "T"s from the 5' end of reverse reads instead of three base pairs and clipping ten "A"s and subsequent sequences from the read ends. On average, 11.2 million reads were available per sample, with 99.9% passing quality control, and the average mapping rate was 9.3%. All data analysis was performed in R (versions 4.2.2 and 4.1.2).

4.4 Differential gene expression analysis

We conducted two separate analyses to assess the differences in gene content between sEV and RNA granule samples under control and HD conditions. The first analysis focused on the presence or absence of genes in each condition. We identified genes consistently detected in HD samples (i.e., with an abundance of ≥ 10 counts in all HD samples, allowing for one exception) but absent in control samples (i.e., zero counts in all control samples), and vice versa, for both sEV and RNA granule samples. This method highlights the genes that most clearly distinguish HD from control conditions, making them strong candidates for marker genes.

In the second analysis, gene abundance was also considered by performing a differential gene expression analysis using DESeq2 [394] to identify changes between control and HD conditions in sEV and RNA granule samples. All genes with an abundance of ≥ 10 counts in at least one sample were included in the analysis. An adjusted p-value of 0.05 was used, and log-fold changes were moderated for visualization using the adaptive shrinkage estimator ashR [395]. The results from both analyses were then combined into a unified list of marker genes specific to the conditions.

4.5 cDNA synthesis and Quantitative Real Time PCR

Reverse transcription is the process used to convert total RNA into complementary DNA (cDNA). In this procedure, both oligo(dT) primers and random hexamers were employed to ensure comprehensive coverage of RNA species. Total RNA was isolated using the NEB Monarch kit (New England Biolabs). cDNA synthesis was carried out with the TaqMan reverse transcription reagents kit (Applied Biosystems), following the manufacturer's instructions. The detailed reaction setup is provided in Table 10. All steps were carried out on ice to preserve RNA integrity. The reaction mixture was then incubated in a thermocycler with the following conditions: 25°C for 10 minutes, 48°C for 60 minutes, and 95°C for 5 minutes to complete the reverse transcription process.

Quantitative real-time PCR (qRT-PCR) was then performed using the SYBRGreen PCR master mix (qPCR BIO SyGreen Mix, Nippon) (**Table 3**). The following thermal cycles were used to amplify the gene of interest: 95 °C for 3 min, 95 °C for 15 sec, 60 °C for 1 min, 60 °C for 15 sec and 95 °C for 15 sec. Housekeeping genes GAPDH and RLP22 were used as an internal control

for data normalization, no template control (NTC) was taken as the negative control and total cell RNA isolate was taken as the positive control. qRT-PCR is a highly sensitive method that allows for the quantification of specific DNA sequences by monitoring the amplification process in real-time. SYBRGreen dye binds to double-stranded DNA, and as amplification proceeds, the fluorescence increases, correlating with the amount of target DNA present. Each sample was analyzed in triplicate to ensure the precision and reliability of the results.

Table 3. Components for the cDNA synthesis reaction (left) and qRT-PCR reaction (right). For the cDNA synthesis, the reaction mixture includes primers (such as oligo(dT) and random hexamers), reverse transcription buffer, dNTPs, reverse transcriptase enzyme, and RNA template. On the right, the qRT-PCR setup consists of the target cDNA, SYBRGreen PCR master mix, forward and reverse primers, and nuclease-free water. Both reactions are crucial steps: cDNA synthesis converts RNA into a DNA template, while qRT-PCR quantifies gene expression by amplifying the cDNA in real-time, using fluorescence to monitor the reaction progress.

Constituents	Volume	Constituents	Volume
RNA	1 µg	SYBR green master mix	7.5 µL
10X RT-PCR buffer	5 µL	Primer mix (M)	0.5 µL
DNTP mix	10 µL	Nuclease free water	2.5 µL
Random hexamers	2.5 µL	cDNA	4.5 µL
MgCl ₂	2.5 µL		
RNase inhibitor	2.5 µL		
RT (MultiScribe)	2.5 µL		
Nuclease free water	Make up volume:50 µL		

4.6 RNA-fluorescence in situ hybridization (FISH)

RNA-FISH is a powerful technique to visualize and study the localization of RNA targets in fixed cells. RNA-FISH was done using the ViewRNA™ Cell Plus Assay Kit (Invitrogen). This kit is specifically optimized to co-stain RNA by FISH and proteins by immunofluorescence. The assay was done according to the manufacturer’s protocol. Briefly, 10,000 cells were seeded in a poly lysine coated 8 chamber slides. The cells were then incubated for 72 hours at 37 °C and 8% CO₂. After the incubation, the chambers meant for studying the stressed conditions were treated with 0.5 mM arsenite solution for 55 minutes. After 55 minutes, the medium was removed, and the cells were fixed and permeabilized using the Fixation/Permeabilization solution for 30 minutes at RT. Next, the cells were washed 3 times with PBS+ RNase inhibitor solution and blocked with Blocking/Antibody Diluent with RNase Inhibitor for 20 minutes at RT. The solution was removed, primary antibody was added and incubated for 1 hour at RT.

Further, the cells were washed 3 times with PBS+ RNase inhibitor solution, fluorophore-conjugated secondary antibody was added for 1 hour at RT and the cells were washed 3 times in PBS with RNase Inhibitor after the incubation. Then fixation solution was used for 1 hour at RT. After that, the cells were again washed 3 times with PBS+ RNase inhibitor solution and the cells were hybridised with target probes for 2 hours at 40°C. Finally, the cells were washed five times with wash buffer and stored in wash buffer overnight. Next day, the Pre-Amplifier was hybridized for 1 hour at 40°C, washed with wash buffer 5 times, the Amplifier was hybridized for 1 hour at 40°C, washed with wash buffer 5 times, the Label Probe was hybridised for 1 hour at 40°C and washed with wash buffer 5 times. The final wash was done with PBS and the mount and coverslip was done using Fluoromount-G with DAPI. The edge of the cover glass was sealed with clear nail polish. The slides were protected from light and dried for 1-2 hours before visualisation.

5. Mass spectroscopic analysis

5.1 Sample preparation for mass spectrometry

Mass spectroscopic analyses were conducted at the Luxembourg institute of health, Luxembourg. The samples were prepared according to the SP3 protocol [396]. Briefly, the samples were incubated with a 1:1 mix of Sera-Mag SpeedBeads (GE Healthcare (45152105050250)) and Sera-Mag SpeedBeads, (GE Healthcare (65152105050250)) The absorbed proteins were washed with decreasing concentrations of Ethanol and finally digested with sequencing grade trypsin (Promega) over night. Next day, the peptide was released from the beads with 0.1% formic acid and prepared for mass spectrometric analysis.

5.2 Mass spectrometry

LC-MS/MS was performed using an Ultimate 3000 RSLCnano (Thermo Fisher Scientific) LC system equipped with an Acclaim PepMap RSLC column (15 cm × 75 µm, C18, 2 µm, 100 Å, Thermo Fisher Scientific). Peptides were eluted at a flow rate of 300nL/min in a linear gradient of 2-35% solvent B over 70 min (solvent A: 0.1% formic acid; B: 0.1% formic acid in acetonitrile (ACN)), followed by a 5 min washing step (90% solvent B) and a 10 min equilibration step (2% solvent B). Mass spectrometry was performed on a Q-Exactive HF mass spectrometer (Thermo Fisher Scientific) equipped with a nano-electrospray source and using uncoated SilicaTips (12cm, 360µm o.d., 20µm i.d., 10µm tip i.d.) for ionization, applying a 1500 V liquid junction

voltage at 250°C capillary temperature. MS/MS analysis were performed in data dependent acquisition (DDA) mode, and the 12 most intense parent ions were fragmented with a resolving power of 17500 (at 200m/z). Automatic gain control (AGC), maximum fill time and dynamic exclusion were set to 1e6, 60 ms and 30 ms, respectively.

5.3 Data analysis for mass spectrometry

Protein quantification was performed with MaxQuant (version 2.2.0.0) [397-399]. using the following parameters: carbamidomethyl cysteine as fixed modification, methionine oxidation and N-acetylation as variable modifications, digestion mode trypsin specific with maximum 2 missed cleavages, and an initial mass tolerance of 4.5 ppm for precursor ions and 0.5 Da for-fragment ions. The abundance of assembled proteins was determined using label-free quantification (standard MaxQuant parameters) and match between run option was selected. Protein identification was performed searching against the Uniprot reference proteome (Uniprot ID 9606, downloaded on 15 April 2022). Further data analysis and visualization were performed in R (version 4.2)

5.4 Bioinformatic analysis of the mass spectroscopic data

The proteins identified upon the pull down were grouped into the following categories for further analysis.

- 1) Proteins present in control sEVs.
- 2) Proteins present in HD sEVs.
- 3) Proteins present control RNA granules.
- 4) Proteins present in HD RNA granules.

The proteins in each category involved proteins that were only present in control/HD sEVs /RNA granules and proteins that were overrepresented in the control than in HD and vice versa in RNA granules/ sEVs. This data was also compared with the list of proteins that binds to *mHTT*-RNA published by Schilling et.al., 2019 [400]. The overlaps and the distinctions were analysed, and further analysis was done.

5.4.1 KEGG mapper analysis

The Kyoto Encyclopedia of Genes and Genomes (KEGG) is a database collection that includes information on genomes, biological pathways, diseases, drugs, and chemical substances. It is

widely used to analyze gene functions and link genomic data with functional information. The database contains experimental data from published research, focusing on cellular and organism-level functions derived from large-scale molecular datasets, particularly gene sets from complete genomes [401].

The KEGG pathway represents networks of metabolic processes, signaling pathways, and other molecular interactions or reactions. It organizes biological functions into a set of interconnected pathways, allowing for the visualization of how molecules interact within a system to perform specific biological processes.

The KEGG module is a functional unit within these pathways, representing specific molecular complexes, reactions, or sub-pathways. KEGG modules can be reused across multiple pathways, demonstrating their flexibility and functional importance in various biological contexts.

The BRITE hierarchy is another feature of KEGG that captures the functional relationships between different biological entities, known as KEGG objects. These objects, stored as database entries, range from molecular components (e.g., genes, proteins, small molecules) to higher-level biological structures (e.g., pathways, diseases). The BRITE hierarchy organizes these entities into a structured framework, showing how they relate to one another across different biological levels.

The KEGG mapper tool provides access to these databases for mapping analyses. Initially, separate tools were used for different databases, but in 2019, KEGG introduced a new version that integrated these databases into three main tools: "Reconstruct Pathway," "Search Pathway," and "Search & Colour Pathway" [402].

In this study, the "Search Pathway" tool, set to human-specific mode and aliases were included. These settings were used to analyse protein sets from control and HD sEVs and RNA granules. Common proteins between HD RNA granules and sEVs were analysed separately. Finally, proteins that bind to mutant *HTT*-RNA, HD sEVs, and RNA granules were also analysed.

5.4.2 Enrichment analysis

Gene set enrichment analysis (GSEA) / functional enrichment analysis / pathway enrichment analysis is an analytical method to interpret gene expression data. This method provides a platform to recognize and understand gene sets that share same biological function, location

or regulation. The gene sets are defined based on *priori* gene sets (a *priori* gene set is a preselected group of genes chosen based on existing knowledge, such as known pathways or biological roles, before performing an analysis. These sets help determine if specific genes in a dataset are significantly associated with particular biological functions or conditions like diseases.) that have been grouped together based on previously published data that defines their involvement in biochemical pathways, location or co-expression. It is a technique for identifying groups of objects (e.g., pathways) that are overrepresented statistically in another group (e.g., genes that are significantly unregulated in an experiment). For example, enrichment analysis helps us know whether a gene set has more genes regulated by a particular transcription regulator than one would assume to be have occurred by chance [403]. HumanCyc.org was used to run the enrichment analysis [403]. This online tool computes enrichment by implementing the Fischer exact test by using hypergeometric distribution. The reference gene set used for the analysis depends upon the enrichment options selected from the dropdown dialog box. GO term enrichments were used for the study (genes enriched for Gene ontology aspects; Biological process, cellular component and molecular function). For this, the reference gene set would be the gene sets that have products with the given GO terms.

For the enrichment analysis, the cut-off p-value was set to 0.1. the Benjamini- Hochberg correction that controls the “False Discovery Rate” was selected and the analysis was done.

5.4.3 STRING

STRING is a web resource that has information on protein-protein interactions from various sources like literature, experimental data, and computer predictions. It derives information from five important sources: known databases, co- expression studies, lab experiments, genome context predictions and automated text mining. The STRING database currently has over 67,592,464 proteins from 14,094 organisms [404].

STRING V12.0 was used for performing string analysis. On the search mode, multiple protein option was selected, and the query proteins were uploaded. It included the list of proteins found in WT and HD sEVs and RNA granules, the list of proteins that were common between them and the list of proteins that were common between HD sEVs and proteins that bind to

mutant *HTT*-RNA. The analysis was done on the *Homo sapiens* mode and the interaction score of 0.9 was chosen at highest confidence rate.

5.4.4 Statistical Tests in Data Analysis

Statistical tests are essential for validating experimental findings and quantifying relationships between variables. In this thesis, various statistical approaches were used to analyze gene expression differences, protein abundance, colocalization patterns, and other key parameters. Below is an overview of the statistical tests employed and their applications.

- **Descriptive Statistics**

Before performing inferential tests, the data was summarized using:

1. **Mean and Median:** To determine central tendencies in RNA expression and protein levels.
2. **Standard Deviation (SD) and Standard Error of the Mean (SEM):** To measure data dispersion and reliability of estimates.

- **Normality Testing**

To determine whether data followed a normal distribution, the Shapiro-Wilk test was applied to gene expression values and protein abundance levels. This step helped in deciding whether to use parametric or non-parametric tests.

- **Differential Gene Expression Analysis**

1. **DESeq2 Analysis:** Used for RNA sequencing data, employing a negative binomial regression model to identify differentially expressed genes (DEGs) between control and HD samples. Log-fold changes (logFC) were adjusted using an adaptive shrinkage estimator to improve interpretability.
2. **False Discovery Rate (FDR) Correction:** Multiple hypothesis testing was controlled using the Benjamini-Hochberg FDR correction, ensuring that significant DEGs were not false positives.

- **Comparative Analysis of Gene Presence and Absence**

A binary classification approach was used to determine whether certain genes were consistently present in control or HD conditions. Genes were considered condition-specific if

they had an abundance count of ≥ 10 in one condition but were completely absent in the other.

- **Principal Component Analysis (PCA)**

PCA was performed to visualize clustering patterns in gene expression data, reducing dimensionality and highlighting differences between control and HD conditions.

- **Outlier Detection**

An outlier was identified in the HD sEV samples, but instead of exclusion, a relaxed inclusion criterion was used to prevent loss of statistical power.

- **Protein Abundance Analysis**

1. **Wilcoxon Rank-Sum Test:** A non-parametric test used to compare protein abundance between control and HD samples based on mass spectrometry data.

- **Colocalization Analysis**

To quantify RNA localization within stress granules, several colocalization coefficients were employed:

Pearson's Correlation Coefficient (PC): Measures the linear correlation between the intensity distributions of two fluorescent channels. Values range from -1 (perfect negative correlation) to 1 (perfect positive correlation).

Spearman's Correlation Coefficient (SC): A non-parametric test capturing monotonic relationships between colocalized signals.

Manders' Colocalization Coefficients (M1 and M2): Measure the fraction of fluorescence from one marker overlapping with another. M1 represents the proportion of marker A overlapping with marker B (e.g., RNA signal in stress granules), while M2 represents the fraction of marker B overlapping with marker A.

These coefficients were calculated across multiple regions of interest to ensure robust colocalization quantification between marker RNAs and YB1-positive stress granules.

- **Multiple Testing Correction**

1. **Bonferroni Correction:** Applied in cases with multiple comparisons, adjusting the p-value threshold to control for false positives.

2. **False Discovery Rate (FDR):** Used when testing thousands of genes and proteins to ensure meaningful yet statistically rigorous conclusions.

Results

1. Isolation of sEVs and RNA granules

To perform a comparative analysis of extracellular sEVs and intracellular RNA granules in an HD cell model, sEVs and cytoplasmic RNA granule cores (RNA granules) were isolated from the culture medium and from HEKQ83 cells, respectively. Five biological replicates were done. To confirm the presence of sEVs and RNA granules in the purified samples, the sEVs and RNA granules from all five replicate batches were analyzed using Western blotting to detect specific marker proteins (**Figure 6**). For RNA granules, EIF4E, G3BP1, FMRP, and YB1 were used as markers, while Lamin A/C, a nuclear marker, served as a negative control.

As anticipated, bands for EIF4E, G3BP1, YB1, and FMRP were observed in both control and HD RNA granule samples, as well as in the nuclear and cytosolic fractions (**Figure 6.a**), since these proteins are known to localize in the nucleus and cytoplasm under normal conditions [405-409]. Given that cells are constantly exposed to some level of stress, faint bands were also seen in the control RNA granule fractions. Additionally, because not all of these proteins localize exclusively to RNA granules and some remain in the cytosol, bands in the cytosolic fractions were expected. As predicted, lamin A/C was not detected in RNA granule samples, indicating the purity of the isolated granules.

The marker proteins for sEVs included Flotillin-1, HSP70 and Alix. An ER membrane marker, calnexin, and a nuclear marker, Lamin A/C, were used as negative controls. As expected, no calnexin or Lamin A/C bands were detectable in the sEV fractions (**Figure 6.b**).

In the case of sEVs, further validation and characterization were done using SEM and NTA. **Figures 7 and 8** show representative images for NTA and SEM analysis respectively. NTA analysis confirmed the size of the sEVs between 80-150 nm. The mean concentration of sEVs in control sample was 4.74×10^7 particles/mL (1:1000 dilution). 50% of the particles had the median size below 113.74 nm (X50). 90% of the particles had the median size below 178.98 nm (X90). The mean concentration of sEVs in HD sample was 5.48×10^7 particles/mL (1:1000 dilution). 50% of the particles had the median size below 110.10 nm (X50). 90% of the particles had the median size below 172.12 nm (X90).

SEM images confirmed the size and the circular morphology of sEVs. Images are obtained at the highest magnification to visualise the smallest EVs. Higher magnifications in HR-SEM (High resolution-SEM) require a dynamic and manual adjustment of focus and magnification to

achieve high quality images. The SEM user interface adjusts the scale bar to the focus position automatically. Both the focus and magnification are adjusted simultaneously in order to obtain a clear image. Therefore, the images were captured at slightly different scale size. These data clearly confirm the presence of sEVs in the isolated samples through Western blot, NTA, and SEM, as well as the presence of RNA granules through Western blot analysis.

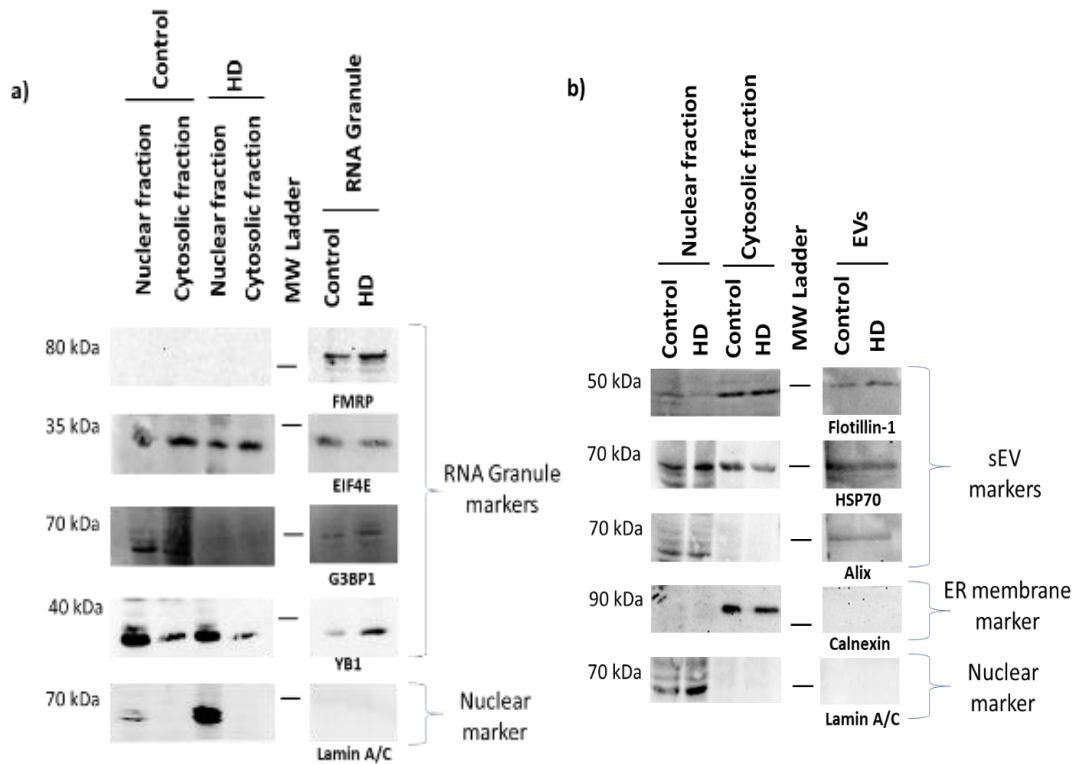


Figure 6: Western blot analysis of RNA granules and sEVs: a) lanes 1-4 contain the nuclear and cytosolic lysates of control and HD samples (positive controls) lanes 5 and 6 contain the RNA granule samples from control and HD samples respectively. The presence of bands in the marker proteins indicate the presence of RNA granules in the sample and the absence of lamin bands in the lane 6 and 7 indicates the absence of any potential nuclear contamination. b) lanes 1-4 contain the nuclear and cytosolic lysates of control and HD samples (positive controls) and lanes 5 and 6 contain the sEV fractions for control and HD samples respectively. The bands in the lanes 5 and 6 of marker proteins indicate the presence of sEVs in the samples and the absence of bands in the control and HD lanes of calnexin and lamin A/C indicate the absence any possible microvesicular, nuclear and ER contamination.

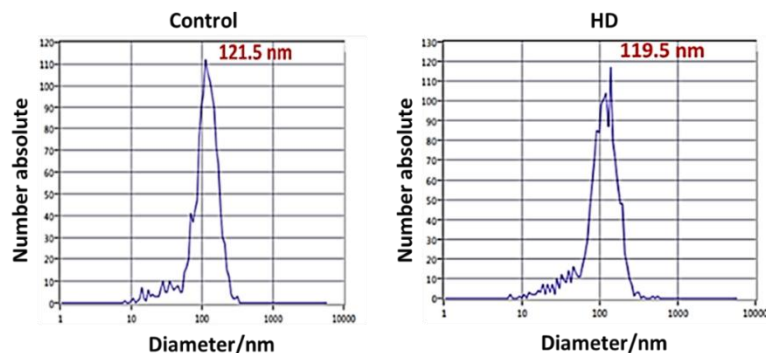


Figure 7. NTA analysis of sEVs. Representative graphs of NTA analysis for control and HD sEVs respectively. The highest number of sEVs in the control sample were recorded to have the size of 121.5 nm. This number was 119.5 nm in the case of HD samples.

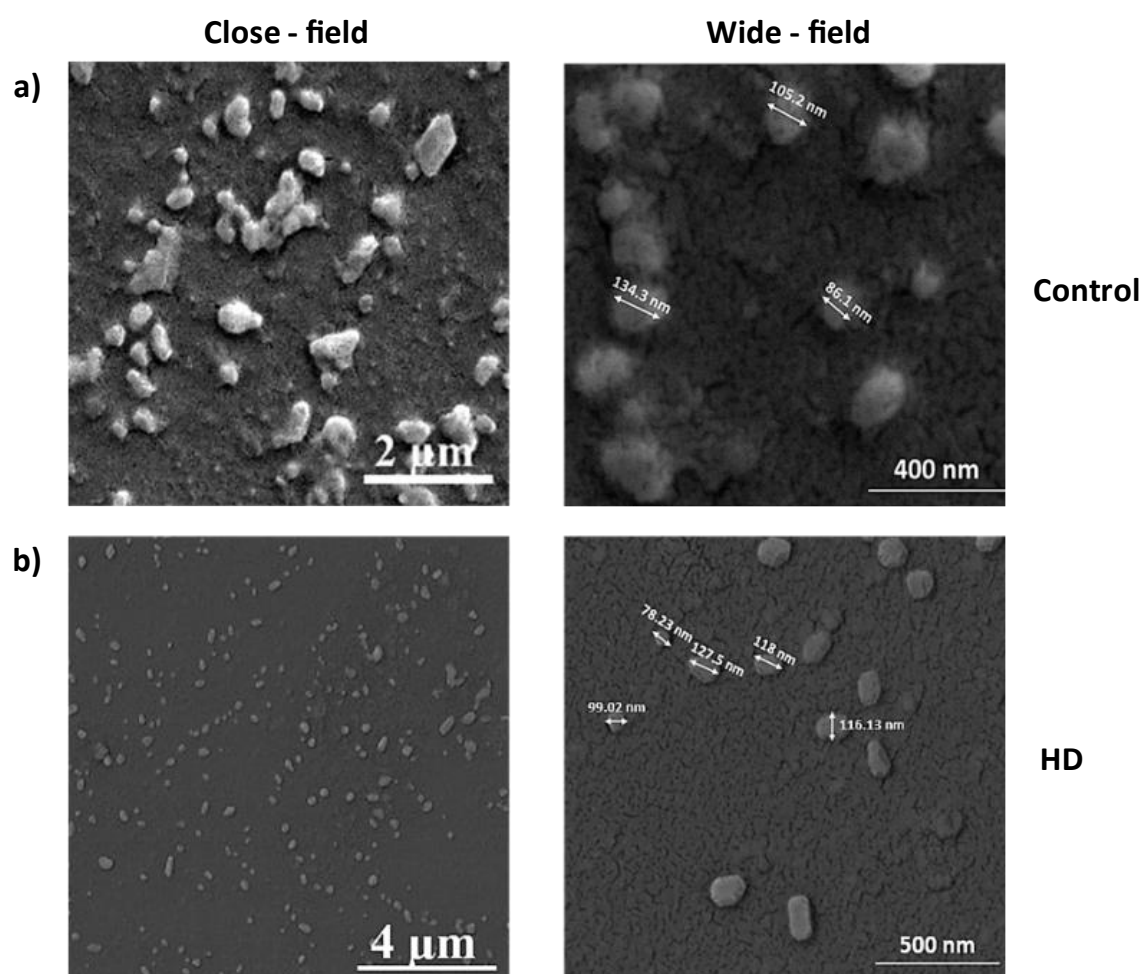


Figure 8. Characterization of the sEV morphology by SEM. a and b are the representative close – field and wide - field SEM images of Control and HD samples respectively. The images show the characteristic spherical shape and size within the sEV range i.e., 30-150 nm.

2. Transcriptomic analysis of sEVs and RNA granules

To analyse the transcriptomic content of sEVs and cytoplasmic RNA granule cores, RNA was isolated from the sEV and RNA granule fractions described above. **Table 4.** Shows the RNA concentrations of the samples determined using Qubit™. Bioanalyzer analysis was performed to assess the quality and integrity of RNA samples prior to RNA-sequencing. The Bioanalyzer system uses microfluidics to provide RNA integrity numbers (RIN), electropherograms, and gel-like images that indicate the quality of the RNA samples. **Table 5** shows the RNA quality assessment based on RIN scores and 28S/18S ratios. The RIN serves as a quantitative indicator of RNA quality, with higher values reflecting reduced degradation. The ideal ratio of 28S to

18S rRNA should be around 2.0, serving as a critical measure of RNA integrity; ratios below this value indicate potential degradation of the RNA. **Figure 9.1** shows the Virtual Gel Image of RNA Integrity. **Figure 9.2** displays an electropherogram of RNA quality in all control and HD sEVs and RNA granule samples, showcasing distinct peaks for 5S, 18S, and 28S rRNA, mostly indicating good RNA integrity, with a balanced 28S/18S ratio suggestive of minimal degradation.

Table 4. RNA concentration of the replicates. The RNA concentrations in the samples were determined using the Qubit™ RNA Assay Kit (Q32855).

Replicates	Control sEVs	HD sEVs	Control RNA granules	HD RNA granules
Replicate 1	3.72 ng/μL	5.45 ng/μL	66 ng/μL	37.1 ng/μL
Replicate 2	5.2 ng/μL	45.5 ng/μL	83 ng/μL	12.7 ng/μL
Replicate 3	3.87 ng/μL	6.82 ng/μL	28 ng/μL	23.3 ng/μL
Replicate 4	5.22 ng/μL	10.2 ng/μL	35.4 ng/μL	24.3 ng/μL
Replicate 5	6.12 ng/μL	10.7 ng/μL	31.8 ng/μL	17.3 ng/μL

Table 5. RIN scores, RNA concentrations and 28S/18S Ratio of control and HD sEVs and RNA granules. The numbers 1, 2, 3, 4, and 5 following control/ HD, sEVs/RNA granules (RNAG) indicate the replicate number. The **RNA RIN** is a scale from 1 to 10, where 10 indicates the highest quality, fully intact RNA, and 1 represents severely degraded RNA. In the table, colours reflect the RNA quality: **green** represents excellent RNA quality with a RIN of 8.0 to 10.0, which is ideal for sensitive applications like transcriptomics; **yellow** indicates high-quality RNA with a RIN between 7.0 and 8.0, showing only minor degradation; **orange** signifies moderate degradation with RIN values from 5.0 to 7.0; and **red**, with RIN scores below 5.0, denotes poor-quality RNA. The **28S/18S ribosomal RNA ratio** is also used to assess RNA integrity. Ideally, the 28S band should be about twice as intense as the 18S band, giving a ratio close to 2.0. Ratios between 1.8 and 2.0 are considered excellent and indicate minimal degradation. A ratio of 1.5 to 1.8 is still good, showing slight degradation. Ratios between 1.0 and 1.5 indicate moderate degradation, while ratios below 1.0 suggest significant degradation.

Well	Sample	RIN	28S/18S (Area)	Conc. [ng/μl]	Observations
-	Ladder 1	-	-		Issue with ladder peak detection (too few peaks detected)
A1	Control sEVs 1	8.4	1.3	67.1	Excellent quality RNA; moderate degradation
B1	Control sEVs 2	6.7	1.1	41.0	Moderate degradation of RNA
C1	Control sEVs 3	6.2	1.0	72.1	Moderate degradation of RNA
D1	Control sEVs 4	6.0	0.8	65.9	Moderate degradation of RNA
E1	Control sEVs 5	7.4	1.2	70.7	High quality RNA; minor degradation
F1	HD sEVs 1	9.1	1.6	46.7	Excellent quality RNA

G1	HD sEVs 2	6.8	1.3	64.0	Moderate degradation of RNA
H1	HD sEVs 3	9.0	1.5	50.7	Excellent quality RNA
A2	HD sEVs 4	6.8	1.1	70.9	Moderate degradation of RNA
B2	HD sEVs 5	8.9	1.3	46.2	Excellent quality RNA
C2	Control RNAG 1	7.0	1.2	67.3	High quality RNA; moderate degradation
D2	Control RNAG 2	9.2	1.6	55.7	Excellent quality RNA
E2	Control RNAG 3	6.8	1.2	75.1	Moderate degradation of RNA
F2	Control RNAG 4	8.9	2.0	41.6	Excellent quality RNA
G2	Control RNAG 5	7.0	1.1	48.7	High quality RNA; moderate degradation
H2	HD RNAG 1	8.9	1.6	45.0	Excellent quality RNA
A3	HD RNAG 2	8.6	1.5	67.7	Excellent quality RNA
B3	HD RNAG 3	6.3	1.1	57.1	Moderate degradation of RNA
C3	HD RNAG 4	9.1	1.6	54.5	Excellent quality RNA
D3	HD RNAG 5	8.4	1.5	45.6	Excellent quality RNA

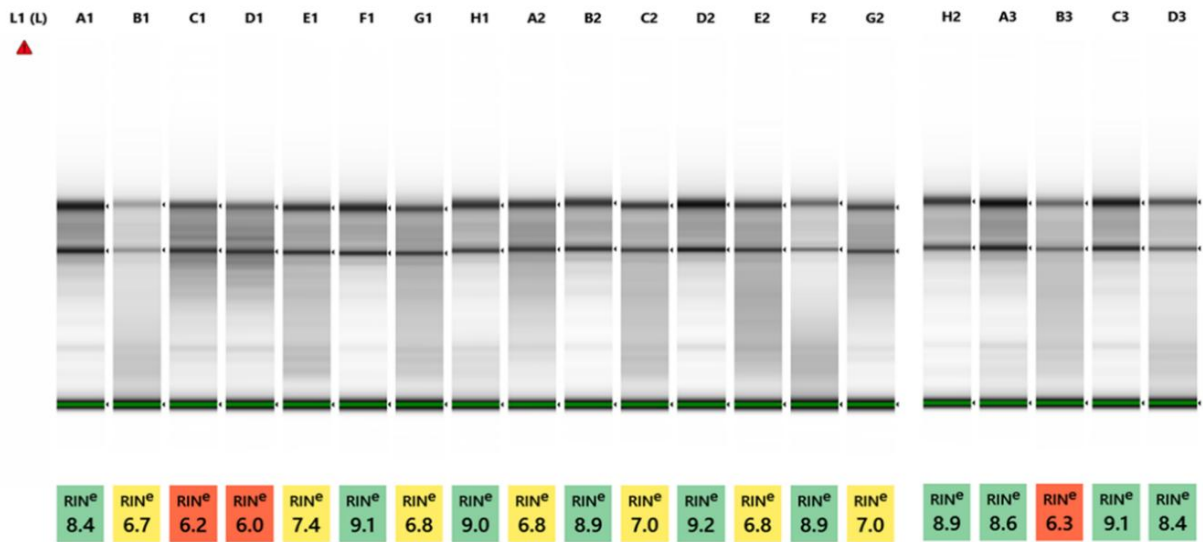
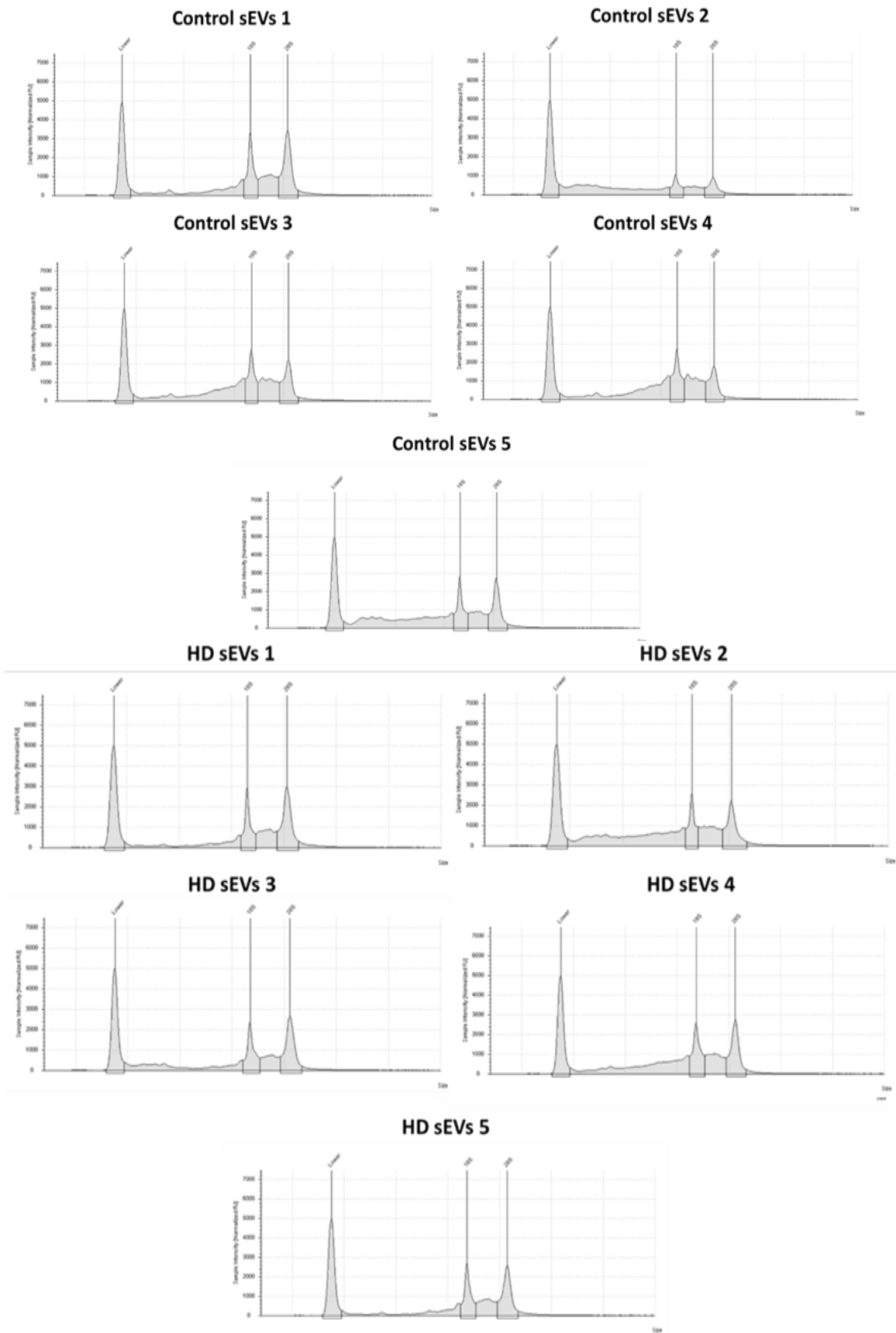
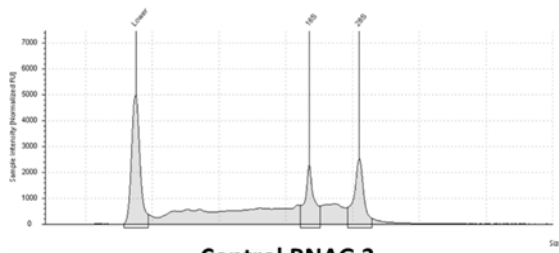


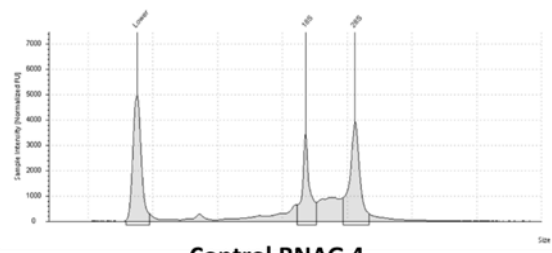
Figure 9.1 Virtual Gel Image of RNA Integrity. The wells in the virtual gel image are labelled at the top as A1, B1, C1, and so on, corresponding to the different RNA samples loaded in each well. For specific sample names corresponding to each well (A1, B1, C1, etc.), refer to **Table 5**. The virtual gel image shows two distinct, sharp bands, representing different RNA species that are used to assess RNA integrity. The 28S rRNA Band (**top Band**) is the largest and most prominent band in the gel and corresponds to the 28S ribosomal RNA. The 18S rRNA Band (**middle Band**) is the band that represents the 18S ribosomal RNA. The relative intensity of the 18S band compared to the 28S band is used to calculate the 28S/18S ratio, a key indicator of RNA degradation. The **green bands** at the bottom of each lane represent the lower marker, typically used in RNA quality control assessments to denote the baseline or background signal.



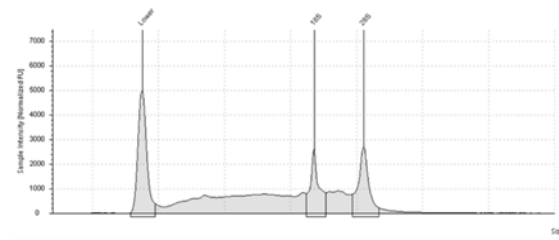
Control RNAG 1



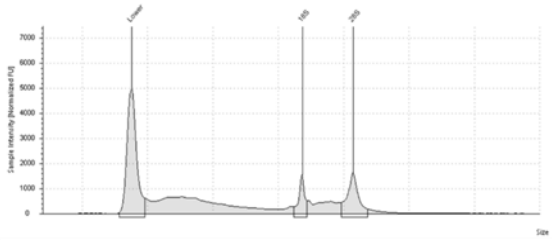
Control RNAG 2



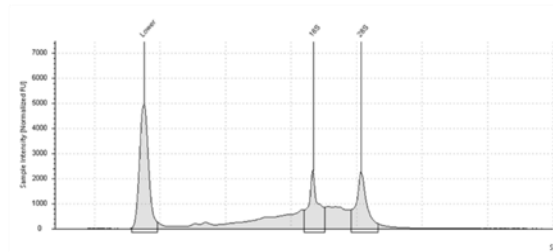
Control RNAG 3



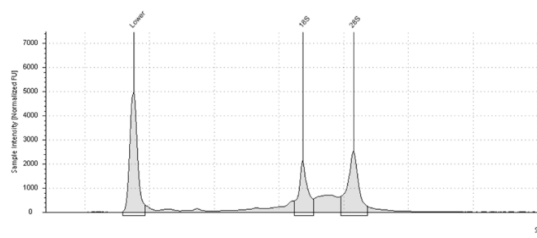
Control RNAG 4



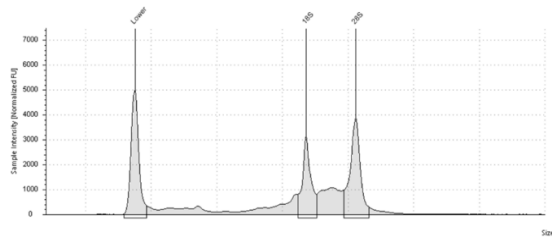
Control RNAG 5



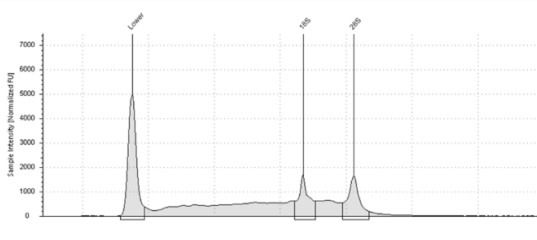
HD RNAG 1



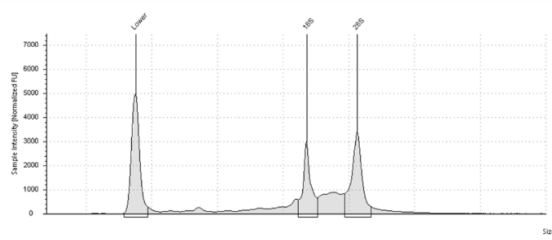
HD RNAG 2



HD RNAG 3



HD RNAG 4



HD RNAG 5

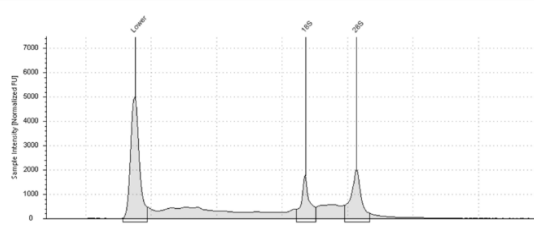


Figure 9.2. Electropherogram analysis of RNA from different samples. The graphs shown in the figure are called electropherograms and produced by an RNA integrity analysis tool. In this plot, the **x-axis** indicates the size of RNA in nucleotides, while the **y-axis** displays the fluorescence intensity, measured in Relative Fluorescence Units (RFU), reflecting the concentration of RNA detected at various sizes. Three peaks can be observed: the Lower peak (**1st peak from the left**), which corresponds to smaller RNA species like 5S rRNA or tRNA, and the two major peaks for 18S and 28S rRNA (**the second and third peaks from the left**). Sharp, well-defined peaks for both the 18S and 28S rRNA suggest that the RNA in this sample is intact. A degraded RNA sample shows a significant reduction in the height and sharpness of the 28S peak, and the 18S peak may also appear diminished or completely absent. Instead of clear peaks, a broad smear can be seen, indicating fragmentation of the RNA.

After completing a thorough quality control check, we proceeded with RNA sequencing on the samples. The resulting data were processed to identify genes with sufficient expression levels for analysis. Of the 303,919 genes detected, 95,856 (31.5%) displayed an abundance count of ≥ 10 reads in at least one sample, which indicates a meaningful level of gene expression. In this context, an "abundance count of ≥ 10 reads" means that, for a gene to be included in downstream analyses, it needed to have at least 10 reads (sequenced RNA fragments) in at least one sample. This threshold helps filter out genes with low or negligible expression, likely due to background noise or sequencing errors, allowing us to focus on genes with robust evidence of expression.

During the analysis, we encountered an outlier in the HD sEV samples. While outliers are often excluded to avoid skewing results, removing this sample would have left the HD sEV group with fewer samples than the other conditions, potentially affecting the balance of the analysis. For this reason, we decided to retain the outlier, allowing its gene expression data to be considered as part of the HD conditions. To accommodate this outlier, the analysis allowed for one absence in samples for gene expression, meaning that genes needed to be consistently detected across samples, but the outlier's unique profile did not disqualify genes from being included as long as they were present in the other HD sEV samples.

To further explore the gene expression patterns, we utilized Principal Component Analysis (PCA), a statistical method that helps simplify complex datasets and clarifies relationships among samples. The PCA plot revealed how samples clustered along the first two principal components (PC1 and PC2), where PC1 accounted for the greatest variance and PC2 represented the second highest source. While the outlier appeared somewhat separate in the plot, it remained within a comparable expression range to the other HD samples, justifying its

inclusion in the dataset. This PCA visualization indicated that the overall gene expression profiles between control and HD conditions showed only minor differences (**Figure 10**).

Among the total RNA extracted from all samples, including control and HD RNA granules as well as sEVs, long non-coding RNAs (lncRNAs) constituted 62-68%, while ncRNAs made up 17-18%. Additionally, protein-coding genes accounted for 7-10% of the RNA content (**Figure 11**). In only RNA granule samples, a small number of miRNAs were detected, specifically 25 in the control samples and 23 in the HD samples.

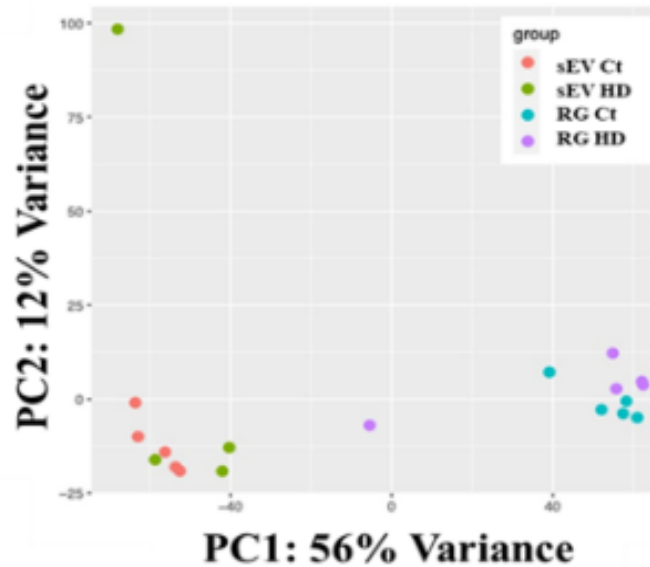


Figure 10. Principal Component Analysis (PCA) plot. In order to assess the similarity between the gene composition across samples, PCA plot of gene content in sEV and RNA granule samples from control and HD cells was plotted.

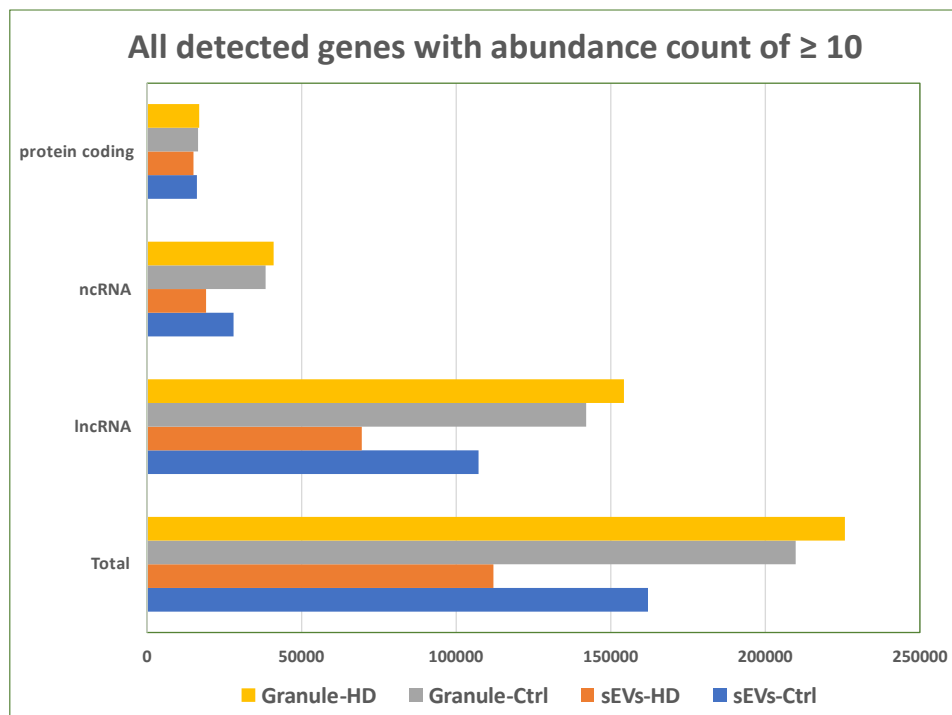


Figure 11. RNA Composition in samples. Relative composition of genes that were consistently detected in all samples belonging to a condition.

3. Analysis of commonly detected genes in control and HD sample

A comprehensive analysis of gene expression profiles in sEVs and RNA granules under control and HD conditions, highlighting distinct differences in gene content, RNA composition, and the distribution of unique and shared genes across these samples was done. Of the 303,919 genes initially identified, 95,856 genes were consistently detected with an abundance count of ≥ 10 in at least one sample, forming the foundation for further analysis. From this subset, a more refined set of 45,882 genes was detected across samples that belonged to at least one condition (control or HD). When we analyzed these genes specifically within RNA granules and sEVs, the RNA granules exhibited a higher gene count, with a median of 44,048 genes in control samples and 44,319 genes in HD samples. In contrast, the sEV samples showed a lower gene count, with a median of 34,439 genes under control conditions and 26,100 genes in HD conditions (**Figure 12**).

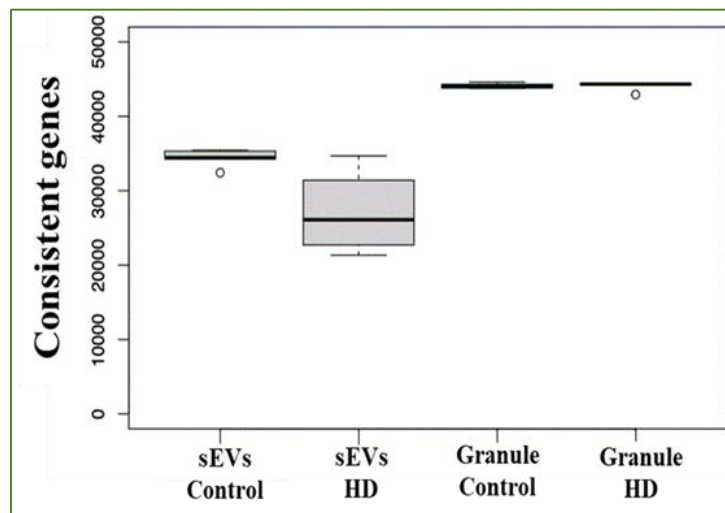


Figure 12. Consistently detected genes. Number of genes consistently detected in samples belonging to one condition.

Additionally, when comparing control and HD conditions, sEVs showed a significant drop in the number of detected genes in HD samples, highlighting a notable change in gene expression. This suggests that the two types of samples behave differently, especially under HD conditions.

By retaining the outlier and allowing for a single sample absence in gene detection, we preserved a more comprehensive dataset for the HD condition, ensuring consistency in

sample representation while minimizing potential bias from the outlier. This approach enabled us to confirm a substantial decrease in gene expression in HD sEV samples compared to controls. Importantly, this observed reduction appears to reflect a broader, biologically relevant trend associated with the HD condition rather than being an artifact introduced by the outlier.

In the earlier analysis, we found that lncRNAs made up a significant portion of the total RNA extracted from all samples, including control and HD RNA granules as well as sEVs, accounting for 62-68% of the RNA content. ncRNAs contributed 17-18%, while protein-coding genes comprised 7-10%. However, when focusing specifically on the refined set of genes detected across samples that belonged to at least one condition (control or HD), the proportions shifted. LncRNAs represented a smaller share, at 46-49%, while protein-coding genes accounted for a larger portion, 26-28%. The proportion of ncRNAs remained relatively stable at 16-18% (**Figure 13**).

When unique and shared consistent genes were compared in all the samples, the difference between sEVs and RNA granule cores became apparent. 12,229 (26.7%) genes were present in all the conditions, 27,987 genes (61.0%) were unique to RNA granules and 5,666 genes (11.3%) were unique to sEVs. Upon comparing control and HD samples, several common genes were discovered. With respect to sEVs, 12,505 genes (27.3%) were common. In RNA granule samples, 36,138 genes (78.8%) were common between control and HD.

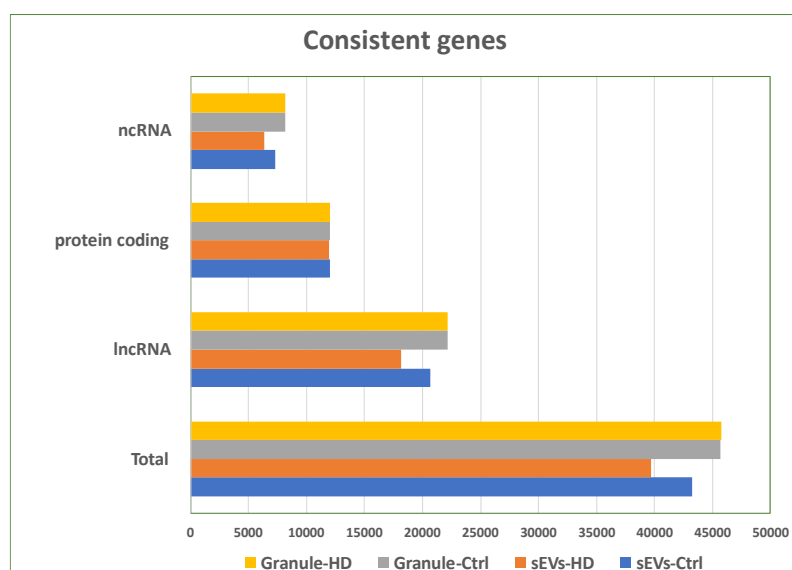


Figure 13. RNA composition of samples. Genes that were consistently detected in all samples belonging to one condition.

The number of unique genes in control sEV samples were 5,046 genes (11.0%). The number reduced to 344 genes (0.7%) for HD sEV samples. In control RNA granule samples, the exclusivity of mere 6.8% was observed with 3,140 unique genes. In HD RNA granule samples, 5,626 genes (12.3%) were exclusive (**Table 6**).

Table 6. Gene distribution across sEV and RNA granule samples. The table summarizes the distribution of genes detected across control and HD conditions in sEVs and RNA granules. It highlights three main categories of gene presence. Genes shared across all conditions represents the number of genes that are consistently present across both sEVs and RNA granule samples under control and HD conditions. Common genes (Control vs HD) indicate the number of genes shared between control and HD samples within each sample type (sEVs or RNA granules). Unique genes show the number of genes exclusive to each sample type and condition, highlighting differences between control and HD samples in both sEVs and RNA granules. Unique genes in each organelle represents the number of unique genes in sEVs and RNA granules.

Category	sEVs Control	sEVs HD	RNA granules control	RNA Granules (HD)	All conditions
Genes Shared Across All Conditions	N/A	N/A	N/A	N/A	12,229 (26.7%)
Common Genes (Control vs HD)	12,505 (27.3%)		36,138 (78.8%)		N/A
Unique Genes	5,046 (11.0%)	344 (0.7%)	3,140 (6.80%)	5,626 (12.3%)	
Unique genes in each organelle	5,666 genes (11.3%)		27,987 (61.0%)		

Taken together, several common RNAs are present between control and HD conditions in both RNA granule and sEV samples. The exclusive gene count was extremely low with 11% and 0.7% in control and HD sEVs and 6.8% and 12.3% in control and HD RNA granules respectively. LncRNAs were the most abundant RNAs present in all samples.

4. Comparative Analysis of Gene Expression Profiles in Control and HD Conditions Using Presence-Absence and Differential Expression Approaches

To further examine the differences in gene expression between control and HD samples, two complementary approaches were employed. This builds on the earlier gene detection analysis, which focused on the number and types of genes expressed in both sEVs and RNA granules, by now incorporating two key parameters: gene presence/absence and abundance levels.

First Approach: presence or absence of genes

This method is focused on identifying genes present in one condition (control or HD) but entirely absent in the other. In the control sEVs, 81 genes were found that were completely absent in the HD sEV samples, while in HD sEVs, 17 genes were uniquely expressed.

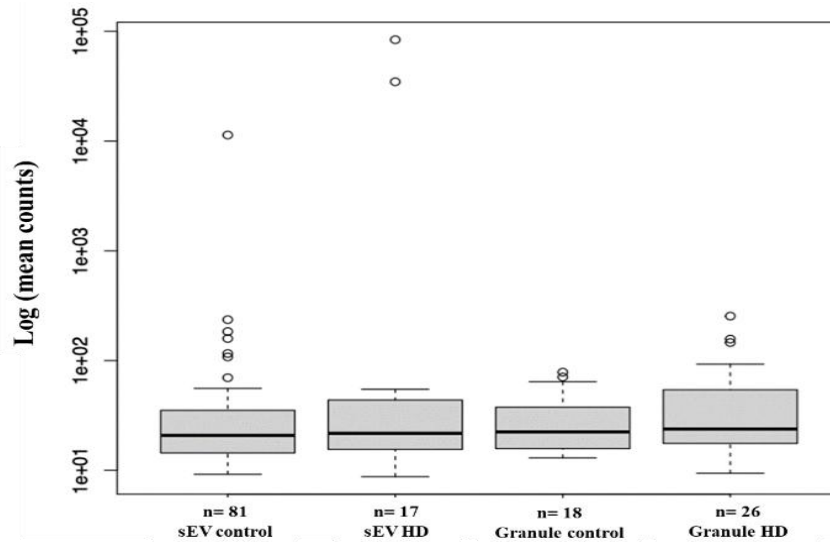


Figure 14. Approach one. Mean count abundance genes that were consistently present in samples of one condition (x-axis), but fully absent in the other (i.e., control for HD samples and HD for control samples).

A similar pattern was observed in RNA granules, where 18 genes were unique to the control condition, and 26 genes were specific to the HD condition (**Figure 14**).

Second Approach: Differential Gene Expression with DESeq2

To add depth to this analysis, a second approach was used to account for gene abundance. While the presence-absence method provided a binary comparison, it did not reflect how much of a given gene was being expressed. To fill this gap, we performed a differential gene expression analysis using DESeq2, a statistical tool that identifies changes in gene abundance between conditions while accounting for variability between replicates. Out of the 95,856 genes with an abundance count of ≥ 10 in at least one sample, 948 genes were found to be differentially expressed in sEVs. Specifically, in HD sEVs, 707 genes were upregulated, meaning their expression increased compared to the control, while 241 genes were downregulated, showing reduced expression. In RNA granules, a more modest number of 86 genes were differentially expressed, with 53 being upregulated and 33 downregulated in HD samples. This approach helped to capture not only the presence of genes but also how their expression

levels shifted under HD conditions, revealing a broader range of transcriptional changes (**Figure 15**).

By integrating the results from both the presence-absence analysis and the DESeq2-based differential expression analysis, we identified a total of 1,091 differentially expressed genes across sEVs and RNA granules under HD conditions. 57 genes had double entry due to the agreement of both approaches. Overall, more genes were upregulated in HD conditions (707 genes in sEVs and 53 genes in RNA granules) than in control conditions (286 genes in sEVs and 48 genes in RNA granules). LncRNAs were the most abundant RNAs (**Figure 16**). While lncRNAs also constituted a major portion of total RNA in the earlier analysis, the elevated presence of lncRNAs in HD sEVs here could indicate a specific pattern of enrichment related to disease-associated regulatory functions or signaling mechanisms. This aligns with the general understanding that ncRNAs are more abundant than protein-coding RNAs in most cellular environments, but the particular increase observed in HD sEVs might reflect a shift in RNA composition that could be relevant to the molecular changes in HD pathology. **Table 7** shows the number of differentially expressed genes identified by both the approaches. List of marker genes in control and HD conditions are listed as appendix 1 and 2 respectively along with mean abundance values and log₂ fold change values.

In our comparison between sEVs and RNA granules, we identified the top 5 most abundant genes in both Control and HD samples for each sample type (sEVs and RNA granules), resulting in a total of 10 entries in the table (**Table 8 and 9**).

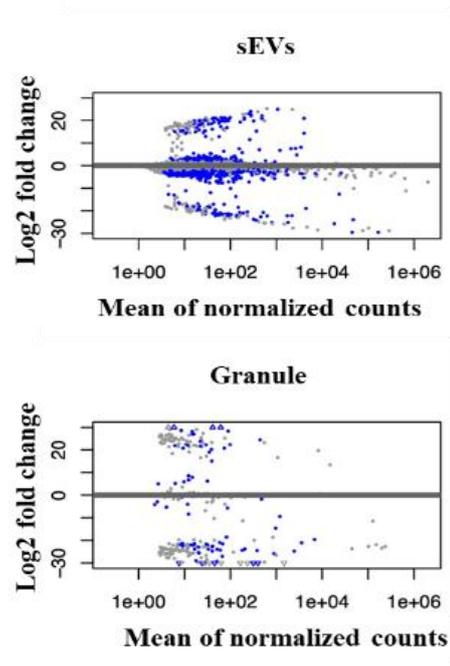


Figure 15. Approach two. Differential gene expression analysis. Increase in HD cells is depicted by negative fold changes and decrease upon HD is depicted by positive fold changes. Before plotting, adaptive shrinkage estimator was used to reduce the fold-changes in order to reduce noise due to low count of genes and to enhance visualization (adjusted p-value 0.05). a) Up and downregulated genes in sEVs b) Up and downregulated genes in RNA granules.

These specific genes were selected based on their abundance to prioritize those most likely to play significant roles in cellular processes, particularly in the context of HD. High-abundance genes are often more functionally relevant as they can drive key biological pathways or serve as reliable biomarkers for disease conditions. Since control is set as the baseline, a positive log2 fold change indicates that the gene is more highly expressed in control samples compared to HD. Conversely, a negative log2 fold change means that the gene is expressed at lower levels in HD samples relative to control.

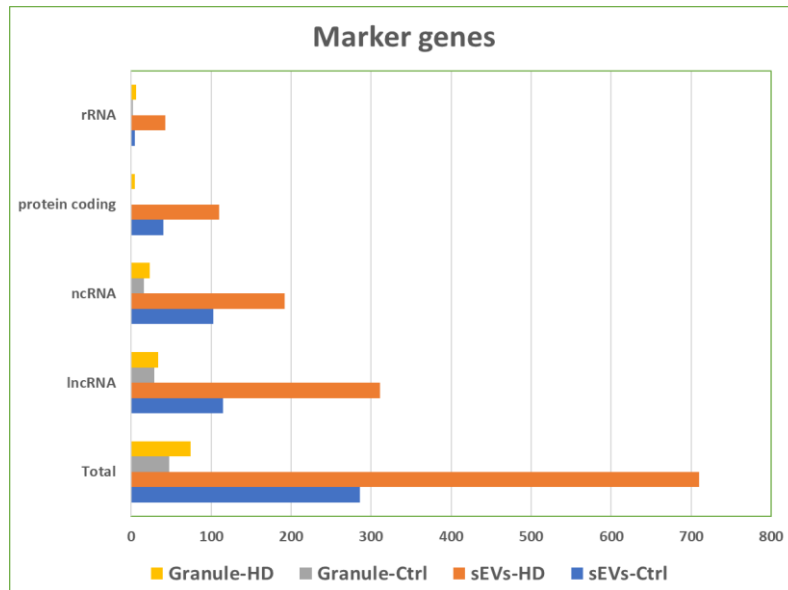


Figure 16. Biotype of marker transcripts. The biotype of marker transcripts was analyzed to understand the distribution of different RNA types in each sample. The graph highlights the diverse RNA populations present, with lncRNAs being the most abundant across all samples. Notably, lncRNAs were significantly elevated in HD sEVs compared to control sEVs and control and HD RNA granules, indicating a potential role for these RNAs in disease-related processes.

Table 7. Differential gene expression data for control and HD conditions across sEVs and RNA granules. Unique genes are genes present in one condition (control or HD) and completely absent in the other. Upregulated genes are genes showing an increase in expression in the HD condition compared to control. Downregulated genes are genes showing a decrease in expression in the HD condition compared to control and differentially expressed genes are the total genes identified as significantly different between conditions based on the DESeq2 analysis.

Analysis approach	sEVs control	sEVs HD	RNAG Control	RNAG HD
Presence-absence approach				
Unique Genes	81	17	18	26
DESeq2 (Abundance) approach				
Upregulated Genes	286	707	48-	53
Downregulated Genes	-	241	-	33
Combined Total (Both Approaches)				

Differentially Expressed Genes		948		86
--------------------------------	--	-----	--	----

Table 8. Marker genes for control sEVs and RNA granules. Marker genes for control sEVs and RNA granules (RG) were selected based on their abundance rates (MA). positive log2 fold change (L2fc) indicates that the gene is more highly expressed in control samples (Cont) compared to HD. Low adjusted p-value (padj) ensures that these differences are statistically significant.

Control markers for sEVs and RNA granules						
Gene	Name	MA	L2fc	padj	type	State
URS0000D57449_9606	lnc-LRR1-1:3	934.6	23.17556869	5.42E-05	sEVs	cont
URS0000D57449_9606	lnc-LRR1-1:4	16.2	23.28887262	1.98E-05	RG	cont
URS0000D5A5B3_9606	non-protein coding XIST:48	47.4	20.31061854	0.00077084	sEVs	cont
URS0000D5A5B3_9606	non-protein coding XIST:49	90	24.84981419	1.87E-06	RG	cont
URS0000E960A4_9606	HSALNT0145531	15.6	18.65032413	0.00278609	sEVs	cont
URS0000E960A4_9606	HSALNT0145531	12.2	22.73550553	2.38E-05	RG	cont
URS00023427AC_9606	HSALNT0328745	6.4	18.68018997	0.00364404	sEVs	cont
URS00023427AC_9606	HSALNT0328745	45.4	23.54428497	1.40E-05	RG	cont
URS0002559B84_9606	Non-coding RNA (CM034952-450)	20.6	19.05783994	0.00260065	sEVs	cont
URS0002559B84_9606	Non-coding RNA (CM034952-450)	7.4	21.60796024	0.00017319	RG	cont

Table 9. Marker genes for HD sEVs and RNA granules. Marker genes for HD sEVs and RNA granules were selected based on their abundance rates (MA). Since control is set as the baseline, negative log2 fold change (L2fc) indicates that the gene is more highly expressed in HD samples compared to control. Low adjusted p-value (padj) ensures that these differences are statistically significant.

HD markers for sEVs and RNA granules						
Gene	Name	MA	L2fc	padj	type	State
URS00009AEE5C_9606	HSALNT0088996 (lnc-SLC30A5-6)	8	-19.6436084	0.0014999	sEVs	HD
URS00009AEE5C_9606	HSALNT0088996 (lnc-SLC30A5-6)	25.8	-32.69316161	7.12E-12	RG	HD
URS0000D5B666_9606	SNHG7:8	23.5	-22.05460356	0.0001542	sEVs	HD
URS0000D5B666_9606	SNHG7:8	22.8	-32.05822125	1.74E-11	RG	HD
URS0001BE5FEC_9606	HSALNT0003934 (SNHG12:13)	23.2	-21.83829852	0.0001957	sEVs	HD
URS0001BE5FEC_9606	HSALNT0003934 (SNHG12:13)	56.4	-30.77493885	1.82E-10	RG	HD
URS0001BF179B_9606	HSALNT0279541 (LHR1-LNC1610-1)	209	-25.68918639	2.25E-06	sEVs	HD
URS0001BF179B_9606	HSALNT0279541 (LHR1-LNC1610-1)	371.	-32.47659779	9.73E-12	RG	HD
URS000233D421_9606	HSALNT0398958 (lnc-DUXA1)	24.7	-22.71702652	7.70E-05	sEVs	HD
URS000233D421_9606	HSALNT0398958 (lnc-DUXA1)	96	-33.74471476	1.10E-12	RG	HD

5. Validation of HD Marker Gene Abundance Using qRT-PCR Analysis

In order to validate the increased abundance rates of HD marker genes, qRT-PCR was done. With respect to HD RNA granule samples, we confirmed the increase of all five marker genes. with respect to sEVs, the increase was only seen in 3 markers. The other two failed to be statistically significant due to high replicate variability (**Figure 17**).

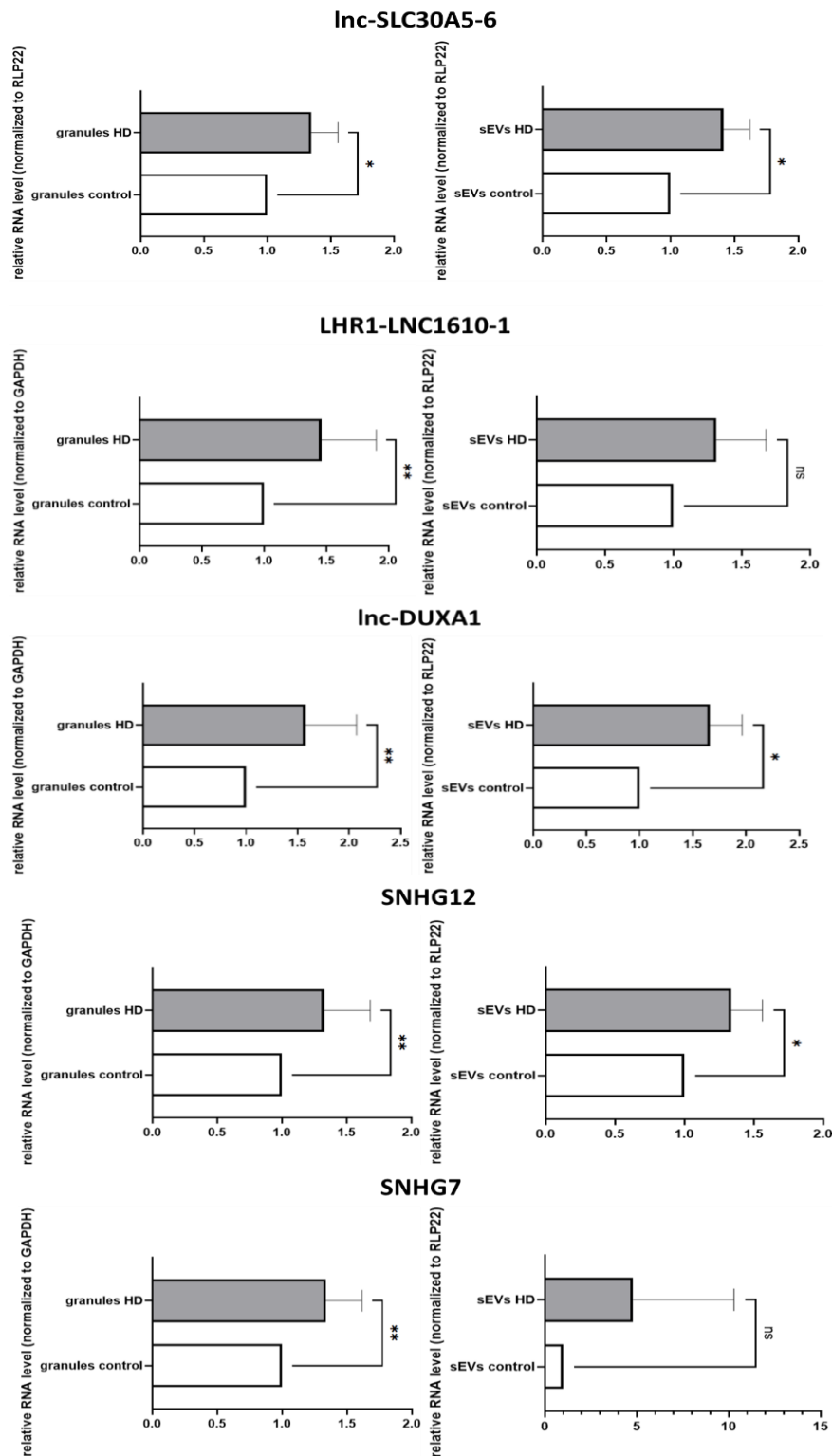


Figure 17. Validation of HD marker genes by qRT-PCR. Relative RNA levels of marker genes in RNA granule and sEV samples. Lnc-SLC30A5-6 ($n_{\text{RNA granules}} = 3$; $n_{\text{sEVs}} = 3$), LHR1-LNC1610-1 ($n_{\text{RNA granules}} = 10$; $n_{\text{sEVs}} = 5$), Lnc-DUXA-1 ($n_{\text{RNA granules}} = 8$; $n_{\text{sEVs}} = 3$), SNHG12 ($n_{\text{RNA granules}} = 15$; $n_{\text{sEVs}} = 4$), SNHG7 ($n_{\text{RNA granules}} = 10$; $n_{\text{sEVs}} = 4$). Relative expression level of these genes was normalized to housekeeping genes RPL22 or GAPDH. Columns indicate mean values \pm SEM. * $p < 0,05$

6. Validation of HD Marker Transcripts in YB1-Positive RNA Granules Using RNA-FISH

Three marker genes (SNHG7, LHR1-LNC1610-1 and Lnc-DUXA-1) were selected based on abundance values and their presence in RNA granules was validated using RNA-FISH. Controls with GAPDH (**Figure 18**) and no probe (NPC) (**Figure 19**) were analysed using the same parameters. YB1 (Y-box binding protein 1) was used to stain SGs because it is a well-known marker for stress granule formation and is involved in RNA binding and stabilization under stress conditions [410, 411].

In our RNA-FISH experiments, YB1 staining allowed us to visualize SGs, while the RNA-FISH probes targeted the marker transcripts of interest. This approach helped validate whether these transcripts colocalized with SGs, providing insight into their potential role in stress responses within HD and control cells.

Partial co-localization of the selected transcripts with YB1-positive RNA granules was observed, likely due to the inherent variability in the composition of stress-induced granules [376]. To better understand this partial overlap, we quantified the colocalization to assess the extent of association between the marker genes and SGs (**Figure 20**). This approach allowed us to determine whether the observed partial colocalization reflects selective interactions rather than uniform association with all stress-induced granules.

To quantify the colocalization, we calculated and compared several correlation coefficients, including Pearson's coefficient, Spearman's coefficient, and Manders' M1 and M2 coefficients. Pearson's coefficient assesses the linear correlation between the intensity distributions of two channels, with values ranging from -1 (perfect negative correlation) to 1 (perfect positive correlation). Spearman's coefficient measures rank correlation, capturing monotonic relationships between variables. Manders' M1 and M2 coefficients specifically quantify the proportion of marker overlap, with values closer to 1 indicating higher colocalization.

In our study, all transcripts showed higher colocalization in stressed HD cells compared to controls, except for SNHG7, which exhibited only a slight increase, likely due to a high background signal (**Table 10**). Altogether, colocalization studies validated the presence of transcripts SNHG7, LHR1-LNC1610-1 and Inc-DUXA-1 in YB1-positive RNA granules.

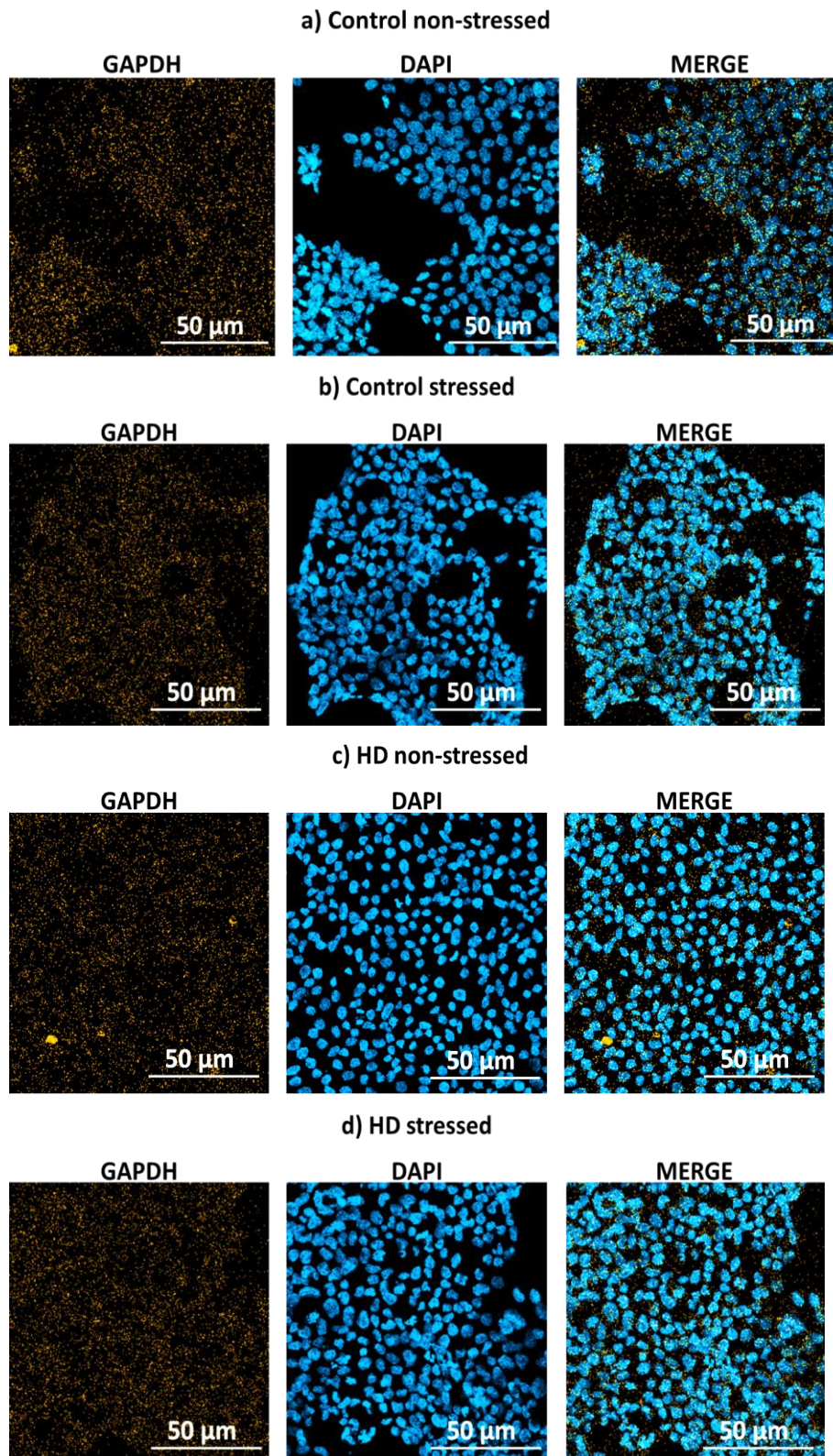


Figure 18. Controls for RNA-FISH. GAPDH staining was performed on control and HD cells under both non-stressed and stressed conditions. The images were captured at 20X magnification and include the following panels: **(a)** control non-stressed cells, **(b)** control stressed cells, **(c)** HD non-stressed cells, and **(d)** HD stressed cells. In each set, the left panel shows GAPDH probe staining, the middle panel displays nuclear staining with DAPI, and the right panel presents the merged image, highlighting the overlap between GAPDH and nuclear signals under varying conditions.

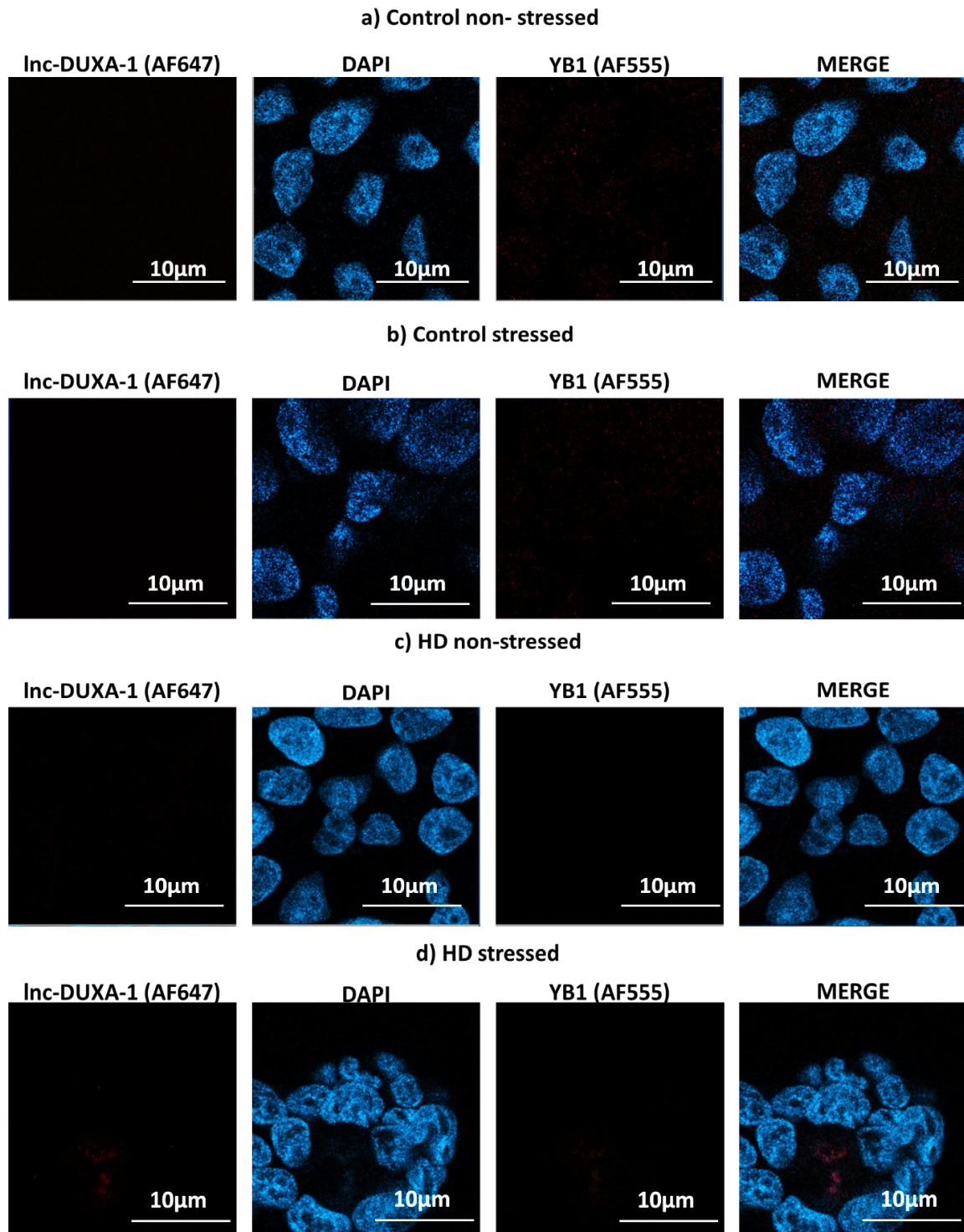
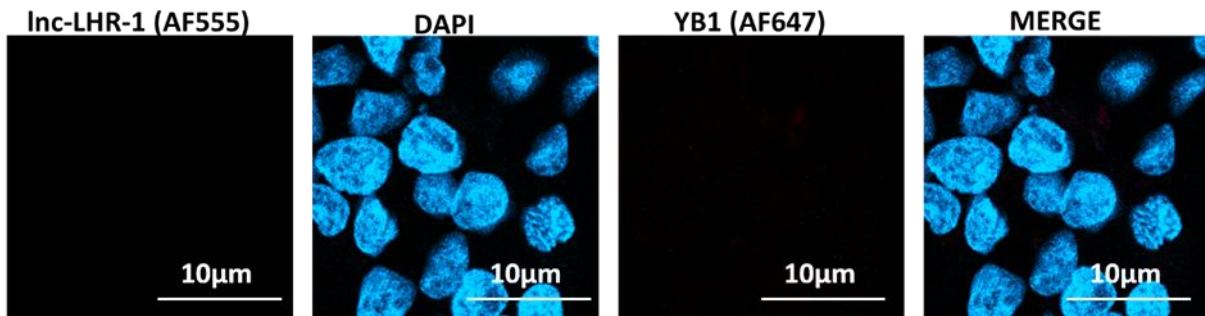


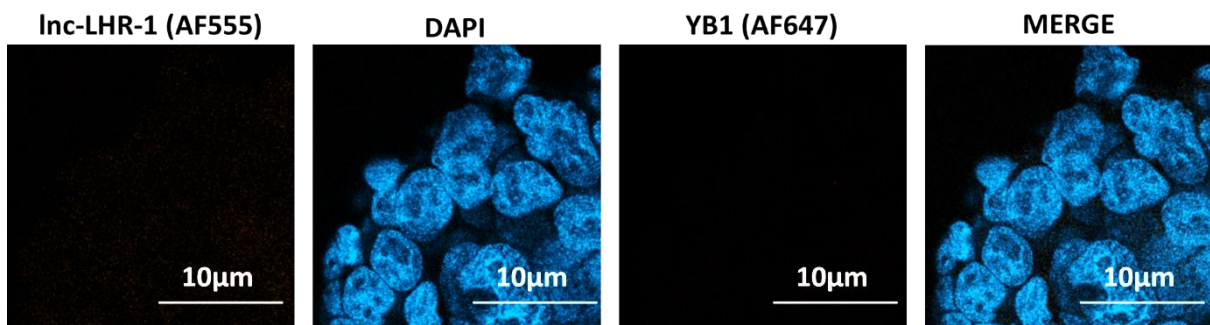
Figure 19.1. No probe controls for Inc-DUXA1. No probe controls for Inc-DUXA1 were performed using an oil immersion 60X microscope, capturing images under four conditions: **(a)** control non-stressed cells, **(b)** control

stressed cells, **(c)** HD non-stressed cells, and **(d)** HD stressed cells. Each set of images includes four panels. The first panel shows no Inc-DUXA1 probe staining, the second panel shows DAPI nuclear staining, the third panel displays YB1 stress granule staining without primary antibody, and the final panel presents the merged image. The absence of signal in the no-probe and YB1 panels confirms staining specificity without background interference.

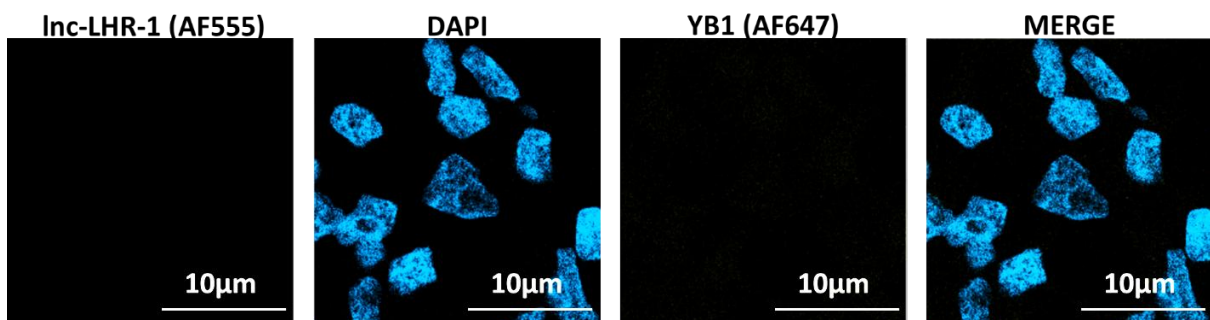
a) Control non-stressed



b) Control stressed



c) HD non-stressed



d) HD stressed

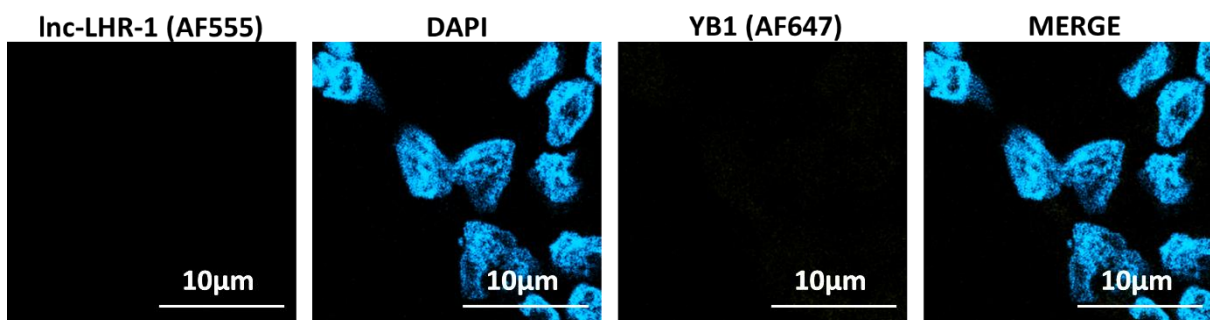
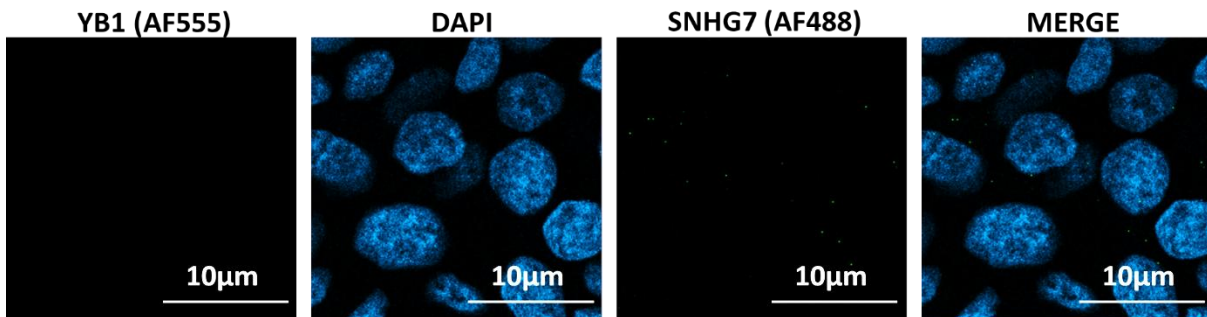
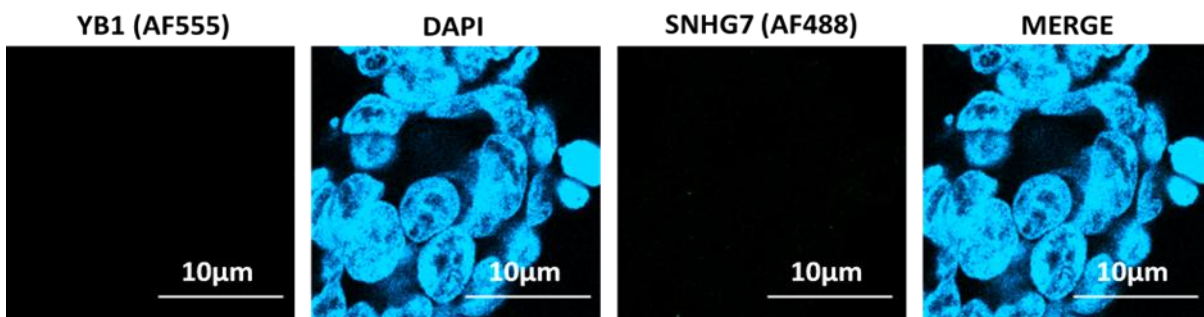


Figure 19.2. No probe controls for Inc-LHR-1. No probe controls for Inc-LHR-1 were performed using an oil immersion 60X microscope, capturing images under four conditions: (a) control non-stressed cells, (b) control stressed cells, (c) HD non-stressed cells, and (d) HD stressed cells. The first panel shows no Inc-DUXA1 probe staining, the second panel shows DAPI nuclear staining, the third panel displays YB1 stress granule staining without primary antibody, and the final panel presents the merged image. The absence of signal in the no-probe and YB1 panels confirms staining specificity without background interference.

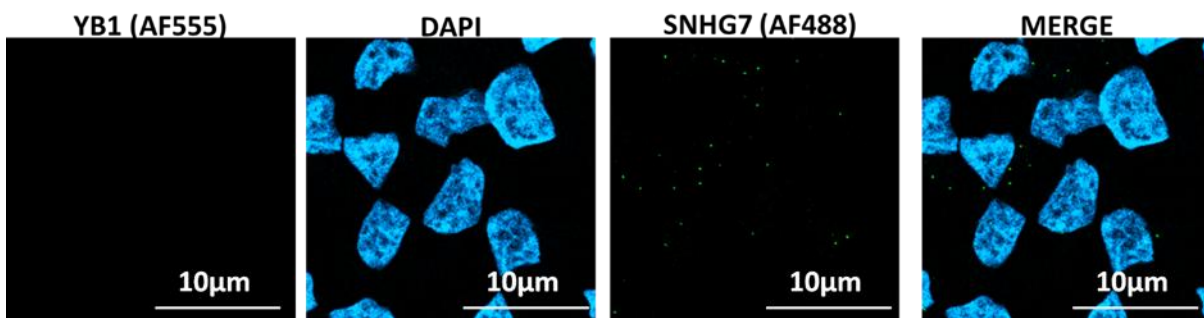
a) Control non-stressed



b) Control stressed



c) HD non-stressed



d) HD stressed

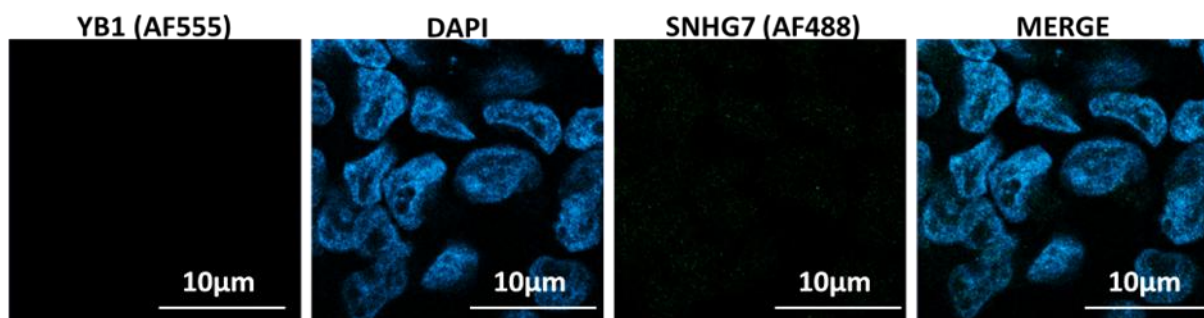


Figure 19.3. No probe controls for SNHG7. No probe controls for SNHG7 were performed using an oil immersion 60X microscope, capturing images under four conditions: **(a)** control non-stressed cells, **(b)** control stressed cells, **(c)** HD non-stressed cells, and **(d)** HD stressed cells. The first panel shows the absence of YB1-positive stress granule staining without the primary antibody, the second panel displays nuclear staining with DAPI, the third panel demonstrates no SNHG7 probe staining, and the final panel presents the merged image. Faint signals were observed in the third panel. This could be due to high background interference.

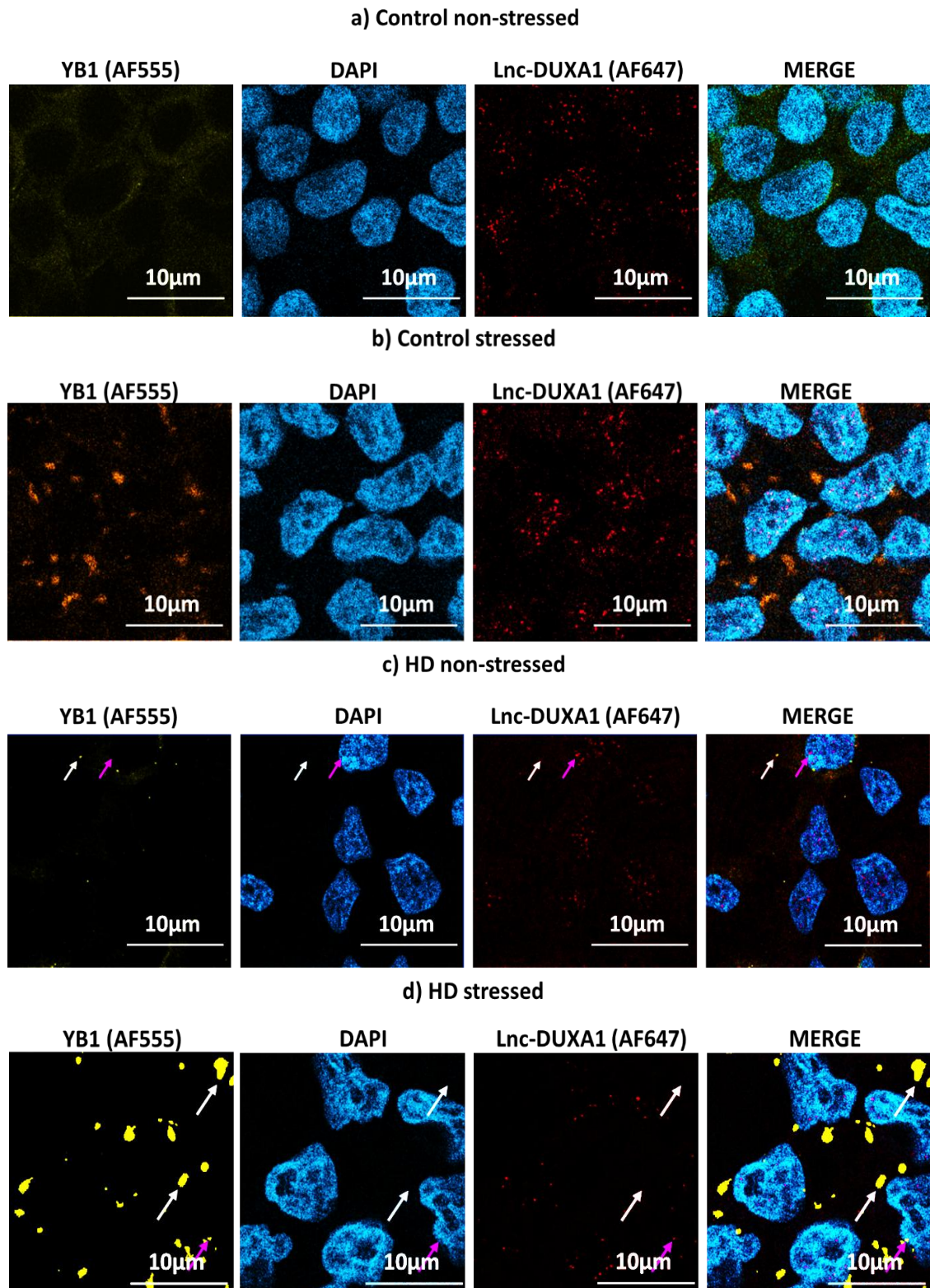
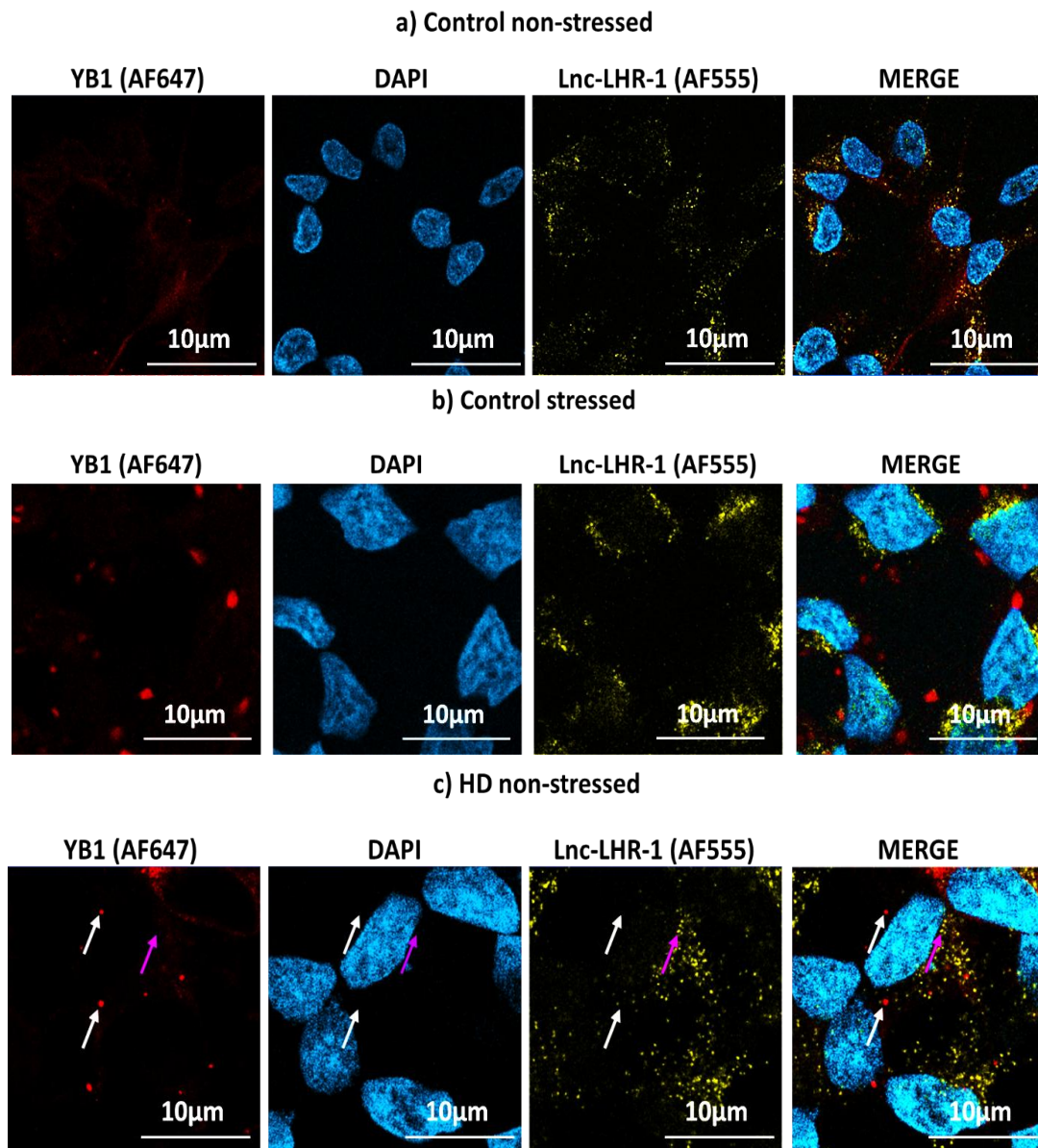


Figure 20.1: RNA-FISH analysis for lnc-DUXA1. RNA-FISH analysis for lnc-DUXA1 was performed using an oil immersion 60X microscope, capturing images under four experimental conditions: **(a)** control non-stressed cells, **(b)** control stressed cells, **(c)** HD non-stressed cells, and **(d)** HD stressed cells. In these images, YB1 antibody was used to mark YB1-positive RNA granules. The presence and colocalization of lnc-DUXA1 and YB1-positive granules were highlighted with specific color-coded arrows. In HD non-stressed cells, pink arrows indicate the location of the lnc-DUXA1 probe, while white arrows show YB1-positive RNA granules. In the HD stressed condition, colocalization of lnc-DUXA1 and YB1-positive RNA granules is marked by pink arrows, with white arrows indicating YB1-positive granules. In control non-stressed cells, YB1-positive RNA granules were not detected, and lnc-DUXA1 primarily localized within the nuclear region. However, in control stressed cells, distinct YB1-positive RNA granules were observed, marked by yellow fluorescence (AF555 staining), indicating stress granule formation. In HD non-stressed cells, small YB1-positive RNA granules were observed, and in HD stressed cells, clear colocalization between lnc-DUXA1 and YB1-positive RNA granules was seen.



d) HD stressed

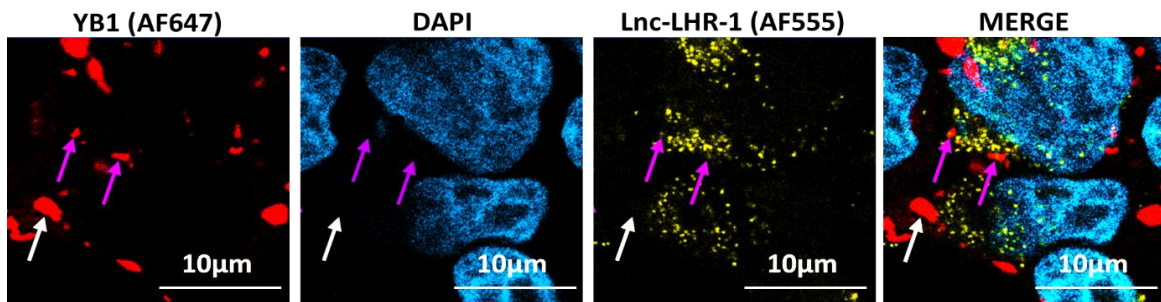
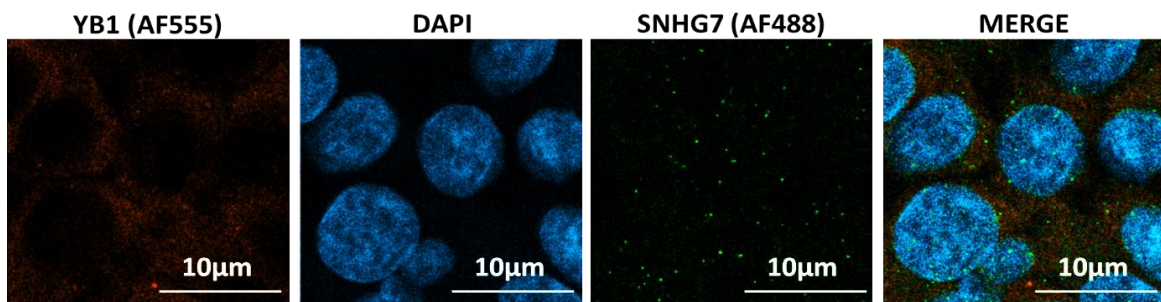
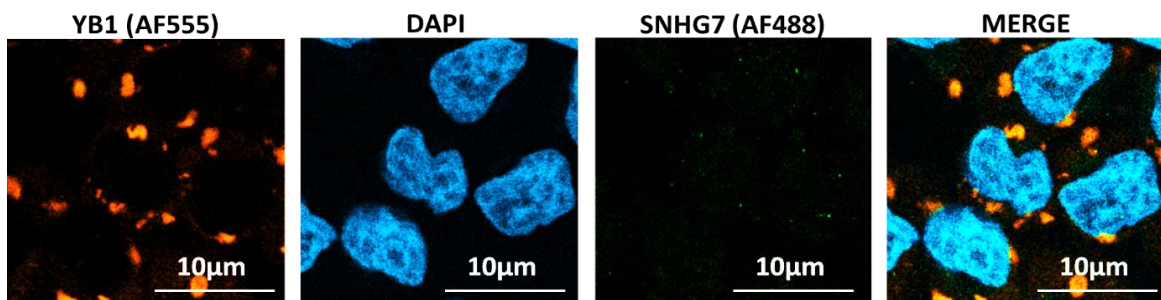


Figure 20.2: RNA-FISH analysis for lnc-LHR-1. RNA-FISH analysis for lnc-LHR-1 was performed on control (a, c) and HD (b, d) cells under non-stressed and stressed conditions using a 60X oil immersion microscope. YB1 antibody marked YB1-positive RNA granules. In HD non-stressed cells, pink arrows indicate lnc-LHR-1 probe, and white arrows mark YB1-positive granules. Under HD stress, colocalization of lnc-LHR-1 and YB1 granules is highlighted by pink arrows. In control non-stressed cells, YB1-positive granules were absent, but appeared under stress (red fluorescence, AF647). HD non-stressed cells showed small YB1 granules, with clear colocalization of lnc-LHR-1 in stressed HD cells.

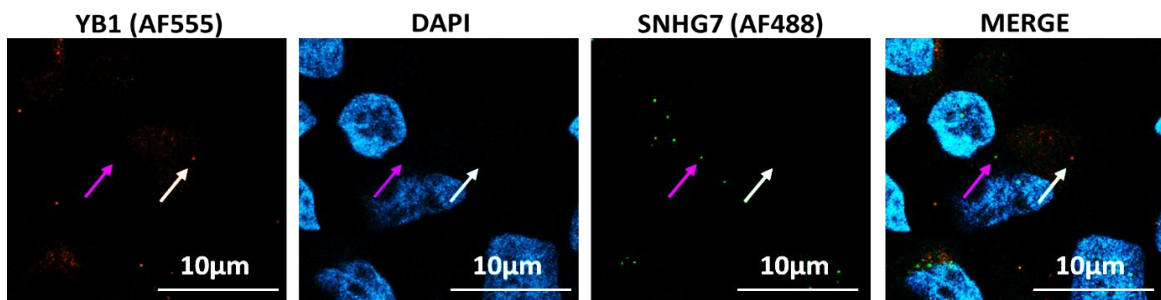
a) Control non-stressed



b) Control stressed



c) HD non-stressed



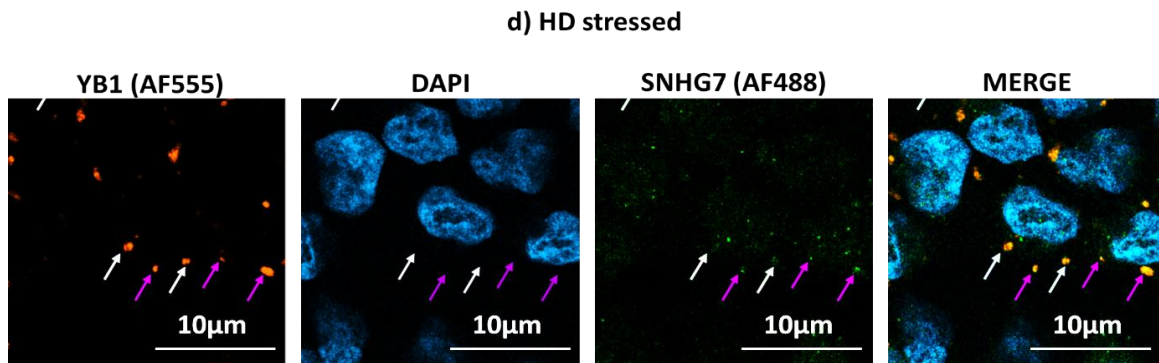


Figure 20.3: RNA-FISH analysis for SNHG7. RNA-FISH analysis for SNHG7 was performed using an oil immersion 60X microscope, capturing images under four experimental conditions: **(a)** control non-stressed cells, **(b)** control stressed cells, **(c)** HD non-stressed cells, and **(d)** HD stressed cells. In these images, YB1 antibody was used to mark YB1-positive RNA granules. The presence and colocalization of SNHG7 and YB1-positive granules were highlighted with specific color-coded arrows. In HD non-stressed cells, pink arrows indicate the location of the SNHG7 probe, while white arrows show YB1-positive RNA granules. In the HD stressed condition, colocalization of SNHG7 and YB1-positive RNA granules is marked by pink arrows, with white arrows indicating YB1-positive granules. In control non-stressed cells, YB1-positive RNA granules were not detected. However, in control stressed cells, distinct YB1-positive RNA granules were observed, marked by orange fluorescence (AF555 staining), indicating stress granule formation. In HD non-stressed cells, small YB1-positive RNA granules were observed, and in HD stressed cells, clear colocalization between SNHG7 and YB1-positive RNA granules was seen

Table 10. Coefficients of correlation in stressed control and HD cells. The top panels for **(a)** lnc-DUXA1, **(b)** LHR1-LNC1610-1, and **(c)** SNHG7 display various correlation coefficients, which provide insights into the colocalization of these transcripts with YB1-positive RNA granules. The coefficients include: **1) Pearson's correlation coefficient (PC):** This measures the linear relationship between two variables, with values ranging from -1 to +1. A value of +1 indicates a perfect positive linear relationship, whereas -1 indicates a perfect inverse linear relationship. **2) Spearman's correlation coefficient (SC):** Similar to Pearson's, but non-parametric, it also ranges between -1 and +1, where +1 indicates a perfect monotonic relationship, and -1 indicates a perfect inverse relationship and **3) Mander's coefficients M1 and M2:** These assess the overlap between two signals. M1 represents the fraction of signal A (e.g., lncRNA) overlapping with signal B (e.g., YB1-positive granules), and M2 represents the fraction of signal B overlapping with A. These correlation values were derived from six different regions of interest in the images, providing a robust quantitative analysis of the degree of colocalization between these marker RNAs and SGs under various conditions. Control stressed is abbreviated as CS and HD stressed as HS.

Sample	PC	CS	HS	SC	CS	HS	M1	CS	HS	M2	CS	HS
Lnc-DUXA1		0.06	0.07		0.01	0.03		0.17	0.45		0.45	0.08
		0.13	0.30		0.12	0.46		0.28	0.22		0.38	0.40
		0.10	0.26		0.08	0.28		0.28	0.69		0.43	0.16
		0.04	0.08		0.04	0.07		0.16	0.77		0.38	0.30
		0.10	0.08		0.08	0.07		0.28	0.77		0.43	0.30

		0.036	0.02		0.03	0.04		0.12	0.50		0.29	0.29
Lnc-LHR1		0.19	0.14		0.18	0.13		0.40	0.08		0.31	0.65
		0.17	0.36		0.17	0.49		0.44	0.30		0.51	0.77
		0.16	0.42		0.16	0.54		0.46	0.24		0.37	0.42
		0.08	0.24		0.11	0.25		0.27	0.16		0.30	0.71
		0.09	0.28		0.13	0.27		0.30	0.29		0.26	0.63
		0.05	0.35		0.07	0.38		0.36	0.12		0.27	0.90
SNHG7		0.52	0.51		0.45	0.63		0.37	0.92		0.77	0.28
		0.45	0.54		0.47	0.43		0.70	0.94		0.5	0.21
		0.38	0.66		0.37	0.59		0.53	0.94		0.53	0.41
		0.48	0.43		0.36	0.57		0.36	0.86		0.76	0.20
		0.34	0.42		0.24	0.56		0.32	0.59		0.60	0.47
		0.54	0.37		0.42	0.45		0.54	0.88		0.69	0.12

7. Identification of REST-Regulated genes in RNA Granule and sEV samples using the TFLink database

Since our data revealed that long lncRNAs constituted the highest proportion of transcripts in both sEVs and RNA granules, we turned to the literature to explore their role in HD. Previous studies have established that lncRNAs are involved in the progression of HD, particularly through the wild-type HTT protein, which regulates the nuclear translocation of the Repressor Element 1 Silencing Transcription Factor (REST). In HD, mutated HTT leads to abnormal nuclear-cytoplasmic transport of REST, a repressor of neuronal genes, causing dysregulation of its target genes [346, 415, 416].

Given this background, we sought to determine whether the transcripts we identified, particularly the abundant lncRNAs, were linked to REST regulation in HD. To explore this, we utilized the TFLink database, a tool that connects transcription factors to their target genes. Through this analysis, we discovered that 139 genes from our marker gene list were under the regulatory control of REST (**Table 11**).

Table 11.1. REST regulated genes. List of REST regulated genes across all samples.

REST regulated genes across all samples					
ABCA6	EFCAB5	MMP2	CHCHD4	LMAN2L	SLC31A2
ABCG8	EFEMP1	MPPED2	CHD2	LRR4	SLC35F2
ACACB	EGF	MTUS1	CHRM3	LRR9	SPARCL1
ACSL3	EGFR	NEIL1	CLEC16A	LRRN1	ST6GALNAC3
ACTN2	ELOVL6	NELL2	COL1A1	MARCKSL1	SYN2
ADAM9	EXOC1	NMRAL1	CORO1C	MARS1	TINF2

ANKRD1	FBXO42	NUDCD3	CPNE4	MFAP3L	TMC7
APPBP2	FNDC3B	OPA1	CPNE6	MFSD9	TMEM41A
APPL2	GABRE	OVCH1	DIAPH1	MKI67	TMEM74B
AQR	GLB1L	PDZD2	DNAAF2	MLLT10	TNFRSF14
ASAH2	GPAT3	PEX1	DNASE1	ZFP37	TSTD3
ATG2B	GPR63	PEX5L	DOC2B	ZKSCAN7	TXNIP
B3GAT2	GPR78	PHF1	DPCD	ZNF107	UBE2A
BASP1	GREB1	PIGA	ECM2	ZNF233	UNC13D
C19orf44	GSTO2	PIK3CD	EEFSEC	ZNF287	USP37
C1QTNF3	HBG2	PIK3IP1	ZDHHC5	ZNF613	UTS2B
C1R	HLA-DRB1	PLB1	WNK4	WIPI1	IQCH
CA5B	HNRNPA3	PLCB1	WBP2NL	VIL1	RNF187
CACNB4	HUNK	PLLP	CD55	KIF15	SCHIP1
CALCOCO1	IFI44	PLXNC1	CD74	KLHDC7B	SEMA3B
CAPRIN2	IFT172	RAPGEF4	CD8A	KRT5	SEMA3G
CCDC14	IGHMBP2	RETREG1	CDH10	KRTDAP	SFN
CCDC57	IGSF10	RHOQ	CDH8	L1CAM	SHISA7
CCDC80					

Table 11.2 REST regulated genes. List of REST regulated genes in HD sEVs (Top panel) and HD RNA granules (bottom panel).

REST regulated marker genes in HD sEVs							
ABCG8	CPNE6	LRR9	SCHIP1	CCDC80	HLA-DRB1	PHF1	WIPI1
ACACB	CD74	SFN	SEMA3B	RETREG1	IFT172	PLB1	WNK4
ACSL3	DOC2B	MARS1	SEMA3G	KLHDC7B	IGHMBP2	PLCB1	ZDHHC5
ACTN2	DPCD	MFAP3L	MARCKSL1	CHCHD4	IGSF10	PLLP	ZFP37
ADAM9	ECM2	MKI67	SHISA7	C19orf44	IQCH	PLXNC1	ZKSCAN7
APPL2	EFCAB5	MMP2	SPARCL1	COL1A1	KIF15	RAPGEF4	ZNF107
AQR	UBE2A	SYN2	ST6GALNAC3	WBP2NL	DNAAF2	CD55	ZNF233
ASAH2	EGF	MTUS1	MPPED2	KRTDAP	KRT5	RHOQ	
ATG2B	EGFR	NEIL1	CAPRIN2	L1CAM	ZNF613	ZNF287	
VIL1	ELOVL6	NELL2	TMEM41A	CACNB4	GREB1	PDZD2	
BASP1	EXOC1	TINF2	TNFRSF14	NMRAL1	GSTO2	PEX1	
CHD2	GLB1L	OPA1	EFEMP1	CCDC14	HBG2	PEX5L	
C1R	GPR78	CPNE4	B3GAT2	UTS2B	OVCH1	USP37	
REST regulated marker genes in HD RNA granules							
ANKRD1	IFI44	NUDCD3	PIGA	RNF187			

8. Comparison of the control and HD RNA granule and sEVs marker genes with data from HD patients

To determine whether the up- and down-regulated genes identified in our HD cell line model could also be detected in patient samples, we compared our data with a recently published dataset of HD patient plasma extracellular vesicles (EVs) by Neueder *et al.*, 2024 [393]. This dataset included RNA sequencing results from plasma EVs of patients categorized into three groups: "control," "pre-HD," and "early-HD". The patient dataset contained 330,551 genes across all samples, but only 21,848 genes (6.6%) met the abundance threshold of ≥ 10 counts in at least one sample, allowing for robust analysis. We used DESeq2 to calculate fold changes and compared the expression patterns of our HD marker genes between the cell line and patient datasets. To focus on a strong and reliable signal in the patient dataset, we applied a \log_2 fold change cutoff of ± 0.5 .

In our comparison of HD sEV marker genes and the "control" vs "pre-HD" patient samples, 66 genes were available for analysis, with 34 genes (51.5%) showing consistent fold change directions. In the comparison between HD sEV marker genes from the HD cell model and "control" vs "early-HD" patient samples, 73 genes were available, with 28 genes (38.4%) agreeing in fold change direction (**Figure 21**). This higher agreement in the "pre-HD" group suggests that our cell line model may more closely reflect the early stages of HD progression.

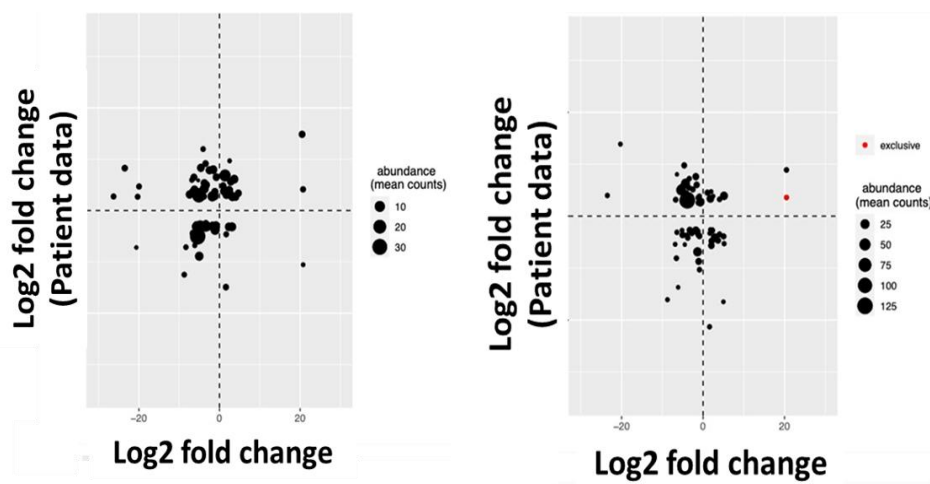


Figure 21: Comparing \log_2 fold changes of patient data with HD sEVs dataset. Control vs pre-HD (left), control vs early-HD (right). X-axis represents \log_2 fold change in patient data. Y-axis represents in data from HD sEVs. The size of the symbol mean count abundance count in patient's data. The genes marked exclusive (red) were absent in the other condition and no fold change was available. Therefore, maximal occurring fold change value was used instead of \log_2 fold change.

Collectively, our cell model system is more comparable to the state of early onset of HD since a better agreement was achieved for the pre-HD condition.

9. Mass spectroscopic data revealed gene sets present in sEVs and RNA granules

To establish a link between sEVs and RNA granules, it was important to study and understand their biomolecular composition. In addition to the above-mentioned transcriptomic analysis, proteomic analysis of control and HD sEVs and RNA granules were done. Protein quantification was performed with MaxQuant [397]. Protein identification was performed by searching against the Uniprot reference proteome (Uniprot ID 9606, downloaded on 15 April 2022) and further data analysis and visualization were performed in R (version 4.2). The obtained data were divided into the following categories:

1. Proteins **exclusively** present in **control sEVs**.
2. Proteins that are **significantly overrepresented in control sEVs** when compared to HD sEVs.
3. Proteins **exclusively** present in **HD sEVs**.
4. Proteins that are **significantly overrepresented in HD sEVs** when compared to control sEVs.
5. Proteins **exclusively** present in **control RNA granules**.
6. Proteins that are **significantly overrepresented in control RNA granules** when compared to HD RNA granules.
7. Proteins **exclusively** present in **HD RNA granules**.
8. Proteins that are **significantly overrepresented in HD RNA granules** when compared to control RNA granules.

The datasets in which proteins were overrepresented in one type were fused with their respective isolated datasets in which they were overrepresented. For instance, the proteins that were overrepresented in control sEVs when compared to HD were added to the proteins exclusively present in control sEV dataset. This was done to ease the comparative analysis of the given samples. **Appendix 3-10** show the list of proteins with P-values and fc values for the obtained sEV and RNA granule proteins.

10. sEVs and RNA granules share content in both control and HD samples

When proteins of control sEVs (253) and RNA granules (62) were compared, we found 3 proteins common between them: namely, **CAMSAP3**, **KIAA1279** and **TCEB2**. When we compared the proteins of HD sEVs (405) and RNA granules (70), we found 13 shared proteins: namely, **ABRACL**, **CHMP4A**, **COMT**, **EGFR**, **FAM171A1**, **ITGA6**, **ITGAV**, **MAN1A1**, **PWP1**, **RANBP6**, **SQSTM1**, **STK24** and **WDR1**. This indicates a distinct protein composition associated with HD, as there were no proteins common to both control and HD samples in either sEVs or RNA granules. These findings suggest that HD pathology may drive a unique molecular profile compared to control conditions (**Figure 22**).

We aimed to identify the HTT protein in our datasets to further explore its distribution in HD-related cellular components. Since mutant HTT is already known to be present in sEVs, detecting it in our sEV samples would support existing evidence of its role in intercellular spread. Additionally, finding HTT in RNA granules would suggest that HTT may contribute to altered RNA-protein interactions in HD, potentially disrupting RNA granule dynamics in disease pathology. However, HTT protein was not present in both control and HD sEV and RNA granule datasets. The absence of HTT in our mass spectrometry (MS) analysis, despite using a cell line stably expressing mutant HTT, likely stems from several factors. First, HTT may be present at low concentrations in sEVs, falling below MS detection thresholds due to the dominance of more abundant proteins. This is consistent with our inability to detect HTT in sEVs using Western blot as well, despite the sensitivity of this technique when high concentrations of target proteins are present. Second, HTT's large size and possible interactions with other proteins might also complicate its detection, especially if it's in a complex that remains undetected by MS under standard conditions. Third, mutant HTT is prone to aggregation due to its polyglutamine (polyQ) expansion. These aggregates might not efficiently solubilize during sample preparation, leading to poor recovery and detection in MS. If HTT forms high-molecular-weight aggregates, it might be lost during the fractionation or filtering steps that precede MS, especially if it is present in insoluble fractions that do not make it into the final soluble protein pool analyzed by MS.

We successfully detected HTT in RNA granules by Western blot (**Figure 22**), which suggests that HTT is more concentrated or stably associated with RNA granules than with sEVs. The

successful detection of HTT in RNA granules via Western blot confirms that HTT is present in our system, but at levels or in forms that challenge MS detection in sEVs and RNA granules.

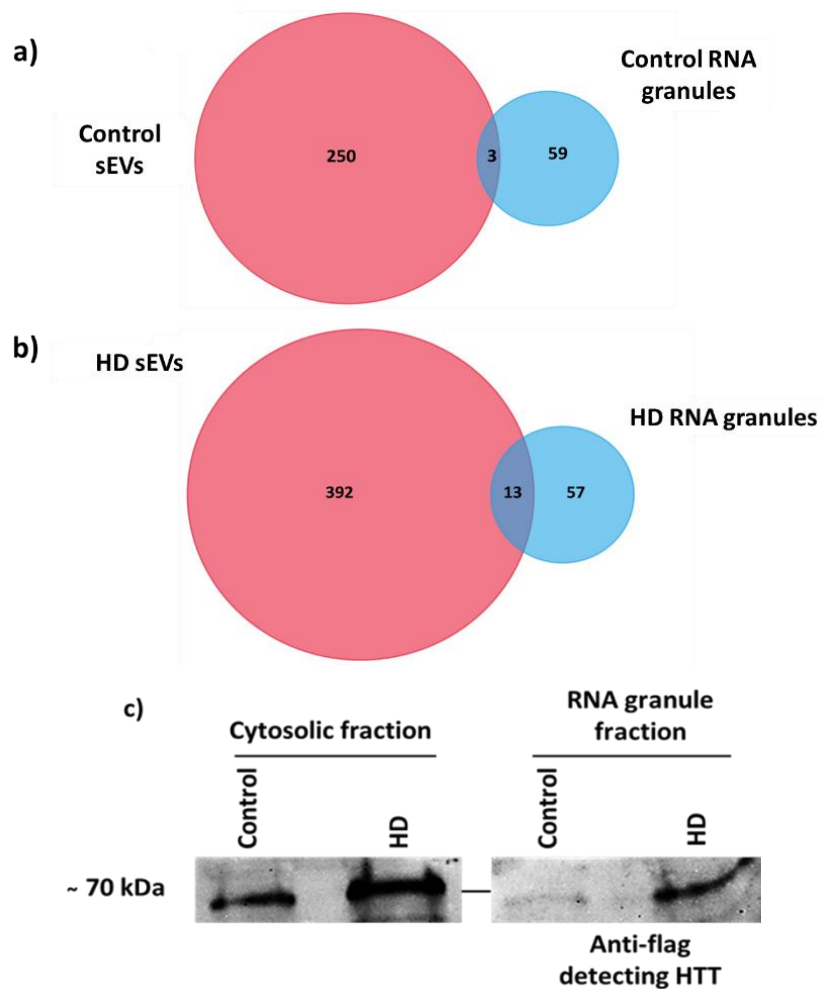


Figure 22. Comparison of proteomic content from sEVs and RNA granules. (a and b) Venn diagrams exhibit the shared content of control sEVs and RNA granules, and HD sEVs and RNA granules. **(c)** Western blot representing the presence of HTT protein in both cytosolic and RNA granule fractions of HD. The full-length HTT protein is expected at approximately 350 kDa, but we observed a band around 75 kDa, corresponding to the HTT exon 1 fragment with an 83 CAG repeat and FLAG tag. This molecular weight is consistent with the truncated exon 1 fragment, which is stably expressed in the cells used. The FLAG tag and polyglutamine expansion contribute to the observed size, confirming the presence of the HTT exon 1 fragment in both fractions.

11. Interactions network predictions between proteins of the sEV and RNA granule dataset

STRING analysis was done to investigate if there are interactions between the protein datasets from sEVs and RNA granules. STRING analysis offers a comprehensive visualization of protein-protein interactions, facilitating the examination of functional relationships among proteins within a dataset. The resulting network comprises nodes that represent individual proteins and edges that signify their interactions, providing insights into the strength and significance

of these connections. This analysis produces various enrichment statistics, including PPI enrichment p-values, which assess the probability of the observed interactions occurring by chance. Additionally, Gene Ontology (GO) terms are utilized to classify proteins based on their biological functions, cellular locations, and molecular processes, while also identifying functional enrichments that underscore important biological themes pertinent to the condition under study.

This analysis was done at an interaction score of 0.9 which is the highest confidence level at which the interaction is considered true according to the available evidence. This leads to the elimination of false positives to a great extent. Weak interaction sources like text mining and neighbourhood were eliminated to further strengthen the analysis. The disconnected nodes of the network were kept hidden.

STRING analysis revealed that there are several protein-protein interactions between proteins of each control dataset for sEVs and RNA granules (**Figures 23 and 25**). Such an enrichment indicates that the proteins are at least partially biologically connected. However, there were no interactions found between the 3 common proteins between Control sEVs and RNA granules.

A small interaction network was observed upon running STRING analysis with proteins of HD RNA granules (**Figure 24**) with an PPI enrichment value of 0.339. This relatively high p-value suggests reduced connectivity.

In control samples, RNA granule-associated proteins exhibit robust functional connectivity, as demonstrated by STRING analysis with a significant Protein-protein interaction (PPI) enrichment p-value of 0.00805. This suggests an organized network of protein-protein interactions essential for maintaining RNA metabolism and cellular homeostasis. However, in HD, this network might be substantially compromised, with a PPI enrichment p-value of 0.339, indicating a marked reduction in protein interactions within RNA granules. The loss of connectivity in HD likely reflects the disruptive effects of mHTT on RNA-binding proteins and their associated complexes. This disorganization may impair critical cellular functions such as RNA transport, splicing, and stress granule assembly, contributing to the dysfunction in RNA metabolism observed in HD. The weakened PPI network underscores the role of mHTT in destabilizing protein complexes, which may intensify neurodegenerative processes by

disrupting the regulatory mechanisms required for cellular stress responses and overall proteostasis.

A robust interaction network was observed in both control and HD sEV datasets following STRING analysis (**Figures 25 and 26**). Control sEVs exhibited significantly more interactions than expected, with a PPI enrichment p-value of 0.000291, while HD sEVs showed an even higher level of interaction, with a PPI enrichment p-value of 3.71×10^{-5} .

These enrichment values indicate that the proteins within both datasets are strongly biologically connected, reflecting well-organized, functionally relevant networks in both normal and disease states. Notably, in HD, the interaction network within sEVs becomes even stronger, contrasting with the reduced connectivity observed in HD RNA granules, where protein interactions are significantly weakened. This indicates that while HD disrupts RNA granule-associated protein networks, leading to impaired RNA processing, the sEV protein network remains highly active, possibly reflecting the packaging of disease-associated proteins into sEVs for export or cell-to-cell communication. This stronger interaction in HD sEVs may play a critical role in the pathogenesis of HD, suggesting an adaptive or pathological mechanism through which cells respond to the accumulation of mHTT.

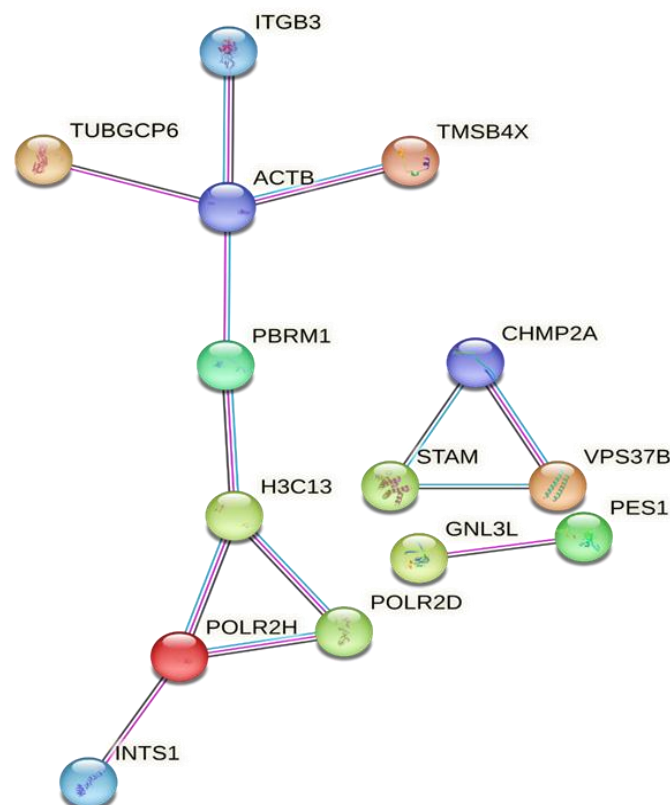


Figure 23: STRING analysis of control RNA granule proteins. STRING analysis of control RNA granules show significantly more interactions than expected with a PPI enrichment p-value of 0.00805. The blue line between the nodes indicates databases as source, the pink line indicates experimentally determined source of interactions, and the black line represents co-expression as a source.

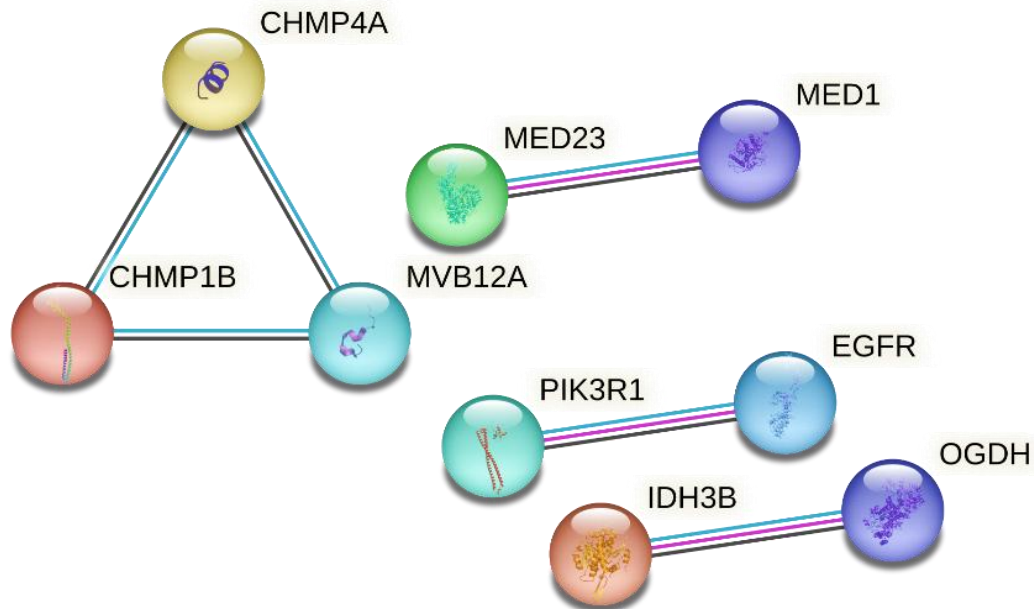


Figure 24: STRING analysis of HD RNA granules. STRING analysis of HD RNA granules showed significantly less interactions than expected with a PPI enrichment p-value of 0.339. The blue line between the nodes indicates databases as source, the pink line indicates experimentally determined source of interactions, and the black line represents co-expression as a source.

In summary, STRING analysis reveals contrasting dynamics between HD sEVs and RNA granules. While RNA granules in HD show reduced connectivity, HD sEVs exhibit stronger protein interactions compared to controls, suggesting their active role in disease progression. This may reflect the packaging of disease-associated proteins into sEVs for intercellular communication, indicating that while mHTT disrupts RNA granules, sEVs may serve as an adaptive or pathological response to cellular stress in HD.

12. Pathway and Interaction Network Analysis of sEV and RNA Granule Proteomes in HD

STRING and KEGG pathway analyses were performed on our samples to explore the functional interactions and biological pathways associated with proteins in sEVs and RNA granules in both control and HD conditions. Given that HD is marked by disruptions in protein networks, particularly those involved in RNA metabolism, these analyses aimed to uncover how mHTT affects protein-protein interactions and cellular pathways.

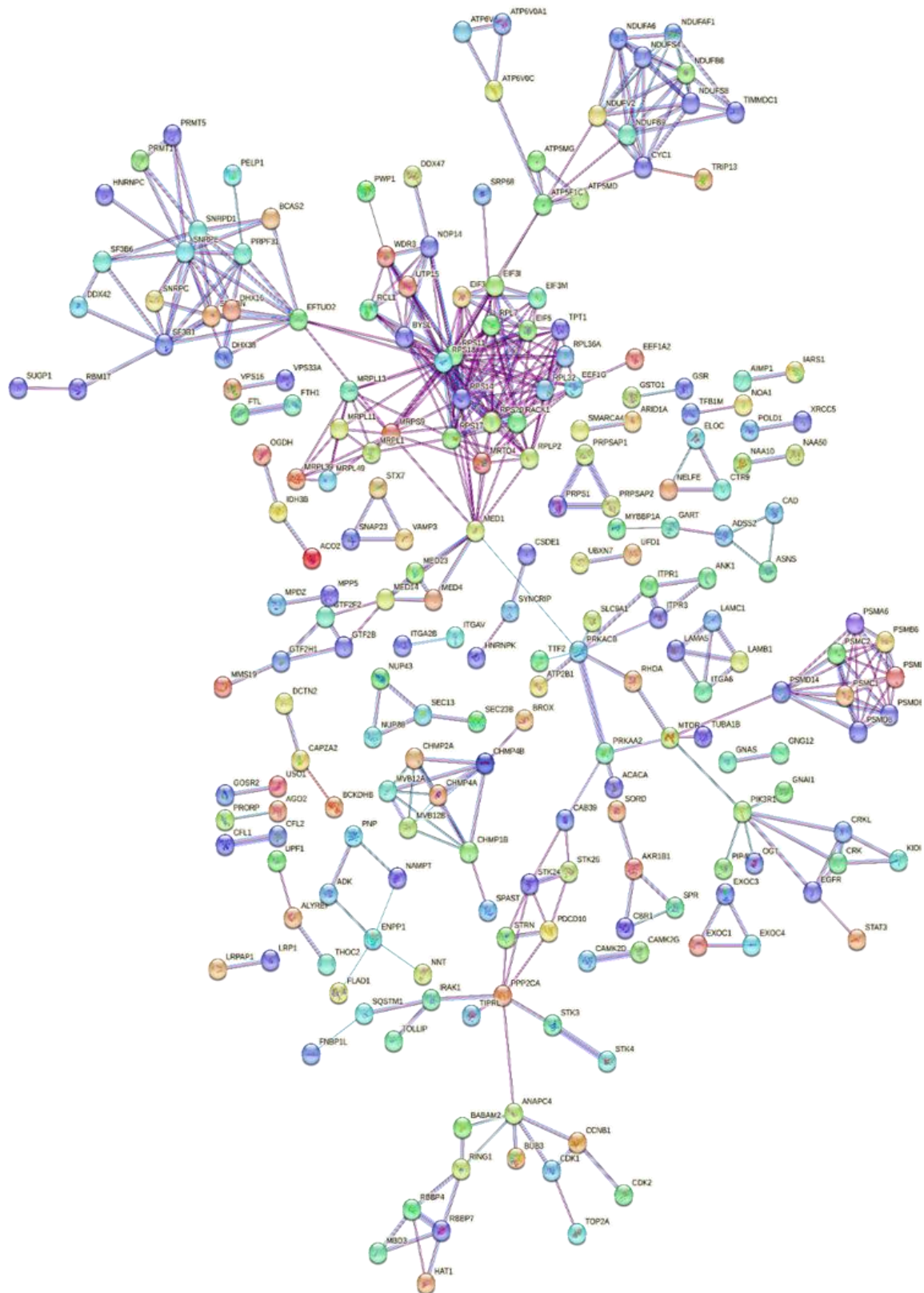


Figure 26: STRING analysis of HD sEVs. STRING analysis of HD sEVs show significantly more interactions than expected with a PPI enrichment p-value of $3.71e-05$. The light blue and the dark lines between the nodes indicate databases and gene co-occurrences as source respectively, the pink line indicates experimentally determined source of interactions, violet coloured line indicates protein homology as a source of network and the black line represents co-expression as a source.

Upon analyzing the functional enrichments in the STRING network of HD sEVs, we identified the GO term "Huntington's Disease," indicating a relevant biological connection between the proteins involved. The network displayed for the GO term "Huntington's Disease" had significantly more interactions than expected, with a PPI enrichment value of $< 1.0e-16$, underscoring the strong biological relevance of these protein interactions.

In **Figure 27** we observe the network of proteins associated with HD, identified under the GO term "Huntington's Disease," which emerged during the functional enrichment analysis of the HD sEVs dataset. The functional enrichment of this network (the GO term "Huntington's Disease") revealed connections to several other neurodegenerative disorders, including Parkinson's disease (PD), Alzheimer's disease (AD), and Amyotrophic Lateral Sclerosis (ALS). Additionally, the analysis indicated associations with psychotic symptoms such as lethargy, confusion and abnormal behaviour, suggesting that these proteins may play roles in a broader spectrum of neurological and psychiatric conditions. These connections are visually mapped in the STRING interaction network, where proteins are color-coded according to their corresponding GO terms. A detailed explanation of each GO term and its corresponding colour code is provided in the table below.

KEGG analysis revealed significant hits for multiple neurodegenerative disorders when both HD sEV and RNA granule datasets were analysed. These hits highlight pathways associated with HD, as well as other related neurodegenerative conditions such as Parkinson's disease (PD), Alzheimer's disease (AD), and Amyotrophic Lateral Sclerosis (ALS). This suggests that the proteins in these datasets are not only involved in HD pathology but may also share molecular mechanisms with a broader spectrum of neurodegenerative diseases, reinforcing the interconnected nature of these conditions at the pathway level (**Appendix 11 and 12**).

Of the proteins that were present in both HD sEVs and RNA granules, COMT showed a hit for obsessive-compulsive disorder, CHMP4A showed a hit for necroptosis and SQSTM1 showed links with ALS, necroptosis, frontotemporal dementia and the GO term, pathways of neurodegeneration - multiple diseases. When KEGG analysis on the control datasets were run, no hits for neurodegenerative diseases in control RNA granules were seen. Some hits for neurological disorders were found in the control sEV proteome. However, these were not neurodegenerative diseases, but mostly either hereditary disorders, or defects at birth (**Appendix 13**). In summary, we found that the HD dataset is connected to neurodegenerative

disorders signifying a corrupted proteome in the sEVs and RNA granules when compared to the control.

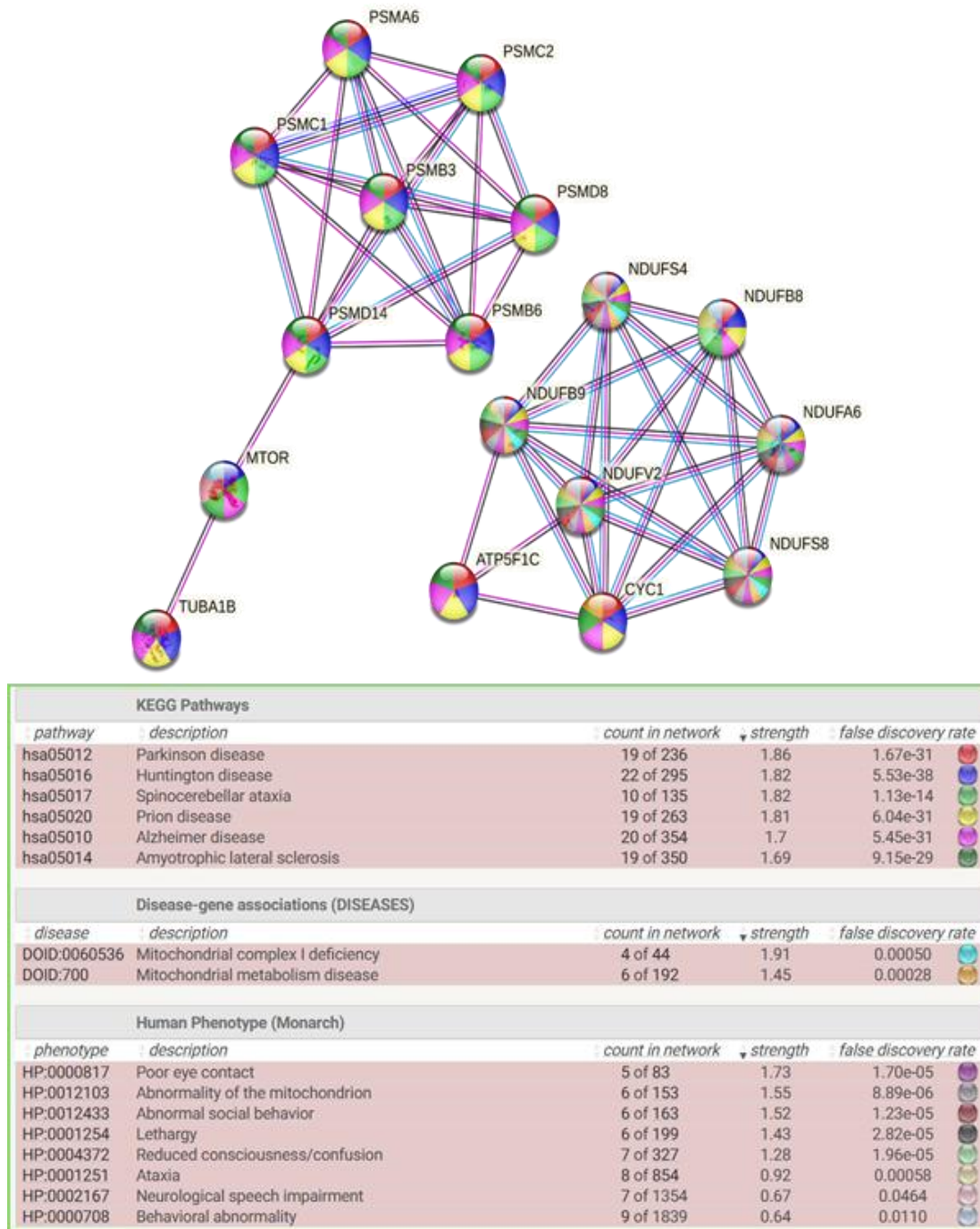


Figure 27: STRING analysis. The STRING analysis of HD sEVs revealed the GO term "Huntington's Disease" upon functional enrichment, with significantly more interactions than expected, indicated by a PPI enrichment p-value of < 1.0e-16. The functional enrichment highlighted the proteins' associations with several diseases. Different colours in the nodes represent various GO terms, with the colour codes displayed in the extreme right of the lower panel. The connections between the nodes are shown using different line colours: light blue for database-sourced interactions, dark lines for gene co-occurrences, pink for experimentally determined interactions, violet for protein homology, and black for co-expression. The table in the lower panel lists the associated disorders

with their **false discovery rates (FDR)**, where the low FDR values reflect the high significance of these associations. In STRING functional enrichment analysis, "**count in network**" refers to the number of proteins from the dataset linked to a specific GO term or pathway. "**Strength**" measures the enrichment level of proteins within that term, where higher values indicate stronger associations; typical strength values range from small positive numbers, indicating weak enrichment, to larger values (above 1.5), showing stronger enrichment. The FDR assesses the statistical significance of the enrichment, with lower FDR values (<0.05) indicating high confidence that the enrichment is biologically meaningful rather than due to chance.

13. Functional Enrichment Analysis Revealed RNA Granule-Related GO Terms in sEV Dataset and sEV-Related GO Terms in RNA Granule Dataset

Functional enrichment analysis is a powerful tool used to identify overrepresented biological functions, pathways, or processes within a dataset of genes or proteins. This type of analysis often involves looking for GO terms or pathway associations to see how a dataset corresponds to known biological functions. HumanCyc.org is a curated database that provides information about human metabolic pathways and gene functions [412]. It runs functional enrichment analysis on datasets to identify connections to metabolic pathways, molecular functions or processes known to humans.

The aim of this analysis was to examine whether there are shared biological pathways between sEVs and RNA granules. By running functional enrichment analysis on datasets from sEVs and RNA granules, we sought to uncover any overlapping or cross-functional GO terms that may provide insight into the relationship between these two cellular components.

When performing the analysis on HumanCyc, we found notable overlaps between the sEV and RNA granule fractions. GO terms related to RNA granules, such as intracellular non-membrane-bounded organelle, stress granule, P-body, and ribonucleoprotein granule, were identified in the control sEV datasets. Conversely, GO terms associated with sEV biogenesis, such as multivesicular body assembly and the ESCRT complex, were detected within the control RNA granule dataset (**Appendix 14 and 15**). This cross-appearance of GO terms in the opposite fractions suggests a potential functional interaction or shared pathway between sEVs and RNA granules, which may reflect their coordinated role in the transport, processing, and regulation of RNA.

Upon performing enrichment analysis on HD datasets, a recurring pattern of cross-associated GO terms emerged, indicating substantial interaction between RNA granules and sEVs. Several

key GO terms were identified in the proteins overrepresented in HD sEVs, such as P-body, nuclear speck, Cajal body, U4 snRNP, cytoplasmic ribonucleoprotein granule, ribonucleoprotein complex biogenesis, and supramolecular complex (**Appendix 16**). These terms point to components involved in RNA metabolism, RNA-protein granule assembly, and stress responses. Interestingly, while these proteins were not directly identified in our HD RNA granule dataset, their presence in sEVs suggests they may still play functional roles in the dynamic interactions between sEVs and RNA granules.

The presence of both nuclear and cytoplasmic RNA granule-associated GO terms within both control and HD sEVs strongly hints at an exchange or interaction between these cellular structures. RNA granules play a role in managing RNA transport and stability, and recent research suggests that sEVs might aid in cellular communication by carrying RNA and RNA-binding proteins. For instance, cytoplasmic RNA granules, like SGs and p-bodies, frequently share proteins and RNA molecules with nuclear RNA granules, such as nuclear specks and Cajal bodies, which function in RNA processing and gene expression regulation in the nucleus [413]. This sharing of protein components underscores the dynamic nature of RNA granules, especially in response to cellular stress, and suggests that RNA granules may be linked through both direct intracellular trafficking and indirect intercellular transport via sEVs.

The identification of GO terms like "membrane-bounded organelle," "extracellular exosome," "extracellular vesicle," and "ESCRT complex" in RNA granules from the HD dataset reinforces the idea that proteins traditionally associated with RNA granules could be packaged into sEVs as part of cellular communication (**Appendix 17**). This pattern is evident even in healthy conditions, where functional enrichment reflects shared biological roles between sEVs and RNA granules despite the lack of direct protein overlap.

In essence, the identification of GO terms related to both nuclear and cytoplasmic RNA granules in the control and HD sEV datasets—and the presence of sEV-related GO terms in the control and HD RNA granule datasets—suggests a complex interplay between these cellular compartments. This interaction could mean that even when proteins are not physically present in both datasets, the underlying functional connections still exist, allowing for RNA metabolism and cellular transport processes to be coordinated across these structures. The shared GO terms further imply that cellular communication and regulation of RNA dynamics may involve a collaborative network between sEVs and RNA granules, potentially influencing

the pathophysiology of conditions such as HD. Distinct Protein Associations in Shared Signaling Pathways of sEVs and RNA Granules

14. Distinct Protein Associations in Shared Signaling Pathways of sEVs and RNA Granules

In our study, we aimed to investigate the biological pathways associated with proteins found in sEVs and RNA granules to understand their potential roles in HD pathology. To achieve this, we conducted KEGG pathway analysis, a powerful tool used to map proteins to key biological pathways and assess their functional relevance. This approach allowed us to examine how sEVs and RNA granules contribute to cellular processes in both control and HD conditions. A noteworthy pattern emerged during the analysis: while several signaling pathways were consistently identified in both control and HD datasets, the specific proteins linked to these pathways differed significantly between the two conditions. Pathways such as Hippo, MAPK, AMPK, JAK-STAT, and mTOR, which are central to cellular regulation—including processes like cell growth, apoptosis, metabolism, and stress responses—were enriched in both sEVs and RNA granules (**Table 12 and 13**). However, the distinct protein associations within these pathways between the control and HD datasets highlight the profound impact of HD on cellular function. This finding suggests that sEV cargo and RNA granule composition are not static but are dynamically influenced by the disease state. One key discovery was the presence of the JAK/STAT3 pathway in HD sEVs and RNA granules. Inhibition of this pathway is known to increase the formation of mHTT aggregates, suggesting that both sEVs and RNA granules may play a role in regulating the pathological accumulation of toxic proteins in HD [410]. This observation underscores the potential involvement of these structures in HD pathogenesis, particularly in how they modulate signaling pathways that govern cellular stress and protein aggregation. In conclusion, KEGG analysis revealed that sEVs and RNA granules, while sharing common signaling pathways, differ markedly in their protein composition between control and HD conditions. This differential protein association highlights the influence of the disease state on protein loading into sEVs and RNA granule dynamics. These findings suggest that sEVs and RNA granules may be pivotal in regulating key processes such as RNA metabolism, intercellular communication, and stress signaling in HD. The alteration of these pathways in HD offers potential insights into therapeutic strategies targeting these mechanisms to mitigate disease progression.

Table 12. Pathway Proteins in Control and HD sEVs. This table presents the results of KEGG pathway analysis, illustrating the proteins identified in control and HD sEVs associated with specific signaling pathways. The pathways listed in the first column are labeled using their unique KEGG identifiers, with "hsa" denoting the human organism (*Homo sapiens*) followed by the specific pathway number. The second and third columns list the proteins found in control and HD sEVs, respectively, that are linked to each pathway. This comparison reveals distinct differences in protein composition between control and HD conditions within the same signaling pathways, suggesting that HD influences protein loading into sEVs.

Pathway	Control sEVs	HD sEVs
hsa04666 Fc gamma R-mediated phagocytosis	MARCKSL1	CFL1
	ARPC2	CFL2
		CRKL
		CRK
hsa03015 mRNA surveillance pathway	CASC3	PPP2CA
	PPP2R2A	EIF3I
	CPSF1	ALYREF
	CPSF2	GSPT2
	RBM8A	
hsa04151 PI3K-Akt signaling pathway	EIF4E2	EGFR
	TP53	ITGAV
	PPP2R2A	LAMB1
	CDC37	ITGA6
	RPTOR	CDK2
		PPP2CA
		GNG12
		COL2A1
hsa04066 HIF-1 signaling pathway	EIF4E2	EGFR
	HK1	STAT3
	HMOX1	CAMK2G
hsa04150 mTOR signaling pathway	EIF4E2	PRKAA2
	RICTOR	SEC13
	RPTOR	MTOR
	TELO2	CAB39
hsa04310 Wnt signaling pathway	TP53	PRKACB
	CUL1	CAMK2G
	CSNK2A2	
hsa04010 MAPK signaling pathway	TP53	GNG12
	STMN1	EGFR
	TRAF2	PRKACB
		CRK
		CRKL

		IRAK1
		STK3
hsa04071 Sphingolipid signaling pathway	PPP2R2A	CERS2
	CTSD	PPP2CA
	TRAF2	GNAI1
	TP53	
hsa04621 NOD-like receptor signaling pathway	STAT1	GNAI1
	TRAF2	CERS2
	MCU	PPP2CA
		NAMPT
		ITPR1
		ITPR3
		TRIP6
hsa04630 JAK-STAT signaling pathway	STAT1	MTOR
		EGFR
		STAT3
hsa04152 AMPK signaling pathway	PPP2R2A	PRKAA2
	RPTOR	PPP2CA
		ACACA
		CAB39
		MTOR
hsa04390 Hippo signaling pathway	PARD3	DLG1
	PPP2R2A	NF2
	TP53BP2	PPP2CA
	AMOT	STK3
		YWHAG
hsa04064 NF-kappa B signaling pathway	TRAF2	IRAK1
	CSNK2A2	

Table 13. Pathway Proteins in Control and HD RNA granules. This table presents the results of KEGG pathway analysis, illustrating the proteins identified in control and HD RNA granules associated with specific signaling pathways. The pathways listed in the first column are labeled using their unique KEGG identifiers, with "hsa" denoting the human organism (Homo sapiens) followed by the specific pathway number. The second and third columns list the proteins found in control and HD RNA granules, respectively, that are linked to each pathway. This comparison reveals distinct differences in protein composition between control and HD conditions within the same signaling pathways, suggesting that HD influences protein loading into RNA granules.

Pathway	Control RNA granules	HD RNA granules
hsa04151 PI3K-Akt signaling pathway	ITGB3	EGFR
		ITGAV
		ITGA6
		PIK3R1

hsa04150 mTOR signaling pathway	ATP6V1H	PIK3R1
		ATP6V1E1
		RHOA
		SLC7A5
hsa04630 JAK-STAT signaling pathway	STAM	EGFR
		PIK3R1
hsa04810 Regulation of actin cytoskeleton	ACTB	ABI2
	ITGB3	EGFR
	TMSB4X	ITGAV
	RAP1	ITGA6
		RHOA
		PIK3R1
hsa04015 Rap1 signaling pathway	ITGB3	EGFR
	ACTB	RHOA
		PIK3R1

15. Proteins present in HD RNA granules and sEVs also bind to mutant *HTT-RNA*

We compared our dataset with the findings of Schilling *et al.*, 2019 [396] to build on their extensive identification of proteins that bind to mutant *HTT-RNA* and to contextualize our results within the broader landscape of HD research.

Schilling *et al.* identified 509 proteins that associate with *mHTT-RNA*, providing a critical resource for investigating how mutant *HTT* impacts cellular pathways and contributes to disease progression. By aligning our datasets of sEVs and RNA granules from HD models with their *mHTT-RNA* binding proteins, we aimed to identify shared molecular players that could offer insights into the roles of RNA-binding proteins in HD.

Our analysis revealed 49 proteins from the Schilling *et al.* dataset that were also localized within HD sEVs, suggesting that these vesicles may serve as carriers for RNA-protein complexes associated with mutant *HTT*. Interestingly, only one protein—**WDR1**—was found across all three datasets: Schilling *et al.*'s *mHTT-RNA* interactome, our HD sEV dataset, and our RNA granule dataset.

This overlap highlights WDR1 as a potential key player in HD pathology. The presence of multiple proteins associated with *mHTT-RNA* in HD sEVs suggests that, in the disease state, sEVs may actively package and transport the abnormal RNA-protein aggregates formed due to the hairpin structures of mutant *HTT* RNA. This points to a novel hypothesis: in HD, sEVs

could contribute to disease spread by exporting these aberrant RNA-protein complexes to neighboring cells (**Figure 28**).

Additionally, when comparing our data to Schilling *et al.*'s study, which identified 32 spliceosomal proteins bound to *mHTT*-RNA, we found five of these proteins, namely; **splicing factor 3b subunit 1 (SF3B1)**, **elongation factor Tu GTP-binding domain containing 2 (EFTUD2)**, **Heterogeneous Nuclear Ribonucleoprotein C (HNRPC)**, **small nuclear ribonucleoprotein D1 polypeptide (SNRPD1)**, and **pre-mRNA processing factor 31 (PRPF31)** present in HD sEVs. This overlap suggests that sEVs may also play a role in the dysregulation of RNA splicing pathways in HD, further supporting the idea that these vesicles are involved in RNA processing disturbances in the disease. By comparing our results to the established protein interactomes from Schilling *et al.*, 2019 we identified a set of previously underexplored proteins that may play critical roles in HD pathology. This comparison strengthens the hypothesis that sEVs in HD are involved in packaging and possibly spreading mutant RNA-protein aggregates, providing new avenues for investigating therapeutic strategies targeting sEV-mediated disease mechanisms [414].

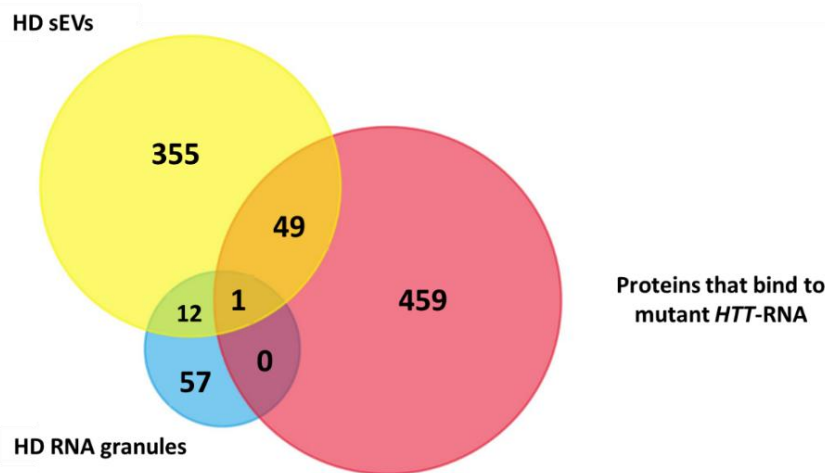


Figure 28. Venn diagram representing the overlapping between HD sEVs, RNA granules and proteins that bind to mutant HTT - RNA. The Venn diagram reveals that only one protein, WDR1, is shared between all three datasets, highlighting its unique role. Its presence in all three datasets suggests that WDR1 may play a pivotal role in the intersection of RNA metabolism, intercellular communication via sEVs, and the pathological processes involving mutant HTT-RNA. WDR1 could be a critical mediator of HD pathology by influencing both intracellular and intercellular dynamics. This overlap hints at WDR1's potential involvement in both RNA granule formation and sEV-mediated RNA/protein transport, possibly linking intracellular RNA granule activity with extracellular signaling in HD. The presence of WDR1 in mutant *HTT*-RBPs also suggests it might influence the regulation or transport of HTT-related mRNA, making it a candidate for further exploration as a target for modulating HD pathology.

DISCUSSCION

HD is a progressive neurodegenerative disorder. Generally, most early symptoms include psychiatric disorders like anxiety and depression. Suicide rate is very high among patients and therefore, diagnosis is challenging. To date, diagnosis is only done by genetic testing and the treatment is of palliative nature only. Several studies have individually investigated and reported the role of RNA granules and sEVs upon HD. RNA granules and sEVs are integral for the regulation and function of cells. RNA granule formation and increased sEV secretion are the cell's way to respond towards stress. RNA granules and sEVs have multiple common features like the involvement of LLPS, site of origin and cargo and a combined study of their molecular cargo is missing. Since both sEVs and RNA granules contribute towards the progression of HD, their molecular cargo can be used as markers of progression of the disease [79, 271, 357, 366, 371]. Therefore, in order to establish a link between sEVs and RNA granules and investigate their transcriptome and proteome upon the expression of mutant *HTT*, we isolated sEVs and RNA granules from an HD cell model.

Both HTT protein and RNA are known to be secreted via EVs [368, 370, 415]. Supporting this, HEK293T cells overexpressing polyQ-expanded HTT-GFP fusion constructs have been shown to release EVs containing both the polyQ-HTT protein and its corresponding RNA [416]. Consistent with these findings, HTT transcripts were detected across all our samples. However, our quantitative analysis revealed a trend towards increased abundance of mHTT in HD RNA granules and decreased abundance in HD sEVs which aligns with our proteomics data. Although HTT was not among the overrepresented proteins in our dataset, we confirmed its presence in RNA granule samples via Western blot, but we did not detect it in sEVs, possibly due to its low abundance in these vesicles. This suggests that mHTT may be preferentially retained and stored intracellularly within RNA granules rather than being actively sorted and secreted via sEVs. These findings highlight a potential mechanism by which cells attempt to manage the toxic effects of mutant HTT by sequestering it in RNA granules, potentially reducing its extracellular spread and associated neurotoxicity. Further research is needed to understand the implications of this differential sorting and its impact on HD pathology and progression.

Our findings reveal a distinct profile of transcripts in the sEVs and RNA granules of HD samples. From this dataset, we selected the top five transcripts based on their abundance levels for further validation using qPCR. In RNA granules, all five marker genes showed a confirmed

increase in HD samples. For sEVs, while an increase was observed across all experiments, two of the five transcripts did not reach statistical significance due to high variability between replicates. This variability highlights a potential limitation in using sEVs as reliable diagnostic markers for HD. Supporting this, a study examining sEVs secreted from platelets of HD patients at various disease stages found that platelets do not consistently secrete sEVs containing valuable biomarkers [417]. These findings suggest that while RNA granules may serve as more stable indicators for HD, the use of sEVs for diagnostic purposes requires further refinement and validation to address the variability and improve reliability.

Generally, RNA granules, such as SGs formed in response to arsenite treatment, consist of both cytosolic proteins and RNAs, with a higher proportion of RNAs compared to proteins relative to the cytoplasm [101, 151]. Our transcriptomic analysis of RNA granule cores formed under stress conditions aligns with this, as various RNA species, including mRNAs and lncRNAs, are known to localize within these granules [418]. Although both mRNAs and ncRNAs can be directed to SGs, their targeting efficiency can vary, with some reaching up to 95% [101]. In our study, we investigated the localization of top three HD marker transcripts based on abundance rates and found that the tested transcripts were only partially localized to intracellular RNA granules under stress conditions, with a significant portion remaining in the cytoplasm outside of these granules. This specific transcript profile highlights how RNA sorting into these cellular compartments is affected by HD, potentially reflecting altered RNA processing or storage mechanisms in the disease. This distinct signature could provide insights into the differential roles of RNA granules and sEVs in HD and inform future research into their potential as biomarkers or therapeutic targets.

1. lncRNAs and REST

Our transcriptomic data revealed **ncRNAs** as the largest chunk of RNAs in both RNA granules and in sEVs. ncRNAs are being exploited for their diagnostic and therapeutic qualities in several neurodegenerative disorders [419]. Among ncRNAs, several microRNAs (miRNAs) have been identified as dysregulated in HD, specifically involved in neurodegeneration and cellular stress pathways. Chang *et al.* (2017) found that miR-218, miR-196a, and miR-486 were highly expressed in the pathological region (Brodmann area 4), while miR-132, miR-9, miR-124a, miR-29b, and miR-22 showed reduced expression. Martí *et al.* (2010) reported additional changes, with miR-100, miR-16, and miR-451 upregulated in HD-affected brain regions, and miR-128,

miR-222, and miR-139-3p downregulated. Studies, including those by Johnson and Buckley (2009) and Kocerha *et al.* (2014), indicate that miRNAs may influence HD pathogenesis, particularly through targets like HIP-1 and SP-1, underscoring their role in HD progression [420-428].

Given that our HD cell model expresses mutant HTT exon 1 with a high CAG repeat count, we anticipated the presence of miRNAs like miR-27a, miR-124, miR-196a, and miR-128 due to their established links to HD pathology. However, we detected only a few miRNAs in the RNA granule samples and none in the sEV samples. This discrepancy may result from the lower read abundance (approximately threefold lower) and reduced quality (13.5% fewer reads passing quality filtering) observed in sEV samples compared to RNA granule samples. Supporting this, a study suggests that around 76% of sEV content is coding RNA, with non-coding RNA, primarily lncRNAs, making up about 21%, which leaves little room for capturing miRNAs in sEVs [429]. This finding aligns with our observations and may explain why HD-associated miRNAs were detectable only in RNA granules, where they contribute to RNA metabolism and stress response pathways.

On the contrary, our dataset showed highest abundance rates for **long non-coding RNAs (lncRNAs)** both in the control and HD samples. lncRNAs are highly conserved ncRNAs which are more than 200 nucleotides long. lncRNAs are sites for intermolecular interactions due to their nature of forming complex secondary structures. These interactions are crucial for various biological functions, including cell growth, development, proliferation, differentiation, and apoptosis [430-432]. lncRNAs engage with biomolecules, including proteins and miRNAs, to influence their target expression at the genetic, transcriptional, and post-transcriptional stages. Given that lncRNAs play a role in numerous biological processes, their dysregulation is linked to the development of various neurodegenerative disorders, including HD [433].

Multiple studies have confirmed the involvement of lncRNAs in the progression of HD. One example is the HTT-dependent nuclear translocation of the **Repressor element 1 silencing transcription factor (REST)**. HTT mutations lead to aberrant nuclear-cytoplasmic transport of REST, a transcriptional repressor resulting in the abnormal expression of its target genes [298, 434, 435]. Given that mutant HTT is known to influence the expression of REST target genes, one might expect to detect a higher number of these genes in HD samples, particularly in cellular compartments like RNA granules and sEVs. Interestingly, our analysis of the dataset

using the TFlink database identified 139 genes under the regulatory control of REST. Of these, 104 genes (98 in sEVs and 5 in RNA granules) were detected in HD samples, emphasizing the relevance of REST signaling in HD. Supporting this, other studies have shown that in patients with HD, the expression of the lncRNA **Human Accelerated Region 1 (HAR1)** is reduced in the striatum. This reduction is caused by an increased translocation of REST into the nucleus, which inhibits HAR1 transcription [436]. This reduction aligns with the idea that mutant HTT leads to increased expression of REST target genes, potentially driving a compensatory response from the cell to manage these aberrantly expressed transcripts. Thus, one might hypothesize that the increased presence of REST target genes in RNA granules and sEVs could represent an attempt by the cell to clear or regulate these disrupted transcripts as part of its stress response mechanisms.

The presence of transcripts of over 100 REST regulated genes in HD sEVs and RNA granules and only a handful in the control samples show the importance of REST mediated signalling upon HD. Also, when comparing the list of REST-regulated genes with our proteomic data from HD sEVs and RNA granules, we identified two common genes: **Epidermal Growth Factor Receptor (EGFR)** and **Exocyst Complex Component 1 (EXOC1)**.

This result aligns with known HD pathology, where REST's dysregulation affects both neurodevelopmental and neuroprotective functions [437]. EGFR and EXOC1's presence in HD samples, rather than in controls, may suggest an HD-specific regulatory shift. EGFR, for instance, plays a role in neuronal survival and is implicated in neurodegenerative conditions [438], while EXOC1 is involved in intracellular transport, a process often disrupted in HD [439, 440]. Their inclusion in HD sEVs and RNA granules may reflect HD cells' attempt to modulate neuroprotective and transport-related pathways to cope with mutant HTT-induced stress, marking them as potential targets for further study. Given that REST regulates not only protein-coding genes but also lncRNAs and miRNAs, further investigation into this dataset could deepen our understanding of REST's expanded regulatory role in HD, revealing potential points for therapeutic intervention.

Similarly, the expression of other lncRNAs, such as NEAT1 and MEG3, is also disrupted in HD due to abnormal nuclear translocation of REST [441-443]. Notably, NEAT1 has neuroprotective properties in HD and has been reported to be overexpressed in the brains of HD patients and in R6/2 mice models [444]. Given NEAT1's elevated expression in HD, we would expect to see

higher levels of this lncRNA in HD samples. However, in our dataset, NEAT1 was found only in the control sEV samples and was absent from the HD sEVs.

This pattern could suggest that although Nuclear Paraspeckle Assembly Transcript 1 (NEAT1) is upregulated in HD cells, it may be selectively retained within the cell rather than packaged into sEVs for secretion. Since NEAT1 supports cellular functions that protect against HD-associated stress and neurodegeneration, HD cells might retain it intracellularly as part of a defensive strategy, preserving its neuroprotective effects where they are most beneficial. This selective retention highlights a potential cellular response in HD, prioritizing the intracellular retention of certain lncRNAs—such as NEAT1—to maintain necessary protective mechanisms under stress rather than releasing them into the extracellular space [445, 446].

In typical cellular environments, lncRNAs represent approximately 2-5% of total RNA content, though this proportion can vary across cell types and conditions. In SGs, lncRNAs tend to be enriched as part of the cell's stress response, contributing to RNA stability and regulation [447]. sEVs, however, typically contain fewer lncRNAs, with protein-coding mRNAs often predominating [429]. The enrichment of lncRNAs in our HD samples, particularly in RNA granules, may indicate a cellular adaptation to HD pathology, where lncRNAs are sequestered to help manage RNA stability and gene expression under disease conditions [448-450]. Further studies on our acquired HD lncRNA datasets are required to delineate how their involvement contributes towards the onset, progression and pathology of the disease. Given the regulatory role of lncRNAs, further investigations could exploit them as novel therapeutic and biomarker targets for HD. In our study, we aimed to validate the abundance of specific HD marker lncRNAs using qRT-PCR. The tested lncRNAs included Lnc-SLC30A5-6 SNHG7, SNHG12, LHR1-LNC1610-1 and Lnc-DUXA-1. qRT-PCR results confirmed an increased expression of all five lncRNAs in HD RNA granule samples. In sEVs, however, only three markers showed statistically significant increases, while the remaining two did not, likely due to high variability among replicates. To further examine localization, we used RNA-FISH on the three lncRNAs with the highest abundance LHR1-LNC1610-1, SNHG12, and Lnc-DUXA-1, which showed partial localization in HD RNA granules, supporting their potential role in HD pathology. In early and pre-symptomatic HD patient samples, these lncRNAs were not detectable, which could be attributed to several factors. One of the most important factors could be that our study utilized a HEK cell model to generate sEVs, whereas the patient samples contained plasma

EVs. Plasma EVs are derived from a complex mix of cell types and tissues throughout the body, diluting any disease-specific signal from individual cell types. In contrast, sEVs from HEK cells in our model are more uniform and controlled, focusing specifically on HD-relevant changes within these cells. This difference could lead to the reduced detectability of HD-specific lncRNAs in plasma EVs, as any HD-related changes may be masked or diluted by the diverse sources of EVs in plasma.

In addition to lncRNAs, we identified five **zinc finger protein (ZNF)** transcripts in HD sEVs, including four protein-coding ZNFs (**ZNF107, ZNF287, ZNF613, and ZNF233**) and one lncRNA (**novel transcript, antisense to ZNF578**). Interestingly, some ZNF transcriptional repressors have been shown to lower mutant HTT levels *in vivo*. While engineered zinc finger nucleases (ZFNs) are being explored as potential therapies to reduce mutant HTT levels, the ZNFs we detected are endogenous proteins that do not directly target mutant HTT [451]. The presence of these ZNFs in HD sEVs suggests that HD cells may release them as part of a stress response, possibly to alleviate the transcriptional burden caused by mutant HTT. This export of ZNFs might be a cellular strategy to manage HD-related stress, with potential implications for intercellular signaling in HD.

2. Shared transcriptomic and proteomic cargo of sEVs and RNA granules

In our study, we observed that there were no common proteins between control and HD samples in both sEVs and RNA granules, suggesting that the expression of the mutant HTT gene alters the composition of these components. Interestingly, the overlap in proteins was greater in HD samples, with 13 shared proteins between HD sEVs and RNA granules compared to only 3 in control conditions, indicating a stronger link between sEVs and RNA granules under diseased conditions. This enhanced overlap in HD may point to a highly selective and regulated sorting and loading system for sEVs. Among the 13 common proteins in HD samples were **RANBP6, EGFR, ITGAV, COMT, ITGA6, MAN1A1, PWP1, FAM171A1, CHMP4A, ABRACL, STK24, SQSTM1, and WDR1**. Notably, only one protein, **WDR1**, was common between HD RNA granules, HD sEVs, and the known list of proteins that bind to mutant HTT-RNA [414].

The presence of overlapping transcripts and proteins between sEVs and RNA granules suggests a link between these cellular components, potentially involving the encapsulation of RNA granules by sEVs to manage toxic RNA aggregates under diseased conditions. **WDR1**'s detection in HD sEVs and RNA granules, along with **cofilins (CFLs)**, which are critical for actin

cytoskeleton dynamics, further supports this hypothesis. Dysregulation of WDR1 and CFLs can impair actin remodeling, crucial for cell structure, motility, and transport—functions essential for neuronal health. In HD, compromised actin dynamics may worsen neurodegeneration by disrupting normal cellular functions [452-454].

Furthermore, given that WDR1 has been identified as a promising therapeutic target among hundreds of HD-linked genes (Kalathure *et al.*), its inclusion in HD sEVs raises the intriguing possibility that cells may selectively package WDR1 within sEVs to modulate cytoskeletal stress linked to HD pathology [452, 455]. We hypothesize that this selective loading may reflect an attempt by cells to buffer or counteract the impact of mutant HTT on cytoskeleton-associated pathways, either by transporting these regulatory proteins to affected regions or by signaling to other cells. This targeted inclusion of WDR1 in sEVs might represent an endogenous mechanism to help restore cytoskeletal stability under HD conditions, a process that could be explored further for potential therapeutic strategies.

While the exact role of **RAN Binding Protein 6 (RANBP6)** in neurodegeneration is not fully understood, it is known to facilitate the transport of proteins across the nuclear envelope. In neurodegenerative diseases like AD and HD, the nuclear transport mechanism is often disrupted, leading to the accumulation of misfolded proteins and increased cellular stress which can ultimately cause neuronal death. Given RANBP6's role in regulating the nuclear import of the STAT3 transcription factor—a key player in cell survival and neuroinflammation—it's possible that RANBP6 could be indirectly involved in neurodegenerative processes. Furthermore, studies indicate that cellular stress can disrupt nucleocytoplasmic transport by causing key transport factors to localize into SGs. The presence of RANBP6, a nuclear transporter, in both HD sEVs and RNA granules supports this disruption, highlighting its potential involvement in neurodegenerative processes [456].

We identified **integrins α V and α 6 (ITGAV and ITGA6)** in HD sEVs and RNA granules, which is particularly noteworthy given their established roles in binding to the extracellular matrix (ECM) and activating matrix metalloproteinases (MMPs). MMPs are linked to neurodegeneration and inflammation, two hallmark processes in HD pathology [457, 458].

sEVs and RNA granules could play a role in transporting ECM-related proteins like ITGAV and ITGA6, potentially influencing MMP activation and ECM interactions beyond their cells of origin. Such activity might represent an attempt by the cell to adapt to HD pathology by

regulating ECM composition and signaling. The selective inclusion of ITGAV and ITGA6 in HD sEVs and RNA granules might thus reflect an adaptive mechanism where cells attempt to mitigate or signal responses to the inflammatory or ECM-disruptive aspects of HD, aligning with our findings on other HD-associated proteins selectively packaged in sEVs.

The detection of **catechol-O-methyltransferase (COMT)** in HD sEVs and RNA granules may provide insight into dopamine dysregulation in HD. COMT is critical for degrading dopamine, and its presence in HD sEVs and RNA granules suggests that these vesicles could play a role in managing dopamine-associated toxicity. In HD, dopamine imbalance—especially in the striatum—is a known issue, and altered COMT activity could exacerbate this imbalance, influencing disease progression [459, 460]. The appearance of COMT in HD sEVs and RNA granules might indicate a cellular response to elevated dopamine toxicity or dysregulation, with these vesicles potentially aiding in modulating dopamine levels in the extracellular environment.

Mannosidase Alpha Class 1A Member 1 (MAN1A1), involved in glycosylation, is crucial for protein folding and stability. In HD, where mutant HTT aggregates, MAN1A1 is downregulated. This downregulation could disrupt glycosylation, potentially exacerbating mHTT aggregation and toxicity [461]. MAN1A1's presence in HD sEVs and RNA granules could indicate a cellular attempt to redistribute glycosylation enzymes to mitigate the effects of mHTT misfolding. This suggests that HD cells may selectively package MAN1A1 in sEVs and RNA granules as part of a response to glycosylation stress caused by mHTT. By distributing MAN1A1 through sEVs and RNA granules, the cell might be attempting to support protein folding and prevent aggregation, reflecting an adaptive strategy to counterbalance the glycosylation deficits associated with HD pathology.

Charged multivesicular body protein 4A (CHMP4A) is a key component of the ESCRT-III complex, essential for endosomal trafficking, cytokinesis, and protein degradation by sealing intraluminal vesicles and recycling ESCRT components. Upon HD, disruptions in these pathways could involve CHMP4A, worsening mHTT accumulation and toxicity [462, 463]. Finding CHMP4A in HD sEVs and RNA granules suggests that cells may attempt to manage the increased burden of mHTT through enhanced involvement of the ESCRT-III machinery. By selectively loading CHMP4A into sEVs and RNA granules, cells might be facilitating endosomal trafficking or aiding in the sequestration and degradation of toxic aggregates associated with

mHTT. This selective inclusion in sEVs and RNA granules may reflect an adaptive response to counteract the buildup of mHTT, emphasizing sEVs' potential role in cellular "clean-up" processes under HD conditions.

The presence of **Actin-binding Rho-activating C-terminus-like protein (ABRACL)** in HD sEVs and RNA granules in our study suggests a relevant link to actin cytoskeleton dysregulation observed in HD. As ABRACL is known to play a role in actin regulation, its inclusion in both sEVs and RNA granules points towards a cellular response potentially aimed at managing cytoskeletal disturbances induced by mHTT expression [464].

In HD, actin and intracellular transport pathways are often disrupted, which can impair neuronal integrity and function. ABRACL's selective loading into sEVs and RNA granules may indicate an attempt by the cell to regulate cytoskeletal dynamics under stress conditions. By packaging ABRACL into sEVs, cells might be transporting or redistributing components essential for actin stabilization, possibly to other areas within the cell or to neighboring cells, to mitigate the impact of cytoskeletal abnormalities in HD. This suggests that ABRACL's presence in sEVs and RNA granules could be part of a targeted adaptation to maintain cellular transport and structural stability, which aligns with its known function and highlights its relevance to HD pathology.

Serine/Threonine Kinase 24 (STK24) is involved in cell cycle regulation, apoptosis, development of the central nervous system and cytoskeletal organization. Upon HD, dysregulation of STK24 may impair neuronal apoptosis and disrupt cytoskeletal stability, potentially worsening neurodegeneration and HD pathology [465, 466]. Its presence in HD sEVs and RNA granules may indicate an attempt by cells to either redistribute or signal essential factors that support cytoskeletal stability and controlled apoptosis, perhaps as a protective mechanism in response to mHTT-induced stress. By packaging STK24 into sEVs, cells could be modulating its availability to other cellular regions or to neighboring cells, potentially aiding in a collective response to counteract HD pathology.

Finding **Sequestosome 1 (SQSTM1)** in HD sEVs and RNA granules in our data aligns with SQSTM1's critical roles in autophagy and protein degradation, functions that are notably disrupted in HD. SQSTM1 is essential for recognizing ubiquitinated protein aggregates and facilitating their degradation via autophagy. In HD, however, mutant huntingtin (mHTT) has

been hypothesized to interfere with SQSTM1's cargo recognition, potentially leading to autophagic dysfunction and the accumulation of toxic protein aggregates [467, 468].

The presence of SQSTM1 in HD sEVs and RNA granules could reflect an adaptive cellular mechanism aimed at mitigating autophagic stress. By packaging SQSTM1 into sEVs, cells may be attempting to redistribute or signal the need for enhanced autophagic and proteostasis activity, potentially helping to address the buildup of harmful protein aggregates. Similarly, its presence in RNA granules may relate to cellular efforts to sequester and regulate mHTT-associated proteins or RNAs in response to compromised autophagy. Thus, the selective inclusion of SQSTM1 in these HD-associated structures not only aligns with its role in proteostasis but also points to a broader cellular response aimed at counteracting mHTT-induced autophagic disruption. This finding highlights SQSTM1 as a potential focus for therapeutic approaches targeting autophagic regulation in HD.

In our analysis of HD sEVs, six common genes—**ALYREF**, **DARS2**, **EGFR**, **EXOC1**, **KRT6B**, and **LLPH**—were identified both at the transcript and protein levels, underscoring their potential significance in HD pathology. Investigating the presence of both RNA and protein forms of these genes in sEVs is critical for understanding the selective loading and transport mechanisms in HD. The identification of both transcript and protein suggests that these molecules might serve specific, adaptive functions within sEVs, potentially aiding in cellular responses to HD-associated stressors.

For example, **ALYREF**, which is known to be upregulated in neurodegenerative disorders such as amyotrophic lateral sclerosis (ALS) and frontotemporal dementia (FTD), has a recognized role in mRNA export and could impact RNA metabolism and stress response in HD cells. Its presence in sEVs might indicate an attempt to modulate or correct dysfunctional RNA processing under HD conditions [469]. Similarly, **DARS2** functions protectively against neuroinflammation and neuronal loss. Given that HD pathology involves neuroinflammatory cascades and mitochondrial dysfunction, the dual presence of DARS2 RNA and protein in sEVs may signify a neuroprotective adaptation, possibly as a means to counteract the inflammatory and apoptotic effects of Mhtt [470]. **EGFR** has a critical function in the nervous system; mHTT can impede the EGFR-mediated activation of ERK, which is crucial for the expression of glutamate transporters (EAATs) in glial cells. This blockage leads to the accumulation of synaptic glutamate, causing toxicity to surrounding neurons. Additionally, mutant HTT alters

EGFR degradation and recycling, disrupting the ubiquitination cycle and forming high-molecular-weight protein aggregates that impair EGFR trafficking. This disruption affects cell migration and proliferation by inhibiting ERK signaling. The detection of EGFR in both forms suggests that sEVs could be involved in redistributing EGFR or supporting signaling pathways disrupted in HD. This could have implications for cellular communication, as sEVs carrying EGFR transcripts or protein might attempt to restore or modulate pathways affected by mHTT's toxic effects. **EXOC1** is essential for vesicle targeting and exocytosis, processes directly relevant to sEV formation and cargo release. Its appearance in both RNA and protein forms within sEVs implies a regulatory role in maintaining vesicle docking and transport under diseased conditions, potentially compensating for trafficking deficits associated with HD. **LLPH**'s role in synaptic transmission and dendritic growth may be relevant to the impaired neuronal connectivity observed in HD. Its presence in sEVs could indicate an effort by cells to preserve synaptic plasticity or compensate for synaptic loss, possibly by transporting LLPH to areas in need of neuronal support.[470-475].

Further research into the specific roles and localization of the shared HD sEV proteins could clarify how sEV-mediated transport might counterbalance HD-associated dysregulations. Investigating these proteins—many of which are integral to cytoskeletal and endosomal-lysosomal pathways—may reveal their role in modulating cellular dysfunctions caused by mutant HTT, uncovering new therapeutic targets for HD.

Although some proteins among those identified have established links to HD, most remain underexplored, necessitating thorough experimental validation. This research could improve our understanding of how disruptions in cytoskeletal regulation and intracellular trafficking contribute to HD progression and potentially offer novel intervention strategies.

3. Crosstalk Between sEVs and RNA Granules in HD: Pathway Disruption and Mitochondrial Dysfunction

STRING and GO term enrichment analysis suggest a functional association between the transcripts and proteins of sEVs and RNA granules. However, it is crucial to recognize a significant limitation of our STRING and GO term enrichment analysis: these tools do not include genes catalogued in RNA Central. Our RNA sequencing dataset contained three times more genes from RNA Central than from Ensembl, highlighting a gap in the comprehensiveness of our downstream analysis. Additionally, our proteomic analysis of RNA

granules yielded a smaller dataset compared to sEVs. This is because of two reasons: one, we isolated only the RNA granule cores, rather than the full RNA granules and two, RNA granules primarily consist of RNA—about 80% [101]. As a result, the number of transcripts and proteins identified in the RNA granule dataset was inherently restricted, leading to less significant functional enrichment outcomes. These constraints not only affect the scope of our findings but also emphasize the need for more inclusive databases to capture a broader range of molecular interactions.

Upon conducting STRING, GO term enrichment, and KEGG analysis of the HD proteome, we identified numerous proteins associated with neurodegenerative diseases such as HD, AD, PD, and ALS, as well as with psychiatric conditions like anxiety and depression. In contrast, no GO terms related to neurodegenerative or psychiatric disorders were found in the control proteome. This suggests that the expression of mHTT not only disrupts the cellular proteome but also leads to the secretion of a dysfunctional proteome through sEVs. Additionally, the presence of mHTT appears to alter the proteome composition of RNA granules, indicating a broad impact on cellular processes and contributing to the pathology of HD and related conditions. Given that these proteins are present in sEVs and are translationally arrested within RNA granules, it is possible that their dysregulation in HD represents a cellular response to the disease state. The accumulation of these proteins in sEVs or RNA granules may indicate an attempt by the cells to manage or eliminate proteins that are contributing to pathological processes. Further research could explore whether overexpression of these proteins within the cell exacerbates HD pathology, or if their knockdown or removal could mitigate the disease's effects (**Figure 29**).

Enrichment analysis also revealed that GO terms associated with RNA granules were also found in sEVs, and vice versa. While there were only a few proteins common to both RNA granules and sEVs, KEGG analysis highlighted that several proteins within the sEVs belong to the RNA granule protein family. Furthermore, this analysis demonstrated that RNA granule proteins are associated with sEVs. These findings were consistent in both control and HD datasets, suggesting a significant crosstalk between RNA granules and sEVs, regardless of the disease state. This indicates a fundamental interplay between these cellular components, which may reflect their collaborative role in managing cellular stress and protein homeostasis. Exploring this interaction further could enhance our understanding of the molecular

mechanisms underlying both normal cellular function and disease progression. In the context of HD, this interaction may reflect the cell's attempt to manage the accumulation of mHTT and other dysregulated proteins. The presence of RNA granule proteins in sEVs and their association with RNA granules could suggest a cellular strategy to sequester or dispose of aberrant proteins.

Several pathways, including JAK/STAT3 and mTOR, were identified as GO terms in both control and HD sEVs and RNA granules, and these pathways are known to be dysregulated in HD [476, 477]. Although the same types of pathways appeared in both control and HD samples, there was no overlap in the specific proteins associated with these pathways in each condition. This lack of shared proteins underscores the substantial impact of HD on cellular processes, revealing how HD disrupts protein composition within these critical pathways. The distinct proteins observed in HD sEVs and RNA granules may play a central role in HD pathology.

We reviewed the literature to evaluate the significance of proteins identified within the JAK/STAT3 and mTOR pathways, as these pathways were

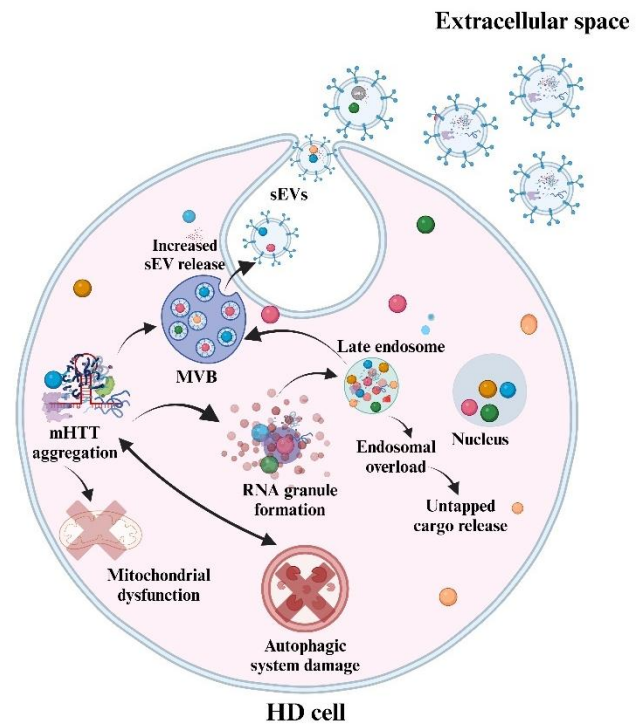


Figure 29. Hypothetical model of cellular adaptations to manage mHTT pathology in HD cells. This model illustrates how HD cells attempt to handle mHTT-induced toxicity through RNA granules and sEVs.

The presence of mHTT leads to protein aggregation, disrupting cellular processes like mitochondrial and autophagic systems and resulting in the formation of RNA granules. This damage subsequently impairs the endosomal-lysosomal pathways, limiting the cell's ability to degrade and recycle dysfunctional proteins. To mitigate these toxic effects, HD cells increase the release of sEVs, packaging dysregulated proteins and RNA into MVBs for secretion into the extracellular space. RNA and proteins from RNA granules are also taken up by the endosome to alleviate cellular stress, which arises from increased RNA granule formation and the failure to disassemble granules due to continuous stress. However, as mHTT continues to disrupt cellular processes, endosomal overload and leaking occurs, indicating incomplete processing of dysfunctional proteins. This ongoing release and sequestration of disease-associated molecules via sEVs and RNA granules reflect the cell's attempt to manage and expel abnormal cargo. (Created with Biorender)

common to both RNA granules and sEVs and are known to be dysregulated in HD. The JAK/STAT3 pathway is essential for regulating cellular stress responses, immune signaling, and protein homeostasis, while the mTOR pathway controls cell growth, autophagy, and protein synthesis [478-482]. In our analysis, two key components of the JAK/STAT3 pathway, EGFR and PIK3R1, were found in HD RNA granules, while mTOR, EGFR, and STAT3 were detected in HD sEVs. Notably, prior studies show that HD cells display increased STAT3 expression and elevated phosphorylation levels in StHdhQ111 cells, homozygous for the HD mutation [480]. Studies also show that mHTT disrupts EGFR signaling and trafficking, impairing essential cellular functions like proliferation and migration. mHTT delays EGFR's progression through the endosomal pathway, causing it to remain in early endosomes and delaying degradation in lysosomes. This extended lifetime of EGFR, combined with mHTT's inhibition of EGFR ubiquitination (by reducing c-Cbl recruitment), results in phosphorylated EGFR accumulating within cells instead of being degraded. mHTT also forms high-molecular-weight aggregates with EGFR, further interfering with its normal trafficking and signaling (**Figure 30**) [472].

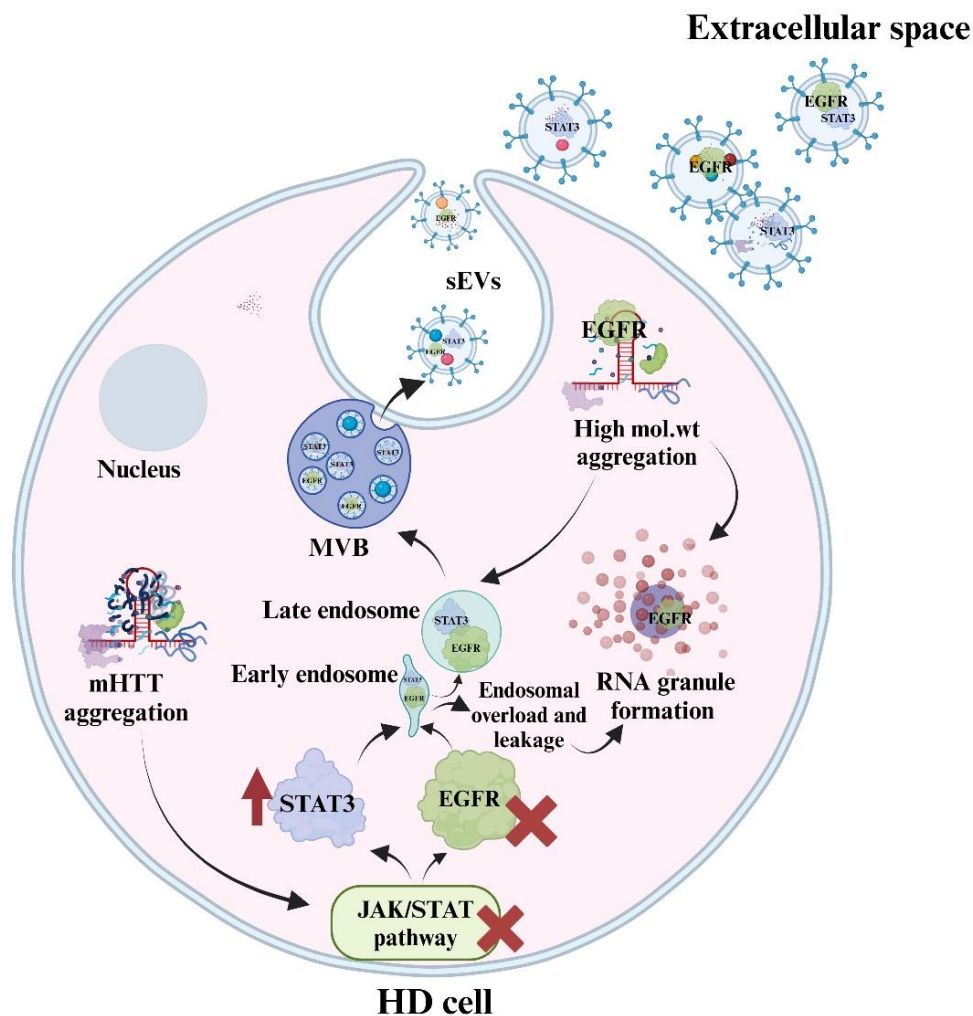


Figure 30. Schematic representation of JAK/STAT dysregulation and its cellular handling in HD cells. JAK/STAT pathway is dysregulated in HD. We found proteins from this pathway both in HD sEVs and RNA granules. increasing STAT3 expression contributes to cellular stress leading to expulsion through sEVs. mHTT aggregation disrupts EGFR signaling and trafficking pathways within the HD cell. The delayed trafficking of EGFR from early endosomes to late endosomes prevents its degradation in lysosomes, resulting in the accumulation of phosphorylated EGFR, endosomal overloading and leakage. This in turn leads to cellular stress and leads to the formation of RNA granules. EGFR could also be loaded into sEVs after delayed trafficking allowing for its removal from the cell.

We hypothesize that the accumulation of these proteins in sEVs could reflect a mechanism for the cell to actively expel toxic components, while their presence in RNA granules may indicate sequestration in response to dysregulation or cellular stress. This dual localization in sEVs and RNA granules likely represents an adaptive response to protein dysregulation, aimed at managing cellular stress. However, this response may ultimately be insufficient to prevent HD-related cellular damage. Further studies on these proteins could illuminate the mechanisms behind their dysregulation and reveal therapeutic targets within these pathways, potentially reducing cellular toxicity in HD.

These findings suggest that further investigation into these proteins could significantly enhance our understanding of HD pathology and potentially identify therapeutic targets to restore cellular function and maintain homeostasis in HD.

In addition to the above-mentioned pathway findings, the observed enrichment of mitochondria-related GO terms, including mitochondrial electron transport, ATP synthesis, oxidative phosphorylation, primary mitochondrial diseases, and mitochondrial metabolism disorders, in the HD sEV protein datasets highlights a pronounced dysregulation of mitochondrial function in HD. Such mitochondrial dysfunctions are well-documented in HD literature, supporting the notion that impaired mitochondrial function is a key driver of HD pathology.

Previous studies extensively illustrate how mHTT impacts mitochondrial processes. For instance, research has shown that mHTT can impair the electron transport chain (ETC) complexes, reducing ATP production and leading to increased oxidative stress, which accelerates neuronal cell death [483-485]. Additionally, mHTT has been linked to impaired mitochondrial calcium buffering and disrupted mitochondrial dynamics, which collectively contribute to neuronal dysfunction and degeneration [486, 487].

The enrichment of mitochondria-related GO terms in HD sEVs aligns with these findings, suggesting that mitochondrial proteins may be selectively loaded into sEVs in response to mitochondrial stress or damage. This may reflect a cellular attempt to expel dysfunctional mitochondrial components, although it may also indicate broader mitochondrial dysregulation in HD. Given the fundamental role of mitochondrial dysfunction in HD progression, mitochondria present a promising target for therapeutic strategies aimed at restoring energy balance and reducing oxidative stress, potentially alleviating neurodegeneration.

These findings underscore the substantial mitochondrial dysregulation associated with HD, linking HD pathology to impaired energy production and metabolic dysfunction. Further exploration of these mitochondrial disruptions may yield insights into the molecular mechanisms underlying HD and inform new therapeutic approaches to combat disease progression.

4. Differential RNA Sorting and Early Biomarkers in HD sEVs and RNA Granules

Our study was conducted using a HEK cell model stably expressing mHTT. When we compared our sEVs transcriptomic data to a study analysing EVs isolated from patient plasma, we found a 51.5% overlap with genes that are differentially expressed in pre-symptomatic HD samples [393]. This overlap is greater than that observed with genes detected in symptomatic HD patients (38.4%). This difference may be because our cell model represents an early disease phenotype, given that the mHTT construct was expressed for a relatively short period (72 hours) before analysis. The fact that we did not detect all the genes differentially expressed in pre-HD samples in our HD cell line model could be due to the influence of other factors beyond the expression of mutant HTT alone, such as lifestyle or other genetic variants, which may affect the composition of EVs. For instance, G3BP1, which has previously been linked to HD [79, 356] and was found to be more than twofold upregulated in early HD [393] was detected in all of our samples. It showed a trend of increased abundance in HD RNA granules but decreased abundance in HD sEVs. This difference in abundance between our cell model and the study by Neueder *et al.* could be explained by the fact that EVs isolated from blood are derived from various cell types throughout the body, primarily platelets. Neueder *et al.* also reported high expression levels of many deregulated proteins in the liver, suggesting that the liver might be a significant source of the observed changes in EV protein content and

composition. Consequently, these gene expression patterns might not be mirrored in HEK cells, which originate from the kidney [393].

Next, upon comparing our list of marker genes from the transcriptomics dataset with the top 20 differentially expressed genes in HD across ten categories [488], we identified two overlaps: **PLCB1** and **CDH10**. Our data showed that **PLCB1** was up-regulated under HD conditions in sEVs, whereas previous studies reported **PLCB1** as being down-regulated in HD [489]. This discrepancy may be due to the different nature of the analyses; our study focused on transcripts contained within sEVs, which represent extracellular RNA, while the other studies analysed intracellular transcript levels. This suggests that the regulation of **PLCB1** may differ between intracellular and extracellular contexts, potentially reflecting distinct roles in cellular communication or disease mechanisms in HD. Further investigation into these differences could provide valuable insights into how HD pathology affects RNA sorting and secretion processes.

Additionally, when we compared our proteomics dataset from HD sEVs and RNA granules with the same list of top differentially expressed genes in HD, we found two common proteins: **FNBP1L** in the HD sEV dataset and **FTH1** in the HD RNA granule dataset. Future studies should explore how these differential expressions and protein associations affect HD pathology, and whether they offer novel targets for therapeutic intervention or serve as early indicators of disease state.

5. Conclusions

In conclusion, our study represents the first comprehensive comparison of the transcriptome and proteome of sEVs and RNA granule cores in a HD cell model. Our datasets reveal a notable overlap in the transcriptomic and proteomic cargo of sEVs and RNA granules, regardless of the disease state, highlighting their significant crosstalk. Enrichment analyses using KEGG, STRING, and GO terms further support this interaction, showing that while some proteins may not be prominently listed due to low abundance, they are extensively linked to both sEVs and RNA granules in other research. This indicates a complex and dynamic relationship between these cellular compartments in HD.

Additionally, our downstream analysis identified specific subsets of proteins in both sEVs and RNA granules associated with neurodegenerative disorders and mitochondrial dysfunction.

Notably, we observed distinct differences in the protein loading of sEVs and the molecular composition of RNA granules with respect to cellular pathways between control and HD conditions, reflecting the profound impact of mutant HTT expression on these processes.

The transcriptomic analysis of HD sEVs and RNA granules predominantly revealed a high abundance of lncRNAs. Several of these transcripts were found to be regulated by REST, underscoring the crucial role of REST signaling in HD. Our validation of key marker genes provides a foundation for developing novel diagnostic markers and therapeutic interventions.

Overall, this study not only offers new insights into the cellular mechanisms underlying HD but also opens up numerous avenues for future research. The datasets and findings can be further explored to elucidate the molecular mechanisms of HD and identify potential therapeutic targets. This work marks a significant step forward in understanding the intricate biological changes in HD and presents opportunities for advancing diagnosis and treatment strategies.

BIBLIOGRAPHY

1. Stroberg, W. and S. Schnell, *On the origin of non-membrane-bound organelles, and their physiological function*. J Theor Biol, 2017. **434**: p. 42-49.
2. Mathivanan, S., H. Ji, and R.J. Simpson, *Exosomes: extracellular organelles important in intercellular communication*. J Proteomics, 2010. **73**(10): p. 1907-20.
3. Friedman, J.R. and J. Nunnari, *Mitochondrial form and function*. Nature, 2014. **505**(7483): p. 335-43.
4. Glisovic, T., et al., *RNA-binding proteins and post-transcriptional gene regulation*. FEBS Lett, 2008. **582**(14): p. 1977-86.
5. Luzio, J.P., P.R. Pryor, and N.A. Bright, *Lysosomes: fusion and function*. Nat Rev Mol Cell Biol, 2007. **8**(8): p. 622-32.
6. Battistelli, M., & Falcieri, E. (2020), *Apoptotic Bodies: Particular Extracellular Vesicles Involved in Intercellular Communication*. Biology. **9**(1): p. 21.
7. Boisvert, F.M., et al., *The multifunctional nucleolus*. Nat Rev Mol Cell Biol, 2007. **8**(7): p. 574-85.
8. Bond, C.S. and A.H. Fox, *Paraspeckles: nuclear bodies built on long noncoding RNA*. J Cell Biol, 2009. **186**(5): p. 637-44.
9. Xie, S.Q., et al., *Splicing speckles are not reservoirs of RNA polymerase II, but contain an inactive form, phosphorylated on serine2 residues of the C-terminal domain*. Mol Biol Cell, 2006. **17**(4): p. 1723-33.
10. Gall, J.G., *The centennial of the Cajal body*. Nat Rev Mol Cell Biol, 2003. **4**(12): p. 975-80.
11. Morimoto, M. and C.F. Boerkoel, *The role of nuclear bodies in gene expression and disease*. Biology (Basel), 2013. **2**(3): p. 976-1033.
12. Sandqvist, A. and L. Sistonen, *Nuclear stress granules: the awakening of a sleeping beauty?* J Cell Biol, 2004. **164**(1): p. 15-7.
13. Anderson, P., & Kedersha, N. (2006) *RNA granules*. The Journal of cell biology. **172**(6): p. 803-808.
14. Woodruff, J.B., et al., *Centrosomes. Regulated assembly of a supramolecular centrosome scaffold in vitro*. Science, 2015. **348**(6236): p. 808-12.
15. Stubbe, J., et al., *Nontemplate-dependent polymerization processes: polyhydroxyalkanoate synthases as a paradigm*. Annu Rev Biochem, 2005. **74**: p. 433-80.
16. Li, P., et al., *Phase transitions in the assembly of multivalent signalling proteins*. Nature, 2012. **483**(7389): p. 336-40.
17. Banjade, S. and M.K. Rosen, *Phase transitions of multivalent proteins can promote clustering of membrane receptors*. Elife, 2014. **3**.
18. Ritter, R., *Die Entwicklung der Geschlechtsorgane und des Darmes bei Chiromomus*. 1890. p. Bd. 50.
19. Hegner, R.W., *Studies on Germ Cells I. The History of the Germ Cells in Insects with Special Reference to the Keimbahn-Determinants, II. The Origin and Significance of the Keimbahn-Determinants in Animals*. Vol. 25. 1914: Journal of Morphology.
20. Schisa, J.A., J.N. Pitt, and J.R. Priess, *Analysis of RNA associated with P granules in germ cells of C. elegans adults*. Development, 2001. **128**(8): p. 1287-98.
21. Leatherman, J.L. and T.A. Jongens, *Transcriptional silencing and translational control: key features of early germline development*. Bioessays, 2003. **25**(4): p. 326-35.
22. Navarro, R.E. and T.K. Blackwell, *Requirement for P granules and meiosis for accumulation of the germline RNA helicase CGH-1*. Genesis, 2005. **42**(3): p. 172-80.
23. Daniel R Schoenberg and L.E. Maquat, *Regulation of cytoplasmic mRNA decay*. Nature reviews. Genetics, 2012. **13**(4): p. 246-59.
24. Tafer, H., *Bioinformatics of siRNA design*. Methods Mol Biol, 2014. **1097**: p. 477-90.
25. Macdonald, P.M. and G. Struhl, *cis-acting sequences responsible for anterior localization of bicoid mRNA in Drosophila embryos*. Nature, 1988. **336**(6199): p. 595-8.
26. Hussey, G.S., et al., *Identification of an mRNP complex regulating tumorigenesis at the translational elongation step*. Mol Cell, 2011. **41**(4): p. 419-31.
27. Reed, R. and E. Hurt, *A conserved mRNA export machinery coupled to pre-mRNA splicing*. Cell, 2002. **108**(4): p. 523-31.
28. Le Hir, H., et al., *The exon-exon junction complex provides a binding platform for factors involved in mRNA export and nonsense-mediated mRNA decay*. EMBO J, 2001. **20**(17): p. 4987-97.
29. Barreau, C., L. Paillard, and H.B. Osborne, *AU-rich elements and associated factors: are there unifying principles?* Nucleic Acids Res, 2005. **33**(22): p. 7138-50.
30. Lal, A., et al., *Concurrent versus individual binding of HuR and AUF1 to common labile target mRNAs*. EMBO J, 2004. **23**(15): p. 3092-102.

31. Sobue, S., et al., *v-Src oncogene product increases sphingosine kinase 1 expression through mRNA stabilization: alteration of AU-rich element-binding proteins*. *Oncogene*, 2008. **27**(46): p. 6023-33.
32. Lin, Y., et al., *Formation and Maturation of Phase-Separated Liquid Droplets by RNA-Binding Proteins*. *Mol Cell*, 2015. **60**(2): p. 208-19.
33. Molliex, A., et al., *Phase separation by low complexity domains promotes stress granule assembly and drives pathological fibrillization*. *Cell*, 2015. **163**(1): p. 123-33.
34. Van Treeck, B. and R. Parker, *Emerging Roles for Intermolecular RNA-RNA Interactions in RNP Assemblies*. *Cell*, 2018. **174**(4): p. 791-802.
35. Tian, S., Curnutte, H. A., & Trcek, T. (2020), *RNA Granules: A View from the RNA Perspective*. *Molecules* (Basel, Switzerland). **25**(14): p. 3130.
36. Han, J., et al., *Pre-mRNA splicing: where and when in the nucleus*. *Trends Cell Biol*, 2011. **21**(6): p. 336-43.
37. Galloway, A. and V.H. Cowling, *mRNA cap regulation in mammalian cell function and fate*. *Biochim Biophys Acta Gene Regul Mech*, 2019. **1862**(3): p. 270-279.
38. Passmore, L.A. and J. Collier, *Roles of mRNA poly(A) tails in regulation of eukaryotic gene expression*. *Nat Rev Mol Cell Biol*, 2022. **23**(2): p. 93-106.
39. Shiina, N., *Liquid- and solid-like RNA granules form through specific scaffold proteins and combine into biphasic granules*. *J Biol Chem*, 2019. **294**(10): p. 3532-3548.
40. Wheeler, J.R., et al., *Distinct stages in stress granule assembly and disassembly*. *Elife*, 2016. **5**.
41. Wolf, N., J. Priess, and D. Hirsh, *Segregation of germline granules in early embryos of *Caenorhabditis elegans*: an electron microscopic analysis*. *J Embryol Exp Morphol*, 1983. **73**: p. 297-306.
42. Brangwynne, C.P., et al., *Germline P granules are liquid droplets that localize by controlled dissolution/condensation*. *Science*, 2009. **324**(5935): p. 1729-32.
43. Brangwynne, C.P., T.J. Mitchison, and A.A. Hyman, *Active liquid-like behavior of nucleoli determines their size and shape in *Xenopus laevis* oocytes*. *Proc Natl Acad Sci U S A*, 2011. **108**(11): p. 4334-9.
44. Doi, M., *Soft matter physics*. First edition. ed. 2013, Oxford ; New York: Oxford University Press. xi, 257 pages.
45. AJ, B., *Theory of phase-ordering kinetics*. *Advances in Physics*, 1994. **43**(3): p. 357-459.
46. Straube, E., *Scaling concepts in polymer physics*. Cornell University Press 1980, 1981. **32**(5).
47. Safran, S., *Statistical Thermodynamics Of Surfaces, Interfaces, And Membranes*. 1 ed. CRC Press. 2003. 288.
48. Kröger, M.a.V., J, *The Structure and Rheology of Complex Fluids*. *Applied Rheology*, 2000. **10**(3): p. 110-111.
49. Majumdar, A., et al., *Liquid-Liquid Phase Separation Is Driven by Large-Scale Conformational Unwinding and Fluctuations of Intrinsically Disordered Protein Molecules*. *The Journal of Physical Chemistry Letters*, 2019. **10**(14): p. 3929-3936.
50. Jain, S., et al., *ATPase-Modulated Stress Granules Contain a Diverse Proteome and Substructure*. *Cell*, 2016. **164**(3): p. 487-98.
51. Kim, H.J., et al., *Mutations in prion-like domains in *hnRNPA2B1* and *hnRNPA1* cause multisystem proteinopathy and ALS*. *Nature*, 2013. **495**(7442): p. 467-73.
52. Andersen, J.S., et al., *Nucleolar proteome dynamics*. *Nature*, 2005. **433**(7021): p. 77-83.
53. Fong, K.W., et al., *Whole-genome screening identifies proteins localized to distinct nuclear bodies*. *J Cell Biol*, 2013. **203**(1): p. 149-64.
54. Oldfield, C.J. and A.K. Dunker, *Intrinsically disordered proteins and intrinsically disordered protein regions*. *Annu Rev Biochem*, 2014. **83**: p. 553-84.
55. Varadi, M., et al., *Functional Advantages of Conserved Intrinsic Disorder in RNA-Binding Proteins*. *PLoS One*, 2015. **10**(10): p. e0139731.
56. Kato, M., et al., *Cell-free formation of RNA granules: low complexity sequence domains form dynamic fibers within hydrogels*. *Cell*, 2012. **149**(4): p. 753-67.
57. Wei, M.T., et al., *Phase behaviour of disordered proteins underlying low density and high permeability of liquid organelles*. *Nat Chem*, 2017. **9**(11): p. 1118-1125.
58. Wang, J., et al., *A Molecular Grammar Governing the Driving Forces for Phase Separation of Prion-like RNA Binding Proteins*. *Cell*, 2018. **174**(3): p. 688-699 e16.
59. Zhang, X., et al., *RNA stores tau reversibly in complex coacervates*. *PLoS Biol*, 2017. **15**(7): p. e2002183.
60. Feric, M., et al., *Coexisting Liquid Phases Underlie Nucleolar Subcompartments*. *Cell*, 2016. **165**(7): p. 1686-1697.

61. Boeynaems, S., Alberti, S., Fawzi, N. L., Mittag, T., Polymenidou, M., Rousseau, F., Schymkowitz, J., Shorter, J., Wolozin, B., Van Den Bosch, L., Tompa, P., & Fuxreiter, M. (2018). *Protein Phase Separation: A New Phase in Cell Biology*. *Trends in cell biology*, **28**(6): p. 420–435.
62. D, B.K.S., *Statistical theory of nucleation, condensation and coagulation*. *Advances in Physics*, 1976. **25**(4): p. 343-396.
63. Malinowska, L., S. Kroschwald, and S. Alberti, *Protein disorder, prion propensities, and self-organizing macromolecular collectives*. *Biochim Biophys Acta*, 2013. **1834**(5): p. 918-31.
64. Gonczy, P., *Towards a molecular architecture of centriole assembly*. *Nat Rev Mol Cell Biol*, 2012. **13**(7): p. 425-35.
65. Heald, R., et al., *Self-organization of microtubules into bipolar spindles around artificial chromosomes in Xenopus egg extracts*. *Nature*, 1996. **382**(6590): p. 420-5.
66. Ostwald, W., *Über die vermeintliche Isomerie des roten und gelben Quecksilberoxyds und die Oberflächenspannung fester Körper*. *Zeitschrift für Physikalische Chemie*, 1900. **34U**(1): p. 495-503.
67. Decker, M., et al., *Limiting amounts of centrosome material set centrosome size in C. elegans embryos*. *Curr Biol*, 2011. **21**(15): p. 1259-67.
68. Brangwynne, C.P., *Phase transitions and size scaling of membrane-less organelles*. *J Cell Biol*, 2013. **203**(6): p. 875-81.
69. Goehring, N.W. and A.A. Hyman, *Organelle growth control through limiting pools of cytoplasmic components*. *Curr Biol*, 2012. **22**(9): p. R330-9.
70. Zwicker, D., et al., *Centrosomes are autocatalytic droplets of pericentriolar material organized by centrioles*. *Proc Natl Acad Sci U S A*, 2014. **111**(26): p. E2636-45.
71. Lee, C.F., et al., *Spatial organization of the cell cytoplasm by position-dependent phase separation*. *Phys Rev Lett*, 2013. **111**(8): p. 088101.
72. Li, Y.R., et al., *Stress granules as crucibles of ALS pathogenesis*. *J Cell Biol*, 2013. **201**(3): p. 361-72.
73. Weber, S.C. and C.P. Brangwynne, *Getting RNA and protein in phase*. *Cell*, 2012. **149**(6): p. 1188-91.
74. Doyle, S.M., O. Genest, and S. Wickner, *Protein rescue from aggregates by powerful molecular chaperone machines*. *Nat Rev Mol Cell Biol*, 2013. **14**(10): p. 617-29.
75. Pickett, J., *Folding away the bad guys*. *Nat Rev Mol Cell Biol*, 2006. **7**: p. 792.
76. Tyedmers, J., A. Mogk, and B. Bukau, *Cellular strategies for controlling protein aggregation*. *Nat Rev Mol Cell Biol*, 2010. **11**(11): p. 777-88.
77. Wippich, F., et al., *Dual specificity kinase DYRK3 couples stress granule condensation/dissolution to mTORC1 signaling*. *Cell*, 2013. **152**(4): p. 791-805.
78. Hubstenberger, A., et al., *Translation repressors, an RNA helicase, and developmental cues control RNP phase transitions during early development*. *Dev Cell*, 2013. **27**(2): p. 161-173.
79. Sanchez, II, et al., *Huntington's disease mice and human brain tissue exhibit increased G3BP1 granules and TDP43 mislocalization*. *J Clin Invest*, 2021. **131**(12).
80. An, H., Tan, J. T., & Shelkovich, T. A. (2019), *Stress granules regulate stress-induced paraspeckle assembly*. *The Journal of cell biology*. **218**(12): p. 4127–4140
81. Cougot, N., et al., *Dendrites of mammalian neurons contain specialized P-body-like structures that respond to neuronal activation*. *J Neurosci*, 2008. **28**(51): p. 13793-804.
82. Zeitelhofer, M., et al., *Dynamic interaction between P-bodies and transport ribonucleoprotein particles in dendrites of mature hippocampal neurons*. *J Neurosci*, 2008. **28**(30): p. 7555-62.
83. Bauer, K.E., et al., *RNA supply drives physiological granule assembly in neurons*. *Nat Commun*, 2022. **13**(1): p. 2781.
84. (2017), K.D., *There Is an Inclusion for That: Material Properties of Protein Granules Provide a Platform for Building Diverse Cellular Functions*. *Trends in biochemical sciences*. **42**(10): p. 765–776.
85. Nover, L., K.D. Scharf, and D. Neumann, *Cytoplasmic heat shock granules are formed from precursor particles and are associated with a specific set of mRNAs*. *Mol Cell Biol*, 1989. **9**(3): p. 1298-308.
86. Anderson, P. and N. Kedersha, *Stressful initiations*. *J Cell Sci*, 2002. **115**(Pt 16): p. 3227-34.
87. Wek, R.C., H.Y. Jiang, and T.G. Anthony, *Coping with stress: eIF2 kinases and translational control*. *Biochem Soc Trans*, 2006. **34**(Pt 1): p. 7-11.
88. Anderson, P. and N. Kedersha, *Stress granules: the Tao of RNA triage*. *Trends Biochem Sci*, 2008. **33**(3): p. 141-50.
89. Protter, D., & Parker, R. (2016), *Principles and Properties of Stress Granules*. *Trends in cell biology*,. **26**(9): p. 668–679.

90. Souquere, S., Mollet, S., Kress, M., Dautry, F., Pierron, G., & Weil, D. (2009), *Unravelling the ultrastructure of stress granules and associated P-bodies in human cells*. *Journal of cell science*. **122**: p. 3619–3626.
91. Mahboubi, H., M. Kodiha, and U. Stochaj, *Automated detection and quantification of granular cell compartments*. *Microsc Microanal*, 2013. **19**(3): p. 617-28.
92. Anderson, P. and N. Kedersha, *Stress granules*. *Curr Biol*, 2009. **19**(10): p. R397-8.
93. Arimoto, K., Fukuda, H., Imajoh-Ohmi, S., Saito, H., & Takekawa, M. (2008), *Formation of stress granules inhibits apoptosis by suppressing stress-responsive MAPK pathways*. *Nature cell biology*. **10**(11): p. 1324–1332.
94. Mahboubi, H. and U. Stochaj, *Cytoplasmic stress granules: Dynamic modulators of cell signaling and disease*. *Biochim Biophys Acta Mol Basis Dis*, 2017. **1863**(4): p. 884-895.
95. Buchan, J.R., *mRNP granules. Assembly, function, and connections with disease*. *RNA Biol*, 2014. **11**(8): p. 1019-30.
96. Gilks, N., et al., *Stress granule assembly is mediated by prion-like aggregation of TIA-1*. *Mol Biol Cell*, 2004. **15**(12): p. 5383-98.
97. Tourrière, H., Chebli, K., Zekri, L., Courselaud, B., Blanchard, J. M., Bertrand, E., & Tazi, J. (2003), *The RasGAP-associated endoribonuclease G3BP assembles stress granules*. *The Journal of cell biology*. **160**(6): p. 823–831.
98. Kedersha, N., et al., *Dynamic shuttling of TIA-1 accompanies the recruitment of mRNA to mammalian stress granules*. *J Cell Biol*, 2000. **151**(6): p. 1257-68.
99. Mazroui, R., et al., *Trapping of messenger RNA by Fragile X Mental Retardation protein into cytoplasmic granules induces translation repression*. *Hum Mol Genet*, 2002. **11**(24): p. 3007-17.
100. Stoecklin, G., et al., *MK2-induced tristetraprolin:14-3-3 complexes prevent stress granule association and ARE-mRNA decay*. *EMBO J*, 2004. **23**(6): p. 1313-24.
101. Khong, A., Matheny, T., Jain, S., Mitchell, S. F., Wheeler, J. R., & Parker, R. (2017), *The Stress Granule Transcriptome Reveals Principles of mRNA Accumulation in Stress Granules*. *Molecular Cell*. **68**(4): p. 808–820.e5.
102. Thomas, M.G., et al., *RNA granules: the good, the bad and the ugly*. *Cell Signal*, 2011. **23**(2): p. 324-34.
103. Kedersha, N., Ivanov, P., & Anderson, P. (2013), *Stress granules and cell signaling: more than just a passing phase?* *Trends in biochemical sciences*. **38**(10): p. 494–506.
104. Pothof, J., et al., *MicroRNA responses and stress granule formation modulate the DNA damage response*. *Cell Cycle*, 2009. **8**(21): p. 3462-8.
105. Aulas, A. and C. Vande Velde, *Alterations in stress granule dynamics driven by TDP-43 and FUS: a link to pathological inclusions in ALS?* *Front Cell Neurosci*, 2015. **9**: p. 423.
106. Leung, A., et al., *Poly(ADP-ribose) regulates post-transcriptional gene regulation in the cytoplasm*. *RNA Biol*, 2012. **9**(5): p. 542-8.
107. Mahboubi, H., et al., *Identification of Novel Stress Granule Components That Are Involved in Nuclear Transport*. *PLoS One*, 2013. **8**(6): p. e68356.
108. Kedersha, N., et al., *Evidence that ternary complex (eIF2-GTP-tRNA(i)(Met))-deficient preinitiation complexes are core constituents of mammalian stress granules*. *Mol Biol Cell*, 2002. **13**(1): p. 195-210.
109. Kedersha, N., Stoecklin, G., Ayodele, M., Yacono, P., Lykke-Andersen, J., Fritzler, M. J., Scheuner, D., Kaufman, R. J., Golan, D. E., & Anderson, P. (2005), *Stress granules and processing bodies are dynamically linked sites of mRNP remodeling*. *The Journal of cell biology*. **169**(6): p. 871–884.
110. Nonhoff, U., et al., *Ataxin-2 interacts with the DEAD/H-box RNA helicase DDX6 and interferes with P-bodies and stress granules*. *Mol Biol Cell*, 2007. **18**(4): p. 1385-96.
111. Kedersha, N.L., et al., *RNA-binding proteins TIA-1 and TIAR link the phosphorylation of eIF-2 alpha to the assembly of mammalian stress granules*. *J Cell Biol*, 1999. **147**(7): p. 1431-42.
112. Wilczynska, A., et al., *The translational regulator CPEB1 provides a link between dcp1 bodies and stress granules*. *J Cell Sci*, 2005. **118**(Pt 5): p. 981-92.
113. Yang, W.H., et al., *RNA-associated protein 55 (RAP55) localizes to mRNA processing bodies and stress granules*. *RNA*, 2006. **12**(4): p. 547-54.
114. Vessey, J.P., et al., *Dendritic localization of the translational repressor Pumilio 2 and its contribution to dendritic stress granules*. *J Neurosci*, 2006. **26**(24): p. 6496-508.
115. Baez, M.V. and G.L. Boccaccio, *Mammalian Smaug is a translational repressor that forms cytoplasmic foci similar to stress granules*. *J Biol Chem*, 2005. **280**(52): p. 43131-40.
116. Yang, F., et al., *Polysome-bound endonuclease PMR1 is targeted to stress granules via stress-specific binding to TIA-1*. *Mol Cell Biol*, 2006. **26**(23): p. 8803-13.

117. Stohr, N., et al., *ZBP1 regulates mRNA stability during cellular stress*. J Cell Biol, 2006. **175**(4): p. 527-34.
118. Maroney, P.A., et al., *Evidence that microRNAs are associated with translating messenger RNAs in human cells*. Nat Struct Mol Biol, 2006. **13**(12): p. 1102-7.
119. Kim, S.H., et al., *Fragile X mental retardation protein shifts between polyribosomes and stress granules after neuronal injury by arsenite stress or in vivo hippocampal electrode insertion*. J Neurosci, 2006. **26**(9): p. 2413-8.
120. Solomon, S., Xu, Y., Wang, B., David, M. D., Schubert, P., Kennedy, D., & Schrader, J. W. (2007), *Distinct structural features of caprin-1 mediate its interaction with G3BP-1 and its induction of phosphorylation of eukaryotic translation initiation factor 2alpha, entry to cytoplasmic stress granules, and selective interaction with a subset of mRNAs*. Molecular and cellular biology. **27**(6): p. 2324–2342.
121. Hua, Y. and J. Zhou, *Survival motor neuron protein facilitates assembly of stress granules*. FEBS Lett, 2004. **572**(1-3): p. 69-74.
122. Goodier, J.L., et al., *LINE-1 ORF1 protein localizes in stress granules with other RNA-binding proteins, including components of RNA interference RNA-induced silencing complex*. Mol Cell Biol, 2007. **27**(18): p. 6469-83.
123. Kozak, S.L., et al., *The anti-HIV-1 editing enzyme APOBEC3G binds HIV-1 RNA and messenger RNAs that shuttle between polysomes and stress granules*. J Biol Chem, 2006. **281**(39): p. 29105-19.
124. Thomas, M.G., et al., *Staufen recruitment into stress granules does not affect early mRNA transport in oligodendrocytes*. Mol Biol Cell, 2005. **16**(1): p. 405-20.
125. Li, W., et al., *FAST is a survival protein that senses mitochondrial stress and modulates TIA-1-regulated changes in protein expression*. Mol Cell Biol, 2004. **24**(24): p. 10718-32.
126. Yu, C., et al., *An essential function of the SRC-3 coactivator in suppression of cytokine mRNA translation and inflammatory response*. Mol Cell, 2007. **25**(5): p. 765-78.
127. Rothe, F., et al., *Identification of FUSE-binding proteins as interacting partners of TIA proteins*. Biochem Biophys Res Commun, 2006. **343**(1): p. 57-68.
128. Hofmann, I., et al., *Identification of the junctional plaque protein plakophilin 3 in cytoplasmic particles containing RNA-binding proteins and the recruitment of plakophilins 1 and 3 to stress granules*. Mol Biol Cell, 2006. **17**(3): p. 1388-98.
129. Kim, W.J., et al., *Sequestration of TRAF2 into stress granules interrupts tumor necrosis factor signaling under stress conditions*. Mol Cell Biol, 2005. **25**(6): p. 2450-62.
130. Kedersha, N. and P. Anderson, *Stress granules: sites of mRNA triage that regulate mRNA stability and translatability*. Biochem Soc Trans, 2002. **30**(Pt 6): p. 963-9.
131. Edupuganti, R.R., et al., *N(6)-methyladenosine (m(6)A) recruits and repels proteins to regulate mRNA homeostasis*. Nat Struct Mol Biol, 2017. **24**(10): p. 870-878.
132. Wu, Y., et al., *Crystal structure of a dimerization domain of human Caprin-1: insights into the assembly of an evolutionarily conserved ribonucleoprotein complex consisting of Caprin-1, FMRP and G3BP1*. Acta Crystallogr D Struct Biol, 2016. **72**(Pt 6): p. 718-27.
133. Meyer, K.D., et al., *Comprehensive analysis of mRNA methylation reveals enrichment in 3' UTRs and near stop codons*. Cell, 2012. **149**(7): p. 1635-46.
134. Xie, W. and R.B. Denman, *Protein methylation and stress granules: posttranslational remodeler or innocent bystander?* Mol Biol Int, 2011. **2011**: p. 137459.
135. Ohn, T., et al., *A functional RNAi screen links O-GlcNAc modification of ribosomal proteins to stress granule and processing body assembly*. Nat Cell Biol, 2008. **10**(10): p. 1224-31.
136. Dolzhanskaya, N., et al., *Methylation regulates the intracellular protein-protein and protein-RNA interactions of FMRP*. J Cell Sci, 2006. **119**(Pt 9): p. 1933-46.
137. Yamaguchi, A. and K. Kitajo, *The effect of PRMT1-mediated arginine methylation on the subcellular localization, stress granules, and detergent-insoluble aggregates of FUS/TLS*. PLoS One, 2012. **7**(11): p. e49267.
138. Reineke, L.C., et al., *Casein Kinase 2 Is Linked to Stress Granule Dynamics through Phosphorylation of the Stress Granule Nucleating Protein G3BP1*. Mol Cell Biol, 2017. **37**(4).
139. Holcik, M., *Could the eIF2alpha-Independent Translation Be the Achilles Heel of Cancer?* Front Oncol, 2015. **5**: p. 264.
140. Reineke, L.C., et al., *Large G3BP-induced granules trigger eIF2alpha phosphorylation*. Mol Biol Cell, 2012. **23**(18): p. 3499-510.
141. Hamanaka, R.B., et al., *PERK and GCN2 contribute to eIF2alpha phosphorylation and cell cycle arrest after activation of the unfolded protein response pathway*. Mol Biol Cell, 2005. **16**(12): p. 5493-501.

142. Baltzis, D., et al., *The eIF2alpha kinases PERK and PKR activate glycogen synthase kinase 3 to promote the proteasomal degradation of p53*. J Biol Chem, 2007. **282**(43): p. 31675-87.
143. Cencic, R., et al., *Antitumor activity and mechanism of action of the cyclopenta[b]benzofuran, silvestrol*. PLoS One, 2009. **4**(4): p. e5223.
144. Pelletier, J., et al., *Targeting the eIF4F translation initiation complex: a critical nexus for cancer development*. Cancer Res, 2015. **75**(2): p. 250-63.
145. Mokas, S., et al., *Uncoupling stress granule assembly and translation initiation inhibition*. Mol Biol Cell, 2009. **20**(11): p. 2673-83.
146. Farny, N.G., N.L. Kedersha, and P.A. Silver, *Metazoan stress granule assembly is mediated by P-eIF2alpha-dependent and -independent mechanisms*. RNA, 2009. **15**(10): p. 1814-21.
147. Mazroui, R., et al., *Inhibition of ribosome recruitment induces stress granule formation independently of eukaryotic initiation factor 2alpha phosphorylation*. Mol Biol Cell, 2006. **17**(10): p. 4212-9.
148. Emara, M.M., et al., *Angiogenin-induced tRNA-derived stress-induced RNAs promote stress-induced stress granule assembly*. J Biol Chem, 2010. **285**(14): p. 10959-68.
149. Fujimura, K., A.T. Sasaki, and P. Anderson, *Selenite targets eIF4E-binding protein-1 to inhibit translation initiation and induce the assembly of non-canonical stress granules*. Nucleic Acids Res, 2012. **40**(16): p. 8099-110.
150. Kim, W.J., J.H. Kim, and S.K. Jang, *Anti-inflammatory lipid mediator 15d-PGJ2 inhibits translation through inactivation of eIF4A*. EMBO J, 2007. **26**(24): p. 5020-32.
151. Bounedjah, O., et al., *Free mRNA in excess upon polysome dissociation is a scaffold for protein multimerization to form stress granules*. Nucleic Acids Res, 2014. **42**(13): p. 8678-91.
152. Buchan, J.R., J.H. Yoon, and R. Parker, *Stress-specific composition, assembly and kinetics of stress granules in Saccharomyces cerevisiae*. J Cell Sci, 2011. **124**(Pt 2): p. 228-39.
153. Sidrauski, C., et al., *The small molecule ISRIB reverses the effects of eIF2alpha phosphorylation on translation and stress granule assembly*. Elife, 2015. **4**.
154. Moutaoufik, M.T., et al., *UVC-induced stress granules in mammalian cells*. PLoS One, 2014. **9**(11): p. e112742.
155. Cherkasov, V., et al., *Coordination of translational control and protein homeostasis during severe heat stress*. Curr Biol, 2013. **23**(24): p. 2452-62.
156. Buchan, J.R., et al., *Eukaryotic stress granules are cleared by autophagy and Cdc48/VCP function*. Cell, 2013. **153**(7): p. 1461-74.
157. Seguin, S.J., et al., *Inhibition of autophagy, lysosome and VCP function impairs stress granule assembly*. Cell Death Differ, 2014. **21**(12): p. 1838-51.
158. Kwon, S., Y. Zhang, and P. Matthias, *The deacetylase HDAC6 is a novel critical component of stress granules involved in the stress response*. Genes Dev, 2007. **21**(24): p. 3381-94.
159. Krisenko, M.O., et al., *Syk Is Recruited to Stress Granules and Promotes Their Clearance through Autophagy*. J Biol Chem, 2015. **290**(46): p. 27803-15.
160. Mazroui, R., et al., *Inhibition of the ubiquitin-proteasome system induces stress granule formation*. Mol Biol Cell, 2007. **18**(7): p. 2603-18.
161. Ganassi, M., et al., *A Surveillance Function of the HSPB8-BAG3-HSP70 Chaperone Complex Ensures Stress Granule Integrity and Dynamism*. Mol Cell, 2016. **63**(5): p. 796-810.
162. Walters, R.W., et al., *Differential effects of Ydj1 and Sis1 on Hsp70-mediated clearance of stress granules in Saccharomyces cerevisiae*. RNA, 2015. **21**(9): p. 1660-71.
163. Adjibade, P., et al., *Sorafenib, a multikinase inhibitor, induces formation of stress granules in hepatocarcinoma cells*. Oncotarget, 2015. **6**(41): p. 43927-43.
164. Hu, W. and J. Collier, *What comes first: translational repression or mRNA degradation? The deepening mystery of microRNA function*. Cell Res, 2012. **22**(9): p. 1322-4.
165. Eulalio, A., I. Behm-Ansmant, and E. Izaurralde, *P bodies: at the crossroads of post-transcriptional pathways*. Nat Rev Mol Cell Biol, 2007. **8**(1): p. 9-22.
166. Eulalio, A., Behm-Ansmant, I., Schweizer, D., & Izaurralde, E. (2007), *P-body formation is a consequence, not the cause, of RNA-mediated gene silencing*. Molecular and cellular biology. **27**(11): p. 3970-3981.
167. Teixeira, D., et al., *Processing bodies require RNA for assembly and contain nontranslating mRNAs*. RNA, 2005. **11**(4): p. 371-82.
168. Bashkurov, V.I., et al., *A mouse cytoplasmic exoribonuclease (mXRN1p) with preference for G4 tetraplex substrates*. J Cell Biol, 1997. **136**(4): p. 761-73.
169. Wang, C., et al., *Context-dependent deposition and regulation of mRNAs in P-bodies*. Elife, 2018. **7**.

170. Hubstenberger, A., Courel, M., Bénard, M., Souquere, S., Ernoult-Lange, M., Chouaib, R., Yi, Z., Morlot, J. B., Munier, A., Fradet, M., Daunesse, M., Bertrand, E., Pierron, G., Mozziconacci, J., Kress, M., & Weil, D. (2017), *P-Body Purification Reveals the Condensation of Repressed mRNA Regulons*. *Molecular cell*. **68**(1): p. 144–157.e5.
171. Aulas, A., et al., *G3BP1 promotes stress-induced RNA granule interactions to preserve polyadenylated mRNA*. *J Cell Biol*, 2015. **209**(1): p. 73-84.
172. Parker, R. and H. Song, *The enzymes and control of eukaryotic mRNA turnover*. *Nat Struct Mol Biol*, 2004. **11**(2): p. 121-7.
173. Houseley, J., J. LaCava, and D. Tollervey, *RNA-quality control by the exosome*. *Nat Rev Mol Cell Biol*, 2006. **7**(7): p. 529-39.
174. Wilusz, C.J. and J. Wilusz, *Bringing the role of mRNA decay in the control of gene expression into focus*. *Trends Genet*, 2004. **20**(10): p. 491-7.
175. Fenger-Gron, M., et al., *Multiple processing body factors and the ARE binding protein TTP activate mRNA decapping*. *Mol Cell*, 2005. **20**(6): p. 905-15.
176. Yu, J.H., et al., *Ge-1 is a central component of the mammalian cytoplasmic mRNA processing body*. *RNA*, 2005. **11**(12): p. 1795-802.
177. Ingelfinger, D., et al., *The human LSm1-7 proteins colocalize with the mRNA-degrading enzymes Dcp1/2 and Xrn1 in distinct cytoplasmic foci*. *RNA*, 2002. **8**(12): p. 1489-501.
178. Tanaka, K.J., et al., *RAP55, a cytoplasmic mRNP component, represses translation in Xenopus oocytes*. *J Biol Chem*, 2006. **281**(52): p. 40096-106.
179. Behm-Ansmant, I., et al., *mRNA degradation by miRNAs and GW182 requires both CCR4:NOT deadenylase and DCP1:DCP2 decapping complexes*. *Genes Dev*, 2006. **20**(14): p. 1885-98.
180. Unterholzner, L. and E. Izaurralde, *SMG7 acts as a molecular link between mRNA surveillance and mRNA decay*. *Mol Cell*, 2004. **16**(4): p. 587-96.
181. Fukuhara, N., et al., *SMG7 is a 14-3-3-like adaptor in the nonsense-mediated mRNA decay pathway*. *Mol Cell*, 2005. **17**(4): p. 537-47.
182. Liu, J., et al., *MicroRNA-dependent localization of targeted mRNAs to mammalian P-bodies*. *Nat Cell Biol*, 2005. **7**(7): p. 719-23.
183. Sen, G.L. and H.M. Blau, *Argonaute 2/RISC resides in sites of mammalian mRNA decay known as cytoplasmic bodies*. *Nat Cell Biol*, 2005. **7**(6): p. 633-6.
184. Stoecklin, G., T. Mayo, and P. Anderson, *ARE-mRNA degradation requires the 5'-3' decay pathway*. *EMBO Rep*, 2006. **7**(1): p. 72-7.
185. Andrei, M.A., et al., *A role for eIF4E and eIF4E-transporter in targeting mRNPs to mammalian processing bodies*. *RNA*, 2005. **11**(5): p. 717-27.
186. Yang, Z., et al., *GW182 is critical for the stability of GW bodies expressed during the cell cycle and cell proliferation*. *J Cell Sci*, 2004. **117**(Pt 23): p. 5567-78.
187. Collier, J., & Parker, R. (2005), *General translational repression by activators of mRNA decapping*. *Cell*. **122**(6): p. 875–886.
188. Yoon, J.H., Choi, E. J., & Parker, R. (2010), *Dcp2 phosphorylation by Ste20 modulates stress granule assembly and mRNA decay in Saccharomyces cerevisiae*. *The Journal of cell biology*. **189**(5): p. 813–827.
189. Tenekeci, U., Poppe, M., Beuerlein, K., Buro, C., Müller, H., Weiser, H., Kettner-Buhrow, D., Porada, K., Newel, D., Xu, M., Chen, Z. J., Busch, J., Schmitz, M. L., & Kracht, M. (2016), *K63-Ubiquitylation and TRAF6 Pathways Regulate Mammalian P-Body Formation and mRNA Decapping*. *Molecular cell*. **62**(6): p. 943–957.
190. Serman, A., et al., *GW body disassembly triggered by siRNAs independently of their silencing activity*. *Nucleic Acids Res*, 2007. **35**(14): p. 4715-27.
191. Brahms, H., et al., *Symmetrical dimethylation of arginine residues in spliceosomal Sm protein B/B' and the Sm-like protein LSm4, and their interaction with the SMN protein*. *RNA*, 2001. **7**(11): p. 1531-42.
192. Franks, T.M. and J. Lykke-Andersen, *The control of mRNA decapping and P-body formation*. *Mol Cell*, 2008. **32**(5): p. 605-15.
193. Kamenska, A., et al., *The DDX6-4E-T interaction mediates translational repression and P-body assembly*. *Nucleic Acids Res*, 2016. **44**(13): p. 6318-34.
194. Decker, C.J., D. Teixeira, and R. Parker, *Edc3p and a glutamine/asparagine-rich domain of Lsm4p function in processing body assembly in Saccharomyces cerevisiae*. *J Cell Biol*, 2007. **179**(3): p. 437-49.
195. Reijns, M.A., et al., *A role for Q/N-rich aggregation-prone regions in P-body localization*. *J Cell Sci*, 2008. **121**(Pt 15): p. 2463-72.

196. Arribas-Layton, M., et al., *The C-Terminal RGG Domain of Human Lsm4 Promotes Processing Body Formation Stimulated by Arginine Dimethylation*. *Mol Cell Biol*, 2016. **36**(17): p. 2226-35.
197. Sheth, U. and R. Parker, *Decapping and decay of messenger RNA occur in cytoplasmic processing bodies*. *Science*, 2003. **300**(5620): p. 805-8.
198. Parker, R., & Sheth, U. (2007), *P bodies and the control of mRNA translation and degradation*. *Molecular cell*. **25**(5): p. 635–646.
199. Kim, Y. and S. Myong, *RNA Remodeling Activity of DEAD Box Proteins Tuned by Protein Concentration, RNA Length, and ATP*. *Mol Cell*, 2016. **63**(5): p. 865-76.
200. Mugler, C.F., et al., *ATPase activity of the DEAD-box protein Dhh1 controls processing body formation*. *Elife*, 2016. **5**.
201. Sweet, T.J., et al., *Microtubule disruption stimulates P-body formation*. *RNA*, 2007. **13**(4): p. 493-502.
202. Shav-Tal, Y. and R.H. Singer, *RNA localization*. *J Cell Sci*, 2005. **118**(Pt 18): p. 4077-81.
203. Fusco, D., et al., *Single mRNA molecules demonstrate probabilistic movement in living mammalian cells*. *Curr Biol*, 2003. **13**(2): p. 161-167.
204. Blower, M.D., et al., *Genome-wide analysis demonstrates conserved localization of messenger RNAs to mitotic microtubules*. *J Cell Biol*, 2007. **179**(7): p. 1365-73.
205. Aizer, A., et al., *The dynamics of mammalian P body transport, assembly, and disassembly in vivo*. *Mol Biol Cell*, 2008. **19**(10): p. 4154-66.
206. Gerdes, H.H., N.V. Bukoreshtliev, and J.F. Barroso, *Tunneling nanotubes: a new route for the exchange of components between animal cells*. *FEBS Lett*, 2007. **581**(11): p. 2194-201.
207. Aryani, A. and B. Denecke, *Exosomes as a Nanodelivery System: a Key to the Future of Neuromedicine?* *Mol Neurobiol*, 2016. **53**(2): p. 818-834.
208. Théry, C., Zitvogel, L., & Amigorena, S. (2002). *Exosomes: composition, biogenesis and function*. *Nature reviews. Immunology*. **2**(8): p. 569–579 <https://doi.org/10.1038/nri855>.
209. Welsh, J.A., et al., *Minimal information for studies of extracellular vesicles (MISEV2023): From basic to advanced approaches*. *J Extracell Vesicles*, 2024. **13**(2): p. e12404.
210. Ratajczak, J., Miekus, K., Kucia, M., Zhang, J., Reca, R., Dvorak, P., & Ratajczak, M. Z. (2006), *Embryonic stem cell-derived microvesicles reprogram hematopoietic progenitors: evidence for horizontal transfer of mRNA and protein delivery*. *Leukemia*. **20**(5): p. 847–856.
211. Valadi, H., Ekström, K., Bossios, A., Sjöstrand, M., Lee, J. J., & Lötvall, J. O. (2007), *Exosome-mediated transfer of mRNAs and microRNAs is a novel mechanism of genetic exchange between cells*. *Nature cell biology*. **9**(6): p. 654–659.
212. Kalra, H., Drummen, G. P., & Mathivanan, S. (2016), *Focus on Extracellular Vesicles: Introducing the Next Small Big Thing*. *International journal of molecular sciences*. **17**(2): p. 170.
213. Logozzi, M., et al., *Prostate cancer cells and exosomes in acidic condition show increased carbonic anhydrase IX expression and activity*. *J Enzyme Inhib Med Chem*, 2019. **34**(1): p. 272-278.
214. Pegtel, D.M. and S.J. Gould, *Exosomes*. *Annu Rev Biochem*, 2019. **88**: p. 487-514.
215. Matsumoto, J., Stewart, T., Banks, W. A., & Zhang, J. (2017), *The Transport Mechanism of Extracellular Vesicles at the Blood-Brain Barrier*. *Current pharmaceutical design*. **23**(40): p. 6206–6214.
216. Ahmed, F., Tamma, M., Pathigadapa, U., Reddanna, P., & Yenuganti, V. R. (2022), *Drug Loading and Functional Efficacy of Cow, Buffalo, and Goat Milk-Derived Exosomes: A Comparative Study*. *Molecular pharmaceutics*. **19**(3): p. 763–774.
217. Chargaff, E., *CELL STRUCTURE AND THE PROBLEM OF BLOOD COAGULATION*. *Journal of Biological Chemistry*, September 1945. **160**(1): p. 351-359.
218. Chargaff, E. and R. West, *The biological significance of the thromboplastin protein of Wood*. *Journal of Biological Chemistry*, 1946. **166**: p. 189-197.
219. Wolf, P., *The nature and significance of platelet products in human plasma*. *Br J Haematol*, 1967. **13**(3): p. 269-88.
220. Crawford, N., *The presence of contractile proteins in platelet microparticles isolated from human and animal platelet-free plasma*. *Br J Haematol*, 1971. **21**(1): p. 53-69.
221. Harding, C., J. Heuser, and P. Stahl, *Receptor-mediated endocytosis of transferrin and recycling of the transferrin receptor in rat reticulocytes*. *J Cell Biol*, 1983. **97**(2): p. 329-39.
222. Pan, B.T. and R.M. Johnstone, *Fate of the transferrin receptor during maturation of sheep reticulocytes in vitro: selective externalization of the receptor*. *Cell*, 1983. **33**(3): p. 967-78.
223. Lotvall, J., et al., *Minimal experimental requirements for definition of extracellular vesicles and their functions: a position statement from the International Society for Extracellular Vesicles*. *J Extracell Vesicles*, 2014. **3**: p. 26913.

224. Thery, C., et al., *Minimal information for studies of extracellular vesicles 2018 (MISEV2018): a position statement of the International Society for Extracellular Vesicles and update of the MISEV2014 guidelines*. J Extracell Vesicles, 2018. **7**(1): p. 1535750.
225. Colombo, M., G. Raposo, and C. Thery, *Biogenesis, secretion, and intercellular interactions of exosomes and other extracellular vesicles*. Annu Rev Cell Dev Biol, 2014. **30**: p. 255-89.
226. Kalluri, R. and V.S. LeBleu, *The biology, function, and biomedical applications of exosomes*. Science, 2020. **367**(6478).
227. Mashouri, L., Yousefi, H., Aref, A. R., Ahadi, A. M., Molaei, F., & Alahari, S. K. (2019), *Exosomes: composition, biogenesis, and mechanisms in cancer metastasis and drug resistance*. Molecular cancer. **18**(1): p. 75.
228. Gould, S.J., A.M. Booth, and J.E. Hildreth, *The Trojan exosome hypothesis*. Proc Natl Acad Sci U S A, 2003. **100**(19): p. 10592-7.
229. Radulovic, M. and H. Stenmark, *ESCRTs in membrane sealing*. Biochem Soc Trans, 2018. **46**(4): p. 773-778.
230. Schmidt, O. and D. Teis, *The ESCRT machinery*. Curr Biol, 2012. **22**(4): p. R116-20.
231. Baietti, M.F., et al., *Syndecan-syntenin-ALIX regulates the biogenesis of exosomes*. Nat Cell Biol, 2012. **14**(7): p. 677-85.
232. Larios, J., et al., *ALIX- and ESCRT-III-dependent sorting of tetraspanins to exosomes*. J Cell Biol, 2020. **219**(3).
233. Buschow, S.I., et al., *Exosomes contain ubiquitinated proteins*. Blood Cells Mol Dis, 2005. **35**(3): p. 398-403.
234. Putz, U., et al., *Nedd4 family-interacting protein 1 (Ndfip1) is required for the exosomal secretion of Nedd4 family proteins*. J Biol Chem, 2008. **283**(47): p. 32621-7.
235. van Niel, G., et al., *Dendritic cells regulate exposure of MHC class II at their plasma membrane by oligoubiquitination*. Immunity, 2006. **25**(6): p. 885-94.
236. Trajkovic, K., et al., *Ceramide triggers budding of exosome vesicles into multivesicular endosomes*. Science, 2008. **319**(5867): p. 1244-7.
237. Garcia-Seisdedos, D., et al., *Curcumin stimulates exosome/microvesicle release in an in vitro model of intracellular lipid accumulation by increasing ceramide synthesis*. Biochim Biophys Acta Mol Cell Biol Lipids, 2020. **1865**(5): p. 158638.
238. Hemler, M.E., *Tetraspanin proteins mediate cellular penetration, invasion, and fusion events and define a novel type of membrane microdomain*. Annu Rev Cell Dev Biol, 2003. **19**: p. 397-422.
239. Escola, J.M., et al., *Selective enrichment of tetraspan proteins on the internal vesicles of multivesicular endosomes and on exosomes secreted by human B-lymphocytes*. J Biol Chem, 1998. **273**(32): p. 20121-7.
240. Perez-Hernandez, D., et al., *The intracellular interactome of tetraspanin-enriched microdomains reveals their function as sorting machineries toward exosomes*. J Biol Chem, 2013. **288**(17): p. 11649-61.
241. Mazurov, D., L. Barbashova, and A. Filatov, *Tetraspanin protein CD9 interacts with metalloprotease CD10 and enhances its release via exosomes*. FEBS J, 2013. **280**(5): p. 1200-13.
242. Ghossoub, R., et al., *Tetraspanin-6 negatively regulates exosome production*. Proc Natl Acad Sci U S A, 2020. **117**(11): p. 5913-5922.
243. Gross, J.C., et al., *Active Wnt proteins are secreted on exosomes*. Nat Cell Biol, 2012. **14**(10): p. 1036-45.
244. Bobrie, A., et al., *Exosome secretion: molecular mechanisms and roles in immune responses*. Traffic, 2011. **12**(12): p. 1659-68.
245. Chaput, N. and C. Thery, *Exosomes: immune properties and potential clinical implementations*. Semin Immunopathol, 2011. **33**(5): p. 419-40.
246. Smith, S.A., et al., *The Endosomal Escape of Nanoparticles: Toward More Efficient Cellular Delivery*. Bioconjug Chem, 2019. **30**(2): p. 263-272.
247. Sung, B.H., et al., *A live cell reporter of exosome secretion and uptake reveals pathfinding behavior of migrating cells*. Nat Commun, 2020. **11**(1): p. 2092.
248. Faure, J., et al., *Exosomes are released by cultured cortical neurones*. Mol Cell Neurosci, 2006. **31**(4): p. 642-8.
249. Kramer-Albers, E.M., et al., *Oligodendrocytes secrete exosomes containing major myelin and stress-protective proteins: Trophic support for axons? Proteomics Clin Appl*, 2007. **1**(11): p. 1446-61.
250. Lachenal, G., et al., *Release of exosomes from differentiated neurons and its regulation by synaptic glutamatergic activity*. Mol Cell Neurosci, 2011. **46**(2): p. 409-18.

251. Bakhti, M., C. Winter, and M. Simons, *Inhibition of myelin membrane sheath formation by oligodendrocyte-derived exosome-like vesicles*. J Biol Chem, 2011. **286**(1): p. 787-96.
252. Wang, S., et al., *Synapsin I is an oligomannose-carrying glycoprotein, acts as an oligomannose-binding lectin, and promotes neurite outgrowth and neuronal survival when released via glia-derived exosomes*. J Neurosci, 2011. **31**(20): p. 7275-90.
253. Rajendran, L., et al., *Alzheimer's disease beta-amyloid peptides are released in association with exosomes*. Proc Natl Acad Sci U S A, 2006. **103**(30): p. 11172-7.
254. Gomes, C., et al., *Evidence for secretion of Cu,Zn superoxide dismutase via exosomes from a cell model of amyotrophic lateral sclerosis*. Neurosci Lett, 2007. **428**(1): p. 43-6.
255. Emmanouilidou, E., et al., *Cell-produced alpha-synuclein is secreted in a calcium-dependent manner by exosomes and impacts neuronal survival*. J Neurosci, 2010. **30**(20): p. 6838-51.
256. Nabariya, D.K., Pallu, R., & Yenuganti, V. R. (2020), *Exosomes: The protagonists in the tale of colorectal cancer?* iochimica et biophysica acta. Reviews on cancer. **1874**(2): p. 188426.
257. Nolte-'t Hoen, E., et al., *Extracellular vesicles and viruses: Are they close relatives?* Proc Natl Acad Sci U S A, 2016. **113**(33): p. 9155-61.
258. Toyofuku, M., N. Nomura, and L. Eberl, *Types and origins of bacterial membrane vesicles*. Nat Rev Microbiol, 2019. **17**(1): p. 13-24.
259. Herrmann, I.K., M.J.A. Wood, and G. Fuhrmann, *Extracellular vesicles as a next-generation drug delivery platform*. Nat Nanotechnol, 2021. **16**(7): p. 748-759.
260. Alvarez-Llamas, G., et al., *Recent advances in atherosclerosis-based proteomics: new biomarkers and a future perspective*. Expert Rev Proteomics, 2008. **5**(5): p. 679-91.
261. Simpson, R.J., et al., *Exosomes: proteomic insights and diagnostic potential*. Expert Rev Proteomics, 2009. **6**(3): p. 267-83.
262. Sandfeld-Paulsen, B., et al., *Exosomal proteins as prognostic biomarkers in non-small cell lung cancer*. Mol Oncol, 2016. **10**(10): p. 1595-1602.
263. Melo, S.A., et al., *Glypican-1 identifies cancer exosomes and detects early pancreatic cancer*. Nature, 2015. **523**(7559): p. 177-82.
264. Zhou, H., et al., *Exosomal Fetuin-A identified by proteomics: a novel urinary biomarker for detecting acute kidney injury*. Kidney Int, 2006. **70**(10): p. 1847-57.
265. Syed, F., et al., *82-OR: Exosomes from Human β -Cells Incorporate Stress Granule Components and May Serve as Biomarkers of β -Cell Stress in Type 1 Diabetes*. Diabetes, 2020. **69**(Supplement_1): p. 82-OR.
266. Nabariya, D.K., et al., *Intracellular and intercellular transport of RNA organelles in CXG repeat disorders: The strength of weak ties*. Front Mol Biosci, 2022. **9**: p. 1000932.
267. Liu, X.M., Ma, L., & Schekman, R. (2021), *Selective sorting of microRNAs into exosomes by phase-separated YBX1 condensates*. eLife. **10**: p. e71982.
268. Saudou, F. and S. Humbert, *The Biology of Huntingtin*. Neuron, 2016. **89**(5): p. 910-26.
269. Caron NS, W.G., Hayden MR., *Huntington Disease*. GeneReviews® [Internet]. 1998 Oct 23 [Updated 2020 Jun 11].
270. Lipe, H., A. Schultz, and T.D. Bird, *Risk factors for suicide in Huntingtons disease: a retrospective case controlled study*. Am J Med Genet, 1993. **48**(4): p. 231-3.
271. Medina, A., et al., *Prevalence and Incidence of Huntington's Disease: An Updated Systematic Review and Meta-Analysis*. Mov Disord, 2022. **37**(12): p. 2327-2335.
272. Wyant, K.J., A.J. Ridder, and P. Dayalu, *Huntington's Disease-Update on Treatments*. Curr Neurol Neurosci Rep, 2017. **17**(4): p. 33.
273. Gonzalez-Alegre, P. and A.K. Afifi, *Clinical characteristics of childhood-onset (juvenile) Huntington disease: report of 12 patients and review of the literature*. J Child Neurol, 2006. **21**(3): p. 223-9.
274. Paulsen, J.S., et al., *Neuropsychiatric aspects of Huntington's disease*. J Neurol Neurosurg Psychiatry, 2001. **71**(3): p. 310-4.
275. Aylward, E.H., et al., *Longitudinal change in regional brain volumes in prodromal Huntington disease*. J Neurol Neurosurg Psychiatry, 2011. **82**(4): p. 405-10.
276. Rosas, H.D., et al., *Cerebral cortex and the clinical expression of Huntington's disease: complexity and heterogeneity*. Brain, 2008. **131**(Pt 4): p. 1057-68.
277. van der Burg, J.M., M. Bjorkqvist, and P. Brundin, *Beyond the brain: widespread pathology in Huntington's disease*. Lancet Neurol, 2009. **8**(8): p. 765-74.
278. Kremer, B., et al., *A worldwide study of the Huntington's disease mutation. The sensitivity and specificity of measuring CAG repeats*. N Engl J Med, 1994. **330**(20): p. 1401-6.

279. Atwal, R.S., et al., *Huntingtin has a membrane association signal that can modulate huntingtin aggregation, nuclear entry and toxicity*. Hum Mol Genet, 2007. **16**(21): p. 2600-15.
280. Tartari, M., et al., *Phylogenetic comparison of huntingtin homologues reveals the appearance of a primitive polyQ in sea urchin*. Mol Biol Evol, 2008. **25**(2): p. 330-8.
281. Rockabrand, E., et al., *The first 17 amino acids of Huntingtin modulate its sub-cellular localization, aggregation and effects on calcium homeostasis*. Hum Mol Genet, 2007. **16**(1): p. 61-77.
282. Maiuri, T., et al., *The huntingtin N17 domain is a multifunctional CRM1 and Ran-dependent nuclear and ciliary export signal*. Hum Mol Genet, 2013. **22**(7): p. 1383-94.
283. Steffan, J.S., et al., *SUMO modification of Huntingtin and Huntington's disease pathology*. Science, 2004. **304**(5667): p. 100-4.
284. Thompson, L.M., et al., *IKK phosphorylates Huntingtin and targets it for degradation by the proteasome and lysosome*. J Cell Biol, 2009. **187**(7): p. 1083-99.
285. Lin, B., et al., *Differential 3' polyadenylation of the Huntington disease gene results in two mRNA species with variable tissue expression*. Hum Mol Genet, 1993. **2**(10): p. 1541-5.
286. Gafni, J. and L.M. Ellerby, *Calpain activation in Huntington's disease*. J Neurosci, 2002. **22**(12): p. 4842-9.
287. Goldberg, Y.P., et al., *Cleavage of huntingtin by apopain, a proapoptotic cysteine protease, is modulated by the polyglutamine tract*. Nat Genet, 1996. **13**(4): p. 442-9.
288. Hermel, E., et al., *Specific caspase interactions and amplification are involved in selective neuronal vulnerability in Huntington's disease*. Cell Death Differ, 2004. **11**(4): p. 424-38.
289. Kim, Y.J., et al., *Caspase 3-cleaved N-terminal fragments of wild-type and mutant huntingtin are present in normal and Huntington's disease brains, associate with membranes, and undergo calpain-dependent proteolysis*. Proc Natl Acad Sci U S A, 2001. **98**(22): p. 12784-9.
290. Kim, Y.J., et al., *Lysosomal proteases are involved in generation of N-terminal huntingtin fragments*. Neurobiol Dis, 2006. **22**(2): p. 346-56.
291. Lunkes, A., et al., *Proteases acting on mutant huntingtin generate cleaved products that differentially build up cytoplasmic and nuclear inclusions*. Mol Cell, 2002. **10**(2): p. 259-69.
292. Ratovitski, T., et al., *Mutant huntingtin N-terminal fragments of specific size mediate aggregation and toxicity in neuronal cells*. J Biol Chem, 2009. **284**(16): p. 10855-67.
293. Benn, C.L., et al., *Contribution of nuclear and extranuclear polyQ to neurological phenotypes in mouse models of Huntington's disease*. Hum Mol Genet, 2005. **14**(20): p. 3065-78.
294. Saudou, F., et al., *Huntingtin acts in the nucleus to induce apoptosis but death does not correlate with the formation of intranuclear inclusions*. Cell, 1998. **95**(1): p. 55-66.
295. Valor, L.M., *Transcription, epigenetics and ameliorative strategies in Huntington's Disease: a genome-wide perspective*. Mol Neurobiol, 2015. **51**(1): p. 406-23.
296. Steffan, J.S., et al., *The Huntington's disease protein interacts with p53 and CREB-binding protein and represses transcription*. Proc Natl Acad Sci U S A, 2000. **97**(12): p. 6763-8.
297. Takano, H. and J.F. Gusella, *The predominantly HEAT-like motif structure of huntingtin and its association and coincident nuclear entry with dorsal, an NF-kB/Rel/dorsal family transcription factor*. BMC Neurosci, 2002. **3**: p. 15.
298. Zuccato, C., et al., *Huntingtin interacts with REST/NRSF to modulate the transcription of NRSE-controlled neuronal genes*. Nat Genet, 2003. **35**(1): p. 76-83.
299. Holbert, S., et al., *The Gln-Ala repeat transcriptional activator CA150 interacts with huntingtin: neuropathologic and genetic evidence for a role in Huntington's disease pathogenesis*. Proc Natl Acad Sci U S A, 2001. **98**(4): p. 1811-6.
300. Bae, B.I., et al., *p53 mediates cellular dysfunction and behavioral abnormalities in Huntington's disease*. Neuron, 2005. **47**(1): p. 29-41.
301. Seong, I.S., et al., *Huntingtin facilitates polycomb repressive complex 2*. Hum Mol Genet, 2010. **19**(4): p. 573-83.
302. White, J.K., et al., *Huntingtin is required for neurogenesis and is not impaired by the Huntington's disease CAG expansion*. Nat Genet, 1997. **17**(4): p. 404-10.
303. Elias, S., et al., *Huntingtin regulates mammary stem cell division and differentiation*. Stem Cell Reports, 2014. **2**(4): p. 491-506.
304. Van Raamsdonk, J.M., et al., *Body weight is modulated by levels of full-length huntingtin*. Hum Mol Genet, 2006. **15**(9): p. 1513-23.
305. Ho, L.W., et al., *Wild type Huntingtin reduces the cellular toxicity of mutant Huntingtin in mammalian cell models of Huntington's disease*. J Med Genet, 2001. **38**(7): p. 450-2.

306. Leavitt, B.R., et al., *Wild-type huntingtin protects neurons from excitotoxicity*. J Neurochem, 2006. **96**(4): p. 1121-9.
307. Marques Sousa, C. and S. Humbert, *Huntingtin: here, there, everywhere!* J Huntingtons Dis, 2013. **2**(4): p. 395-403.
308. Sun, M., et al., *NuMA regulates mitotic spindle assembly, structural dynamics and function via phase separation*. Nat Commun, 2021. **12**(1): p. 7157.
309. Godin, J.D., et al., *Huntingtin is required for mitotic spindle orientation and mammalian neurogenesis*. Neuron, 2010. **67**(3): p. 392-406.
310. Karam, A., et al., *A novel function of Huntingtin in the cilium and retinal ciliopathy in Huntington's disease mice*. Neurobiol Dis, 2015. **80**: p. 15-28.
311. Keryer, G., et al., *Ciliogenesis is regulated by a huntingtin-HAP1-PCM1 pathway and is altered in Huntington disease*. J Clin Invest, 2011. **121**(11): p. 4372-82.
312. Palidwor, G.A., et al., *Detection of alpha-rod protein repeats using a neural network and application to huntingtin*. PLoS Comput Biol, 2009. **5**(3): p. e1000304.
313. Warby, S.C., et al., *Activated caspase-6 and caspase-6-cleaved fragments of huntingtin specifically colocalize in the nucleus*. Hum Mol Genet, 2008. **17**(15): p. 2390-404.
314. Caviston, J.P., et al., *Huntingtin facilitates dynein/dynactin-mediated vesicle transport*. Proc Natl Acad Sci U S A, 2007. **104**(24): p. 10045-50.
315. Colin, E., et al., *Huntingtin phosphorylation acts as a molecular switch for anterograde/retrograde transport in neurons*. EMBO J, 2008. **27**(15): p. 2124-34.
316. Engelender, S., et al., *Huntingtin-associated protein 1 (HAP1) interacts with the p150Glued subunit of dynactin*. Hum Mol Genet, 1997. **6**(13): p. 2205-12.
317. Twelvetrees, A.E., et al., *Delivery of GABAARs to synapses is mediated by HAP1-KIF5 and disrupted by mutant huntingtin*. Neuron, 2010. **65**(1): p. 53-65.
318. Wong, Y.C. and E.L. Holzbaur, *The regulation of autophagosome dynamics by huntingtin and HAP1 is disrupted by expression of mutant huntingtin, leading to defective cargo degradation*. J Neurosci, 2014. **34**(4): p. 1293-305.
319. Caviston, J.P., et al., *Huntingtin coordinates the dynein-mediated dynamic positioning of endosomes and lysosomes*. Mol Biol Cell, 2011. **22**(4): p. 478-92.
320. Zala, D., et al., *Vesicular glycolysis provides on-board energy for fast axonal transport*. Cell, 2013. **152**(3): p. 479-91.
321. Engqvist-Goldstein, A.E., et al., *The actin-binding protein Hip1R associates with clathrin during early stages of endocytosis and promotes clathrin assembly in vitro*. J Cell Biol, 2001. **154**(6): p. 1209-23.
322. Legendre-Guillemain, V., et al., *HIP1 and HIP12 display differential binding to F-actin, AP2, and clathrin. Identification of a novel interaction with clathrin light chain*. J Biol Chem, 2002. **277**(22): p. 19897-904.
323. Waelter, S., et al., *The huntingtin interacting protein HIP1 is a clathrin and alpha-adaptin-binding protein involved in receptor-mediated endocytosis*. Hum Mol Genet, 2001. **10**(17): p. 1807-17.
324. Kaltenbach, L.S., et al., *Huntingtin interacting proteins are genetic modifiers of neurodegeneration*. PLoS Genet, 2007. **3**(5): p. e82.
325. Modregger, J., et al., *Characterization of Endophilin B1b, a brain-specific membrane-associated lysophosphatidic acid acyl transferase with properties distinct from endophilin A1*. J Biol Chem, 2003. **278**(6): p. 4160-7.
326. Sittler, A., et al., *SH3GL3 associates with the Huntingtin exon 1 protein and promotes the formation of polyglutamine-containing protein aggregates*. Mol Cell, 1998. **2**(4): p. 427-36.
327. Li, X., et al., *A function of huntingtin in guanine nucleotide exchange on Rab11*. Neuroreport, 2008. **19**(16): p. 1643-7.
328. Pal, A., et al., *Huntingtin-HAP40 complex is a novel Rab5 effector that regulates early endosome motility and is up-regulated in Huntington's disease*. J Cell Biol, 2006. **172**(4): p. 605-18.
329. Jeong, H., et al., *Acetylation targets mutant huntingtin to autophagosomes for degradation*. Cell, 2009. **137**(1): p. 60-72.
330. Luo, S., et al., *Cdk5 phosphorylation of huntingtin reduces its cleavage by caspases: implications for mutant huntingtin toxicity*. J Cell Biol, 2005. **169**(4): p. 647-56.
331. Schilling, B., et al., *Huntingtin phosphorylation sites mapped by mass spectrometry. Modulation of cleavage and toxicity*. J Biol Chem, 2006. **281**(33): p. 23686-97.
332. Martin, D.D., et al., *Identification of a post-translationally myristoylated autophagy-inducing domain released by caspase cleavage of huntingtin*. Hum Mol Genet, 2014. **23**(12): p. 3166-79.

333. Kegel, K.B., et al., *Huntingtin expression stimulates endosomal-lysosomal activity, endosome tubulation, and autophagy*. J Neurosci, 2000. **20**(19): p. 7268-78.
334. Ravikumar, B., et al., *Inhibition of mTOR induces autophagy and reduces toxicity of polyglutamine expansions in fly and mouse models of Huntington disease*. Nat Genet, 2004. **36**(6): p. 585-95.
335. Rui, Y.N., et al., *Huntingtin functions as a scaffold for selective macroautophagy*. Nat Cell Biol, 2015. **17**(3): p. 262-75.
336. Chuang, C.L. and F. Demontis, *Systemic manifestation and contribution of peripheral tissues to Huntington's disease pathogenesis*. Ageing Res Rev, 2021. **69**: p. 101358.
337. Rub, U., et al., *Huntington's disease (HD): the neuropathology of a multisystem neurodegenerative disorder of the human brain*. Brain Pathol, 2016. **26**(6): p. 726-740.
338. Guo, W., K. Stoklund Dittlau, and L. Van Den Bosch, *Axonal transport defects and neurodegeneration: Molecular mechanisms and therapeutic implications*. Semin Cell Dev Biol, 2020. **99**: p. 133-150.
339. Labbadia, J. and R.I. Morimoto, *Huntington's disease: underlying molecular mechanisms and emerging concepts*. Trends Biochem Sci, 2013. **38**(8): p. 378-85.
340. Gomez-Jaramillo, L., et al., *A New Perspective on Huntington's Disease: How a Neurological Disorder Influences the Peripheral Tissues*. Int J Mol Sci, 2022. **23**(11).
341. Cattaneo, E., C. Zuccato, and M. Tartari, *Normal huntingtin function: an alternative approach to Huntington's disease*. Nat Rev Neurosci, 2005. **6**(12): p. 919-30.
342. Takahashi, T., S. Katada, and O. Onodera, *Polyglutamine diseases: where does toxicity come from? what is toxicity? where are we going?* J Mol Cell Biol, 2010. **2**(4): p. 180-91.
343. Hsu, R.J., et al., *Long tract of untranslated CAG repeats is deleterious in transgenic mice*. PLoS ONE, 2011. **6**(1): p. e16417.
344. Lawlor, K.T., et al., *Double-stranded RNA is pathogenic in Drosophila models of expanded repeat neurodegenerative diseases*. Hum Mol Genet, 2011. **20**(19): p. 3757-68.
345. Wang, L.C., et al., *Muscleblind participates in RNA toxicity of expanded CAG and CUG repeats in Caenorhabditis elegans*. Cell Mol Life Sci, 2011. **68**(7): p. 1255-67.
346. Bernat, V. and M.D. Disney, *RNA Structures as Mediators of Neurological Diseases and as Drug Targets*. Neuron, 2015. **87**(1): p. 28-46.
347. Nalavade, R., et al., *Mechanisms of RNA-induced toxicity in CAG repeat disorders*. Cell Death Dis, 2013. **4**: p. e752.
348. Schilling, J., N. Griesche, and S. Krauß, *Mechanisms of RNA-Induced Toxicity in Diseases Characterised by CAG Repeat Expansions*. eLS. John Wiley & Sons, Ltd: Chichester., 2016.
349. Heinz, A., Nabariya, D.K., Krauß, S., *Huntington's Disease and Neurodegeneration*. , in *Handbook of Neurotoxicity*. , R.M.e. Kostrzewa, Editor. 2022, Springer, Cham.
350. Heinz, A., Nabariya, D. K., & Krauss, S. (2021), *Huntingtin and Its Role in Mechanisms of RNA-Mediated Toxicity*. Toxins. **13**(7): p. 487.
351. America, H.s.D.S.o. *Therapies in pipeline*. [cited 2025 19/3/2025]; Available from: <https://hdsa.org/hd-research/therapies-in-pipeline/>.
352. McColgan, P., et al., *Tominersen in Adults with Manifest Huntington's Disease*. N Engl J Med, 2023. **389**(23): p. 2203-2205.
353. Deeptose, C., *Looking Forward*. EHDN News, July 2021(43).
354. Deeptose, C.R., A. , *Looking Back, Looking Forward.*, in *EHDN News*. . 2021.
355. ; Available from: <https://hdsa.org/hd-research/therapies-in-pipeline/>
356. Gutierrez-Garcia, R., et al., *G3BP1-dependent mechanism suppressing protein aggregation in Huntington's models and its demise upon stress granule assembly*. Hum Mol Genet, 2023. **32**(10): p. 1607-1621.
357. Savas, J.N., et al., *Huntington's disease protein contributes to RNA-mediated gene silencing through association with Argonaute and P bodies*. Proc Natl Acad Sci U S A, 2008. **105**(31): p. 10820-5.
358. Savas, J.N., Ma, B., Deinhardt, K., Culver, B. P., Restituto, S., Wu, L., Belasco, J. G., Chao, M. V., & Tanese, N. (2010), *A role for huntington disease protein in dendritic RNA granules*. The Journal of biological chemistry. **285**(17): p. 13142–13153.
359. Ma, B., Savas, J. N., Yu, M. S., Culver, B. P., Chao, M. V., & Tanese, N. (2011), *Huntingtin mediates dendritic transport of β -actin mRNA in rat neurons*. Scientific reports. **1**: p. 140.
360. Ren, P.H., et al., *Cytoplasmic penetration and persistent infection of mammalian cells by polyglutamine aggregates*. Nat Cell Biol, 2009. **11**(2): p. 219-25.

361. Yang, X., Shen, Y., Garre, E., Hao, X., Krumlinde, D., Cvijović, M., Arens, C., Nyström, T., Liu, B., & Sunnerhagen, P. (2014), *Stress granule-defective mutants deregulate stress responsive transcripts*. PLoS genetics. **10**(11): p. e1004763.
362. Herrera, F., et al., *Visualization of cell-to-cell transmission of mutant huntingtin oligomers*. PLoS Curr, 2011. **3**: p. RRN1210.
363. Costanzo, M., Abounit, S., Marzo, L., Danckaert, A., Chamoun, Z., Roux, P., & Zurzolo, C. (2013), *Transfer of polyglutamine aggregates in neuronal cells occurs in tunneling nanotubes*. Journal of cell science. **126**: p. 3678–3685.
364. Pecho-Vrieseling, E., Rieker, C., Fuchs, S., Bleckmann, D., Esposito, M. S., Botta, P., Goldstein, C., Bernhard, M., Galimberti, I., Müller, M., Lüthi, A., Arber, S., Bouwmeester, T., van der Putten, H., & Di Giorgio, F. P. (2014), *Transneuronal propagation of mutant huntingtin contributes to non-cell autonomous pathology in neurons*. Nature neuroscience. **17**(8): p. 1064–1072.
365. Cicchetti, F., Lacroix, S., Cisbani, G., Vallières, N., Saint-Pierre, M., St-Amour, I., Tolouei, R., Skepper, J. N., Hauser, R. A., Mantovani, D., Barker, R. A., & Freeman, T. B. (2014), *Mutant huntingtin is present in neuronal grafts in Huntington disease patients*. Annals of neurology. **76**(1): p. 31–42.
366. Jeon, I., Cicchetti, F., Cisbani, G., Lee, S., Li, E., Bae, J., Lee, N., Li, L., Im, W., Kim, M., Kim, H. S., Oh, S. H., Kim, T. A., Ko, J. J., Aubé, B., Oueslati, A., Kim, Y. J., & Song, J. (2016), *Human-to-mouse prion-like propagation of mutant huntingtin protein*. Acta neuropathologica. **132**(4): p. 577–592.
367. Hong, Y., Zhao, T., Li, X. J., & Li, S. (2017), *Mutant Huntingtin Inhibits α B-Crystallin Expression and Impairs Exosome Secretion from Astrocytes*. The Journal of neuroscience : the official journal of the Society for Neuroscience. **37**(39): p. 9550–9563.
368. Ananbeh, H., Novak, J., Juhas, S., Juhasova, J., Klempir, J., Doleckova, K., Rysankova, I., Turnovcova, K., Hanus, J., Hansikova, H., Vodicka, P., & Kupcova Skalnikova, H. (2022), *Huntingtin Co-Isolates with Small Extracellular Vesicles from Blood Plasma of TgHD and KI-HD Pig Models of Huntington's Disease and Human Blood Plasma*. International journal of molecular sciences. **23**(10): p. 5598.
369. Ananbeh, H., Vodicka, P., & Kupcova Skalnikova, H. (2021), *Emerging Roles of Exosomes in Huntington's Disease*. International journal of molecular sciences **22**(8): p. 4085.
370. Zhang, X., Abels, E. R., Redzic, J. S., Margulis, J., Finkbeiner, S., & Breakefield, X. O. (2016), *Potential Transfer of Polyglutamine and CAG-Repeat RNA in Extracellular Vesicles in Huntington's Disease: Background and Evaluation in Cell Culture*. Cellular and molecular neurobiology. **36**(3): p. 459–470.
371. Jin, Y.N., & Johnson, G. V. (2010), *The interrelationship between mitochondrial dysfunction and transcriptional dysregulation in Huntington disease*. Journal of bioenergetics and biomembranes. **42**(3): p. 199–205.
372. Beatriz, M., Vilaça, R., Anjo, S.I., Manadas, B., Januário, C., Rego, C.A., Lopes, C. (2022), *Defective mitochondrial-lysosomal axis promotes extracellular vesicles release of mitochondrial components in Huntington's Disease*.
373. Pircs, K., Petri, R., Madsen, S., Brattås, P. L., Vuono, R., Ottosson, D. R., St-Amour, I., Hersbach, B. A., Matusiak-Brückner, M., Lundh, S. H., Petersén, Å., Déglon, N., Hébert, S. S., Parmar, M., Barker, R. A., & Jakobsson, J. (2018) *Huntingtin Aggregation Impairs Autophagy, Leading to Argonaute-2 Accumulation and Global MicroRNA Dysregulation*. Cell reports. **24**(6): p. 1397–1406.
374. Bahar, R., et al., *Neuroprotective effect of human cord blood-derived extracellular vesicles by improved neuromuscular function and reduced gliosis in a rat model of Huntington's disease*. J Chem Neuroanat, 2024. **138**: p. 102419.
375. Solana-Balaguer, J., et al., *Motor skill learning modulates striatal extracellular vesicles' content in a mouse model of Huntington's disease*. Cell Commun Signal, 2024. **22**(1): p. 321.
376. Markmiller, S., Soltanieh, S., Server, K. L., Mak, R., Jin, W., Fang, M. Y., Luo, E. C., Krach, F., Yang, D., Sen, A., Fulzele, A., Wozniak, J. M., Gonzalez, D. J., Kankel, M. W., Gao, F. B., Bennett, E. J., Lécuyer, E., & Yeo, G. W. (2018), *Context-Dependent and Disease-Specific Diversity in Protein Interactions within Stress Granules*. Cell. **172**(3): p. 590–604.e13.
377. Leidal, A.M., Huang, H. H., Marsh, T., Solvik, T., Zhang, D., Ye, J., Kai, F., Goldsmith, J., Liu, J. Y., Huang, Y. H., Monkkonen, T., Vlahakis, A., Huang, E. J., Goodarzi, H., Yu, L., Wiita, A. P., & Debnath, J. (2020), *The LC3-conjugation machinery specifies the loading of RNA-binding proteins into extracellular vesicles*. Nature cell biology. **22**(2): p. 187–199.
378. Mittelbrunn, M., Gutiérrez-Vázquez, C., Villarroya-Beltri, C., González, S., Sánchez-Cabo, F., González, M.A., Bernad, A., Sánchez-Madrid, F. (2011), *Unidirectional transfer of microRNA-loaded exosomes from T cells to antigen-presenting cells*. Nature Communications. **2**(1): p. 282.

379. Haimovich, G., Ecker, C. M., Dunagin, M. C., Eggan, E., Raj, A., Gerst, J. E., & Singer, R. H. (2017), *Intercellular mRNA trafficking via membrane nanotube-like extensions in mammalian cells*. Proceedings of the National Academy of Sciences of the United States of America. **114**(46): p. E9873–E9882.
380. Wozniak, A.L., Adams, A., King, K. E., Dunn, W., Christenson, L. K., Hung, W. T., & Weinman, S. A. (2020), *The RNA binding protein FMR1 controls selective exosomal miRNA cargo loading during inflammation*. The Journal of cell biology. **219**(10): p. e201912074.
381. Waelter, S., et al., *Accumulation of mutant huntingtin fragments in aggresome-like inclusion bodies as a result of insufficient protein degradation*. Mol Biol Cell, 2001. **12**(5): p. 1393-407.
382. Scherzinger, E., et al., *Huntingtin-encoded polyglutamine expansions form amyloid-like protein aggregates in vitro and in vivo*. Cell, 1997. **90**(3): p. 549-58.
383. Matthes, F., et al., *Reducing Mutant Huntingtin Protein Expression in Living Cells by a Newly Identified RNA CAG Binder*. ACS Chemical Neuroscience, 2018. **9**(6): p. 1399-1408.
384. Mangiarini, L., et al., *Exon 1 of the HD gene with an expanded CAG repeat is sufficient to cause a progressive neurological phenotype in transgenic mice*. Cell, 1996. **87**(3): p. 493-506.
385. Davies, S.W., et al., *Formation of neuronal intranuclear inclusions underlies the neurological dysfunction in mice transgenic for the HD mutation*. Cell, 1997. **90**(3): p. 537-48.
386. Ross, C.A., *Polyglutamine pathogenesis: emergence of unifying mechanisms for Huntington's disease and related disorders*. Neuron, 2002. **35**(5): p. 819-22.
387. Raposo, G., et al., *B lymphocytes secrete antigen-presenting vesicles*. J Exp Med, 1996. **183**(3): p. 1161-72.
388. Namkoong, S., Ho, A., Woo, Y. M., Kwak, H., & Lee, J. H. (2018), *Systematic Characterization of Stress-Induced RNA Granulation*. Molecular cell. **70**(1): p. 175–187.e8.
389. Théry, C., Witwer, K. W., Aikawa, E., Alcaraz, M. J., Anderson, J. D., Andriantsitohaina, R., Antoniou, A., Arab, T., Archer, F., Atkin-Smith, G. K., Ayre, D. C., Bach, J. M., Bachurski, D., Baharvand, H., Balaj, L., Baldacchino, S., Bauer, N. N., Baxter, A. A., Bebawy, M., Beckham, C., ... Zuba-Surma, E. K. (2018). , *Minimal information for studies of extracellular vesicles 2018 (MISEV2018): a position statement of the International Society for Extracellular Vesicles and update of the MISEV2014 guidelines*. Journal of extracellular vesicles. **7**(1): p. 1535750.
390. S., A., *FastQC: a quality control tool for high throughput sequence data*. . 2010.
391. Bolger, A.M., M. Lohse, and B. Usadel, *Trimmomatic: a flexible trimmer for Illumina sequence data*. Bioinformatics, 2014. **30**(15): p. 2114-20.
392. martin, M., *Cutadapt Removes Adapter Sequences From High-Throughput Sequencing Reads*.
393. Neueder, A., et al., *Huntington disease alters the actionable information in plasma extracellular vesicles*. Clin Transl Med, 2024. **14**(1): p. e1525.
394. Love, M.I., W. Huber, and S. Anders, *Moderated estimation of fold change and dispersion for RNA-seq data with DESeq2*. Genome Biol, 2014. **15**(12): p. 550.
395. Stephens, M., *False discovery rates: a new deal*. Biostatistics, 2017. **18**(2): p. 275-294.
396. Hughes, C.S., et al., *Single-pot, solid-phase-enhanced sample preparation for proteomics experiments*. Nat Protoc, 2019. **14**(1): p. 68-85.
397. Cox, J. and M. Mann, *MaxQuant enables high peptide identification rates, individualized p.p.b.-range mass accuracies and proteome-wide protein quantification*. Nat Biotechnol, 2008. **26**(12): p. 1367-72.
398. Cox, J., et al., *Accurate proteome-wide label-free quantification by delayed normalization and maximal peptide ratio extraction, termed MaxLFQ*. Mol Cell Proteomics, 2014. **13**(9): p. 2513-26.
399. Cox, J., et al., *Andromeda: a peptide search engine integrated into the MaxQuant environment*. J Proteome Res, 2011. **10**(4): p. 1794-805.
400. Schilling, J., Broemer, M., Atanassov, I., Duernberger, Y., Vorberg, I., Dieterich, C., Dagane, A., Dittmar, G., Wanker, E., van Roon-Mom, W., Winter, J., & Krauß, S. (2019), *Deregulated Splicing Is a Major Mechanism of RNA-Induced Toxicity in Huntington's Disease*. Journal of Molecular Biology. **431**(9): p. 1869-1877.
401. Kanehisa, M. and S. Goto, *KEGG: kyoto encyclopedia of genes and genomes*. Nucleic Acids Res, 2000. **28**(1): p. 27-30.
402. Kanehisa, M. and Y. Sato, *KEGG Mapper for inferring cellular functions from protein sequences*. Protein Sci, 2020. **29**(1): p. 28-35.
403. Romero, P., et al., *Computational prediction of human metabolic pathways from the complete human genome*. Genome Biol, 2005. **6**(1): p. R2.

404. Szklarczyk, D., et al., *The STRING database in 2023: protein-protein association networks and functional enrichment analyses for any sequenced genome of interest*. *Nucleic Acids Res*, 2023. **51**(D1): p. D638-D646.
405. Kim, M., M. Bellini, and S. Ceman, *Fragile X mental retardation protein FMRP binds mRNAs in the nucleus*. *Mol Cell Biol*, 2009. **29**(1): p. 214-28.
406. Kretov, D.A., et al., *Inhibition of Transcription Induces Phosphorylation of YB-1 at Ser102 and Its Accumulation in the Nucleus*. *Cells*, 2019. **9**(1).
407. Mehta, S., et al., *Dephosphorylation of YB-1 is Required for Nuclear Localisation During G(2) Phase of the Cell Cycle*. *Cancers (Basel)*, 2020. **12**(2).
408. Winslow, S., K. Leandersson, and C. Larsson, *Regulation of PMP22 mRNA by G3BP1 affects cell proliferation in breast cancer cells*. *Mol Cancer*, 2013. **12**(1): p. 156.
409. Westmark, C.J., et al., *FMRP Regulates the Nuclear Export of Adam9 and Psen1 mRNAs: Secondary Analysis of an N(6)-Methyladenosine Dataset*. *Sci Rep*, 2020. **10**(1): p. 10781.
410. Somasekharan, S.P., et al., *YB-1 regulates stress granule formation and tumor progression by translationally activating G3BP1*. *J Cell Biol*, 2015. **208**(7): p. 913-29.
411. Alkrekshi, A., et al., *A comprehensive review of the functions of YB-1 in cancer stemness, metastasis and drug resistance*. *Cell Signal*, 2021. **85**: p. 110073.
412. Karp, P.D., et al., *The BioCyc collection of microbial genomes and metabolic pathways*. *Brief Bioinform*, 2019. **20**(4): p. 1085-1093.
413. Anderson, P., & Kedersha, N. (2009). , *RNA granules: post-transcriptional and epigenetic modulators of gene expression*. *Nature reviews. Molecular cell biology*. **10**(6): p. 430–436.
414. Schilling, J., et al., *Deregulated Splicing Is a Major Mechanism of RNA-Induced Toxicity in Huntington's Disease*. *J Mol Biol*, 2019.
415. Pink, D., et al., *Cysteine String Protein Controls Two Routes of Export for Misfolded Huntingtin*. *Front Neurosci*, 2021. **15**: p. 762439.
416. Zhang, J., et al., *MicroRNA-542-3p suppresses cellular proliferation of bladder cancer cells through post-transcriptionally regulating survivin*. *Gene*, 2016. **579**(2): p. 146-52.
417. Denis, H.L., et al., *Platelet-derived extracellular vesicles in Huntington's disease*. *J Neurol*, 2018. **265**(11): p. 2704-2712.
418. Campos-Melo, D., et al., *The Integral Role of RNA in Stress Granule Formation and Function*. *Front Cell Dev Biol*, 2021. **9**: p. 621779.
419. Mo, M., *Editorial: Non-coding RNAs in neurodegenerative diseases*. *Front Neurosci*, 2023. **17**: p. 1241737.
420. Cheng, P.H., et al., *miR-196a ameliorates phenotypes of Huntington disease in cell, transgenic mouse, and induced pluripotent stem cell models*. *Am J Hum Genet*, 2013. **93**(2): p. 306-12.
421. Johnson, R., et al., *A microRNA-based gene dysregulation pathway in Huntington's disease*. *Neurobiol Dis*, 2008. **29**(3): p. 438-45.
422. Packer, A.N., et al., *The bifunctional microRNA miR-9/miR-9* regulates REST and CoREST and is downregulated in Huntington's disease*. *J Neurosci*, 2008. **28**(53): p. 14341-6.
423. Zhang, W.H., et al., *MicroRNA-124: an emerging therapeutic target in central nervous system disorders*. *Exp Brain Res*, 2023. **241**(5): p. 1215-1226.
424. Ban, J.J., et al., *MicroRNA-27a reduces mutant huntingtin aggregation in an in vitro model of Huntington's disease*. *Biochem Biophys Res Commun*, 2017. **488**(2): p. 316-321.
425. Finotti, A., et al., *MicroRNAs and Long Non-coding RNAs in Genetic Diseases*. *Mol Diagn Ther*, 2019. **23**(2): p. 155-171.
426. Chang, K.H., Y.R. Wu, and C.M. Chen, *Down-regulation of miR-9* in the peripheral leukocytes of Huntington's disease patients*. *Orphanet J Rare Dis*, 2017. **12**(1): p. 185.
427. Marti, E., et al., *A myriad of miRNA variants in control and Huntington's disease brain regions detected by massively parallel sequencing*. *Nucleic Acids Res*, 2010. **38**(20): p. 7219-35.
428. Johnson, R. and N.J. Buckley, *Gene dysregulation in Huntington's disease: REST, microRNAs and beyond*. *Neuromolecular Med*, 2009. **11**(3): p. 183-99.
429. Boudna, M., et al., *Investigation of long non-coding RNAs in extracellular vesicles from low-volume blood serum specimens of colorectal cancer patients*. *Clin Exp Med*, 2024. **24**(1): p. 67.
430. Huarte, M., et al., *A large intergenic noncoding RNA induced by p53 mediates global gene repression in the p53 response*. *Cell*, 2010. **142**(3): p. 409-19.
431. Matouk, I.J., et al., *The H19 non-coding RNA is essential for human tumor growth*. *PLoS One*, 2007. **2**(9): p. e845.

432. Prensner, J.R., et al., *Transcriptome sequencing across a prostate cancer cohort identifies PCAT-1, an unannotated lincRNA implicated in disease progression*. Nat Biotechnol, 2011. **29**(8): p. 742-9.
433. Zhang, M., P. He, and Z. Bian, *Long Noncoding RNAs in Neurodegenerative Diseases: Pathogenesis and Potential Implications as Clinical Biomarkers*. Front Mol Neurosci, 2021. **14**: p. 685143.
434. Lipovich, L., et al., *Activity-dependent human brain coding/noncoding gene regulatory networks*. Genetics, 2012. **192**(3): p. 1133-48.
435. Shimojo, M., *Huntingtin regulates RE1-silencing transcription factor (REST/NRSF) nuclear trafficking indirectly through a complex with REST/NRSF-interacting LIM domain protein (RILP) and dynactin p150Glued*. J Biol Chem, 2008.
436. Johnson, R., et al., *Human accelerated region 1 noncoding RNA is repressed by REST in Huntington's disease*. Physiol Genomics, 2010. **41**(3): p. 269-74.
437. Maksour, S., L. Ooi, and M. Dottori, *More than a Corepressor: The Role of CoREST Proteins in Neurodevelopment*. eNeuro, 2020. **7**(2).
438. Romano, R. and C. Bucci, *Role of EGFR in the Nervous System*. Cells, 2020. **9**(8).
439. Maib, H. and D.H. Murray, *A mechanism for exocyst-mediated tethering via Arf6 and PIP5K1C-driven phosphoinositide conversion*. Curr Biol, 2022. **32**(13): p. 2821-2833 e6.
440. Mochel, F. and R.G. Haller, *Energy deficit in Huntington disease: why it matters*. J Clin Invest, 2011. **121**(2): p. 493-9.
441. Johnson, R., *Long non-coding RNAs in Huntington's disease neurodegeneration*. Neurobiol Dis, 2012. **46**(2): p. 245-54.
442. Johnsson, P., et al., *Evolutionary conservation of long non-coding RNAs; sequence, structure, function*. Biochim Biophys Acta, 2014. **1840**(3): p. 1063-71.
443. Smeenk, L., et al., *Role of p53 serine 46 in p53 target gene regulation*. PLoS One, 2011. **6**(3): p. e17574.
444. Sunwoo, J.S., et al., *Altered Expression of the Long Noncoding RNA NEAT1 in Huntington's Disease*. Mol Neurobiol, 2017. **54**(2): p. 1577-1586.
445. Cherbonneau, F., et al., *TRACE-seq: A transgenic system for unbiased and non-invasive transcriptome profiling of living cells*. iScience, 2022. **25**(2): p. 103806.
446. Gezer, U., et al., *Long non-coding RNAs with low expression levels in cells are enriched in secreted exosomes*. Cell Biol Int, 2014. **38**(9): p. 1076-9.
447. Sato, K., K.I. Takayama, and S. Inoue, *Stress granules sequester Alzheimer's disease-associated gene transcripts and regulate disease-related neuronal proteostasis*. Aging (Albany NY), 2023. **15**(10): p. 3984-4011.
448. Carninci, P., et al., *The transcriptional landscape of the mammalian genome*. Science, 2005. **309**(5740): p. 1559-63.
449. Mercer, T.R., et al., *Specific expression of long noncoding RNAs in the mouse brain*. Proc Natl Acad Sci U S A, 2008. **105**(2): p. 716-21.
450. Ponjavic, J., et al., *Genomic and transcriptional co-localization of protein-coding and long non-coding RNA pairs in the developing brain*. PLoS Genet, 2009. **5**(8): p. e1000617.
451. Gangwani, M.R., et al., *Neuronal and astrocytic contributions to Huntington's disease dissected with zinc finger protein transcriptional repressors*. Cell Rep, 2023. **42**(1): p. 111953.
452. Ono, S., *Functions of actin-interacting protein 1 (AIP1)/WD repeat protein 1 (WDR1) in actin filament dynamics and cytoskeletal regulation*. Biochem Biophys Res Commun, 2018. **506**(2): p. 315-322.
453. Shehjar, F., et al., *The Multifaceted Role of Cofilin in Neurodegeneration and Stroke: Insights into Pathogenesis and Targeting as a Therapy*. Cells, 2024. **13**(2).
454. Tousley, A., et al., *Huntingtin associates with the actin cytoskeleton and alpha-actinin isoforms to influence stimulus dependent morphology changes*. PLoS One, 2019. **14**(2): p. e0212337.
455. Kalathur, R.K., M.A. Hernandez-Prieto, and M.E. Futschik, *Huntington's disease and its therapeutic target genes: a global functional profile based on the HD Research Crossroads database*. BMC Neurol, 2012. **12**: p. 47.
456. Zhang, K., et al., *Stress Granule Assembly Disrupts Nucleocytoplasmic Transport*. Cell, 2018. **173**(4): p. 958-971 e17.
457. Bano, D., et al., *Neurodegenerative processes in Huntington's disease*. Cell Death Dis, 2011. **2**: p. e228.
458. Yue, J., K. Zhang, and J. Chen, *Role of integrins in regulating proteases to mediate extracellular matrix remodeling*. Cancer Microenviron, 2012. **5**(3): p. 275-83.
459. Chen, J.Y., et al., *Dopamine imbalance in Huntington's disease: a mechanism for the lack of behavioral flexibility*. Front Neurosci, 2013. **7**: p. 114.

460. Julio-Costa, A., et al., *Count on dopamine: influences of COMT polymorphisms on numerical cognition*. Front Psychol, 2013. **4**: p. 531.
461. Al-Ramahi, I., et al., *High-Throughput Functional Analysis Distinguishes Pathogenic, Nonpathogenic, and Compensatory Transcriptional Changes in Neurodegeneration*. Cell Syst, 2018. **7**(1): p. 28-40 e4.
462. Benyair, R., et al., *Upregulation of the ESCRT pathway and multivesicular bodies accelerates degradation of proteins associated with neurodegeneration*. Autophagy Rep, 2023. **2**(1).
463. Akbergenova, Y. and J.T. Littleton, *Pathogenic Huntington Alters BMP Signaling and Synaptic Growth through Local Disruptions of Endosomal Compartments*. J Neurosci, 2017. **37**(12): p. 3425-3439.
464. Wurz, A.I., et al., *Cytoskeletal dysregulation and neurodegenerative disease: Formation, monitoring, and inhibition of cofilin-actin rods*. Front Cell Neurosci, 2022. **16**: p. 982074.
465. Densham, R.M., et al., *MST kinases monitor actin cytoskeletal integrity and signal via c-Jun N-terminal kinase stress-activated kinase to regulate p21Waf1/Cip1 stability*. Mol Cell Biol, 2009. **29**(24): p. 6380-90.
466. Qiu, J., et al., *Molecular mechanisms involved in regulating protein activity and biological function of MST3*. Cell Div, 2023. **18**(1): p. 8.
467. Kumar, A.V., J. Mills, and L.R. Lapierre, *Selective Autophagy Receptor p62/SQSTM1, a Pivotal Player in Stress and Aging*. Front Cell Dev Biol, 2022. **10**: p. 793328.
468. Yang, J., X. Chen, and H. Xu, *SQSTM1/p62 droplet -mediated autophagosome formation: insights into Huntington disease*. Autophagy, 2021. **17**(10): p. 3256-3259.
469. Shi, M., et al., *ALYREF mainly binds to the 5' and the 3' regions of the mRNA in vivo*. Nucleic Acids Res, 2017. **45**(16): p. 9640-9653.
470. Aradjanski, M., et al., *DARS2 protects against neuroinflammation and apoptotic neuronal loss, but is dispensable for myelin producing cells*. Hum Mol Genet, 2017. **26**(21): p. 4181-4189.
471. Berson, A., et al., *Drosophila Ref1/ALYREF regulates transcription and toxicity associated with ALS/FTD disease etiologies*. Acta Neuropathol Commun, 2019. **7**(1): p. 65.
472. Melone, M.A., et al., *Mutant huntingtin regulates EGF receptor fate in non-neuronal cells lacking wild-type protein*. Biochim Biophys Acta, 2013. **1832**(1): p. 105-13.
473. Bodai, L. and J.L. Marsh, *A novel target for Huntington's disease: ERK at the crossroads of signaling. The ERK signaling pathway is implicated in Huntington's disease and its upregulation ameliorates pathology*. Bioessays, 2012. **34**(2): p. 142-8.
474. Heider, M.R. and M. Munson, *Exorcising the exocyst complex*. Traffic, 2012. **13**(7): p. 898-907.
475. Yu, N.K., et al., *A transducible nuclear/nucleolar protein, mLLP, regulates neuronal morphogenesis and synaptic transmission*. Sci Rep, 2016. **6**: p. 22892.
476. Lee, J.H., *Altered mTOR signaling in Huntington's Disease*. University of Iowa.
477. Ben Haim, L., et al., *The JAK/STAT3 pathway is a common inducer of astrocyte reactivity in Alzheimer's and Huntington's diseases*. J Neurosci, 2015. **35**(6): p. 2817-29.
478. Abjean, L., et al., *Reactive astrocytes promote proteostasis in Huntington's disease through the JAK2-STAT3 pathway*. Brain, 2023. **146**(1): p. 149-166.
479. NCBI. *STAT3 signal transducer and activator of transcription 3 [Homo sapiens (human)]*
- Gene ID: 6774. 2024 [cited Updated on 12-Nov-2024 13-Nov-2024]; Available from: <https://www.ncbi.nlm.nih.gov/gene/6774>.
480. Bowles, K. and L. Jones, *B18 The Role of STAT3 Transcriptional Regulation in an Immortalised Cell Model of HD*. Journal of Neurology, Neurosurgery & Psychiatry, 2014. **85**(Suppl 1): p. A15-A15.
481. Maiese, K., *Targeting molecules to medicine with mTOR, autophagy and neurodegenerative disorders*. Br J Clin Pharmacol, 2016. **82**(5): p. 1245-1266.
482. Lee, J.H., et al., *Reinstating aberrant mTORC1 activity in Huntington's disease mice improves disease phenotypes*. Neuron, 2015. **85**(2): p. 303-15.
483. Johri, A. and M.F. Beal, *Mitochondrial dysfunction in neurodegenerative diseases*. J Pharmacol Exp Ther, 2012. **342**(3): p. 619-30.
484. Paul, B.D. and S.H. Snyder, *Impaired Redox Signaling in Huntington's Disease: Therapeutic Implications*. Front Mol Neurosci, 2019. **12**: p. 68.
485. Giorgini, F., et al., *A genomic screen in yeast implicates kynurenine 3-monooxygenase as a therapeutic target for Huntington disease*. Nat Genet, 2005. **37**(5): p. 526-31.
486. Pandey, M., K.P. Mohanakumar, and R. Usha, *Mitochondrial functional alterations in relation to pathophysiology of Huntington's disease*. Journal of Bioenergetics and Biomembranes, 2010. **42**(3): p. 217-226.

487. Oliveira, J.M.A., *Mitochondrial bioenergetics and dynamics in Huntington's disease: tripartite synapses and selective striatal degeneration*. Journal of Bioenergetics and Biomembranes, 2010. **42**(3): p. 227-234.
488. Malla, B., et al., *A Systematic Review of Transcriptional Dysregulation in Huntington's Disease Studied by RNA Sequencing*. Front Genet, 2021. **12**: p. 751033.
489. Kuhn, A., et al., *Mutant huntingtin's effects on striatal gene expression in mice recapitulate changes observed in human Huntington's disease brain and do not differ with mutant huntingtin length or wild-type huntingtin dosage*. Hum Mol Genet, 2007. **16**(15): p. 1845-61.

APPENDIX

Appendix 1. List of Marker Genes for control sEVs and RNA granules. In particular, the log2 fold change (L2fc) values provide insight into the relative upregulation or downregulation of specific genes under control conditions compared to controls. A positive log2 fold change suggests an increase in expression, while a negative value signifies a decrease.

Marker genes for control sEVs and RNA granules						
Gene	Name	Gene type	MAV	L2fc	padj	Type
URS000256C3F7_9606			11353	0	-1	sEVs
URS000256C3F7_9606			11353	14.39531577	3.62E-30	sEVs
ENSG00000131504.18	DIAPH1	protein_coding	10851.4	0.456316788	0.032820303	sEVs
ENSG00000170144.22	HNRNPA3	protein_coding	4825.8	0.406142085	0.042799663	sEVs
URS00018DB349_9606	HSALNT0210606		4275.2	27.11173714	3.97E-07	sEVs
URS0000D5AE5F_9606			4274.8	27.10122308	3.97E-07	sEVs
ENSG00000110880.11	CORO1C	protein_coding	2160.8	0.474570104	0.035366943	sEVs
URS00019B4D9E_9606			1680	2.266256827	0.0433959	sEVs
URS0000D57449_9606			934.6	23.17556869	5.42E-05	sEVs
URS000254CCB4_9606			923.4	25.14249702	5.60E-06	sEVs
ENSG00000062725.10	APPBP2	protein_coding	713.4	0.679859242	0.045228696	sEVs
URS0002593118_9606			666.2	26.16721498	1.44E-06	sEVs
ENSG00000110660.15	SLC35F2	protein_coding	604.6	0.342445655	0.04783353	sEVs
URS00019E7FBE_9606			575.6	2.390934603	0.009871723	sEVs
ENSG00000078403.17	MLLT10	protein_coding	533.4	0.492934728	0.032781228	sEVs
ENSG00000037637.11	FBXO42	protein_coding	399.2	0.898676656	0.025319179	sEVs
ENSG00000075420.13	FNDC3B	protein_coding	389.4	0.880069031	0.000681813	sEVs
ENSG00000038532.17	CLEC16A	protein_coding	327.4	0.778241455	0.041609506	sEVs
URS0000EA0E79_9606	HSALNT0031278		318.8	24.76737995	6.30E-28	granule
ENSG00000265972.6	TXNIP	protein_coding	289.6	0.92568515	0.023873206	sEVs
URS00023390C2_9606	HSALNT0279530		276.2	29.57747147	8.32E-10	granule
URS0000D5C19B_9606			252.2	8.971654701	2.78E-05	sEVs
ENSG00000245532.11	NEAT1	lncRNA	236	0	-1	sEVs
ENSG00000245532.11	NEAT1	lncRNA	236	23.66617026	9.86E-10	sEVs
URS000234885A_9606	HSALNT0291027		213	3.626073282	0.005691151	sEVs
URS00005303E4_9606			210.6	8.666758766	5.46E-05	sEVs
URS0001BD26FD_9606	HSALNT0289343		201.8	8.587122649	6.52E-05	sEVs
ENSG00000176155.21	CCDC57	protein_coding	196	1.381216656	9.80E-05	sEVs
ENSG00000132394.11	EEFSEC	protein_coding	188.4	0.963611378	0.0030325	sEVs
URS0000204428_9606	NEAT1	lncRNA	184	0	-1	sEVs
URS0000204428_9606	NEAT1	lncRNA	184	8.515999197	0.000321801	sEVs
URS00002017A0_9606			178.6	22.86822621	1.37E-12	sEVs
ENSG00000112218.9	GPR63	protein_coding	163.6	0.601895268	0.027229664	sEVs
URS000255F359_9606			158.8	0	-1	sEVs

Appendix

URS000255F359_9606			158.8	8.11625524	3.71E-07	sEVs
URS00009AD36F_9606			157.8	8.176439798	0.00019668	sEVs
ENSG00000135953.11	MFSD9	protein_coding	146.6	1.455484504	0.002250395	sEVs
ENSG00000068615.20	REEP1	protein_coding	141.8	0.589349826	0.038479482	sEVs
URS0000D59036_9606			141	23.10582437	5.70E-05	sEVs
ENSG00000114988.12	LMAN2L	protein_coding	140.8	0.763912854	0.033460461	sEVs
ENSG00000012822.16	CALCOCO1	protein_coding	136.6	1.060281386	0.019550136	sEVs
ENSG00000263740.2	RN7SL4P	misc_RNA	123.4	22.57186159	0.000103065	sEVs
ENSG00000202198.1	7SK	misc_RNA	121.2	22.86030119	7.54E-05	sEVs
ENSG00000278771.1	RN7SL3	misc_RNA	119.2	23.19583803	5.35E-05	sEVs
URS000075D95B_9606			116.4	22.47444487	4.90E-31	sEVs
URS00009B3359_9606			116	0	-1	sEVs
URS00009B3359_9606			116	22.53907566	5.46E-05	sEVs
URS0000026886_9606	GABRE		111.2	9.232109116	0.02771961	granule
URS00019ACBCA_9606			109.8	3.969898186	0.001877906	sEVs
ENSG00000273590.6		artifact	108	0	-1	sEVs
ENSG00000273590.6		artifact	108	7.702042457	0.000151265	sEVs
ENSG00000142149.9	HUNK	protein_coding	98.2	1.820557999	0.016973012	sEVs
URS0000EBEF2E_9606	HSALNT0179085		96	28.19868186	1.28E-08	granule
URS0001BF9137_9606	HSALNT0179085		96	28.19868186	1.28E-08	granule
URS000233B49C_9606	HSALNT0368328		96	3.86204243	0.038052475	sEVs
URS0000D5A5B3_9606			90	24.84981419	1.87E-06	granule
URS00025452EF_9606			89.8	29.36270798	1.87E-09	granule
URS0000D598DD_9606			86.8	22.05546506	1.86E-08	sEVs
URS00008BD144_9606			86.6	28.30783037	1.13E-08	granule
ENSG00000277925.1	Telomerase-vert	misc_RNA	86.4	6.90215227	0.003114801	sEVs
URS0000EC1CB7_9606	HSALNT0099824		83.6	29.83064967	8.32E-10	granule
URS0001BD75DE_9606	HSALNT0099824		83.6	29.83064967	8.32E-10	granule
URS00000A48F5_9606			83	21.79129632	0.000227517	sEVs
ENSG00000202363.1	SNORA62	snoRNA	78.4	0	-1	granule
URS0000D591DD_9606			70.8	0	-1	granule
URS0000EA8750_9606	HSALNT0005757		69.8	0	-1	sEVs
URS0000EA8750_9606	HSALNT0005757		69.8	7.109058953	0.000553725	sEVs
URS0002336A71_9606	HSALNT0295987		67.2	8.627084943	0.0042394	granule
ENSG00000213918.11	DNASE1	protein_coding	65.6	2.162155684	0.006125974	sEVs
URS0000D5CE7E_9606			65.2	21.8263116	0.000219951	sEVs
URS0001BF8812_9606	HSALNT0239248		64.8	2.513886318	0.026744729	sEVs
URS0000EB4FEA_9606	HSALNT0066310		64.2	8.526677347	6.07E-06	granule
URS0000EB4FEA_9606	HSALNT0066310		64.2	0	-1	granule
URS0001BD6B40_9606	HSALNT0066310		64.2	8.526677347	6.07E-06	granule
URS0001BD6B40_9606	HSALNT0066310		64.2	0	-1	granule
ENSG00000288947.2		lncRNA	63.8	0.984243001	0.015689011	sEVs
ENSG00000138678.11	GPAT3	protein_coding	63.4	0.952661868	0.001077735	sEVs

Appendix

ENSG00000171608.18	PIK3CD	protein_coding	63.4	1.790546699	0.029305696	sEVs
ENSG00000285967.1	NIPBL-DT	lncRNA	63	21.76014578	0.000234427	sEVs
URS000005D6F9_9606			60.2	21.57924626	5.34E-22	sEVs
ENSG00000133019.12	CHRM3	protein_coding	56.4	2.011242196	0.000506565	sEVs
URS000008B30DF_9606			56.4	21.92824156	0.000197543	sEVs
URS0000057866_9606			56.2	21.32968717	3.57E-21	sEVs
URS0001BD8814_9606	HSALNT0245455		55.8	0	-1	sEVs
URS0001BD8814_9606	HSALNT0245455		55.8	6.630858337	2.44E-07	sEVs
ENSG00000272054.1		lncRNA	55.2	7.012163703	0.001774874	granule
URS0001BD21AD_9606	HSALNT0030033		55.2	7.012163703	0.001774874	granule
URS00025C0BCB_9606			53.2	21.7340591	5.17E-17	sEVs
URS0000569A4A_9606	SCARNA10	snoRNA	52.4	21.01523459	7.86E-16	sEVs
URS00002DB004_9606			52.2	0	-1	sEVs
URS000005D8CC_9606			52	21.62379126	0.000267507	sEVs
URS0000064472_9606			51.8	32.00224716	1.82E-11	granule
URS000008B81E6_9606			51.4	0	-1	sEVs
ENSG00000170537.13	TMC7	protein_coding	51	1.660352576	0.04262696	sEVs
URS00025144EA_9606			51	0	-1	sEVs
ENSG00000288663.1		lncRNA	50.6	1.966297826	0.040369297	sEVs
URS000008B2B99_9606			49	21.31866572	6.84E-17	sEVs
URS0001BDC508_9606	HSALNT0123196		49	21.67650317	3.88E-17	sEVs
URS00000EB81EB_9606	HSALNT0229429		48.8	0	-1	sEVs
URS00000EB81EB_9606	HSALNT0229429		48.8	6.424518508	1.92E-06	sEVs
URS000005A5B3_9606			47.4	20.31061854	0.00077084	sEVs
ENSG00000262660.1		protein_coding	46.4	21.37883262	4.72E-05	sEVs
URS00023427AC_9606	HSALNT0328745		45.4	23.54428497	1.40E-05	granule
URS000005A84E_9606			45	0	-1	sEVs
URS000005A84E_9606			45	6.664517829	0.04375306	sEVs
URS0002336C62_9606	HSALNT0408074		42.8	23.20641382	2.16E-05	granule
URS000005B289_9606			42	0	-1	sEVs
ENSG00000289316.1		lncRNA	41.6	31.49739681	1.10E-12	granule
URS00023420B9_9606	HSALNT0388335		41.4	0	-1	sEVs
URS0000057C3B_9606			40.8	2.268621384	0.029543625	sEVs
URS00000EAD756_9606	HSALNT0053809		40.2	0	-1	sEVs
URS00000EAD756_9606	HSALNT0053809		40.2	6.319417631	1.50E-05	sEVs
URS0001BCF9A3_9606	HSALNT0053809		40.2	0	-1	sEVs
URS0001BCF9A3_9606	HSALNT0053809		40.2	6.319417631	1.50E-05	sEVs
URS000005D836_9606			40	20.90967098	0.000506565	sEVs
URS000258B503_9606			39.2	21.19885225	0.000389437	sEVs
ENSG00000169239.14	CASB	protein_coding	39	1.676616452	0.048271397	sEVs
URS00025F31D5_9606		lncRNA	38.4	21.08835147	4.73E-05	sEVs
URS000233C7FD_9606	HSALNT0402587		37.8	20.95998523	3.90E-17	sEVs
URS0002618710_9606			37.8	3.342677823	0.023873206	sEVs

Appendix

ENSG00000249931.5	GOLGA8K	protein_coding	37.6	1.747100673	0.023073815	sEVs
URS0000EAB636_9606	HSALNT0254337		37.6	0	-1	granule
URS0001BE337A_9606	HSALNT0254337		37.6	0	-1	granule
URS0000D57BD1_9606			37.4	6.337478992	0.025319179	sEVs
URS0000E9971A_9606	HSALNT0193207		37.2	0	-1	sEVs
URS0001BCBA29_9606	HSALNT0289338		37.2	20.74186678	0.000416083	sEVs
URS0001BE5C7F_9606	HSALNT0289415		37.2	20.71583713	0.000591951	sEVs
URS0001BE8D50_9606	HSALNT0193207		37.2	0	-1	sEVs
URS000253A91D_9606			36.6	21.33499585	7.45E-06	sEVs
ENSG00000279170.3	TSTD3	protein_coding	35.8	2.347224714	0.000564652	sEVs
URS0000D6DF82_9606			35.6	4.628324339	0.030829	sEVs
URS00019D9359_9606			35.6	1.787405275	0.006347156	sEVs
URS0000EAE1F0_9606	HSALNT0174581		35.2	0	-1	sEVs
URS0000EAE1F0_9606	HSALNT0174581		35.2	6.055825244	0.00888435	sEVs
URS0001BE77C7_9606	HSALNT0174581		35.2	0	-1	sEVs
URS0001BE77C7_9606	HSALNT0174581		35.2	6.055825244	0.00888435	sEVs
ENSG00000280852.2		transcribed_processed_pseudogene	34.2	4.390533262	0.004747285	sEVs
URS0000D5D83B_9606			34	2.821586232	0.00286728	sEVs
URS0000D5CADC_9606			33.6	0	-1	granule
URS000233EADD_9606	HSALNT0315399		33.6	0	-1	sEVs
URS0000D6D53E_9606			33	6.385396265	0.008614215	sEVs
URS000075C245_9606	HSALNT0402498		32.8	7.920204546	0.016790137	granule
URS0002336DD8_9606	HSALNT0396921		32.2	2.108425612	0.013031455	sEVs
ENSG00000270872.2	SRGAP2D	unprocessed_pseudogene	31.6	0	-1	sEVs
ENSG00000270872.2	SRGAP2D	unprocessed_pseudogene	31.6	5.821260618	0.000449515	sEVs
URS0000D5A7D5_9606			31.6	1.646519653	0.017721637	sEVs
URS0000E96361_9606	HSALNT0003812		31.4	20.60450508	3.14E-17	sEVs
ENSG00000245937.10	SLC12A2-DT	lncRNA	31.2	1.778818634	0.049450673	sEVs
URS000253CE42_9606			31.2	0	-1	sEVs
URS0000636A2E_9606	SNORA53	snoRNA	30.6	19.7953668	0.001379188	sEVs
URS0002574DF4_9606			30.4	22.38872137	2.62E-19	granule
URS0000D57905_9606			30.2	20.5700603	0.000681813	sEVs
URS0002339020_9606	HSALNT0387825		29.2	0	-1	granule
URS000025784F_9606	TSIX transcript, antisense RNA	lncRNA	29	20.90061946	0.000507584	sEVs
URS00008B6C25_9606			29	0	-1	sEVs
URS0000D578C1_9606			28.8	2.041380968	0.019455196	sEVs
URS0000D6E29A_9606			28.8	22.63116102	4.41E-05	granule
URS000075E5AD_9606			28.6	19.37482209	0.002012526	sEVs
URS000061B15C_9606			28.4	0	-1	sEVs
URS00009C1756_9606			28.2	1.587657723	0.029543625	sEVs
ENSG00000235501.8	CNN3-DT	lncRNA	27.8	0	-1	sEVs
ENSG00000235501.8	CNN3-DT	lncRNA	27.8	5.709434912	0.013510402	sEVs

Appendix

URS0000E9E171_9606	HSALNT0176132		27.8	0	-1	sEVs
URS0001BDF43A_9606	HSALNT0152853		27.2	20.40076022	0.000794056	sEVs
ENSG00000091262.17	ABCC6	protein_coding	26.8	2.805665499	0.016071113	sEVs
ENSG00000092929.13	UNC13D	protein_coding	26.8	3.111339783	0.049879514	sEVs
URS0000D5747D_9606			25.8	5.62455077	0.013355509	sEVs
URS0000D5787B_9606			25.8	0	-1	granule
URS0001BDA968_9606	HSALNT0101266		25.4	5.165377678	0.016764757	sEVs
URS00023412E6_9606	HSALNT0342667		25.4	32.43081062	1.03E-11	granule
URS0000D5ABB9_9606			25	0	-1	sEVs
URS0000D5ABB9_9606			25	5.545995169	0.000332181	sEVs
URS00019E9892_9606			25	20.16186805	5.36E-07	sEVs
URS0001BD5F06_9606	HSALNT0263045		25	0	-1	sEVs
URS0001BD5F06_9606	HSALNT0263045		25	5.545995169	0.000332181	sEVs
ENSG00000290793.1		lncRNA	24.8	0	-1	sEVs
ENSG00000290793.1		lncRNA	24.8	5.535823466	8.89E-05	sEVs
ENSG00000150394.14	CDH8	protein_coding	24.4	2.236633701	0.006210823	sEVs
URS0001BD644D_9606	HSALNT0244243		24.4	0	-1	sEVs
URS00009AE115_9606	HSALNT0207778		24	20.55786918	2.81E-17	sEVs
URS00009B2E45_9606			24	19.59762933	0.001634581	sEVs
URS00023412A8_9606	HSALNT0349015		24	0	-1	sEVs
URS00025BC20E_9606			24	0	-1	sEVs
URS00025BC20E_9606			24	5.392264627	0.017858384	sEVs
URS000251F55D_9606			23.8	5.373579541	0.002690206	sEVs
ENSG00000128594.8	LRRC4	protein_coding	23.6	2.832945832	0.006812671	sEVs
ENSG00000136867.11	SLC31A2	protein_coding	23	4.495899992	0.004205107	sEVs
ENSG00000125895.6	TMEM74B	protein_coding	22.8	3.951117451	0.006835899	sEVs
ENSG00000290690.1		lncRNA	22.2	0	-1	sEVs
ENSG00000290690.1		lncRNA	22.2	5.137073963	0.044183315	sEVs
URS0000EA45F1_9606	HSALNT0083820		22.2	0	-1	sEVs
URS0000EA45F1_9606	HSALNT0083820		22.2	5.500261216	0.000677024	sEVs
URS0002349BED_9606	HSALNT0381614		21.8	7.096685192	0.016790137	granule
URS00008BA2D7_9606			21.6	5.20459015	0.017688562	sEVs
URS0001BE4C4A_9606	HSALNT0231480		21.6	5.108552726	0.030147869	sEVs
URS00022B1D90_9606		lncRNA	21.6	20.30015374	1.09E-17	sEVs
URS00009BD29F_9606	HSALNT0044329		21.4	20.17076608	7.80E-17	sEVs
URS000233C518_9606	HSALNT0406892		21.4	0	-1	sEVs
URS00009BB13F_9606	HSALNT0395848		21.2	2.736202277	0.031394696	sEVs
URS0000E96C34_9606	HSALNT0282358		21.2	0	-1	sEVs
URS00023444D1_9606	HSALNT0312491		21.2	5.436297278	0.016727229	sEVs
ENSG00000244879.10	GABPB1-AS1	lncRNA	20.8	0	-1	sEVs
URS0000D5AE9B_9606			20.8	0	-1	sEVs
URS0001BCCC88_9606	HSALNT0176348		20.8	0	-1	sEVs
URS000233EB40_9606	HSALNT0408087		20.8	5.420016624	0.015346199	sEVs

Appendix

ENSG00000100626.17	GALNT16	protein_coding	20.6	2.31683307	0.047253404	sEVs
URS0002559B84_9606			20.6	19.05783994	0.002600654	sEVs
URS000256D45A_9606			20.4	0	-1	sEVs
ENSG00000290674.1		lncRNA	20	32.68770837	7.12E-12	granule
URS0000D56FA5_9606			20	0	-1	sEVs
URS0000D56FA5_9606			20	5.210851705	0.023909485	sEVs
URS00023366B1_9606	HSALNT0363267		19.6	19.89596674	0.001269821	sEVs
URS00023490A9_9606	HSALNT0326598		19.6	5.250900224	0.000267368	sEVs
URS0002567586_9606			19.6	0	-1	sEVs
URS0002567586_9606			19.6	5.258673744	0.024379912	sEVs
URS0000D5C41D_9606			19.4	4.923590157	0.030759098	sEVs
URS00025D6461_9606			19.4	5.40290082	0.042137226	sEVs
URS000234847E_9606	HSALNT0406215		19.2	0	-1	sEVs
URS000234847E_9606	HSALNT0406215		19.2	4.990521482	0.004797597	sEVs
URS000234463B_9606	HSALNT0314716		19	6.927418272	0.016790137	granule
URS000234463B_9606	HSALNT0314716		19	0	-1	granule
URS0000D56FA2_9606			18.8	19.93046899	2.50E-24	sEVs
URS000253553C_9606			18.8	3.838011871	0.041515034	sEVs
URS00025AA833_9606			18.8	0	-1	sEVs
URS0000D58518_9606			18.6	0	-1	sEVs
URS0000EB8DB6_9606	HSALNT0229518		18.6	0	-1	sEVs
URS0001BE341A_9606	HSALNT0229518		18.6	0	-1	sEVs
URS000234607A_9606	HSALNT0383149		18.6	5.165201932	0.047718721	sEVs
URS00025E0492_9606			18.6	3.777288631	0.023873206	sEVs
URS0000D58B29_9606			18.4	4.918967407	0.028182667	sEVs
URS0002567C05_9606			18.4	3.717077779	0.017701848	sEVs
URS00025BA947_9606			18.2	0	-1	sEVs
URS00025BA947_9606			18.2	5.18344326	0.023600814	sEVs
URS000234137E_9606	HSALNT0407405		17.6	1.891868475	0.04262696	sEVs
URS0002582D3B_9606			17.6	2.679554214	0.04783353	sEVs
URS00025E2259_9606			17.6	4.888229003	0.012468952	sEVs
URS0002349858_9606	HSALNT0317622		17.4	0	-1	granule
URS0002591392_9606			17.4	20.41366659	0.000391894	sEVs
URS00008BE0FE_9606			17.2	0	-1	sEVs
URS00008BF569_9606			16.4	19.74449204	2.78E-05	sEVs
URS0000D5D15B_9606			16.4	0	-1	sEVs
URS0000D5D15B_9606			16.4	5.040986032	0.044037737	sEVs
URS0001BCDCA7_9606	HSALNT0218902		16.4	19.31394971	0.002132174	sEVs
URS0000D57449_9606			16.2	23.28887262	1.98E-05	granule
URS0002215033_9606			16.2	0	-1	sEVs
URS00008B5B55_9606			16	0	-1	sEVs
URS0000D5766A_9606			16	0	-1	granule
URS0000D5CFFE_9606			16	20.47560077	1.26E-12	sEVs

Appendix

URS0001BCDD8C_9606	HSALNT0266034		16	0	-1	granule
URS00008BCA91_9606			15.8	0	-1	granule
URS00008C23E8_9606			15.8	0	-1	sEVs
URS00009B9B85_9606	HSALNT0011052		15.8	5.418560566	0.0063045	sEVs
URS0000E960A4_9606	HSALNT0145531		15.6	18.65032413	0.002786094	sEVs
URS0002212B3E_9606			15.4	19.02684396	0.002504626	sEVs
URS0002348824_9606	HSALNT0347784		15.4	0	-1	granule
ENSG00000100100.13	PIK3IP1	protein_coding	15.2	2.314529283	0.031617382	sEVs
URS00008D48FC_9606			15.2	21.60643216	0.00017275	granule
URS0000D5A8CF_9606			15.2	0	-1	sEVs
URS000256FC45_9606			15.2	4.390305227	0.01872377	sEVs
ENSG00000174384.9	PMS2P6	unprocessed_pseudogene	15	0	-1	sEVs
ENSG00000291044.1		lncRNA	15	2.302786113	0.040824607	sEVs
URS00008B7B42_9606			15	0	-1	granule
URS0000D5A2F2_9606			15	0	-1	sEVs
URS000234477D_9606	HSALNT0292170		14.8	3.219303514	0.032577241	sEVs
URS00023455DF_9606	HSALNT0299566		14.8	0	-1	sEVs
URS000253FB4D_9606			14.8	0	-1	sEVs
URS000253FB4D_9606			14.8	4.745199385	0.011814708	sEVs
URS000233A5FF_9606	HSALNT0327165		14.6	4.710963711	0.006217584	sEVs
URS0002341176_9606	HSALNT0363271		14.6	19.66473228	0.001542762	sEVs
URS0000D57A0F_9606			14.4	0	-1	sEVs
URS0000E92334_9606	HSALNT0130836		14.2	0	-1	sEVs
URS0000E92334_9606	HSALNT0130836		14.2	5.129761001	0.031123423	sEVs
URS0000EBF952_9606	HSALNT0189682		14.2	0	-1	sEVs
URS0001BD501C_9606	HSALNT0189682		14.2	0	-1	sEVs
URS0002342B20_9606	HSALNT0331521		14.2	4.466981362	0.02080489	sEVs
URS0000D5E00B_9606			14	4.760032126	0.002156933	sEVs
URS0000EADB27_9606	HSALNT0258663		14	0	-1	sEVs
URS0000EADB27_9606	HSALNT0258663		14	4.7335723	0.002060293	sEVs
URS0001BDF7AA_9606	HSALNT0258663		14	0	-1	sEVs
URS0001BDF7AA_9606	HSALNT0258663		14	4.7335723	0.002060293	sEVs
URS00019B25C1_9606			13.8	19.18007505	0.002362551	sEVs
URS0002337FBC_9606	HSALNT0327166		13.8	0	-1	sEVs
URS0002337FBC_9606	HSALNT0327166		13.8	4.828832521	0.003558885	sEVs
URS00008C081D_9606	HSALNT0154177		13.4	4.766982033	0.048989387	sEVs
URS0002340373_9606	HSALNT0395798		13.4	0	-1	sEVs
URS0002543CC8_9606			13.4	4.26214292	0.014534727	sEVs
URS0001BE87D1_9606	HSALNT0103180		13.2	4.633884137	0.046255345	sEVs
URS000233733A_9606	HSALNT0305138		13.2	4.02995468	0.017309023	sEVs
URS00008C2FC8_9606			13	4.650894144	0.023288928	sEVs
URS0000D5935A_9606			13	0	-1	granule
URS0001BD972E_9606	HSALNT0246058		13	0	-1	granule

Appendix

URS0001BE86F6_9606	HSALNT0025205		13	4.650894144	0.023288928	sEVs
URS000233E103_9606	HSALNT0405344		13	0	-1	sEVs
URS000233E103_9606	HSALNT0405344		13	4.676147448	0.004259743	sEVs
URS0002545BFC_9606			13	4.44474322	0.047883196	sEVs
URS00008C0481_9606			12.8	0	-1	sEVs
URS000233CCF0_9606	HSALNT0356514		12.8	4.555521303	0.018097765	sEVs
URS000258BB0F_9606			12.8	4.329115839	0.012251249	sEVs
ENSG00000249492.3		lncRNA	12.6	4.316160793	0.02543796	sEVs
ENSG00000266992.1	DHX40P1	transcribed_unprocessed_pseudogene	12.6	4.634196278	0.011814708	sEVs
URS0000D574EF_9606			12.6	4.702778996	0.036439871	sEVs
URS00025B651F_9606			12.6	4.384781567	0.013355509	sEVs
URS0000E960A4_9606	HSALNT0145531		12.2	22.73550553	2.38E-05	granule
URS0000EA93D7_9606	HSALNT0075941		12.2	4.017384793	0.022835782	sEVs
URS0001BCCC96_9606	HSALNT0075941		12.2	4.017384793	0.022835782	sEVs
URS0002341A73_9606	HSALNT0403962		12.2	0	-1	sEVs
URS0002341A73_9606	HSALNT0403962		12.2	4.626743503	0.008368941	sEVs
ENSG00000153563.17	CD8A	protein_coding	12	3.221859532	0.033002034	sEVs
URS0000E94CAA_9606	HSALNT0153994		12	0	-1	sEVs
URS0000EF4557_9606	HSALNT0391759		12	21.15701533	0.000301089	granule
URS0001BD3397_9606	HSALNT0153994		12	0	-1	sEVs
URS0001BDDA7C_9606	HSALNT0134392		11.8	0	-1	sEVs
URS0001BE806E_9606	HSALNT0209824		11.8	4.498163342	0.044262916	sEVs
URS000259A8F0_9606			11.8	0	-1	sEVs
URS000259A8F0_9606			11.8	4.795823245	0.007664879	sEVs
URS0000D56EC6_9606			11.6	0	-1	sEVs
URS0000D57256_9606			11.6	4.47466789	0.017378279	sEVs
URS000233968D_9606	HSALNT0291861		11.6	4.383723811	0.017701848	sEVs
URS000258D3FC_9606			11.6	0	-1	sEVs
ENSG00000175928.6	LRRN1	protein_coding	11.4	2.384599372	0.049808223	sEVs
URS0000D58735_9606			11.2	4.396416972	0.031394696	sEVs
URS0000D5BD64_9606			11.2	4.044322208	0.039451539	sEVs
URS00025B3BCC_9606			11.2	3.736472082	0.040891107	sEVs
URS00025BFF82_9606			11.2	0	-1	sEVs
URS0000D57802_9606	HSALNT0294590		11	3.874739529	0.014931656	sEVs
URS0000D58AC7_9606			10.6	0	-1	sEVs
URS0000EB1F1F_9606	HSALNT0027018		10.6	3.763550858	0.04262696	sEVs
URS0001BD889D_9606	HSALNT0027018		10.6	3.763550858	0.04262696	sEVs
URS00008BF2A5_9606			10.4	18.97462597	0.002792613	sEVs
URS0001BD6071_9606	HSALNT0283654		10.4	18.97462597	0.002792613	sEVs
URS00025A7C2F_9606			10.4	4.271681539	0.041406232	sEVs
URS0002532B98_9606			10.2	4.500781553	0.040292874	sEVs
URS0000EEDFEA_9606	HSALNT0399015		10	18.89968797	6.29E-05	sEVs
URS0002337763_9606	HSALNT0355414		10	3.973470334	0.047480865	sEVs

Appendix

ENSG0000082196.21	C1QTNF3	protein_coding	9.8	3.621488781	0.035408663	sEVs
URS00023477A1_9606	HSALNT0390095		9.8	0	-1	sEVs
URS0000D58524_9606			9.4	4.065702064	0.028182667	sEVs
ENSG00000242094.1	FOXPI-IT1	lncRNA	9.2	4.325493752	0.02638659	sEVs
ENSG00000255062.2	TIRAP-AS1	lncRNA	9.2	3.996495094	0.023073815	sEVs
URS00008C1AC0_9606			9.2	0	-1	sEVs
URS00008C1AC0_9606			9.2	4.192913581	0.018869001	sEVs
URS0000EB19B9_9606	HSALNT0207345		9.2	4.236175886	0.028182667	sEVs
URS0001A0BB74_9606			8.8	3.983324223	0.031491971	sEVs
URS000259D237_9606			8.8	4.000614938	0.03627302	sEVs
URS000233FAC1_9606	HSALNT0335030		8.6	18.96438758	0.002794645	sEVs
URS00025B70FA_9606			8.6	3.881230548	0.044037737	sEVs
ENSG00000233232.8	NPIP7	protein_coding	8.4	4.037988965	0.024359329	sEVs
URS0000D579FA_9606			8	4.055926074	0.019167364	sEVs
URS000257D947_9606			8	3.947058769	0.0492261	sEVs
URS000233CA7B_9606	HSALNT0310650		7.6	4.039895921	0.03080111	sEVs
URS0000D59D0A_9606			7.4	3.823641414	0.04783353	sEVs
URS0002559B84_9606			7.4	21.60796024	0.000173189	granule
URS0002581B28_9606			7.4	4.05478664	0.025630508	sEVs
URS0002618516_9606	SMN2	protein_coding	7.2	3.976236951	0.025140153	sEVs
ENSG00000154262.13	ABCA6	protein_coding	6.8	3.661043007	0.049808223	sEVs
ENSG00000227388.3		lncRNA	6.6	3.674495321	0.045603255	sEVs
URS0002348B52_9606	HSALNT0368717		6.6	19.04232664	0.002660343	sEVs
URS00023415AE_9606	HSALNT0337469		6.4	19.2693275	0.002232292	sEVs
URS00023427AC_9606	HSALNT0328745		6.4	18.68018997	0.003644043	sEVs
URS0000E9263A_9606	HSALNT0257632		6.2	3.792853199	0.04771674	sEVs
URS0000E9506F_9606	HSALNT0046646		6.2	3.665904584	0.040369297	sEVs
URS0001BDECOF_9606	HSALNT0257632		6.2	3.792853199	0.04771674	sEVs
URS0001BE7112_9606	HSALNT0046646		6.2	3.665904584	0.040369297	sEVs
ENSG00000040731.10	CDH10	protein_coding	5.6	3.73819824	0.042160093	sEVs
URS00009BA206_9606	HSALNT0012656		5.4	18.12651211	0.00571972	sEVs
URS0000D59761_9606			5	18.59636157	0.003978412	sEVs
URS0000D5DB0B_9606			4.6	18.10893868	0.002792613	sEVs
URS000036DD5F_9606			4.2	17.96975682	0.000118576	sEVs
URS0000E9C1B7_9606	HSALNT0196438		4.2	19.26421306	1.31E-11	granule
URS00002B3204_9606	SCARNA7	scaRNA	2.8	17.75626645	0.00749839	sEVs
URS00025A9E10_9606			1.6	17.3140055	0.004799802	sEVs
URS000251B188_9606			1.4	18.10651699	0.012935946	granule
URS0000E966E5_9606	HSALNT0027357		1	16.04575338	0.000401095	sEVs

Appendix 2. List of Marker Genes for HD sEVs and RNA granules. In particular, the log₂ fold change (L2fc) values provide insight into the relative upregulation or downregulation of specific genes under HD conditions compared to controls. A positive log₂ fold change suggests

an increase in expression, while a negative value signifies a decrease. This comprehensive list helps highlight key RNA molecules, including long non-coding RNAs (lncRNAs) and protein-coding genes, that might be involved in disease mechanisms.

Marker genes for HD sEVs and RNA granules						
Gene	Name	Gene type	MAV	L2 fc	Padj	Type
URS00004741F9_9606			83877.75	0	-1	sEVs
URS00004741F9_9606			83877.75	-30	1.26E-48	sEVs
URS00001D4207_9606			34714.5	0	-1	sEVs
URS00001D4207_9606			34714.5	-30	4.82E-50	sEVs
URS00002ACB8C_9606			16291	-3.852421039	0.001218302	sEVs
URS0001A0422B_9606			10123.5	-5.27747017	0.00027581	sEVs
URS00002E82E5_9606	SCARNA9	lncRNA	3167	-33.01465733	4.08E-12	granule
URS00025BC04F_9606			2746.5	-5.278533907	0.00928904	sEVs
ENSG00000148677.7	ANKRD1	protein_coding	2432.8	-1.783865154	3.42E-05	granule
URS00019B4177_9606			1825.25	-4.44088748	0.000932689	sEVs
URS0000354645_9606			1435.75	-12.97458568	2.92E-06	sEVs
ENSG00000165195.16	PIGA	protein_coding	1015.4	-0.820073581	0.002337078	granule
URS00025514B4_9606			1013.25	-5.02759709	0.000332181	sEVs
URS0000D58931_9606			1005.5	-5.355262832	0.000817435	sEVs
ENSG00000201098.1	RNY1	misc_RNA	826.4	-26.54905929	3.19E-12	granule
ENSG00000175130.7	MARCKSL1	protein_coding	794.25	-0.712809995	0.010769973	sEVs
ENSG00000166986.15	MARS1	protein_coding	782.5	-0.958779064	0.000584827	sEVs
URS00008BB0ED_9606	HSALNT0226513		733	-2.423161943	0.0089971	sEVs
ENSG00000015676.18	NUDCD3	protein_coding	731.2	-0.468218493	0.022117233	granule
URS000063B690_9606	RNVU1-31	snRNA	688	-26.63679165	4.13E-10	sEVs
URS00025A8ED0_9606			684.25	-4.663419891	0.000154219	sEVs
ENSG00000188536.13	HBA2	protein_coding	646.75	-6.714197917	0.024730409	sEVs
URS00025B3C0F_9606			636.25	-4.684499231	0.04262696	sEVs
URS00025320C0_9606			606	-4.225508932	0.001600503	sEVs
ENSG00000198836.11	OPA1	protein_coding	595.5	-0.645647848	0.024379912	sEVs
URS000010CC88_9606			573.4	-25.25699847	5.14E-15	granule
URS0002584CAD_9606			559.5	-5.409053442	0.010240202	sEVs
ENSG00000148773.14	MKI67	protein_coding	557	-1.079025497	0.006859731	sEVs
URS0001EE2FA8_9606			519.8	-28.17737816	1.28E-08	granule
URS00025166A8_9606			515	-4.800542693	5.64E-05	sEVs
ENSG00000119729.12	RHOQ	protein_coding	453.75	-0.588321552	0.0433959	sEVs
URS00025537FC_9606			422.25	-4.273439444	0.012591093	sEVs
ENSG00000077721.17	UBE2A	protein_coding	416.25	-0.392860605	0.024304663	sEVs
URS0000D5AE6F_9606			396	-25.11099362	1.16E-11	granule
URS000034A3BC_9606	RNU2		388.25	-26.26565425	4.37E-28	sEVs
URS00000C37EC_9606			385.75	-5.480502751	0.011185526	sEVs

Appendix

ENSG00000196565.15	HBG2	protein_coding	385.5	-3.059271356	0.037664929	sEVs
URS0001C423C0_9606			378.5	-24.24959094	3.09E-35	sEVs
URS0001BF179B_9606	HSALNT0279541		371.4	-32.47659779	9.73E-12	granule
ENSG00000021776.11	AQR	protein_coding	367.25	-0.890232203	0.031394696	sEVs
URS0001BF68FD_9606	HSALNT0279516		353	-25.15476634	1.13E-08	granule
ENSG00000135913.11	USP37	protein_coding	348.5	-0.8385993	0.021337822	sEVs
URS0000D5D8CC_9606			335.2	-25.2935139	1.22E-06	granule
ENSG00000173575.24	CHD2	protein_coding	326.25	-0.890397594	0.044695061	sEVs
URS00025B4BAC_9606			326.25	-3.815802338	0.008012153	sEVs
ENSG00000186081.12	KRT5	protein_coding	320.75	-3.478357561	0.028182667	sEVs
ENSG00000176788.9	BASP1	protein_coding	316	-0.753967405	0.011814708	sEVs
URS0002583019_9606			309	-25.95575561	7.06E-18	sEVs
URS0002531AB8_9606			306	-4.93317843	0.009718446	sEVs
URS0001BCDCA7_9606	HSALNT0218902		299.4	-25.77530851	5.85E-07	granule
URS00003D33B3_9606			288	-3.343166199	0.00888435	sEVs
URS00025CBE1F_9606			283	-3.425440908	0.043669451	sEVs
ENSG00000255717.9	SNHG1	lncRNA	282.75	-1.556532154	0.010417463	sEVs
URS000225EAEA_9606			281.75	-9.03425429	0.046255345	sEVs
ENSG00000200795.1	RNU4-1	snRNA	277	-3.10523529	0.011518264	sEVs
URS00022B08FB_9606			254.4	0	-1	granule
URS000257BEDD_9606			238	-4.924597612	0.029071176	sEVs
URS00008B4D79_9606			224.5	-24.7157546	2.56E-22	sEVs
ENSG00000175455.16	CCDC14	protein_coding	218.75	-1.143013715	0.020099285	sEVs
ENSG00000066739.12	ATG2B	protein_coding	211	-0.95781029	0.000933265	sEVs
URS0001BF179B_9606	HSALNT0279541		209	-25.68918639	2.25E-06	sEVs
URS0000D5A9A3_9606			207.6	-24.11993356	2.46E-19	granule
URS000252659D_9606			205.5	-4.312406966	0.006217584	sEVs
ENSG00000129422.15	MTUS1	protein_coding	198.5	-1.081983548	0.026997241	sEVs
URS000220F272_9606			195.75	-3.949460297	0.015494541	sEVs
ENSG00000156599.11	ZDHHC5	protein_coding	191	-0.794600436	0.038479482	sEVs
ENSG00000123983.15	ACSL3	protein_coding	184.5	-0.845420431	0.007901502	sEVs
URS000255D791_9606			181.25	-4.056486286	0.009399424	sEVs
ENSG00000134762.17	DSC3	protein_coding	177	-1.243318427	0.003522841	sEVs
ENSG00000182389.20	CACNB4	protein_coding	175.5	-0.979490113	0.025346503	sEVs
URS0002617B9B_9606	LINC03009	lncRNA	170	-26.70118411	1.38E-07	granule
URS000021BC29_9606	SCARNA1	scaRNA	169.8	-26.39400097	2.23E-07	granule
URS0000D57905_9606			166.6	-24.83781519	2.35E-06	granule
URS000250B32D_9606			157	0	-1	granule
URS000250B32D_9606			157	-9.271534699	0.034702094	granule
URS00025B0C01_9606			147.8	-30.20233712	4.66E-10	granule
URS0001C4E735_9606			146	0	-1	granule
URS0001C4E735_9606			146	-24.12869166	8.90E-36	granule
URS000075B029_9606			143.25	-23.47930315	1.52E-12	sEVs

Appendix

ENSG00000127980.16	PEX1	protein_coding	139.5	-0.810267891	0.005799905	sEVs
ENSG00000289740.1	TALAM1	lncRNA	136	-1.109408167	0.03505628	sEVs
URS00025DE30B_9606			135.75	-4.102810225	0.013355509	sEVs
ENSG00000136044.12	APPL2	protein_coding	127	-0.951518116	0.010240202	sEVs
URS00025C0549_9606			123	-4.363563071	0.018808121	sEVs
ENSG00000163808.17	KIF15	protein_coding	120.5	-0.855741842	0.033460461	sEVs
ENSG00000090989.18	EXOC1	protein_coding	119.75	-0.773663941	0.049450673	sEVs
ENSG00000196247.13	ZNF107	protein_coding	119.25	-0.781964393	0.010614494	sEVs
URS00019E94D2_9606			116.75	-7.478764039	0.000391894	sEVs
URS000251451D_9606			113.5	-4.804354075	0.036043794	sEVs
ENSG00000182621.19	PLCB1	protein_coding	112.75	-0.797493404	0.03627302	sEVs
ENSG00000165506.15	DNAAF2	protein_coding	112	-0.978568433	0.04262696	sEVs
ENSG00000184613.11	NELL2	protein_coding	110.5	-0.60643266	0.049808223	sEVs
ENSG00000108821.14	COL1A1	protein_coding	109.75	-1.447942688	0.029543625	sEVs
URS00002DFE82_9606			108.25	-4.63056681	0.002626326	sEVs
URS000259D8CE_9606			107.5	-1.427165327	0.048271397	sEVs
URS000222A6D5_9606			104.25	-2.18488704	0.048315359	sEVs
URS0002520AA7_9606			103	-3.856474042	0.04262696	sEVs
ENSG00000138002.16	IFT172	protein_coding	102.25	-0.845062438	0.04262696	sEVs
URS000233D421_9606	HSALNT0398958		96	-33.74471476	1.10E-12	granule
ENSG00000132740.10	IGHMBP2	protein_coding	95.5	-1.165414311	0.049281851	sEVs
URS0000D57C9D_9606			95.25	-0.83391952	0.026829122	sEVs
URS0001BF9C77_9606	HSALNT0017659		95.25	-0.83391952	0.026829122	sEVs
ENSG00000270194.2	GOLGA4-AS1	lncRNA	92.8	0	-1	granule
ENSG00000092330.19	TINF2	protein_coding	90.75	-0.955976068	0.029763265	sEVs
URS0002346854_9606	HSALNT0358294		89.6	-23.07045433	1.38E-11	granule
ENSG00000196352.18	CD55	protein_coding	86	-0.940498373	0.010203134	sEVs
URS0000D5DD7A_9606			84.8	-23.35117585	4.16E-10	granule
ENSG00000163900.11	TMEM41A	protein_coding	84.75	-0.897837352	0.002472115	sEVs
URS000233F403_9606	HSALNT0342660		82.4	0	-1	granule
URS000233F403_9606	HSALNT0342660		82.4	-8.459162079	0.000251725	granule
ENSG00000163528.13	CHCHD4	protein_coding	78.5	-0.597181855	0.033761174	sEVs
URS000203DE7D_9606			78.5	-2.026081197	0.002958965	sEVs
ENSG00000170522.10	ELOVL6	protein_coding	78	-1.184545218	0.013355509	sEVs
ENSG00000146648.21	EGFR	protein_coding	77.75	-1.150058566	0.045494361	sEVs
URS000014C5D2_9606			77	-9.673267412	0.000829018	granule
URS00019A5500_9606			75	-6.375217827	7.39E-06	sEVs
ENSG00000186832.9	KRT16	protein_coding	74.75	-4.06028165	0.010084269	sEVs
ENSG00000166171.13	DPCD	protein_coding	73.75	-1.097405221	0.04205805	sEVs
URS0002587F62_9606			72	-23.30766932	4.17E-05	sEVs
URS00025A624A_9606			67.75	-4.275160604	0.013355509	sEVs
ENSG00000110888.19	CAPRIN2	protein_coding	67	-1.357234109	0.006612147	sEVs
ENSG00000137965.11	IFI44	protein_coding	66.2	-2.455263296	0.030076185	granule

Appendix

URS000224D9CC_9606			64.75	-6.694911828	0.038346431	sEVs
URS00025833EA_9606			64.6	-22.37814525	1.06E-05	granule
ENSG00000185479.6	KRT6B	protein_coding	63.25	-5.617308932	0.042447173	sEVs
ENSG00000276232.1		lncRNA	62.75	-24.10968795	1.66E-05	sEVs
ENSG00000154153.15	RETREG1	protein_coding	60.5	-0.674261156	0.026513133	sEVs
ENSG00000199550.1	Y_RNA	misc_RNA	59.75	-2.102100763	0.044695061	sEVs
ENSG00000175793.12	SFN	protein_coding	59.25	-1.957202081	0.015866557	sEVs
URS0001BDA5C0_9606	HSALNT0243024		58.6	-22.50745418	1.15E-13	granule
URS0002617FDC_9606	RNF187	protein_coding	58.2	-22.42261531	5.78E-05	granule
URS0000D64472_9606			57.75	-23.32677758	4.12E-05	sEVs
URS0001BE5FEC_9606	HSALNT0003934		56.4	-30.77493885	1.82E-10	granule
URS0000D5CF70_9606			55.5	-22.30418324	2.88E-32	sEVs
ENSG00000275895.8		artifact	54.75	0	-1	sEVs
ENSG00000275895.8		artifact	54.75	-10.25999607	2.58E-12	sEVs
ENSG00000077522.15	ACTN2	protein_coding	54.25	-1.012265059	0.023294254	sEVs
ENSG00000264207.1		lncRNA	54.2	0	-1	granule
URS0001BF97F0_9606	HSALNT0014860		54.2	0	-1	granule
URS0000D59652_9606			53.2	-22.37829108	3.25E-14	granule
URS000252C360_9606			52.8	-21.61590941	2.19E-08	granule
ENSG00000105072.9	C19orf44	protein_coding	52.5	-1.317155707	0.017868325	sEVs
URS000233FAC1_9606	HSALNT0335030		51.8	-22.68927934	4.13E-05	granule
ENSG00000091428.18	RAPGEF4	protein_coding	51.25	-1.42105741	0.021337822	sEVs
ENSG00000258864.1		protein_coding	51.25	0	-1	sEVs
ENSG00000258864.1		protein_coding	51.25	-8.821302805	0.000151661	sEVs
ENSG00000141040.15	ZNF287	protein_coding	51	-2.089481328	0.027956668	sEVs
URS0001BDF43A_9606	HSALNT0152853		51	-23.8888823	8.83E-06	granule
URS00006422E6_9606	SNORA73B	snoRNA	50.75	-23.48882401	5.15E-08	sEVs
ENSG00000224287.2	MSL3P1	transcribed_processed_pseudogene	49.75	-1.902209681	0.027224099	sEVs
ENSG00000188611.17	ASAH2	protein_coding	49.5	-1.638296293	0.040760748	sEVs
URS00008B524C_9606			49.25	-22.79906761	3.38E-11	sEVs
URS0000D5D10A_9606			48.25	-0.954301314	0.048989387	sEVs
ENSG00000272921.1		protein_coding	47.75	-22.10299733	1.26E-12	sEVs
URS0001D136AB_9606			46.8	-22.30706607	9.06E-19	granule
URS0001BCBA29_9606	HSALNT0289338		45.8	-22.31653577	4.06E-05	granule
ENSG00000165474.8	GJB2	protein_coding	44	-1.02854146	0.009653442	sEVs
ENSG00000289316.1		lncRNA	43.75	0	-1	sEVs
ENSG00000289316.1		lncRNA	43.75	-22.69803339	1.26E-05	sEVs
URS0002577D6D_9606			43.6	-19.81619362	2.46E-19	granule
ENSG00000283782.2		protein_coding	43.25	-22.86177273	7.42E-40	sEVs
URS000256FC11_9606			42.75	-4.484554056	0.041187816	sEVs
ENSG00000198948.12	MFAP3L	protein_coding	42.5	-1.205452156	0.014534727	sEVs
URS0002618364_9606		lncRNA	42.25	-21.92969841	5.27E-23	sEVs
URS0000D58CC4_9606			42.2	-21.8614819	3.09E-08	granule

Appendix

URS0000636A2E_9606	SNORA53	snoRNA	42	-24.80467929	2.44E-06	granule
ENSG00000109944.11	JHY	protein_coding	41.5	-1.24523603	0.038052475	sEVs
ENSG00000076555.16	ACACB	protein_coding	41.25	-1.926572507	0.034701112	sEVs
ENSG00000196353.13	CPNE4	protein_coding	41	-0.899348913	0.016789968	sEVs
URS00022B30C4_9606			40.8	0	-1	granule
URS0001BD3D95_9606	HSALNT0279530		40	-23.05103747	4.03E-05	sEVs
URS00023390C2_9606	HSALNT0279530		40	-23.44763833	2.78E-05	sEVs
URS0002522F18_9606			39.8	-21.87822559	0.000120388	granule
URS00009AD4FD_9606	HSALNT0060647		39.75	-21.92627586	5.39E-24	sEVs
ENSG00000070540.13	WIPI1	protein_coding	39	-1.413574035	0.001073156	sEVs
URS0002592CA0_9606			38.75	-3.80197145	0.003107267	sEVs
URS0001BD0144_9606	HSALNT0118234		38	-22.77997957	8.73E-22	sEVs
URS00009B2E45_9606			37.6	-23.01115399	2.76E-05	granule
ENSG00000065618.21	COL17A1	protein_coding	36.75	-3.422147535	0.019205159	sEVs
URS0000E91E11_9606	HSALNT0248588		36.25	-2.930637788	0.004205107	sEVs
URS000075E5AD_9606			36	-24.04482498	7.18E-06	granule
URS0000D5B15C_9606			35.75	-22.65276851	1.83E-21	sEVs
URS0002342589_9606	HSALNT0293797		35.6	0	-1	granule
URS0002342589_9606	HSALNT0293797		35.6	-7.178851953	0.035848323	granule
ENSG00000169627.9	BOLA2B	protein_coding	35.5	-2.652234321	0.02792611	sEVs
URS00008C394F_9606			34.75	-22.77136882	1.93E-17	sEVs
ENSG00000184005.12	ST6GALNAC3	protein_coding	34	-1.387286952	0.00171706	sEVs
URS0000E5F74C_9606			34	-3.666492062	0.001268089	sEVs
ENSG00000133401.16	PDZD2	protein_coding	33.5	-1.774656706	0.046321856	sEVs
URS0000064325_9606	SNORA23		33.25	-3.22100667	0.012915852	sEVs
ENSG00000112309.11	B3GAT2	protein_coding	32.75	-1.631962543	0.013355509	sEVs
ENSG00000176024.18	ZNF613	protein_coding	32.5	-2.00869632	1.64E-05	sEVs
ENSG00000103599.20	IQCH	protein_coding	31.75	-1.295838679	0.039203619	sEVs
ENSG00000136040.9	PLXNC1	protein_coding	31.75	-1.784627254	0.002250395	sEVs
URS00009C2D30_9606	HSALNT0156837		31.75	0	-1	sEVs
URS00009C2D30_9606	HSALNT0156837		31.75	-9.140751498	0.000374638	sEVs
URS000253131C_9606			31.75	0	-1	sEVs
URS0002575EB0_9606			31.75	-5.933868325	0.002250395	sEVs
URS0000E9EF52_9606	HSALNT0236757		30.8	0	-1	granule
ENSG00000136866.14	ZFP37	protein_coding	30.75	-1.33478567	0.001499896	sEVs
URS00008BF87F_9606			30.5	-20.53643117	0.000648556	sEVs
URS000233C8B7_9606	HSALNT0316151		30	0	-1	granule
URS0002212B3E_9606			28	-23.33973711	1.61E-05	granule
ENSG00000087245.13	MMP2	protein_coding	27.75	-1.898762296	0.016727229	sEVs
ENSG00000199785.1	SNORA52	snoRNA	27.75	-4.180665702	0.019455196	sEVs
URS0000D6EB06_9606			27.75	0	-1	sEVs
URS0000D6EB06_9606			27.75	-8.440805837	0.00051489	sEVs
URS0000EEDFEA_9606	HSALNT0399015		27.6	-22.39861684	4.81E-08	granule

Appendix

URS0000D59F5F_9606			27.25	-1.031592164	0.0473148	sEVs
URS0001BCC7CC_9606	HSALNT0270739		27.25	-8.292326777	0.014931656	sEVs
URS00009AEESC_9606	HSALNT0088996		25.8	-32.69316161	7.12E-12	granule
ENSG00000102934.10	PLLP	protein_coding	25.5	-1.560807908	0.049808223	sEVs
URS0000D6DE5F_9606			25.4	0	-1	granule
ENSG00000157152.17	SYN2	protein_coding	25.25	-1.905961634	0.006659518	sEVs
URS00009BFAE5_9606			25	-21.40871679	3.08E-22	sEVs
URS000233D421_9606	HSALNT0398958		24.75	-22.71702652	7.70E-05	sEVs
URS0000D5B4CC_9606			24.5	-21.53466024	3.82E-05	sEVs
URS0000EBB24C_9606	HSALNT0043030		23.8	0	-1	granule
URS0001BF5228_9606	HSALNT0043030		23.8	0	-1	granule
URS0002337FDC_9606	HSALNT0312743		23.75	-1.276146838	0.043630934	sEVs
ENSG00000124429.18	POF1B	protein_coding	23.5	-2.685347101	0.026034387	sEVs
URS0000D5B666_9606			23.5	-22.05460356	0.000154219	sEVs
URS0001BE5FEC_9606	HSALNT0003934		23.25	-21.83829852	0.000195748	sEVs
URS0000D5B666_9606			22.8	-32.05822125	1.74E-11	granule
URS0000D6E874_9606			22.75	-8.526253993	0.023468437	sEVs
URS00008B2376_9606			22.5	-7.952945143	3.73E-07	sEVs
URS0000D59631_9606			22.5	-21.30733059	4.35E-10	sEVs
ENSG00000151572.18	ANO4	protein_coding	22.25	-1.507227978	0.031323816	sEVs
ENSG00000140398.14	NEIL1	protein_coding	22	-1.604550405	0.04262696	sEVs
ENSG00000188508.11	KRTDAP	protein_coding	22	-3.085332281	0.021141586	sEVs
URS00008B9176_9606			22	-8.74221074	0.000449515	sEVs
ENSG00000273204.1		lncRNA	21.8	0	-1	granule
URS0000D6E745_9606			21.75	0	-1	sEVs
URS0000D6E745_9606			21.75	-22.05914352	0.000142091	sEVs
URS00022AFA38_9606			21.6	0	-1	granule
URS0000D5DFE2_9606			21.25	-19.94246314	7.48E-17	sEVs
URS00025DDEF2_9606			21.25	-3.691830892	0.0063813	sEVs
URS0002617E36_9606	ADAM9	protein_coding	21.25	-21.04750054	5.49E-23	sEVs
ENSG00000159403.18	C1R	protein_coding	21	-2.52947816	0.00569717	sEVs
URS000019E0CD_9606	HELLPAR	lncRNA	21	-20.91053683	1.69E-36	sEVs
URS000233C3B6_9606	HSALNT0388330		21	-2.135694677	0.000391894	sEVs
ENSG00000115380.20	EFEMP1	protein_coding	20.75	-1.421263456	0.00569717	sEVs
ENSG00000235954.9	TTC28-AS1	lncRNA	20.75	-2.72629012	0.038111784	sEVs
URS0000D5BF49_9606			20.75	-6.846822141	1.05E-06	sEVs
URS00009BD750_9606	HSALNT0016228		20.25	-22.44748131	1.49E-12	sEVs
URS0000D6E1B3_9606			20.25	0	-1	sEVs
URS000233A5E0_9606	HSALNT0334394		20.25	-3.431743563	0.031394696	sEVs
ENSG00000019582.17	CD74	protein_coding	20	-3.163690509	0.002792613	sEVs
URS00008B5BBE_9606			20	0	-1	sEVs
URS00008B5BBE_9606			20	-8.820258058	0.000589315	sEVs
URS0000EA5DDE_9606	HSALNT0230196		20	-7.418075267	0.006125974	sEVs

Appendix

URS0001BD807C_9606	HSALNT0230196		20	-7.418075267	0.006125974	sEVs
ENSG00000066382.17	MPPED2	protein_coding	19.75	-1.320082138	0.002559966	sEVs
URS000233D9FA_9606	HSALNT0338887		19.4	0	-1	granule
URS000233D9FA_9606	HSALNT0338887		19.4	-6.279454761	0.049134264	granule
URS00008B2652_9606			19.25	-20.86083718	1.28E-22	sEVs
URS0002343485_9606	HSALNT0348369		19.25	0	-1	sEVs
URS0002231620_9606			19	-19.741584	0.000295817	sEVs
URS00008B9634_9606			18.6	0	-1	granule
URS0001BE095B_9606	HSALNT0193786		18.6	0	-1	granule
URS00025B91A9_9606			18.5	-20.98584073	0.000115397	sEVs
URS00009B2482_9606			18	-6.741565797	0.027229664	sEVs
URS0000D5C22C_9606			18	-5.652758057	0.002032387	granule
URS0001BE2EF3_9606	HSALNT0082942		18	-5.652758057	0.002032387	granule
ENSG00000257800.1	FNBP1P1	processed_pseudogene	17.6	0	-1	granule
URS0001BDD7FC_9606	HSALNT0034104		17.6	0	-1	granule
URS0000D5CEAC_9606			17.5	-21.99345467	1.63E-29	sEVs
ENSG00000180581.7	SRP9P1	processed_pseudogene	17.25	-8.663466404	0.02758734	sEVs
URS000043CC1A_9606			17.25	-7.953961814	0.030203749	sEVs
ENSG00000278274.1	SNORA61	snoRNA	17	-21.22413772	2.61E-22	sEVs
URS0001E61CB3_9606			17	-7.20318031	2.77E-05	sEVs
URS00008BFB28_9606			16.6	0	-1	granule
URS00008B805C_9606			16.5	-21.86251817	2.41E-23	sEVs
URS00008C2CD5_9606			16.5	-19.50202608	2.12E-05	sEVs
URS0001BDD0D9_9606	HSALNT0219218		16.5	-21.86251817	2.41E-23	sEVs
URS0001BE9C9F_9606	HSALNT0015076		16.5	-7.813118495	0.02589169	sEVs
ENSG00000200354.1	SNORA71D	snoRNA	16	-5.841729896	0.026363476	sEVs
ENSG00000091986.16	CCDC80	protein_coding	15.75	-2.053560677	0.035069781	sEVs
ENSG00000163521.16	GLB1L	protein_coding	15.75	-1.394600659	0.049471951	sEVs
ENSG00000188002.13	PDCD6P1	transcribed_unprocessed_pseudogene	15.75	-7.601204981	2.72E-10	sEVs
ENSG00000196126.12	HLA-DRB1	protein_coding	15.5	-1.468430758	0.031394696	sEVs
URS00009BEA8F_9606	HSALNT0258490		15.5	-8.212943803	7.06E-08	sEVs
URS0000EA447B_9606	HSALNT0005755		15.5	0	-1	sEVs
URS0000EA447B_9606	HSALNT0005755		15.5	-7.730473223	0.020700019	sEVs
URS0001BD771A_9606	HSALNT0005755		15.5	0	-1	sEVs
URS0001BD771A_9606	HSALNT0005755		15.5	-7.730473223	0.020700019	sEVs
URS00008BF4B1_9606			15.25	-8.4107036	0.000736512	sEVs
URS00008C1285_9606			15.25	-8.466959492	4.93E-06	sEVs
URS00008C3A52_9606			15.25	-5.620136184	0.022609606	sEVs
URS0000D5956D_9606			15.2	0	-1	granule
URS0000EBA6B5_9606	HSALNT0007474		15	-6.185929793	0.000260735	sEVs
ENSG00000278249.1	SCARNA2	scaRNA	14.75	-19.15932409	3.41E-33	sEVs
URS0000D6E4F4_9606			14.75	-20.4219716	4.52E-05	sEVs
URS00025D162B_9606			14.75	-8.40741249	0.012193125	sEVs

Appendix

ENSG00000254692.1		protein_coding	14.5	-20.72005833	1.09E-05	sEVs
ENSG00000272501.1		lncRNA	14.4	0	-1	granule
URS0001BF2B95_9606	HSALNT0104255		14.4	0	-1	granule
URS0000EBC303_9606	HSALNT0117666		14.25	-8.099016139	5.69E-06	sEVs
URS0000EC19CD_9606	HSALNT0250871		14.25	-1.219500494	0.04783353	sEVs
URS0001BD760B_9606	HSALNT0250871		14.25	-1.219500494	0.04783353	sEVs
ENSG00000126562.17	WNK4	protein_coding	13.75	-3.300340808	0.037523073	sEVs
URS0000D5D470_9606			13.75	0	-1	sEVs
URS0000D5D470_9606			13.75	-8.056814319	0.047828233	sEVs
ENSG00000065621.15	GSTO2	protein_coding	13.5	-2.066649881	0.045800587	sEVs
ENSG00000138798.13	EGF	protein_coding	13.5	-1.838460737	0.01872377	sEVs
ENSG00000157873.18	TNFRSF14	protein_coding	13.5	-3.330035665	0.044753146	sEVs
URS0000D6D756_9606			13.5	-5.115065654	0.028556228	sEVs
URS00008B7854_9606			13.25	-4.449981618	0.011814708	sEVs
URS0001BE193B_9606	HSALNT0123816		13.25	-4.449981618	0.011814708	sEVs
ENSG00000105427.10	CNFN	protein_coding	13	-2.761365977	0.017688562	sEVs
ENSG00000149418.11	ST14	protein_coding	13	-4.0345623	0.001077735	sEVs
ENSG00000154856.13	APCDD1	protein_coding	13	-2.941025413	0.040369297	sEVs
URS00008B6D11_9606			13	-7.243193219	0.019502194	sEVs
URS0001A08290_9606			13	-8.067783112	0.004946968	sEVs
URS0002567D08_9606			13	-7.36579423	0.048785786	sEVs
ENSG00000207523.1	SNORA66	snoRNA	12.75	-4.550987788	0.025140153	sEVs
URS0002342843_9606	HSALNT0344168		12.75	-1.485663567	0.018038849	sEVs
ENSG00000115850.10	LCT	protein_coding	12.5	-1.996420665	0.017721637	sEVs
ENSG00000290682.1	STAG3L5P	lncRNA	12.25	-2.709250187	0.038790913	sEVs
URS00008C0BD9_9606			12.25	-6.88161927	0.020047663	sEVs
URS00009BE4DE_9606	HSALNT0189965		12.25	-8.190610757	0.00123438	sEVs
URS000252DAD9_9606			12.25	-5.376137172	0.006550072	sEVs
ENSG00000273544.1	SNORA44	snoRNA	12	-6.459756299	0.018311421	sEVs
URS0000D5B0B3_9606			12	-3.170109802	0.037523073	sEVs
URS00002C2F40_9606			11.75	-8.329042572	0.007397074	sEVs
URS00008C1164_9606			11.75	-8.325775933	0.000329135	sEVs
URS00009C2925_9606	HSALNT0030031		11.75	-7.428900793	0.006053797	sEVs
ENSG00000255513.1		transcribed_processed_pseudogene	11.5	-1.612278624	0.04783353	sEVs
URS0000D5ABCF_9606			11.5	-1.713530851	0.023873206	sEVs
URS0002348270_9606	HSALNT0363325		11.5	-7.030926318	0.01856307	sEVs
ENSG00000269243.1		lncRNA	11.25	-4.31161165	0.027021998	sEVs
URS0000D6DCFA_9606			11.25	-7.679292292	2.76E-05	sEVs
URS0000EB7679_9606	HSALNT0053211		11.25	-8.128718508	0.0273422	sEVs
URS000075C0B4_9606			11	-7.972218189	0.015859676	sEVs
URS00009AF5E5_9606			11	-6.591876707	5.07E-07	sEVs
URS0000D5CA67_9606			11	-8.329950856	0.001266489	sEVs
URS000256530E_9606			10.8	-19.75628474	0.001736424	granule

Appendix

ENSG0000010319.7	SEMA3G	protein_coding	10.75	-2.540080417	0.04262696	sEVs
ENSG00000144452.15	ABCA12	protein_coding	10.75	-3.391411944	0.000533341	sEVs
ENSG00000247240.10	UBL7-DT	lncRNA	10.75	-3.900353538	2.01E-08	sEVs
URS0000EBF763_9606	HSALNT0006844		10.75	-7.764901197	3.45E-07	sEVs
URS0001BF1A4B_9606	HSALNT0006844		10.75	-7.764901197	3.45E-07	sEVs
URS0001F1C7A4_9606			10.75	-5.923542842	0.024145061	sEVs
URS0000D58BF4_9606			10.5	-1.763422007	0.005691151	sEVs
URS0002348B84_9606	HSALNT0306427		10.5	-2.852760942	0.04262696	sEVs
ENSG00000196208.14	GREB1	protein_coding	10.25	-3.390301276	0.004233755	sEVs
URS00008C10F0_9606			10.25	-1.63354837	0.048271397	sEVs
URS00009C440B_9606	HSALNT0176270		10.25	-6.190606025	0.037577208	sEVs
URS0001BEA1A4_9606	HSALNT0279524		10.25	-4.925352762	0.01049379	sEVs
URS0000D56FBB_9606			10.2	-5.509781583	0.011904205	granule
URS0000D59B36_9606			10	-3.532790138	0.01910624	sEVs
ENSG00000153406.14	NMRAL1	protein_coding	9.75	-2.31818495	0.02221282	sEVs
URS00009AD112_9606			9.75	-7.285827061	0.015866557	sEVs
URS0000D58A87_9606			9.75	-20.29762986	2.01E-08	sEVs
URS0002342D34_9606	HSALNT0312048		9.75	-2.437366718	0.015866557	sEVs
URS00008BF997_9606			9.5	-1.59948477	0.037555143	sEVs
URS0000D57B45_9606			9.5	-3.350585472	0.000295817	sEVs
URS0000D5C47B_9606			9.5	-5.987648387	0.000932689	sEVs
URS0001BD3457_9606	HSALNT0259227		9.5	-3.350585472	0.000295817	sEVs
URS0002341B7A_9606	HSALNT0314715		9.4	0	-1	granule
URS000233A387_9606	HSALNT0374588		9.25	-2.184079962	0.042271359	sEVs
URS000233D5DA_9606	HSALNT0290919		9.25	-5.790691308	0.005035166	sEVs
ENSG00000068781.21	STON1-GTF2A1L	protein_coding	9	-4.556746471	0.001095745	sEVs
ENSG00000152580.9	IGSF10	protein_coding	9	-2.506518004	0.005543821	sEVs
ENSG00000187984.14	ANKRD19P	transcribed_unprocessed_pseudogene	9	0	-1	sEVs
ENSG00000187984.14	ANKRD19P	transcribed_unprocessed_pseudogene	9	-6.809891343	0.00443145	sEVs
URS00008B397B_9606			9	-7.800160438	0.036356209	sEVs
URS0000D5790B_9606			9	-6.878687262	0.000242766	sEVs
URS000233DAFD_9606	HSALNT0363275		9	-7.434508632	7.96E-05	sEVs
URS00023441C7_9606	HSALNT0361709		9	-6.988493885	1.74E-05	sEVs
ENSG00000131951.12	LRRC9	protein_coding	8.75	-3.196081215	0.022157942	sEVs
URS0000D5837F_9606			8.75	-5.909996325	0.006096364	sEVs
URS0000E484D2_9606			8.75	0	-1	sEVs
URS0000E484D2_9606			8.75	-7.00725059	0.004987078	sEVs
ENSG00000231245.2	C1DP1	processed_pseudogene	8.5	-6.476151467	0.04262696	sEVs
URS00008BF7D7_9606			8.5	-4.007707135	0.017688904	sEVs
URS0001BD846E_9606	HSALNT0176354		8.5	-7.010740074	0.000199821	sEVs
ENSG00000154227.14	CERS3	protein_coding	8.25	-5.335695688	0.006445089	sEVs
URS000075C19C_9606			8.25	-5.282254173	0.000299857	sEVs
URS00008B2696_9606			8.25	-6.888226612	0.001298509	sEVs

Appendix

URS0008B9174_9606			8.25	-1.567625474	0.042349244	sEVs
URS0000DEA019_9606			8.25	-4.410629448	0.040367025	sEVs
URS00019A82CE_9606			8.25	-2.834841751	0.030056149	sEVs
URS0001BDD64D_9606	HSALNT0017656		8.25	-1.567625474	0.042349244	sEVs
URS0002342F08_9606	HSALNT0304353		8.25	-20.23003578	0.000864764	sEVs
URS00025A7FB5_9606			8.25	-7.682396702	0.04783353	sEVs
URS00008B39DC_9606			8	-7.246172526	0.001095745	sEVs
URS00009AE5C_9606	HSALNT0088996		8	-19.6436084	0.001499896	sEVs
URS0000EB9B65_9606	HSALNT0243287		8	-4.811832793	0.010942321	sEVs
URS0001BD45B1_9606	HSALNT0243287		8	-4.811832793	0.010942321	sEVs
URS0002552D8D_9606			8	-2.430496338	0.018519892	sEVs
URS0000D57798_9606			7.75	-7.684682212	0.009871723	sEVs
ENSG00000247271.9	ZBED5-AS1	lncRNA	7.5	-5.13555008	0.008733341	sEVs
URS0000D57594_9606			7.5	-5.885142743	0.000138731	sEVs
URS0001A07D18_9606			7.5	-4.600294979	0.017701848	sEVs
ENSG00000114757.19	PEX5L	protein_coding	7.25	-3.176883175	0.023073815	sEVs
ENSG00000167984.18	NLRC3	protein_coding	7.25	-1.745486337	0.031812305	sEVs
URS0000D5918A_9606			7.25	-2.157425039	0.018160963	sEVs
URS0000D5DFF4_9606			7.25	-3.476009059	0.032577241	sEVs
URS0001BCFA4E_9606	HSALNT0092912		7.25	-4.694098516	0.001499896	sEVs
URS0001BE4FBE_9606	HSALNT0165138		7.25	-3.476009059	0.032577241	sEVs
URS0001BF02B9_9606	HSALNT0191033		7.25	-7.584734545	0.000794056	sEVs
ENSG00000280195.2		lncRNA	7	-5.604677782	0.002284299	sEVs
URS0000784FE0_9606			7	-3.406458063	0.021566465	sEVs
URS0000789158_9606			7	-4.189456503	0.031394696	sEVs
URS0002338765_9606	HSALNT0359064		7	-6.199922371	0.000282291	sEVs
URS000233CAB7_9606	HSALNT0296748		7	-2.614341177	0.016973012	sEVs
ENSG00000143921.9	ABCG8	protein_coding	6.75	-1.850163435	0.048989387	sEVs
URS00008B3373_9606			6.75	-6.446117427	0.032820303	sEVs
URS0001BD8B6B_9606	HSALNT0174583		6.75	-3.484047924	0.002414711	sEVs
URS00021FF41C_9606			6.75	-7.80199205	0.012251249	sEVs
URS0002349FC6_9606	HSALNT0174583		6.75	-3.484047924	0.002414711	sEVs
ENSG00000106823.13	ECM2	protein_coding	6.5	-1.974286762	0.036055289	sEVs
ENSG00000130487.9	KLHDC7B	protein_coding	6.5	-3.26508158	0.038906925	sEVs
ENSG00000228526.8	MIR34AHG	lncRNA	6.5	-2.236285991	0.008220153	sEVs
ENSG00000244151.1		lncRNA	6.5	-3.54126378	0.006678477	sEVs
URS0000D5A8D0_9606			6.5	-6.962636248	0.018268123	sEVs
URS0002336EBE_9606	HSALNT0380929		6.5	-7.48433635	0.001441072	sEVs
URS0002346754_9606	HSALNT0386392		6.5	-20.68158821	0.000128335	sEVs
ENSG00000261796.1	ISY1-RAB43	protein_coding	6.25	-6.539704266	0.022409391	sEVs
URS00008BACB4_9606			6.25	-5.286216941	0.009871723	sEVs
URS0000D5BC91_9606			6.25	-7.160121049	0.000145243	sEVs
URS0000D5C43C_9606			6.25	-2.560943282	0.049808223	sEVs

Appendix

URS0000EA8428_9606	HSALNT0111483		6.25	-6.147878955	0.001893861	sEVs
URS0001BCF096_9606	HSALNT0111483		6.25	-6.147878955	0.001893861	sEVs
URS0002339839_9606	HSALNT0305759		6.25	-4.373970552	0.042137226	sEVs
URS0002347315_9606	HSALNT0360413		6.25	-2.129064689	0.033189433	sEVs
URS000234945C_9606	HSALNT0303153		6.25	-6.458043661	0.004987078	sEVs
ENSG00000274978.1	RNU11	snRNA	6	-20.62568324	0.000591951	sEVs
URS00008B6DB9_9606			6	-6.560438199	0.008368941	sEVs
URS00008BF5A2_9606			6	-2.634857467	0.0277522	sEVs
URS0000D56F62_9606			6	-2.510213342	0.024730409	sEVs
URS0000D5DBEB_9606	HSALNT0384819		6	-4.486373047	0.0063813	sEVs
URS0000D6E9CE_9606			6	-20.35413714	0.00077084	sEVs
URS0000E27054_9606			6	-3.24164345	0.038790913	sEVs
URS0001BE771F_9606	HSALNT0287843		6	-6.378696472	0.008603083	sEVs
ENSG00000163141.20	BNIPL	protein_coding	5.75	-2.386784957	0.018097765	sEVs
ENSG00000196345.13	ZKSCAN7	protein_coding	5.75	-4.038563339	0.008629921	sEVs
URS000026CEFF_9606			5.75	-3.395299141	0.036905558	sEVs
URS00005ED4C0_9606			5.75	-4.225994498	0.028556228	sEVs
URS0000D598FF_9606			5.75	-4.612413551	0.048315359	sEVs
URS0000D59F11_9606			5.75	-2.446415011	0.021566465	sEVs
URS0000D5BABF_9606			5.75	-5.889185909	4.62E-05	sEVs
URS0001BF97AA_9606	HSALNT0015855		5.75	-6.325455033	0.034454385	sEVs
URS000257E2E5_9606			5.75	-6.11829274	0.010240202	sEVs
URS0002594C15_9606			5.75	-6.594232194	0.000119282	sEVs
ENSG00000204677.13	FAM153CP	lncRNA	5.5	-2.686059745	0.005188336	sEVs
ENSG00000239280.1	DBTP1	processed_pseudogene	5.5	-2.764055896	0.0448025	sEVs
URS00008B6BC5_9606			5.5	-6.141098454	0.036723154	sEVs
URS0000D57ED0_9606			5.5	-5.368308631	0.003249274	sEVs
URS0000D5B430_9606			5.5	-4.576612122	0.04205805	sEVs
URS0000D5B908_9606			5.5	-7.322979188	0.004130269	sEVs
URS0001BE4B49_9606	HSALNT0229680		5.5	-3.909552268	0.008368941	sEVs
URS000251B1A7_9606			5.5	-5.936776946	0.000390485	sEVs
URS000253E3AC_9606			5.5	-6.12713582	0.000713647	sEVs
ENSG00000012171.20	SEMA3B	protein_coding	5.25	-3.362419976	0.028182667	sEVs
ENSG00000159915.13	ZNF233	protein_coding	5.25	-1.498240197	0.031344325	sEVs
ENSG00000224837.1	GCSHP5	processed_pseudogene	5.25	-6.254532342	0.001070359	sEVs
ENSG00000277128.2		lncRNA	5.25	-3.840170837	0.047661714	sEVs
URS00005BECDE_9606			5.25	-5.625162076	0.014111887	sEVs
URS000075DE72_9606			5.25	-6.845608954	9.99E-06	sEVs
URS000078944A_9606			5.25	-4.374659331	0.020591836	sEVs
URS00008B9DF2_9606			5.25	-6.420810976	0.04262696	sEVs
URS0001BDA164_9606	HSALNT0090315		5.25	-6.420810976	0.04262696	sEVs
URS0001BDFA7_9606	HSALNT0241456		5.25	-2.966174819	0.040369297	sEVs
URS0001BDBD9B_9606	HSALNT0218194		5.25	-4.758177826	0.015866557	sEVs

Appendix

URS0002560E09_9606			5.25	-6.104256083	0.00928904	sEVs
ENSG00000137440.5	FGFBP1	protein_coding	5	-3.176185608	0.009871723	sEVs
ENSG00000187950.9	OVCH1	protein_coding	5	-3.750039649	0.023205643	sEVs
ENSG00000290474.1	GUSBP2	lncRNA	5	-3.89913474	0.027021998	sEVs
URS0000D59BBC_9606			5	-6.688808062	0.030692522	sEVs
URS0000E9841B_9606	HSALNT0011396		5	-5.788936081	0.000308155	sEVs
URS0000E9B8F3_9606	HSALNT0206022		5	-6.635090213	0.000187059	sEVs
URS0000EAA58F_9606	HSALNT0240450		5	-6.298374881	0.002008214	sEVs
URS00019B2368_9606			5	-2.429792193	0.027075776	sEVs
URS0001BE054C_9606	HSALNT0226640		5	-6.784262299	0.005188336	sEVs
URS00022B021A_9606			5	-5.918382028	0.023108386	sEVs
ENSG00000291281.1	COL6A4P1	lncRNA	4.75	-4.021049713	0.010614494	sEVs
URS0000085019_9606			4.75	-4.049908859	0.015495449	sEVs
URS00008BA865_9606			4.75	-5.982510736	0.048123065	sEVs
URS0000EA8654_9606	HSALNT0112874		4.75	-5.138076109	0.023291057	sEVs
URS0000EB8467_9606	HSALNT0053917		4.75	-6.896231591	0.023468437	sEVs
URS0001BE6AF1_9606	HSALNT0219227		4.75	-3.61652507	0.024379912	sEVs
URS0001BF8A58_9606	HSALNT0148756		4.75	-5.982510736	0.048123065	sEVs
URS0001BF9A70_9606	HSALNT0236743		4.75	-7.01899298	0.031491971	sEVs
URS0002338D7E_9606	HSALNT0291362		4.75	-7.106105656	0.038052475	sEVs
URS00023411E8_9606	HSALNT0310900		4.75	-4.003219013	0.023108386	sEVs
ENSG00000241007.1	SEPTIN7P6	processed_pseudogene	4.5	-2.948627177	0.047364603	sEVs
ENSG00000261312.1		lncRNA	4.5	-6.298822725	0.045686482	sEVs
ENSG00000272636.5	DOC2B	protein_coding	4.5	-5.791236076	0.000303366	sEVs
URS0000EB3F80_9606	HSALNT0074649		4.5	-7.03898265	0.022497894	sEVs
URS0001BDBB1B_9606	HSALNT0066671		4.5	-6.442573686	0.000589315	sEVs
URS0001BE8FD5_9606	HSALNT0228511		4.5	-6.298822725	0.045686482	sEVs
URS0001BF9552_9606	HSALNT0095234		4.5	-3.798932836	0.041152897	sEVs
URS000226FCD_9606			4.5	-4.481366971	0.006053797	sEVs
URS0002345159_9606	HSALNT0319314		4.5	-3.191699644	0.042160093	sEVs
URS000234542A_9606	HSALNT0358292		4.5	-5.984646884	0.038479482	sEVs
ENSG00000155269.12	GPR78	protein_coding	4.25	-5.794980918	0.001177621	sEVs
ENSG00000213943.3	KRT18P17	processed_pseudogene	4.25	-3.650791201	0.016175023	sEVs
ENSG00000229183.10	PGA4	protein_coding	4.25	-3.756564133	0.026829122	sEVs
ENSG00000269349.1		lncRNA	4.25	-5.77795842	0.002654185	sEVs
ENSG00000290674.1		lncRNA	4.25	-18.1286317	0.005847596	sEVs
URS0000D5A6CC_9606			4.25	-6.298756663	0.013355509	sEVs
URS0000D5D973_9606			4.25	-5.804753455	0.01734526	sEVs
URS0000E958F7_9606	HSALNT0191010		4.25	-2.345182886	0.048061504	sEVs
URS00019C0110_9606			4.25	-6.024187843	0.012831591	sEVs
URS0001A0B417_9606			4.25	-3.132944029	0.040369297	sEVs
URS0001A1028F_9606			4.25	-5.319437911	0.016777514	sEVs
URS0001BE6450_9606	HSALNT0191010		4.25	-2.345182886	0.048061504	sEVs

Appendix

URS000233D0AA_9606	HSALNT0364269		4.25	-5.085295503	0.007202391	sEVs
URS000233F91B_9606	HSALNT0390954		4.25	-5.727225673	0.026053823	sEVs
URS0002346768_9606	HSALNT0316189		4.25	-3.814232007	0.007664879	sEVs
ENSG00000127831.11	VIL1	protein_coding	4	-3.209470549	0.045686482	sEVs
ENSG00000200983.1	SNORA3A	snoRNA	4	-6.307132276	0.004987078	sEVs
ENSG00000285952.1		lncRNA	4	-5.905826893	0.00830668	sEVs
URS00008B32EF_9606			4	-5.231752709	0.0030325	sEVs
URS00009B0DEF_9606			4	-2.985757793	0.044183315	sEVs
URS0000D5B79D_9606			4	-5.780273717	0.013355509	sEVs
URS0000E9C70F_9606	HSALNT0186432		4	-4.859393368	0.026582006	sEVs
URS0000EAD40E_9606	HSALNT0240313		4	-2.58099664	0.047417203	sEVs
URS0000EBAC4E_9606	HSALNT0211694		4	-5.70497277	0.005188336	sEVs
URS00019ADA5D_9606			4	-3.485622908	0.043156383	sEVs
URS0001BCBE00_9606	HSALNT0117211		4	-6.812510693	0.004946968	sEVs
URS000233652E_9606	HSALNT0408356		4	-4.280129094	0.010063001	sEVs
URS000233A6EB_9606	HSALNT0401244		4	-6.712652622	0.00251843	sEVs
URS000233BA0A_9606	HSALNT0390781		4	-6.748267882	0.029906955	sEVs
URS000234686F_9606	HSALNT0312063		4	-2.698326978	0.043831826	sEVs
URS000254557C_9606			4	-5.528984588	0.008330898	sEVs
URS000254F8FD_9606			4	-5.065593168	0.009987776	sEVs
ENSG00000125804.14	FAM182A	lncRNA	3.75	-4.852082381	0.02221282	sEVs
ENSG00000151967.18	SCHIP1	protein_coding	3.75	-3.463855443	0.025518129	sEVs
URS0000034D55_9606	SNORA10	snoRNA	3.75	-19.79750982	0.001291446	sEVs
URS00008B4E97_9606			3.75	-6.418127808	0.026149658	sEVs
URS00009B269E_9606	HSALNT0074352		3.75	-17.90495149	0.006801233	sEVs
URS00009C1A9F_9606	HSALNT0180380		3.75	-6.780850574	0.004440577	sEVs
URS00009C37DB_9606			3.75	-3.663505217	0.041839966	sEVs
URS0000D5AA3C_9606			3.75	-5.682765139	0.002284299	sEVs
URS0000E995D5_9606	HSALNT0104683		3.75	-5.851297575	0.015329574	sEVs
URS0000EA465E_9606	HSALNT0165391		3.75	-3.119474132	0.023600814	sEVs
URS0000EB47FF_9606	HSALNT0003186		3.75	-3.159449166	0.025172516	sEVs
URS00019C8D11_9606			3.75	-5.610533374	0.008287544	sEVs
URS0001BDE395_9606	HSALNT0003186		3.75	-3.159449166	0.025172516	sEVs
URS0001BE6589_9606	HSALNT0165391		3.75	-3.119474132	0.023600814	sEVs
URS0002337C0B_9606	HSALNT0363429		3.75	-2.760839078	0.034454385	sEVs
URS0002339882_9606	HSALNT0296525		3.75	-5.432906082	0.000190559	sEVs
URS0002341574_9606	HSALNT0394837		3.75	-3.867824556	0.010240202	sEVs
URS0002347B45_9606	HSALNT0323308		3.75	-3.022111489	0.03793101	sEVs
URS000234821B_9606	HSALNT0347627		3.75	-3.310849931	0.021141586	sEVs
ENSG00000201321.1	RNA559	rRNA	3.5	-18.43126206	0.001035973	sEVs
ENSG00000279700.1		TEC	3.5	-3.172548263	0.024304663	sEVs
ENSG00000285841.1		lncRNA	3.5	-3.578455957	0.010123712	sEVs
URS00008B7BBA_9606			3.5	-6.286678352	0.017132386	sEVs

Appendix

URS00008BF11E_9606			3.5	-6.714618943	0.036693105	sEVs
URS00008BF19A_9606			3.5	-5.348049269	0.041839966	sEVs
URS0000D58D37_9606			3.5	-4.718996149	0.027021998	sEVs
URS0000D59C4D_9606			3.5	-5.74766415	0.012032378	sEVs
URS0000D6E930_9606			3.5	-19.76290424	0.001332427	sEVs
URS0000DE5E2B_9606			3.5	-4.517439098	0.04783353	sEVs
URS0000EB83B8_9606	HSALNT0092845		3.5	-6.105432242	0.019455196	sEVs
URS00019D8F28_9606			3.5	-5.507736279	0.005175734	sEVs
URS0001BCE609_9606	HSALNT0131721		3.5	-5.696271857	0.019588942	sEVs
URS0001BE214C_9606	HSALNT0209713		3.5	-4.664505286	0.021337822	sEVs
URS0002337372_9606	HSALNT0363994		3.5	-5.263275352	0.001458473	sEVs
URS000233A129_9606	HSALNT0394580		3.5	-4.946419726	0.049412893	sEVs
URS0002345D6B_9606	HSALNT0381604		3.5	-5.943031103	0.018549158	sEVs
URS0002347132_9606	HSALNT0329895		3.5	-4.842751974	0.027808673	sEVs
URS00025B9CEC_9606			3.5	-5.995457017	0.017309023	sEVs
URS0002587F62_9606			3.4	-30.48489209	3.64E-10	granule
ENSG00000176927.16	EFCAB5	protein_coding	3.25	-5.735738464	0.021337822	sEVs
ENSG00000187902.13	SHISA7	protein_coding	3.25	-2.844600446	0.045228696	sEVs
ENSG00000224117.1	PTPN2P2	processed_pseudogene	3.25	-5.427444977	0.045686482	sEVs
ENSG00000286563.1		lncRNA	3.25	-5.564508823	0.000506565	sEVs
URS00001827BE_9606			3.25	-5.077448434	0.028182667	sEVs
URS00009AD4C6_9606	HSALNT0002239		3.25	-6.420182301	0.040367025	sEVs
URS0000D5BF04_9606			3.25	-5.152340774	0.00720029	sEVs
URS0001BD4CE7_9606	HSALNT0119847		3.25	-5.49377002	0.011455864	sEVs
URS0001BF40EE_9606	HSALNT0277528		3.25	-6.226275005	0.006136742	sEVs
URS000233652A_9606	HSALNT0402292		3.25	-4.687763945	0.017701848	sEVs
URS0002338CC3_9606	HSALNT0305407		3.25	-2.352676856	0.048271397	sEVs
URS000233C1BC_9606	HSALNT0332809		3.25	-3.598239677	0.038630689	sEVs
URS000233DD15_9606	HSALNT0300302		3.25	-5.474133869	0.01734526	sEVs
URS000233FF8C_9606	HSALNT0357815		3.25	-3.415292345	0.035408663	sEVs
URS0002342C3D_9606	HSALNT0290897		3.25	-5.470239867	0.026997241	sEVs
URS000234895B_9606	HSALNT0394013		3.25	-4.379857749	0.012041389	sEVs
ENSG00000152583.13	SPARCL1	protein_coding	3	-4.045188075	0.028182667	sEVs
ENSG00000198910.14	L1CAM	protein_coding	3	-2.893629929	0.033558867	sEVs
ENSG00000226288.3	OR52I2	protein_coding	3	-4.582385964	0.004966343	sEVs
ENSG00000278275.2		transcribed_processed_pseudogene	3	-4.002401982	0.024402373	sEVs
URS00008B31E1_9606			3	-4.777632551	0.021337822	sEVs
URS00008B389D_9606			3	-5.31051687	0.018510068	sEVs
URS00008B38CF_9606			3	-6.289255223	0.049808223	sEVs
URS00008BC0A2_9606			3	-6.311132952	0.013355509	sEVs
URS00008BC1CB_9606			3	-6.437926208	0.032944917	sEVs
URS00008BD817_9606			3	-6.04818663	0.005267969	sEVs
URS0000D58EFC_9606			3	-4.701352055	0.018869001	sEVs

Appendix

URS0000D59E3B_9606			3	-6.15563314	0.00035423	sEVs
URS0000D5A6DF_9606			3	-5.363439669	0.008685008	sEVs
URS0000D5D6FA_9606			3	-6.259022951	0.011879011	sEVs
URS0000DDB436_9606			3	-4.505184421	0.021354193	sEVs
URS0000E94AE3_9606	HSALNT0019578		3	-5.512048764	0.017380484	sEVs
URS0000EA3657_9606	HSALNT0243845		3	-3.879952396	0.026120379	sEVs
URS0000EB0916_9606	HSALNT0082174		3	-5.325398958	0.000283444	sEVs
URS0000EB4EE8_9606	HSALNT0096887		3	-3.991240441	0.031796369	sEVs
URS0000EB7A3D_9606	HSALNT0276140		3	-4.50547363	0.025172516	sEVs
URS0001BCC12C_9606	HSALNT0276140		3	-4.529442944	0.0473148	sEVs
URS0001BCC6C8_9606	HSALNT0246089		3	-5.431363822	0.000589315	sEVs
URS0001BDFF66_9606	HSALNT0219455		3	-6.04818663	0.005267969	sEVs
URS0001BE7E4B_9606	HSALNT0195888		3	-4.208946618	0.023642607	sEVs
URS0001BEB029_9606	HSALNT0019578		3	-5.512048764	0.017380484	sEVs
URS0001BEB30A_9606	HSALNT0082174		3	-5.325398958	0.000283444	sEVs
URS0001BECE3D_9606	HSALNT0096887		3	-3.991240441	0.031796369	sEVs
URS0002336258_9606	HSALNT0327207		3	-4.563390338	0.005188336	sEVs
URS000233CAB8_9606	HSALNT0387881		3	-5.610526723	0.010240202	sEVs
URS000233F167_9606	HSALNT0311704		3	-5.259589648	0.00046634	sEVs
URS000233F9C0_9606	HSALNT0296508		3	-5.536709269	0.011185526	sEVs
URS00023415F1_9606	HSALNT0195888		3	-4.208946618	0.023642607	sEVs
URS00023431C0_9606	HSALNT0405234		3	-4.526319534	0.023108386	sEVs
URS0002343AA8_9606	HSALNT0327985		3	-4.471747044	0.013355509	sEVs
URS0002597829_9606			3	-4.633595401	0.037956284	sEVs
URS00025B4816_9606			3	-5.864917856	0.00183746	sEVs
ENSG00000163803.13	PLB1	protein_coding	2.75	-3.529251373	0.033460461	sEVs
ENSG00000183281.15	PLGLB1	protein_coding	2.75	-4.900106985	0.006859731	sEVs
URS00002B0ED4_9606			2.75	-6.262913391	0.005215992	sEVs
URS000075FF8A_9606			2.75	-5.3372211	0.031394696	sEVs
URS00008B65CC_9606			2.75	-5.193859483	0.001416114	sEVs
URS0000D5B6F7_9606	HSALNT0054460		2.75	-5.970905665	0.00867645	sEVs
URS0000D5CB33_9606			2.75	-6.554523372	0.033460461	sEVs
URS0000E910B2_9606	HSALNT0008532		2.75	-4.030707425	0.021566465	sEVs
URS0000E95F92_9606	HSALNT0259283		2.75	-5.114867984	0.001532112	sEVs
URS0000EB5E5D_9606	HSALNT0115056		2.75	-4.088703705	0.0159932	sEVs
URS00019EDE73_9606			2.75	-6.413838656	0.04783353	sEVs
URS0001BD03FE_9606	HSALNT0212171		2.75	-5.146163605	0.001218302	sEVs
URS0001BD572C_9606	HSALNT0035787		2.75	-6.554523372	0.033460461	sEVs
URS0001BDE65F_9606	HSALNT0008532		2.75	-4.030707425	0.021566465	sEVs
URS0001BE6BD9_9606	HSALNT0259283		2.75	-5.114867984	0.001532112	sEVs
URS0001BE7C76_9606	HSALNT0115056		2.75	-4.088703705	0.0159932	sEVs
URS0002338A09_9606	HSALNT0346400		2.75	-3.762655682	0.040697152	sEVs
URS000233AC36_9606	HSALNT0402270		2.75	-6.100131671	0.005957127	sEVs

Appendix

URS000233F99A_9606	HSALNT0366404		2.75	-4.514024678	0.04262696	sEVs
URS00023412E6_9606	HSALNT0342667		2.75	-18.20438341	0.005385512	sEVs
URS00023415FE_9606	HSALNT0408378		2.75	-3.853255961	0.032577241	sEVs
URS00023460C5_9606	HSALNT0384931		2.75	-5.002357194	0.00855446	sEVs
URS000251F525_9606			2.75	-4.4628917	0.017721637	sEVs
URS00025561FE_9606			2.75	-5.015240634	0.006053797	sEVs
ENSG00000188958.10	UTS2B	protein_coding	2.5	-4.983148735	0.011994413	sEVs
ENSG00000207344.1	SNORA22C	snoRNA	2.5	-5.023732571	0.008603083	sEVs
ENSG00000237268.4		transcribed_unprocessed_pseudogene	2.5	-5.187376659	0.007513083	sEVs
ENSG00000249784.1	SCARNA22	scaRNA	2.5	-5.422110014	0.009871723	sEVs
ENSG00000257698.3	GIHCG	lncRNA	2.5	-6.000287771	0.046255345	sEVs
ENSG00000279434.1		TEC	2.5	-3.884990355	0.049808223	sEVs
URS00007591FD_9606			2.5	-5.634603269	0.010240202	sEVs
URS00009B0DF8_9606	HSALNT0055858		2.5	-5.135690462	0.000636565	sEVs
URS0000A76E61_9606			2.5	-3.879144853	0.028205591	sEVs
URS0000D57COE_9606			2.5	-5.377993292	0.04262696	sEVs
URS0000D5BAA2_9606			2.5	-3.735043992	0.035049084	sEVs
URS0000D5C5D3_9606			2.5	-5.162635304	0.006096364	sEVs
URS0000E18587_9606			2.5	-5.127622809	0.04262696	sEVs
URS00019ECF00_9606			2.5	-5.537667641	0.025109467	sEVs
URS0001BE1494_9606	HSALNT0193858		2.5	-4.45955925	0.025319179	sEVs
URS0001BE6E1D_9606	HSALNT0176944		2.5	-4.226713297	0.045686482	sEVs
URS0001BEFD26_9606	HSALNT0209435		2.5	-3.884990355	0.049808223	sEVs
URS0002339658_9606	HSALNT0308651		2.5	-4.553371582	0.027021998	sEVs
URS000233BFD5_9606	HSALNT0407060		2.5	-4.337735309	0.011667637	sEVs
URS000234425B_9606	HSALNT0359363		2.5	-4.874910338	0.002250395	sEVs
URS0002345C51_9606	HSALNT0395612		2.5	-4.253234379	0.019455196	sEVs
URS00023462EE_9606	HSALNT0407867		2.5	-3.642898154	0.040369297	sEVs
URS0002347073_9606	HSALNT0335519		2.5	-4.785591774	0.038641988	sEVs
URS000234865B_9606	HSALNT0401598		2.5	-4.441030811	0.032146695	sEVs
URS00023490D2_9606	HSALNT0319555		2.5	-4.946137603	0.013199427	sEVs
URS0002349759_9606	HSALNT0321132		2.5	-4.434642697	0.006762891	sEVs
URS00025689A1_9606			2.5	-5.381761382	0.008319039	sEVs
URS00025C3C19_9606			2.5	-5.635979202	0.014931656	sEVs
ENSG00000235919.5	ASH1L-AS1	lncRNA	2.25	-5.061896126	0.021502488	sEVs
URS00008B405B_9606			2.25	-4.351401422	0.015866557	sEVs
URS00008BA6FC_9606			2.25	-4.677893412	0.030203749	sEVs
URS00008C073C_9606			2.25	-4.260029199	0.047417203	sEVs
URS0000D5944B_9606			2.25	-19.03306114	0.000864764	sEVs
URS0000D5A0E8_9606			2.25	-5.387443452	0.014407058	sEVs
URS0000D5B1C7_9606			2.25	-4.769170316	0.005572364	sEVs
URS0000DD9ED7_9606			2.25	-5.154660237	0.019749314	sEVs
URS0000DF225F_9606			2.25	-4.566491392	0.046245612	sEVs

Appendix

URS0000E97152_9606	HSALNT0053777		2.25	-5.805189168	0.030045706	sEVs
URS0000EB3176_9606	HSALNT0046210		2.25	-4.340970533	0.028210134	sEVs
URS0000EBA81D_9606	HSALNT0139382		2.25	-4.984757104	0.038052475	sEVs
URS0000EBD0D6_9606	HSALNT0190753		2.25	-5.017238153	0.006678477	sEVs
URS0001BCC020_9606	HSALNT0053777		2.25	-5.805189168	0.030045706	sEVs
URS0001BD654E_9606	HSALNT0237061		2.25	-4.260029199	0.047417203	sEVs
URS0001BE487C_9606	HSALNT0193392		2.25	-6.172632658	0.046421801	sEVs
URS0001BEA6E1_9606	HSALNT0089255		2.25	-4.219435512	0.043953378	sEVs
URS0001BEFA60_9606	HSALNT0286441		2.25	-5.250933692	0.045696544	sEVs
URS0001BF31D4_9606	HSALNT0139382		2.25	-4.984757104	0.038052475	sEVs
URS0001BF32F0_9606	HSALNT0158950		2.25	-4.351401422	0.015866557	sEVs
URS0001BF726E_9606	HSALNT0190753		2.25	-5.017238153	0.006678477	sEVs
URS0001BF9C19_9606	HSALNT0046210		2.25	-4.340970533	0.028210134	sEVs
URS000223003F_9606			2.25	-5.853749897	0.006812671	sEVs
URS000233A993_9606	HSALNT0286441		2.25	-5.250933692	0.045696544	sEVs
URS000233C8DD_9606	HSALNT0310656		2.25	-5.17653722	0.003387073	sEVs
URS000233DBF4_9606	HSALNT0330470		2.25	-5.264373666	0.008319039	sEVs
URS000233E5B5_9606	HSALNT0318210		2.25	-4.608296483	0.010284492	sEVs
URS0002340FDD_9606	HSALNT0328137		2.25	-4.167074424	0.021141586	sEVs
URS0002346DAF_9606	HSALNT0391817		2.25	-3.95224871	0.042799663	sEVs
URS0002347012_9606	HSALNT0341264		2.25	-5.455545742	0.03330017	sEVs
URS0002347B32_9606	HSALNT0393388		2.25	-4.892997896	0.044183315	sEVs
URS0002348523_9606	HSALNT0385359		2.25	-5.77788983	0.029543625	sEVs
URS0002349083_9606	HSALNT0394838		2.25	-4.197708993	0.034913517	sEVs
URS00023496D2_9606	HSALNT0346012		2.25	-5.381864574	0.010240202	sEVs
URS0002544128_9606			2.25	-5.058067261	0.008692527	sEVs
ENSG00000100884.10	CPNE6	protein_coding	2	-6.341966851	0.042137226	sEVs
ENSG00000261611.6		protein_coding	2	-4.579868753	0.008629921	sEVs
ENSG00000262402.1	MCUR1P1	processed_pseudogene	2	-5.701207579	0.026084344	sEVs
URS00008B5532_9606			2	-4.700944358	0.008328933	sEVs
URS00008B820A_9606			2	-4.699979692	0.005385512	sEVs
URS00008BBECA_9606			2	-5.70117462	0.012251249	sEVs
URS00008C2EDC_9606			2	-5.566677295	0.019065276	sEVs
URS0000D5ABE5_9606			2	-4.240704068	0.044183315	sEVs
URS0000EA836D_9606	HSALNT0281860		2	-4.568804537	0.029543625	sEVs
URS0000EB25B3_9606	HSALNT0075454		2	-5.443645385	0.036364819	sEVs
URS0001BD0204_9606	HSALNT0116691		2	-5.43771403	0.025172516	sEVs
URS0001BDBD27_9606	HSALNT0023059		2	-4.240704068	0.044183315	sEVs
URS0001BEDA41_9606	HSALNT0278905		2	-5.70117462	0.012251249	sEVs
URS0001BEECGF_9606	HSALNT0275929		2	-5.355081335	0.042149013	sEVs
URS0001BF019B_9606	HSALNT0153087		2	-4.699979692	0.005385512	sEVs
URS0001BF01C9_9606	HSALNT0260627		2	-4.700944358	0.008328933	sEVs
URS00022B3F00_9606			2	-5.72901018	0.011994413	sEVs

Appendix

URS00022B8424_9606			2	-4.700216204	0.03086063	sEVs
URS0002337491_9606	HSALNT0367315		2	-4.146922965	0.04262696	sEVs
URS0002337EB3_9606	HSALNT0294557		2	-4.028811765	0.038052475	sEVs
URS00023392EC_9606	HSALNT0301896		2	-4.805705499	0.022569238	sEVs
URS0002340B21_9606	HSALNT0375146		2	-4.891837695	0.013355509	sEVs
URS0002344BD4_9606	HSALNT0303938		2	-4.129130454	0.046255345	sEVs
URS0002345EEA_9606	HSALNT0359481		2	-4.709391523	0.029305696	sEVs
URS00023476EF_9606	HSALNT0338223		2	-5.668283059	0.037577208	sEVs
ENSG00000207165.1	SNORA70	snoRNA	1.75	-5.029988966	0.0473148	sEVs
ENSG00000225014.1	KCTD9P1	transcribed_processed_pseudogene	1.75	-4.173179051	0.048058337	sEVs
URS000075EF5D_9606			1.75	-18.39358462	0.004588243	sEVs
URS00008B42FB_9606			1.75	-5.290740389	0.047417203	sEVs
URS00008B7F70_9606			1.75	-4.439521996	0.010519088	sEVs
URS00008B9C35_9606			1.75	-4.597593752	0.009871723	sEVs
URS00008BC022_9606			1.75	-4.516278329	0.045237556	sEVs
URS00008BC135_9606			1.75	-5.000887605	0.011814708	sEVs
URS00009B173D_9606			1.75	-4.444850534	0.048278945	sEVs
URS00009C5AEE_9606			1.75	-5.406633504	0.023607621	sEVs
URS0000D56EEC_9606			1.75	-5.4402256	0.043154553	sEVs
URS0000E954A0_9606	HSALNT0275077		1.75	-5.359638434	0.027650491	sEVs
URS0000E9D8B5_9606	HSALNT0117665		1.75	-4.479415695	0.04262696	sEVs
URS0000EA26BC_9606	HSALNT0059915		1.75	-5.096371903	0.020832222	sEVs
URS0000EDF6E0_9606			1.75	-3.852343888	0.04660612	sEVs
URS0001BCD914_9606	HSALNT0091590		1.75	-4.439521996	0.010519088	sEVs
URS0001BEC142_9606	HSALNT0207781		1.75	-5.27690954	0.017380484	sEVs
URS0001BEE191_9606	HSALNT0064292		1.75	-4.597593752	0.009871723	sEVs
URS0001BF5A1C_9606	HSALNT0117665		1.75	-4.479415695	0.04262696	sEVs
URS0001BF8AF1_9606	HSALNT0255731		1.75	-5.005820793	0.01914343	sEVs
URS0002272BD8_9606			1.75	-5.589052704	0.013355509	sEVs
URS00023436DA_9606	HSALNT0335196		1.75	-3.97776031	0.046255345	sEVs
URS000257B6A8_9606			1.75	-5.145475638	0.026111829	sEVs
ENSG00000183066.14	WBP2NL	protein_coding	1.5	-4.146583201	0.036055289	sEVs
ENSG00000230154.1	AIDAP1	processed_pseudogene	1.5	-4.320934645	0.04262696	sEVs
ENSG00000282164.4	PEG13	lncRNA	1.5	-5.00550612	0.025394927	sEVs
URS00008B72AE_9606			1.5	-4.376918514	0.037664929	sEVs
URS00008B85CC_9606			1.5	-5.19841523	0.024730409	sEVs
URS00008C08C8_9606	PHF1	lncRNA	1.5	-5.414308052	0.006812671	sEVs
URS00008C3586_9606			1.5	-4.72680559	0.037577208	sEVs
URS0000D58579_9606			1.5	-4.169175012	0.024670652	sEVs
URS0000E936EC_9606	HSALNT0251106		1.5	-5.221945793	0.027021998	sEVs
URS0000E9A982_9606	HSALNT0108282		1.5	-4.229313045	0.043794855	sEVs
URS0000EA3A9D_9606	HSALNT0248125		1.5	-4.549553287	0.026111829	sEVs
URS0000EB8ADA_9606	HSALNT0095079		1.5	-5.014893501	0.031617382	sEVs

Appendix

URS0000EBB098_9606	HSALNT0046647		1.5	-4.019217065	0.029483864	sEVs
URS0001BE14F4_9606	HSALNT0108282		1.5	-4.229313045	0.043794855	sEVs
URS0001BE7C99_9606	HSALNT0248125		1.5	-4.549553287	0.026111829	sEVs
URS0001BE8946_9606	HSALNT0089211		1.5	-4.72680559	0.037577208	sEVs
URS0001BE919E_9606	HSALNT0134371		1.5	-5.19841523	0.024730409	sEVs
URS0001BF074E_9606	HSALNT0159455		1.5	-4.376918514	0.037664929	sEVs
URS0001BF9FE1_9606	HSALNT0046647		1.5	-4.019217065	0.029483864	sEVs
URS0001BFA284_9606	HSALNT0251106		1.5	-5.221945793	0.027021998	sEVs
URS0002335C01_9606	HSALNT0376435		1.5	-4.415699741	0.049936329	sEVs
URS000233E9BD_9606	HSALNT0316063		1.5	-4.126739514	0.034466909	sEVs
URS0002348F45_9606	HSALNT0311066		1.5	-4.566474348	0.03627302	sEVs
URS00025D12D7_9606			1.5	-4.239298637	0.04262696	sEVs
URS00025D7A06_9606			1.5	-4.90397606	0.04783353	sEVs
URS00008BD8F9_9606			1.25	-4.815599968	0.034701112	sEVs
URS00008C021B_9606			1.25	-4.22235843	0.047718721	sEVs
URS0000D59E24_9606			1.25	-4.814605951	0.039283458	sEVs
URS0000D5D554_9606			1.25	-4.241018586	0.048989387	sEVs
URS0000EA4616_9606	HSALNT0013547		1.25	-4.029026178	0.044753146	sEVs
URS0000EA8997_9606	HSALNT0071195		1.25	-4.844276796	0.027021998	sEVs
URS0000EA8C20_9606	HSALNT0114786		1.25	-4.056332924	0.0473148	sEVs
URS0000EBE0AD_9606	HSALNT0051640		1.25	-4.243848607	0.037577208	sEVs
URS0001BCFCF4_9606	HSALNT0051640		1.25	-4.243848607	0.037577208	sEVs
URS0001BD0799_9606	HSALNT0114786		1.25	-4.056332924	0.0473148	sEVs
URS0001BD618F_9606	HSALNT0205415		1.25	-4.22235843	0.047718721	sEVs
URS0001BD62B0_9606	HSALNT0096179		1.25	-4.241018586	0.048989387	sEVs
URS0001BE66C5_9606	HSALNT0013547		1.25	-4.029026178	0.044753146	sEVs
URS0001BEF5BD_9606	HSALNT0071195		1.25	-4.844276796	0.027021998	sEVs
URS0001BF283E_9606	HSALNT0173669		1.25	-4.874403815	0.044183315	sEVs
URS0002338CC5_9606	HSALNT0307814		1.25	-4.073797923	0.047364603	sEVs
URS000233E3BF_9606	HSALNT0322554		1.25	-4.260359311	0.032778919	sEVs
URS00023407EF_9606	HSALNT0363965		1.25	-3.899203724	0.042802173	sEVs
URS0000706530_9606	SNORD10	snoRNA	1	-15.68514722	0.031394696	sEVs
URS0000D5D052_9606			0.75	-17.68256369	0.00820597	sEVs
URS0000074F23_9606			0.4	-15.16980046	0.00087489	granule

Appendix 3. List of proteins exclusively present in control sEVs. This table presents proteins uniquely identified in control sEVs, detailing several key metrics.

Protein ID	Gene	P-Value	Adj P-Value	fc	Logfc
O00273	DFFA	0.07200566	0.07200566	6.3221E-07	-20.593096
O00629	KPNA4	0.4237108	0.4237108	2.5258E-06	-18.5948523
O14617	AP3D1	0.4237108	0.4237108	1.8518E-06	-19.042602
O15078	CEP290	0.17971249	0.17971249	1.2894E-07	-22.8868443

Appendix

O15144	ARPC2	0.4237108	0.4237108	2.2961E-06	-18.7323821
O15234	CASC3	0.4237108	0.4237108	6.6397E-06	-17.2004465
O15382	BCAT2	0.17971249	0.17971249	2.1394E-06	-18.8343618
O15460	P4HA2	0.4237108	0.4237108	1.4608E-05	-16.0629062
O43172	PRPF4	0.4237108	0.4237108	8.8993E-06	-16.777882
O43290	SART1	0.4237108	0.4237108	4.844E-06	-17.6553686
O43395	PRPF3	0.4237108	0.4237108	1.6039E-06	-19.2499856
O43674	NDUFB5	0.4237108	0.4237108	2.2075E-06	-18.7891541
O43847	NRD1	0.4237108	0.4237108	3.7447E-06	-18.0267007
O60566	BUB1B	0.4237108	0.4237108	2.2191E-06	-18.7816184
O60573	EIF4E2	0.02536986	0.02536986	2.9201E-07	-21.7074789
O75190;Q8NHSO;P25686	DNAJB6	0.4237108	0.4237108	4.6542E-06	-17.7130428
O75323	GBAS	0.4237108	0.4237108	1.5614E-07	-22.6106772
O75448	MED24	0.17971249	0.17971249	2.1471E-06	-18.8292105
O94760	DDAH1	0.4237108	0.4237108	4.6313E-06	-17.7201427
O94855	SEC24D	0.4237108	0.4237108	4.7938E-06	-17.6703852
O94903	PROSC	0.17971249	0.17971249	3.9768E-06	-17.9399728
O94992	HEXIM1	0.17971249	0.17971249	1.7906E-06	-19.091096
O95271	TNKS	0.4237108	0.4237108	2.3481E-06	-18.7000902
O95298	NDUFC2	0.07200566	0.07200566	5.1975E-06	-17.5537523
O95453	PARN	0.4237108	0.4237108	6.0133E-06	-17.3434182
P03886	MTND1	0.4237108	0.4237108	6.4249E-06	-17.2478979
P04350	TUBB4A	0.4237108	0.4237108	2.6196E-06	-18.5422339
P04637	TP53	0.4237108	0.4237108	2.5534E-06	-18.5791715
P05198	EIF2S1	0.4237108	0.4237108	1.5551E-06	-19.2945508
P07196	NEFL	0.4237108	0.4237108	8.8276E-06	-16.7895438
P08240	SRPR	0.07200566	0.07200566	5.8281E-07	-20.7104671
P09601	HMOX1	0.4237108	0.4237108	1.0013E-06	-19.9296352
P09661	SNRPA1	0.07200566	0.07200566	2.2744E-06	-18.7461023
P10155	TROVE2	0.17971249	0.17971249	7.4835E-07	-20.3497916
P14314	PRKCSH	0.4237108	0.4237108	2.2707E-06	-18.7484576
P14406	COX7A2	0.4237108	0.4237108	3.0971E-07	-21.622567
P14854	COX6B1	0.4237108	0.4237108	1.2024E-06	-19.6656357
P14927	UQCRB	0.17971249	0.17971249	1.2154E-06	-19.6501483
P16930	FAH	0.4237108	0.4237108	4.2731E-06	-17.8362772
P16949	STMN1	0.4237108	0.4237108	2.128E-06	-18.8420581
P18077	RPL35A	0.17971249	0.17971249	6.6921E-06	-17.1891161
P19022;P55283	CDH2	0.4237108	0.4237108	2.1661E-06	-18.8164737
P19525	EIF2AK2	0.17971249	0.17971249	6.4597E-07	-20.5620305
P21266	GSTM3	0.4237108	0.4237108	1.0237E-05	-16.5759055
P23368	ME2	0.4237108	0.4237108	4.5372E-06	-17.7497699
P24752	ACAT1	0.07200566	0.07200566	2.3582E-07	-22.0158099
P25325	MPST	0.4237108	0.4237108	9.3926E-06	-16.7000441
P26358	DNMT1	0.17971249	0.17971249	1.9739E-06	-18.9504893
P28838	LAP3	0.4237108	0.4237108	3.2787E-06	-18.2184535
P29692	EEF1D	0.17971249	0.17971249	1.5854E-06	-19.2667193

Appendix

P30837	ALDH1B1	0.4237108	0.4237108	4.0707E-07	-21.228232
P33981	TTK	0.4237108	0.4237108	7.5557E-06	-17.0140074
P35520	CBS	0.4237108	0.4237108	3.1977E-06	-18.2545157
P35611	ADD1	0.4237108	0.4237108	1.0848E-05	-16.4921474
P36871	PGM1	0.4237108	0.4237108	7.6824E-07	-20.3119443
P38117	ETFB	0.4237108	0.4237108	3.2099E-06	-18.2490616
P42224	STAT1	0.4237108	0.4237108	4.8412E-06	-17.656207
P46013	MKI67	0.07200566	0.07200566	2.0784E-06	-18.8760984
P48147	PREP	0.4237108	0.4237108	2.1835E-06	-18.8049276
P48681	NES	0.4237108	0.4237108	2.0039E-06	-18.9287404
P49189	ALDH9A1	0.4237108	0.4237108	2.1604E-06	-18.8202812
P49406	MRPL19	0.07200566	0.07200566	1.8118E-06	-19.0741373
P51608	MECP2	0.4237108	0.4237108	5.0673E-06	-17.590359
P51610	HCFC1	0.4237108	0.4237108	5.4077E-07	-20.8184861
P53007	SLC25A1	0.4237108	0.4237108	2.4632E-07	-21.9529775
P53582	METAP1	0.4237108	0.4237108	1.712E-05	-15.8339475
P55039	DRG2	0.4237108	0.4237108	7.6094E-06	-17.0037902
P61201	COPS2	0.4237108	0.4237108	1.4859E-06	-19.3602487
P61962	DCAF7	0.17971249	0.17971249	2.0534E-06	-18.893564
P62861	FAU	0.17971249	0.17971249	7.1138E-06	-17.1009559
P63151;Q00005	PPP2R2A	0.4237108	0.4237108	1.815E-06	-19.0715902
P63173	RPL38	0.4237108	0.4237108	2.357E-07	-22.0165175
P80511	S100A12	0.17971249	0.17971249	3.4919E-07	-21.4494895
P84085	ARF5	0.4237108	0.4237108	5.8312E-06	-17.3877717
P98175	RBM10	0.17971249	0.17971249	2.145E-06	-18.8305913
Q00587	CDC42EP1	0.4237108	0.4237108	6.2732E-06	-17.2823717
Q01105;PODME0	SET	0.17971249	0.17971249	2.2523E-07	-22.08207
Q03001	DST	0.4237108	0.4237108	1.0179E-05	-16.5840641
Q03164	KMT2A	0.17971249	0.17971249	7.6217E-07	-20.3233809
Q04760	GLO1	0.4237108	0.4237108	8.5389E-06	-16.8375146
Q08170	SRSF4	0.4237108	0.4237108	8.1454E-06	-16.9055844
Q08379	GOLGA2	0.17971249	0.17971249	1.5649E-06	-19.2855029
Q10570	CPSF1	0.17971249	0.17971249	1.031E-06	-19.8874714
Q12849	GRSF1	0.17971249	0.17971249	6.1636E-07	-20.6297164
Q12933	TRAF2	0.4237108	0.4237108	8.1952E-07	-20.2187108
Q13084	MRPL28	0.17971249	0.17971249	1.3851E-06	-19.4615606
Q13472	TOP3A	0.17971249	0.17971249	5.9138E-06	-17.3674881
Q13601	KRR1	0.4237108	0.4237108	4.3929E-07	-21.1183232
Q13616	CUL1	0.07200566	0.07200566	8.2653E-07	-20.206433
Q13625	TP53BP2	0.4237108	0.4237108	4.7228E-06	-17.6919398
Q14011	CIRBP	0.4237108	0.4237108	4.6598E-06	-17.7112959
Q14139	UBE4A	0.4237108	0.4237108	1.3899E-05	-16.1346429
Q14195	DPYSL3	0.17971249	0.17971249	1.0204E-06	-19.9024525
Q14562	DHX8	0.07200566	0.07200566	1.2379E-06	-19.6236751
Q14966	ZNF638	0.4237108	0.4237108	5.0468E-06	-17.5961956
Q14C86	GAPVD1	0.4237108	0.4237108	4.4508E-07	-21.0994408

Appendix

Q15025	TNIP1	0.4237108	0.4237108	2.6565E-06	-18.5220635
Q15056	EIF4H	0.4237108	0.4237108	2.7582E-06	-18.4678634
Q15293	RCN1	0.4237108	0.4237108	2.8038E-06	-18.4441931
Q15370	TCEB2	0.4237108	0.4237108	1.9793E-06	-18.9466116
Q15428	SF3A2	0.17971249	0.17971249	3.9015E-06	-17.9675561
Q15637	SF1	0.17971249	0.17971249	6.8474E-07	-20.4779327
Q16352	INA	0.4237108	0.4237108	3.4268E-06	-18.1547232
Q16543	CDC37	0.4237108	0.4237108	8.857E-06	-16.7847473
Q16595	FXN	0.4237108	0.4237108	4.742E-06	-17.6860682
Q16637	SMN1	0.4237108	0.4237108	7.9332E-07	-20.2655885
Q16643	DBN1	0.07200566	0.07200566	7.9357E-07	-20.2651302
Q16740	CLPP	0.4237108	0.4237108	5.9044E-06	-17.3697745
Q2M2I8	AAK1	0.4237108	0.4237108	3.0996E-06	-18.2994799
Q3KQU3	MAP7D1	0.4237108	0.4237108	3.0364E-06	-18.3292217
Q3YEC7	RABL6	0.07200566	0.07200566	3.5664E-06	-18.0971083
Q3ZCQ8	TIMM50	0.4237108	0.4237108	9.0288E-07	-20.0789545
Q49A26	GLYR1	0.4237108	0.4237108	3.1311E-06	-18.2849181
Q4VCS5	AMOT	0.4237108	0.4237108	1.6688E-06	-19.1927282
Q5SW79;Q96L14	CEP170	0.4237108	0.4237108	3.8005E-06	-18.0053658
Q5T2T1	MPP7	0.4237108	0.4237108	2.1143E-06	-18.8513611
Q5T6F2	UBAP2	0.4237108	0.4237108	9.679E-06	-16.6567153
Q5T8D3;Q8NC06	ACBD5	0.4237108	0.4237108	6.1477E-06	-17.3115248
Q5TC82;Q9HBD1	RC3H1	0.4237108	0.4237108	7.5405E-06	-17.016904
Q5TCQ9	MAGI3	0.4237108	0.4237108	7.8922E-06	-16.9511344
Q5UIP0	RIF1	0.4237108	0.4237108	3.6849E-06	-18.0499591
Q5VT06	CEP350	0.07200566	0.07200566	1.1818E-06	-19.6905375
Q5VT52	RPRD2	0.4237108	0.4237108	6.4228E-06	-17.2483612
Q5VUA4	ZNF318	0.4237108	0.4237108	6.1607E-06	-17.3084706
Q66GS9	CEP135	0.4237108	0.4237108	2.2855E-06	-18.739058
Q69YQ0	SPECC1L	0.4237108	0.4237108	2.2663E-06	-18.7512067
Q6P2H3	CEP85	0.4237108	0.4237108	1.9632E-06	-18.9583284
Q6P4A7	SFXN4	0.4237108	0.4237108	6.8596E-06	-17.1534412
Q6P198	INO80C	0.4237108	0.4237108	4.2988E-06	-17.8276206
Q6R327	RICTOR	0.4237108	0.4237108	1.066E-07	-23.1612489
Q6UX04	CWC27	0.4237108	0.4237108	4.2571E-06	-17.8416921
Q6ZXV5	TMTC3	0.4237108	0.4237108	5.4392E-06	-17.4881759
Q76N32	CEP68	0.4237108	0.4237108	7.0778E-06	-17.1082672
Q7Z2E3	APTX	0.17971249	0.17971249	2.0492E-06	-18.8965234
Q7Z5L2	R3HCC1L	0.17971249	0.17971249	1.4419E-06	-19.4036208
Q7Z628	NET1	0.4237108	0.4237108	5.6856E-06	-17.4242549
Q7Z6E9	RBBP6	0.17971249	0.17971249	2.5264E-06	-18.5944653
Q86XZ4	SPATS2	0.4237108	0.4237108	5.1727E-06	-17.5606523
Q86Y07	VRK2	0.4237108	0.4237108	5.1515E-06	-17.5665655
Q86Y39	NDUFA11	0.17971249	0.17971249	1.4711E-06	-19.3747097
Q8IU60	DCP2	0.4237108	0.4237108	1.3518E-06	-19.4966603
Q8IWC1	MAP7D3	0.17971249	0.17971249	1.3779E-06	-19.4691342

Appendix

Q8IZD4	DCP1B	0.17971249	0.17971249	1.2075E-06	-19.6595162
Q8N122	RPTOR	0.4237108	0.4237108	5.1361E-06	-17.5708993
Q8N3U4;Q8WVM7	STAG2	0.4237108	0.4237108	1.165E-06	-19.7112583
Q8N9T8	KRI1	0.4237108	0.4237108	6.958E-06	-17.1328893
Q8NBS9	TXNDC5	0.4237108	0.4237108	1.0457E-06	-19.867105
Q8NBU5	ATAD1	0.17971249	0.17971249	5.6061E-07	-20.7665067
Q8NE86	MCU	0.17971249	0.17971249	7.1801E-07	-20.4094951
Q8NFH5	NUP35	0.17971249	0.17971249	1.6954E-06	-19.1699705
Q8NHH9	ATL2	0.4237108	0.4237108	2.0375E-07	-22.2267041
Q8TAQ2	SMARCC2	0.4237108	0.4237108	2.1097E-06	-18.85453
Q8TCG1	KIAA1524	0.4237108	0.4237108	7.0396E-06	-17.1160677
Q8TEW0	PAR3	0.17971249	0.17971249	2.429E-06	-18.651187
Q8WV22	NSMCE1	0.4237108	0.4237108	1.3433E-05	-16.1838835
Q92541	RTF1	0.4237108	0.4237108	5.5669E-06	-17.4547073
Q92615	LARP4B	0.4237108	0.4237108	2.6307E-06	-18.5360984
Q92759	GTF2H4	0.4237108	0.4237108	3.3647E-06	-18.1810785
Q92922	SMARCC1	0.4237108	0.4237108	4.9039E-06	-17.6376494
Q969Z0	TBRG4	0.4237108	0.4237108	6.5023E-06	-17.2306284
Q96CB9	NSUN4	0.4237108	0.4237108	4.3055E-06	-17.8253862
Q96EK5	KIAA1279	0.4237108	0.4237108	6.6891E-06	-17.1897551
Q96EL3	MRPL53	0.17971249	0.17971249	1.2712E-06	-19.5853818
Q96GC5	MRPL48	0.17971249	0.17971249	4.1844E-06	-17.8665581
Q96H55	MYO19	0.00749496	0.00749496	1.2589E-06	-19.5993899
Q96IZ0	PAWR	0.4237108	0.4237108	5.7036E-06	-17.419687
Q96KR1	ZFR	0.17971249	0.17971249	3.2882E-06	-18.214284
Q96R06	SPAG5	0.4237108	0.4237108	8.2257E-06	-16.8914372
Q96RP9	GFM1	0.17971249	0.17971249	1.2056E-06	-19.6617791
Q96RR1	PEO1	0.07200566	0.07200566	1.9061E-06	-19.0009254
Q96SN8	CDK5RAP2	0.17971249	0.17971249	1.4778E-06	-19.3681155
Q96ST3	SIN3A	0.4237108	0.4237108	1.0282E-05	-16.5695412
Q96T58	SPEN	0.17971249	0.17971249	4.5249E-06	-17.7536908
Q96T60	PNKP	0.17971249	0.17971249	1.6955E-06	-19.1698188
Q96TC7	RMDN3	0.07200566	0.07200566	1.1183E-06	-19.7702064
Q99550	MPHOSPH9	0.4237108	0.4237108	3.873E-06	-17.9781339
Q99598	TSNAX	0.17971249	0.17971249	2.5967E-06	-18.5549058
Q9BRR8	GPATCH1	0.4237108	0.4237108	1.5254E-05	-16.0004578
Q9BRS2	RIOK1	0.4237108	0.4237108	1.1677E-05	-16.3859433
Q9BTV4	TMEM43	0.4237108	0.4237108	2.7369E-06	-18.4790413
Q9BTX1	NDC1	0.17971249	0.17971249	1.7467E-06	-19.1269681
Q9BUK6	MSTO1	0.07200566	0.07200566	6.064E-07	-20.6532303
Q9BVI4	NOC4L	0.4237108	0.4237108	2.2356E-06	-18.7708858
Q9BWM7	SFXN3	0.4237108	0.4237108	3.4945E-06	-18.1264665
Q9BXS6	NUSAP1	0.17971249	0.17971249	8.296E-07	-20.2010813
Q9BYC9	MRPL20	0.4237108	0.4237108	2.0541E-06	-18.8930906
Q9BZE1	MRPL37	0.4237108	0.4237108	2.7456E-06	-18.4744538
Q9C0D9	EPT1	0.4237108	0.4237108	3.4487E-06	-18.1454983

Appendix

Q9GZL7	WDR12	0.4237108	0.4237108	1.7747E-06	-19.1040069
Q9GZS3	WDR61	0.07200566	0.07200566	5.2605E-07	-20.858297
Q9GZT8	NIF3L1	0.4237108	0.4237108	1.5754E-06	-19.2758081
Q9H078	CLPB	0.4237108	0.4237108	4.7304E-06	-17.6896213
Q9H2W6	MRPL46	0.02536986	0.02536986	7.6793E-07	-20.3125132
Q9H4A6	GOLPH3	0.07200566	0.07200566	2.2163E-06	-18.7833896
Q9H4L5	OSBPL3	0.4237108	0.4237108	9.5238E-07	-20.001959
Q9H6W3	NO66	0.4237108	0.4237108	9.2795E-06	-16.7175265
Q9H8V3	ECT2	0.4237108	0.4237108	4.5376E-06	-17.749639
Q9H9Y2	RPF1	0.4237108	0.4237108	2.6226E-06	-18.54057
Q9HAV7	GRPEL1	0.07200566	0.07200566	4.224E-07	-21.1748723
Q9NQ55	PPAN	0.4237108	0.4237108	4.1985E-06	-17.8616976
Q9NRA8	EIF4ENIF1	0.4237108	0.4237108	2.3356E-06	-18.7077932
Q9NRV9	HEBP1	0.4237108	0.4237108	2.3326E-06	-18.7096116
Q9NRW3	APOBEC3C	0.4237108	0.4237108	7.3145E-06	-17.0608099
Q9NRX1	PN01	0.4237108	0.4237108	2.3753E-06	-18.6834634
Q9NUQ3	TXLNG	0.4237108	0.4237108	1.2881E-05	-16.2443787
Q9NVI1	FANCI	0.4237108	0.4237108	4.2301E-06	-17.8508754
Q9NVT9	ARMC1	0.17971249	0.17971249	1.4613E-06	-19.3843129
Q9NYV4	CDK12	0.4237108	0.4237108	4.8449E-06	-17.655089
Q9NZJ4	SACS	0.4237108	0.4237108	4.1183E-06	-17.8895325
Q9P031	CCDC59	0.4237108	0.4237108	4.86E-06	-17.6506086
Q9P0U1	TOMM7	0.4237108	0.4237108	7.8317E-06	-16.9622499
Q9P1Y5	CAMSAP3	0.4237108	0.4237108	2.5645E-06	-18.5728956
Q9P253	VPS18	0.4237108	0.4237108	9.9812E-06	-16.6123617
Q9P2F8	SIPA1L2	0.4237108	0.4237108	5.0101E-06	-17.6067291
Q9P2I0	CPSF2	0.4237108	0.4237108	9.5993E-06	-16.6686468
Q9UBD5	ORC3	0.4237108	0.4237108	2.5897E-06	-18.5587675
Q9UBP6	METTL1	0.17971249	0.17971249	1.9445E-06	-18.9721962
Q9UDY2	TJP2	0.17971249	0.17971249	2.5728E-07	-21.8901665
Q9UI10	EIF2B4	0.17971249	0.17971249	1.5269E-06	-19.3209164
Q9UKX7	NUP50	0.17971249	0.17971249	1.3574E-06	-19.4906797
Q9UL40	ZNF346	0.4237108	0.4237108	3.8956E-06	-17.9697283
Q9ULW0	TPX2	0.17971249	0.17971249	1.8196E-06	-19.0679296
Q9UN86	G3BP2	0.4237108	0.4237108	4.123E-06	-17.8878679
Q9UQR1	ZNF148	0.17971249	0.17971249	2.1834E-06	-18.8050089
Q9Y2T2	AP3M1	0.4237108	0.4237108	1.3494E-06	-19.4992324
Q9Y324	FCF1	0.4237108	0.4237108	1.8837E-06	-19.0180284
Q9Y3Z3	SAMHD1	0.4237108	0.4237108	1.027E-05	-16.5711423
Q9Y467	SALL2	0.4237108	0.4237108	2.9652E-06	-18.3634196
Q9Y4A5	TRRAP	0.4237108	0.4237108	1.1033E-05	-16.4677775
Q9Y4C8	RBM19	0.4237108	0.4237108	1.3481E-06	-19.5006723
Q9Y4P1	ATG4B	0.17971249	0.17971249	1.9011E-06	-19.0047104
Q9Y4R8	TELO2	0.4237108	0.4237108	7.1477E-07	-20.4160272
Q9Y4Z0	LSM4	0.4237108	0.4237108	3.4965E-06	-18.1256597
Q9Y580	RBM7	0.4237108	0.4237108	2.3333E-06	-18.7092077

Q9Y5J1	UTP18	0.4237108	0.4237108	7.2654E-07	-20.3924482
Q9Y5L0	TNPO3	0.4237108	0.4237108	2.5612E-06	-18.5747443
Q9Y5S9	RBM8A	0.4237108	0.4237108	3.3086E-06	-18.2053389
Q9Y673	ALG5	0.4237108	0.4237108	4.7701E-06	-17.67756
Q9Y6G9	DYNC1LI1	0.4237108	0.4237108	3.6985E-06	-18.0446332
Q9Y6Y8	SEC23IP	0.17971249	0.17971249	5.2879E-07	-20.8508099

Appendix 4. List of proteins significantly overrepresented in control sEVs when compared to HD sEVs. This table presents proteins significantly overrepresented in control sEVs when compared to HD sEVs, detailing several key metrics.

Protein.IDs	gene	p.value	adj_pvalue	fc	logfc
O60841	EIF5B	0.007936508	0.007936508	0.257948969	-1.954842416
P07339	CTSD	0.04490859	0.04490859	0.088152535	-3.503854129
P12270	TPR	0.034453637	0.034453637	0.240809244	-2.054037318
P19367;Q2TB90	HK1	0.031746032	0.031746032	0.279081598	-1.841241095
P19784	CSNK2A2	0.007936508	0.007936508	0.381013999	-1.392084089
P34897	SHMT2	0.007936508	0.007936508	0.455428025	-1.134705023
P49006	MARCKSL1	0.031746032	0.031746032	0.419349494	-1.253774981
P61163	ACTR1A	0.04490859	0.04490859	0.089325489	-3.484784285
P82650	MRPS22	0.031141211	0.031141211	0.147825666	-2.75803132
Q8NI36	WDR36	0.031746032	0.031746032	0.362378666	-1.46443007
Q96TA2	YME1L1	0.007936508	0.007936508	0.220144865	-2.183474899
Q9NSD9	FARSB	0.034453637	0.034453637	0.165577246	-2.594423668
Q9UHI8	ADAMTS1	0.007936508	0.007936508	0.444313965	-1.170348608

Appendix 5. List of proteins exclusively present in HD sEVs. This table presents proteins uniquely identified in HD sEVs, detailing several key metrics.

Protein.IDs	gene	p.value	adj_pvalue	fc	logfc
A0FGR8	ESYT2	0.17971249	0.17971249	2920000.6	21.4775372
A6NKT7	RGPD3	0.4237108	0.4237108	150486.8	17.1992774
A8MVW0	FAM171A2	0.17971249	0.17971249	1228160.6	20.2280678
O00154	ACOT7	0.4237108	0.4237108	494900.8	18.9167798
O00161	SNAP23	0.07200566	0.07200566	2389240.4	21.1881206
O00165	HAX1	0.17971249	0.17971249	719620.6	19.456877
O00178	GTPBP1	0.4237108	0.4237108	119654.8	16.8685187
O00192	ARVCF	0.17971249	0.17971249	750840.6	19.5181471
O00217	NDUFS8	0.00749496	0.00749496	1457682	20.4752446
O00487	PSMD14	0.4237108	0.4237108	251580.8	17.9406623
O14497	ARID1A	0.4237108	0.4237108	492060.8	18.9084771
O14653	GOSR2	0.4237108	0.4237108	102318.8	16.6427117
O14737	PDCD5	0.4237108	0.4237108	588620.8	19.166979
O14744	PRMT5	0.4237108	0.4237108	607920.8	19.2135239
O14929	HAT1	0.4237108	0.4237108	383360.8	18.5483433
O15091	KIAA0391	0.17971249	0.17971249	661612.6	19.3356272

Appendix

O15116	LSM1	0.4237108	0.4237108	73324.8	16.1620136
O15258	RER1	0.4237108	0.4237108	474960.8	18.8574489
O15294	OGT	0.07200566	0.07200566	340794.4	18.3785421
O15397	IPO8	0.4237108	0.4237108	307420.8	18.2298553
O15400	STX7	0.17971249	0.17971249	2290140.6	21.1270047
O15484	CAPN5	0.17971249	0.17971249	4219060.6	22.0084904
O43181	NDUFS4	0.4237108	0.4237108	125142.8	16.9332158
O43598	DNPH1	0.4237108	0.4237108	164720.8	17.3296632
O43615	TIMM44	0.17971249	0.17971249	434654.6	18.7295099
O43633	CHMP2A	0.4237108	0.4237108	528760.8	19.0122557
O43684	BUB3	0.17971249	0.17971249	819920.6	19.6451247
O43815	STRN	0.4237108	0.4237108	202100.8	17.6247155
O60231	DHX16	0.4237108	0.4237108	127214.8	16.956907
O60244	MED14	0.4237108	0.4237108	1910680.8	20.8656553
O60256	PRPSAP2	0.4237108	0.4237108	655720.8	19.3227221
O60271;Q9UPT6	SPAG9	0.4237108	0.4237108	270600.8	18.0458066
O60287	URB1	0.4237108	0.4237108	73378.8	16.1630757
O60518	RANBP6	0.17971249	0.17971249	388176.6	18.5663536
O60684;O15131	KPNA6	0.4237108	0.4237108	245380.8	17.9046628
O60884	DNAJA2	0.02536986	0.02536986	2094260.2	20.9980093
O75083	WDR1	0.4237108	0.4237108	1943240.8	20.8900333
O75494	SRSF10	0.17971249	0.17971249	1514020.6	20.5299534
O75534	CSDE1	0.4237108	0.4237108	147750.8	17.1728064
O75683	SURF6	0.4237108	0.4237108	168816.8	17.365099
O75746	SLC25A12	0.4237108	0.4237108	116824.8	16.833987
O75822	EIF3J	0.4237108	0.4237108	2066400.8	20.9786887
O75934	BCAS2	0.17971249	0.17971249	114952.6	16.8106796
O75964	ATP5L	0.07200566	0.07200566	905880.4	19.7889611
O75970	MPDZ	0.4237108	0.4237108	143520.8	17.1309003
O94822	LTN1	0.4237108	0.4237108	239400.8	17.8690684
O94888	UBXN7	0.4237108	0.4237108	398440.8	18.6040059
O94973;O95782	AP2A2	0.4237108	0.4237108	502860.8	18.9397996
O95084	PRSS23	0.17971249	0.17971249	2178460.6	21.0548776
O95169	NDUFB8	0.4237108	0.4237108	169472.8	17.3706942
O95251	KAT7	0.4237108	0.4237108	265780.8	18.0198774
O95630	STAMPB	0.07200566	0.07200566	3042760.4	21.5369493
O95757	HSPA4L	0.17971249	0.17971249	575034.6	19.1332892
O95983	MBD3	0.4237108	0.4237108	451660.8	18.7848802
O95985	TOP3B	0.4237108	0.4237108	306000.8	18.2231759
P00387	CYB5R3	0.4237108	0.4237108	111970.8	16.772763
P00390	GSR	0.17971249	0.17971249	601880.6	19.1991178
P00533	EGFR	0.07200566	0.07200566	1167746.4	20.1552956
P02458	COL2A1	0.02536986	0.02536986	3469620.2	21.7263463
P02792	FTL	0.17971249	0.17971249	380480.6	18.5374634
P03246;P03247	E1B	0.17971249	0.17971249	309710.6	18.2405612
P04083	ANXA1	0.02536986	0.02536986	6750700.2	22.6866057

Appendix

P04181	OAT	0.4237108	0.4237108	749060.8	19.5147233
P04279	SEMG1	0.4237108	0.4237108	1324020.8	20.3364944
P05387	RPLP2	0.07200566	0.07200566	1033060.4	19.9784932
P06493	CDK1	0.17971249	0.17971249	1433500.6	20.4511111
P06756	ITGAV	0.07200566	0.07200566	5900940.4	22.4925135
P07108	DBI	0.17971249	0.17971249	6939460.6	22.7263921
P07942	LAMB1	0.17971249	0.17971249	2576300.6	21.2968695
P08574	CYC1	0.07200566	0.07200566	9365820.4	23.1589739
P08708	RPS17	0.4237108	0.4237108	367260.8	18.4864454
P09234	SNRPC	0.4237108	0.4237108	125006.8	16.931647
P09543	CNP	0.17971249	0.17971249	1046200.6	19.9967281
P12235	SLC25A4	0.4237108	0.4237108	92304.8	16.4941181
P13671	C6	0.17971249	0.17971249	1772900.6	20.7576802
P13693;Q9HAU6	TPT1	0.17971249	0.17971249	2093260.6	20.9973205
P13798	APEH	0.17971249	0.17971249	498220.6	18.9264251
P13984	GTF2F2	0.4237108	0.4237108	195492.8	17.5767559
P14635	CCNB1	0.4237108	0.4237108	800560.8	19.6106514
P63162;P14678	SNRPN	0.4237108	0.4237108	253820.8	17.9534508
P15121	AKR1B1	0.4237108	0.4237108	863920.8	19.7205395
P16152;O75828	CBR1	0.17971249	0.17971249	616480.6	19.233696
P16157	ANK1	0.17971249	0.17971249	1811280.6	20.7885786
P18085	ARF4	0.4237108	0.4237108	347640.8	18.4072379
P18615	NELFE	0.4237108	0.4237108	102528.8	16.6456697
P18887	XRCC1	0.07200566	0.07200566	2238774.4	21.0942777
P19404	NDUFV2	0.4237108	0.4237108	1017480.8	19.9565701
P20962	PTMS	0.17971249	0.17971249	250184.6	17.9326335
P21964	COMT	0.07200566	0.07200566	1081740.4	20.0449229
P22694	PRKACB	0.17971249	0.17971249	407960.6	18.6380703
P23229	ITGA6	0.02536986	0.02536986	24762180.2	24.561635
P24941;Q00526	CDK2	0.07200566	0.07200566	1415880.4	20.433268
P27449	ATP6V0C	0.07200566	0.07200566	1183620.4	20.174775
P27816	MAP4	0.4237108	0.4237108	76568.8	16.224469
P28072	PSMB6	0.4237108	0.4237108	201680.8	17.6217142
P30044	PRDX5	0.4237108	0.4237108	484180.8	18.8851863
P30520	ADSS	0.4237108	0.4237108	249900.8	17.930996
P30533	LRPAP1	0.17971249	0.17971249	758228.6	19.5322733
P30626	SRI	0.07200566	0.07200566	808880.4	19.6255669
P31153;Q00266	MAT2A	0.4237108	0.4237108	128042.8	16.9662666
P31937	HIBADH	0.4237108	0.4237108	547660.8	19.0629231
P32780	GTF2H1	0.17971249	0.17971249	491324.6	18.9063169
P33316	DUT	0.17971249	0.17971249	734860.6	19.4871111
P33908	MAN1A1	0.17971249	0.17971249	963860.6	19.878465
P35240	NF2	0.4237108	0.4237108	206560.8	17.656207
P35270	SPR	0.4237108	0.4237108	335280.8	18.3550103
P35998	PSMC2	0.4237108	0.4237108	308520.8	18.2350082
P36542	ATP5C1	0.07200566	0.07200566	707556.4	19.4324856

Appendix

P40763	STAT3	0.17971249	0.17971249	1124060.6	20.1002884
P41227;Q9BSU3	NAA10	0.4237108	0.4237108	576520.8	19.1370131
P41250	GARS	0.02536986	0.02536986	2624120.2	21.3234024
P42694	HELZ	0.4237108	0.4237108	75424.8	16.2027513
P43250	GRK6	0.4237108	0.4237108	341880.8	18.3831339
P43490	NAMPT	0.4237108	0.4237108	469700.8	18.8413825
P46108	CRK	0.4237108	0.4237108	168338.8	17.3610082
P46109	CRKL	0.07200566	0.07200566	3057460.4	21.5439024
P47755	CAPZA2	0.4237108	0.4237108	171260.8	17.3858354
P48556	PSMD8	0.4237108	0.4237108	289500.8	18.1432078
P49585;Q9Y5K3	PCYT1A	0.4237108	0.4237108	110060.8	16.7479412
P50336	PPOX	0.4237108	0.4237108	320120.8	18.2882569
P51532	SMARCA4	0.4237108	0.4237108	368800.8	18.4924823
P51617	IRAK1	0.4237108	0.4237108	156038.8	17.2515453
P54646	PRKAA2	0.17971249	0.17971249	436470.6	18.735525
P55010	EIF5	0.17971249	0.17971249	1167340.6	20.1547941
P55263	ADK	0.07200566	0.07200566	1930120.4	20.8802594
P55735	SEC13	0.17971249	0.17971249	2211380.6	21.0765159
P56556	NDUFA6	0.4237108	0.4237108	116652.8	16.8318614
P58546	MTPN	0.17971249	0.17971249	411708.6	18.6512641
P60900	PSMA6	0.4237108	0.4237108	5220000.8	22.3156186
P61970	NUTF2	0.4237108	0.4237108	848480.8	19.6945225
P62191	PSMC1	0.4237108	0.4237108	407680.8	18.6370805
P62263	RPS14	0.4237108	0.4237108	288100.8	18.1362141
P62304	SNRPE	0.07200566	0.07200566	2833882.4	21.4343485
P62314	SNRPD1	0.07200566	0.07200566	2641140.4	21.3327296
P67775;P62714	PPP2CA	0.17971249	0.17971249	671380.6	19.3567713
P62910	RPL32	0.17971249	0.17971249	821940.6	19.6486746
P63096	GNAI1	0.4237108	0.4237108	234720.8	17.8405862
P63244	GNB2L1	0.07200566	0.07200566	2619760.4	21.3210034
P68402	PAFAH1B2	0.4237108	0.4237108	340900.8	18.3789925
P78316	NOP14	0.17971249	0.17971249	992340.6	19.9204759
P78406	RAE1	0.4237108	0.4237108	454660.8	18.7944311
P78417	GSTO1	0.17971249	0.17971249	3288200.6	21.6488669
P82933	MRPS9	0.07200566	0.07200566	366450.4	18.4832584
P83881	RPL36A	0.4237108	0.4237108	144656.8	17.1422746
P85037	FOXK1	0.4237108	0.4237108	127308.8	16.9579726
Q00535	CDK5	0.4237108	0.4237108	378660.8	18.5305466
Q00577	PURA	0.17971249	0.17971249	475860.6	18.8601795
Q00796	SORD	0.4237108	0.4237108	760320.8	19.5362487
Q05639	EEF1A2	0.4237108	0.4237108	70718.8	16.1098062
Q06587;Q99496	RING1	0.4237108	0.4237108	524320.8	19.0000903
Q07866	KLC1	0.17971249	0.17971249	731194.6	19.4798959
Q09028	RBBP4	0.17971249	0.17971249	796260.6	19.6028811
Q0ZGT2	NEXN	0.4237108	0.4237108	270380.8	18.0446332
Q12792	TWF1	0.17971249	0.17971249	364086.6	18.4739221

Appendix

Q12872	SFSWAP	0.4237108	0.4237108	879560.8	19.7464238
Q12904	AIMP1	0.17971249	0.17971249	1412180.6	20.4294932
Q12959	DLG1	0.07200566	0.07200566	1268260.4	20.2744196
Q13045	FLII	0.17971249	0.17971249	532880.6	19.0234528
Q13085	ACACA	0.00749496	0.00749496	1938000	20.8861371
Q13188	STK3	0.02536986	0.02536986	2602288.2	21.3113493
Q13405	MRPL49	0.07200566	0.07200566	2176340.4	21.0534728
Q13423	NNT	0.4237108	0.4237108	398780.8	18.6052364
Q13501	SQSTM1	0.07200566	0.07200566	601052.4	19.1971312
Q13555;Q13554;Q9UQM7	CAMK2G	0.4237108	0.4237108	682640.8	19.3807671
Q13561	DCTN2	0.07200566	0.07200566	818622.4	19.6428386
Q13595	TRA2A	0.4237108	0.4237108	222860.8	17.7657834
Q13610	PWP1	0.4237108	0.4237108	732400.8	19.4822738
Q13641	TPBG	0.07200566	0.07200566	1797780.4	20.7777854
Q13895	BYSL	0.02536986	0.02536986	7707360.2	22.8778054
Q14156	EFR3A	0.17971249	0.17971249	1623720.6	20.630872
Q14257	RCN2	0.4237108	0.4237108	81286.8	16.3107335
Q14558	PRPSAP1	0.4237108	0.4237108	147538.8	17.1707349
Q14573	ITPR3	0.4237108	0.4237108	80480.8	16.296357
Q14643	ITPR1	0.4237108	0.4237108	359960.8	18.4574803
Q14671	PUM1	0.17971249	0.17971249	574012.6	19.1307229
Q15059	BRD3	0.4237108	0.4237108	150542.8	17.1998142
Q15125	EBP	0.4237108	0.4237108	1662680.8	20.6650798
Q15437	SEC23B	0.4237108	0.4237108	178618.8	17.4465244
Q15631	TSN	0.17971249	0.17971249	715160.6	19.4479077
Q15645	TRIP13	0.17971249	0.17971249	300558.6	18.1972868
Q15654	TRIP6	0.4237108	0.4237108	327240.8	18.3199931
Q15738	NSDHL	0.17971249	0.17971249	1136600.6	20.116294
Q15836	VAMP3	0.02536986	0.02536986	6179280.2	22.5590074
Q16222	UAP1	0.07200566	0.07200566	1200600.4	20.1953246
Q16576	RBBP7	0.17971249	0.17971249	856212.6	19.7076095
Q4G148	GXYLT1	0.4237108	0.4237108	208740.8	17.6713531
Q4V328	GRIPAP1	0.4237108	0.4237108	221860.8	17.7592953
Q562R1	ACTBL2	0.17971249	0.17971249	1498600.6	20.5151845
Q5BKZ1	ZNF326	0.4237108	0.4237108	707180.8	19.4317196
Q5JRX3	PITRM1	0.4237108	0.4237108	417180.8	18.6703132
Q5JSZ5	PRRC2B	0.07200566	0.07200566	1042180.4	19.9911736
Q93079;Q5QNW6	HIST1H2BH	0.17971249	0.17971249	1285520.6	20.2939213
Q5TON5	FNBP1L	0.4237108	0.4237108	543740.8	19.0525596
Q5T3I0	GPATCH4	0.17971249	0.17971249	606540.6	19.2102447
Q5U7I5	Transthyretin	0.07200566	0.07200566	4924420.4	22.2315225
Q5VUB5	FAM171A1	0.07200566	0.07200566	3568540.4	21.7669027
Q5VW36	FOCAD	0.4237108	0.4237108	236320.8	17.8503871
Q68CZ6	HAUS3	0.4237108	0.4237108	280600.8	18.0981596
Q68E01	INTS3	0.4237108	0.4237108	152002.8	17.2137384
Q6IAN0	DHRS7B	0.17971249	0.17971249	215816.6	17.7194463

Appendix

Q6PD62	CTR9	0.17971249	0.17971249	628420.6	19.2613709
Q6PHR2	ULK3	0.4237108	0.4237108	717860.8	19.4533446
Q6PI48	DARS2	0.07200566	0.07200566	1730360.4	20.7226411
Q6UWE0	LRSAM1	0.4237108	0.4237108	2558400.8	21.2868109
Q6VY07	PACS1	0.17971249	0.17971249	2007700.6	20.9371127
Q6WKZ4	RAB11FIP1	0.07200566	0.07200566	1594158.4	20.6043636
Q7Z406	MYH14	0.4237108	0.4237108	1363580.8	20.3789688
Q7Z4Q2	HEATR3	0.4237108	0.4237108	285560.8	18.1234384
Q7Z4V5;Q9Y3E1	HDGFRP2	0.07200566	0.07200566	2916820.4	21.4759651
Q86V81	ALYREF	0.17971249	0.17971249	679180.6	19.3734357
Q86XP3	DDX42	0.4237108	0.4237108	165868.8	17.339683
Q8IWZ3	ANKHD1	0.4237108	0.4237108	224860.8	17.7786727
Q8IX12	CCAR1	0.17971249	0.17971249	1029120.6	19.9729806
Q8IXB1	DNAJC10	0.17971249	0.17971249	351440.6	18.4229213
Q8IYD1	GSPT2	0.4237108	0.4237108	1327020.8	20.3397596
Q8IZL8	PELP1	0.4237108	0.4237108	403600.8	18.6225695
Q8N0X7	SPG20	0.17971249	0.17971249	1229880.6	20.2300868
Q8N3R9	MPP5	0.4237108	0.4237108	202520.8	17.6277106
Q8N8S7	ENAH	0.4237108	0.4237108	276880.8	18.0789055
Q8NB90	SPATA5	0.4237108	0.4237108	289080.8	18.1411133
Q8NC60	NOA1	0.17971249	0.17971249	215000.6	17.7139812
Q8NDF8	PAPD5	0.4237108	0.4237108	84968.8	16.3746456
Q8NEW0	SLC30A7	0.4237108	0.4237108	529180.8	19.0134012
Q8NFF5	FLAD1	0.4237108	0.4237108	423800.8	18.6930268
Q8NFH3	NUP43	0.4237108	0.4237108	567460.8	19.1141612
Q8NI27	THOC2	0.17971249	0.17971249	473380.6	18.8526411
Q8TCJ2	STT3B	0.4237108	0.4237108	125894.8	16.9418592
Q8TED0	UTP15	0.07200566	0.07200566	1062346.4	20.0188228
Q8WUA2	PPIL4	0.4237108	0.4237108	369960.8	18.4970129
Q8WVM0	TFB1M	0.4237108	0.4237108	235640.8	17.8462298
Q8WVV9	HNRNPLL	0.4237108	0.4237108	196250.8	17.582339
Q8WWY3	PRPF31	0.4237108	0.4237108	309380.8	18.2390241
Q92538	GBF1	0.17971249	0.17971249	402308.6	18.6179431
Q92614	MYO18A	0.4237108	0.4237108	1690460.8	20.6889851
Q92620	DHX38	0.02536986	0.02536986	2129400.2	21.0220157
Q92667	AKAP1	0.4237108	0.4237108	87908.8	16.42372
Q92688	ANP32B	0.4237108	0.4237108	385140.8	18.5550264
Q92890	UFD1L	0.17971249	0.17971249	601340.6	19.1978228
Q93050	ATP6V0A1	0.4237108	0.4237108	752140.8	19.5206432
Q93096;Q12974	PTP4A1	0.4237108	0.4237108	52730.8	15.6863583
Q969V3	NCLN	0.17971249	0.17971249	473520.6	18.8530677
Q96A26	FAM162A	0.4237108	0.4237108	85522.8	16.3840215
Q96A65	EXOC4	0.00749496	0.00749496	3230060	21.6231295
Q96AX1	VPS33A	0.4237108	0.4237108	138982.8	17.0845468
Q96CN7	ISOC1	0.07200566	0.07200566	1085260.4	20.0496098
Q96G23	CERS2	0.4237108	0.4237108	664020.8	19.3408689

Appendix

Q96I25	RBM17	0.4237108	0.4237108	79476.8	16.2782462
Q96IX5	USMG5	0.4237108	0.4237108	814880.8	19.6362295
Q96K17	BTF3L4	0.02536986	0.02536986	950616.2	19.8585035
Q96KP4	CNDP2	0.4237108	0.4237108	119776.8	16.869989
Q96NB2	SFXN2	0.17971249	0.17971249	3508340.6	21.7423574
Q96QC0	PPP1R10	0.4237108	0.4237108	268100.8	18.032416
Q99567	NUP88	0.4237108	0.4237108	367700.8	18.4881728
Q99569;Q9UQB3	PKP4	0.4237108	0.4237108	135526.8	17.0482186
Q99584	S100A13	0.4237108	0.4237108	366140.8	18.482039
Q99733	NAP1L4	0.02536986	0.02536986	3883380.2	21.8888815
Q99798	ACO2	0.4237108	0.4237108	661720.8	19.3358631
Q99873	PRMT1	0.4237108	0.4237108	95142.8	16.5378069
Q9BRT6	LLPH	0.17971249	0.17971249	484540.6	18.886258
Q9BT78	COPS4	0.17971249	0.17971249	747780.6	19.5122555
Q9BUJ2	HNRNPUL1	0.07200566	0.07200566	496254.4	18.9207204
Q9BUL8	PDCD10	0.4237108	0.4237108	666700.8	19.3466799
Q9BV86	NTMT1	0.4237108	0.4237108	103590.8	16.6605364
Q9BW71	HIRIP3	0.4237108	0.4237108	237340.8	17.8566006
Q9BWH6	RPAP1	0.4237108	0.4237108	315980.8	18.2694774
Q9BX55	AP1M1	0.07200566	0.07200566	1359240.4	20.3743692
Q9BXW7	CECR5	0.4237108	0.4237108	574200.8	19.1311958
Q9BY43	CHMP4A	0.17971249	0.17971249	1699866.6	20.6969901
Q9BYD1	MRPL13	0.4237108	0.4237108	42946000.8	25.3560205
Q9BYD6	MRPL1	0.4237108	0.4237108	469820.8	18.8417511
Q9C0C9	UBE2O	0.17971249	0.17971249	849860.6	19.6968667
Q9GZZ1	NAA50	0.4237108	0.4237108	209740.8	17.678248
Q9H074	PAIP1	0.4237108	0.4237108	162714.8	17.311986
Q9H0E2	TOLLIP	0.17971249	0.17971249	3507860.6	21.74216
Q9H0S4	DDX47	0.4237108	0.4237108	523960.8	18.9990994
Q9H299	SH3BGRL3	0.17971249	0.17971249	173398.6	17.4037327
Q9H2U1	DHX36	0.4237108	0.4237108	116570.8	16.8308469
Q9H444	CHMP4B	0.17971249	0.17971249	492424.6	18.9095433
Q9H7P6	MVB12B	0.07200566	0.07200566	2910900.4	21.473034
Q9H7Z3	NRDE2	0.4237108	0.4237108	63676.8	15.9584802
Q9H8Y8	GORASP2	0.4237108	0.4237108	151018.8	17.2043686
Q9H9A6	LRRC40	0.4237108	0.4237108	348480.8	18.4107196
Q9H9E3	COG4	0.4237108	0.4237108	190322.8	17.5380889
Q9HAS0	C17orf75	0.4237108	0.4237108	164396.8	17.3268227
Q9HB07	C12orf10	0.02536986	0.02536986	1365982.2	20.3815073
Q9NP81	SARS2	0.4237108	0.4237108	101726.8	16.6343403
Q9NPA0	EMC7	0.4237108	0.4237108	189502.8	17.5318596
Q9NPJ6	MED4	0.4237108	0.4237108	464260.8	18.8245759
Q9NPL8	TIMMDC1	0.4237108	0.4237108	790900.8	19.5931372
Q9NQW7	XPNPEP1	0.4237108	0.4237108	671460.8	19.3569437
Q9NQX7	ITM2C	0.4237108	0.4237108	379260.8	18.5328307
Q9NR45	NANS	0.07200566	0.07200566	2888360.4	21.4618193

Appendix

Q9NRX4	PHPT1	0.4237108	0.4237108	66086.8	16.0120745
Q9NRZ9	HELLS	0.4237108	0.4237108	80178.8	16.2909332
Q9NS69	TOMM22	0.02536986	0.02536986	1752520.2	20.7409996
Q9NUQ9;Q9H0Q0	FAM49B	0.17971249	0.17971249	474686.6	18.8566158
Q9NV70	EXOC1	0.07200566	0.07200566	1427782.4	20.4453447
Q9NVJ2;Q96BM9	ARL8B	0.02536986	0.02536986	1740384.2	20.7309744
Q9NVV4	MTPAP	0.4237108	0.4237108	230640.8	17.8152882
Q9NWW4	C1orf123	0.4237108	0.4237108	295400.8	18.1723142
Q9NWW4;A8MVJ9	C4orf27	0.4237108	0.4237108	1444760.8	20.4623992
Q9NXR7	BRE	0.4237108	0.4237108	1000380.8	19.9321178
Q9NYB0	TERF2IP	0.4237108	0.4237108	121166.8	16.8866349
Q9NYK5	MRPL39	0.4237108	0.4237108	337660.8	18.3652152
Q9NYU2	UGGT1	0.17971249	0.17971249	945540.6	19.8507799
Q9P003	CNIH4	0.4237108	0.4237108	290860.8	18.1499693
Q9P1F3	ABRACL	0.17971249	0.17971249	2208580.6	21.0746881
Q9P209	CEP72	0.17971249	0.17971249	252686.6	17.9469896
Q9P266	KIAA1462	0.4237108	0.4237108	332920.8	18.3448195
Q9P275	USP36	0.4237108	0.4237108	57252.8	15.8050586
Q9P289	STK26	0.4237108	0.4237108	446600.8	18.7686263
Q9P2W9	STX18	0.17971249	0.17971249	288822.6	18.1398241
Q9UBI6	GNG12	0.17971249	0.17971249	1907820.6	20.8634941
Q9UBP0	SPAST	0.4237108	0.4237108	962220.8	19.8760085
Q9UHB9	SRP68	0.17971249	0.17971249	322486.6	18.2988797
Q9UHD1	CHORDC1	0.02536986	0.02536986	1640560.2	20.6457571
Q9UHD9	UBQLN2	0.17971249	0.17971249	255120.6	17.9608199
Q9UHY1	NRBP1	0.4237108	0.4237108	845340.8	19.6891736
Q9UI26	IPO11	0.4237108	0.4237108	255160.8	17.9610472
Q9UIF9	BAZ2A	0.4237108	0.4237108	66758.8	16.0266704
Q9UJX5	ANAPC4	0.4237108	0.4237108	238300.8	17.8624243
Q9UKD2	MRTO4	0.07200566	0.07200566	1482708.4	20.4998035
Q9ULC4	MCTS1	0.17971249	0.17971249	524878.6	19.0016243
Q9ULH0	KIDINS220	0.17971249	0.17971249	426562.6	18.702398
Q9UNI6	DUSP12	0.4237108	0.4237108	102260.8	16.6418937
Q9UNN8	PROCR	0.07200566	0.07200566	3961220.4	21.9175135
Q9UNX4	WDR3	0.17971249	0.17971249	254452.6	17.9570374
Q9UNY4	TTF2	0.07200566	0.07200566	570200.4	19.1211095
Q9Y281	CFL2	0.4237108	0.4237108	186074.8	17.5055232
Q9Y2B0	CNPY2	0.4237108	0.4237108	195870.8	17.5795428
Q9Y2P8	RCL1	0.17971249	0.17971249	287630.6	18.1338576
Q9Y2V2	CARHSP1	0.4237108	0.4237108	243700.8	17.8947515
Q9Y2W2	WBP11	0.07200566	0.07200566	942130.4	19.8455672
Q9Y371	SH3GLB1	0.4237108	0.4237108	66112.8	16.012642
Q9Y375	NDUFAF1	0.4237108	0.4237108	92536.8	16.4977396
Q9Y3A5	SBDS	0.4237108	0.4237108	324980.8	18.309995
Q9Y3B7	MRPL11	0.4237108	0.4237108	392440.8	18.5821155
Q9Y4E8	USP15	0.4237108	0.4237108	346420.8	18.402166

Q9Y4F3	KIAA0430	0.4237108	0.4237108	609840.8	19.2180731
Q9Y5A9	YTHDF2	0.02536986	0.02536986	1282400.2	20.2904151
Q9Y5K6	CD2AP	0.07200566	0.07200566	2937900.4	21.4863541
Q9Y672	ALG6	0.4237108	0.4237108	199700.8	17.6074806
Q9Y678;Q9UBF2	COPG1	0.02536986	0.02536986	1824860.2	20.7993545
Q9Y679	AUP1	0.4237108	0.4237108	158882.8	17.2776034
Q9Y6E0	STK24	0.17971249	0.17971249	1337240.6	20.3508276
Q9Y6M9	NDUFB9	0.17971249	0.17971249	1264400.6	20.2700222

Appendix 6. List of proteins significantly overrepresented in HD sEVs when compared to control sEVs. This table presents proteins significantly overrepresented in HD sEVs when compared to control sEVs , detailing several key metrics.

Protein.IDs	Gene	p-value	Adj p-value	fc	logfc
O15230	LAMA5	0.021177	0.021177	5.201019	2.378794
O43795;Q9UBC5	MYO1B	0.015873	0.015873	3.05052	1.609055
O60506	SYNCRIP	0.011159	0.011159	23.49965	4.554567
O60763	USO1	0.044909	0.044909	8.025324	3.00456
O75131	CPNE3	0.015873	0.015873	5.390257	2.430354
O75533	SF3B1	0.007937	0.007937	2.313142	1.209854
P00491	PNP	0.01775	0.01775	10.99692	3.459027
P04259	KRT6B	0.034454	0.034454	12.54342	3.648859
P07910;O60812;B2RXH8;PODMR1	HNRNPC	0.031746	0.031746	2.909278	1.540661
P08243	ASNS	0.009701	0.009701	14.35797	3.84378
P08514	ITGA2B	0.036145	0.036145	2.806814	1.488933
PODP25;PODP24;PODP23	CALM3	0.007937	0.007937	2.92754	1.549689
P11047	LAMC1	0.007937	0.007937	4.956764	2.309398
P11171;Q9H4G0	EPB41	0.036145	0.036145	5.005134	2.323409
P11388	TOP2A	0.015873	0.015873	2.519008	1.332856
P11413	G6PD	0.044909	0.044909	19.68141	4.298762
P12109	COL6A1	0.01775	0.01775	22.57485	4.496645
P13010	XRCC5	0.007937	0.007937	3.493158	1.804532
P18124	RPL7	0.031746	0.031746	3.849661	1.944731
P19634	SLC9A1	0.009701	0.009701	16.90061	4.079004
P23528	CFL1	0.031746	0.031746	2.242083	1.16484
P26641	EEF1G	0.007937	0.007937	3.009936	1.589733
P27105	STOM	0.007937	0.007937	2.236372	1.16116
P27708	CAD	0.031746	0.031746	2.818662	1.495011
P28340	POLD1	0.036145	0.036145	3.923112	1.971999

Appendix

P30419;O60551	NMT1	0.034454	0.034454	4.949506	2.307285
P40937	RFC5	0.01775	0.01775	9.350197	3.224997
P41252	IARS	0.031746	0.031746	2.050851	1.036223
P42345	MTOR	0.044909	0.044909	12.79144	3.677106
P43243	MATR3	0.031746	0.031746	3.159466	1.659681
P48426	PIP4K2A	0.015873	0.015873	2.669812	1.416738
P49720	PSMB3	0.01775	0.01775	12.32173	3.623133
P50395	GDI2	0.007937	0.007937	2.44793	1.291562
P52294	KPNA1	0.009701	0.009701	12.5669	3.651557
P54709	ATP1B3	0.015873	0.015873	2.072415	1.051313
P60866	RPS20	0.011159	0.011159	4.473423	2.161379
P60891;P21108	PRPS1	0.034454	0.034454	3.938915	1.977798
P61978	HNRNPK	0.007937	0.007937	4.54299	2.183642
P61981	YWHAG	0.011925	0.011925	4.829529	2.271882
P62269	RPS18	0.031746	0.031746	2.708642	1.43757
P62280	RPS11	0.021177	0.021177	4.000201	2.000073
Q5JWF2;P63092;P38405	GNAS	0.031746	0.031746	2.107307	1.0754
P68363;A6NHL2;Q9H853	TUBA1B	0.007937	0.007937	2.066841	1.047428
Q01081;Q8WU68	U2AF1	0.031746	0.031746	3.963151	1.986648
Q13347	EIF3I	0.009701	0.009701	15.16183	3.922372
Q15008	PSMD6	0.015873	0.015873	3.922331	1.971711
Q15029	EFTUD2	0.031746	0.031746	3.234072	1.693352
Q15286	RAB35	0.031141	0.031141	8.186239	3.033201
Q5VW32	BROX	0.020008	0.020008	3.474571	1.796835
Q6ZRP7	QSOX2	0.011159	0.011159	7.761396	2.956316
Q7L2H7	EIF3M	0.036145	0.036145	3.179758	1.668917
Q8TEX9	IPO4	0.031746	0.031746	2.064114	1.045522
Q92878	RAD50	0.015873	0.015873	2.074313	1.052634
Q92900	UPF1	0.011159	0.011159	5.845346	2.547288
Q96AE4	FUBP1	0.034454	0.034454	12.11526	3.598754
Q96T76	MMS19	0.034454	0.034454	4.286147	2.099681
Q99623	PHB2	0.031746	0.031746	4.394792	2.135795
Q9BQG0	MYBBP1A	0.015873	0.015873	2.723129	1.445266
Q9BXJ4	C1QTNF3	0.031141	0.031141	5.395734	2.431819
Q9Y376	CAB39	0.011925	0.011925	7.959389	2.992658

Appendix 7. List of proteins exclusively present in control RNA granules. This table presents proteins present in control RNA granules, detailing several key metrics.

Protein.IDs	gene	p.value	adj_pvalue	fc	logfc
O15514	POLR2D	0.17971249	0.17971249	1.3478E-05	-16.179058
O43633	CHMP2A	0.4237108	0.4237108	1.1382E-05	-16.422833
O43683	BUB1	0.17971249	0.17971249	7.8852E-06	-16.95243
O95372	LYPLA2	0.07200566	0.07200566	1.7814E-06	-19.098557
O95490;O94910	LPHN2	0.4237108	0.4237108	1.9829E-06	-18.943982
P00488	F13A1	0.4237108	0.4237108	1.8209E-05	-15.745012
P05106	ITGB3	0.4237108	0.4237108	2.3898E-06	-18.674664
P11908	PRPS2	0.17971249	0.17971249	1.1737E-06	-19.700495
P35244	RPA3	0.07200566	0.07200566	7.2497E-08	-23.717496
P36383	GJC1	0.4237108	0.4237108	1.0647E-05	-16.519188
P39060	COL18A1	0.4237108	0.4237108	9.9724E-06	-16.613628
P42356	PI4KA	0.4237108	0.4237108	3.825E-06	-17.996125
P52434	POLR2H	0.17971249	0.17971249	6.7669E-06	-17.173078
P53990	IST1	0.4237108	0.4237108	1.4826E-05	-16.041505
P54687	BCAT1	0.07200566	0.07200566	2.9474E-06	-18.372127
P62328	TMSB4X	0.17971249	0.17971249	3.0761E-06	-18.310456
P82094	TMF1	0.17971249	0.17971249	7.6277E-06	-17.000315
Q12959	DLG1	0.17971249	0.17971249	4.2454E-06	-17.845653
Q12979	ABR	0.07200566	0.07200566	3.1488E-06	-18.276771
Q13427	PPIG	0.17971249	0.17971249	2.6018E-06	-18.552086
Q15020	SART3	0.02536986	0.02536986	1.0721E-06	-19.831171
Q15370	TCEB2	0.07200566	0.07200566	3.784E-07	-21.333571
Q17RS7	GEN1	0.07200566	0.07200566	2.9066E-06	-18.392218
Q5JWR5	DOPEY1	0.17971249	0.17971249	2.2853E-06	-18.739156
Q5TB30	DEPDC1	0.07200566	0.07200566	3.3142E-07	-21.524836
Q6DKJ4	NXN	0.17971249	0.17971249	5.5795E-06	-17.451425
Q86U86	PBRM1	0.17971249	0.17971249	1.561E-06	-19.289066
Q8N201	INTS1	0.17971249	0.17971249	4.42E-06	-17.787511
Q92783	STAM	0.4237108	0.4237108	6.6095E-07	-20.528962
Q92879	CELF1	0.17971249	0.17971249	4.9231E-06	-17.631991
Q96EK5	KIAA1279	0.07200566	0.07200566	1.5653E-06	-19.285137
Q96HY7	DHTKD1	0.17971249	0.17971249	9.4573E-06	-16.690143
Q96PY5;Q8IVF7	FMNL2	0.07200566	0.07200566	1.4234E-06	-19.422267
Q96RT7	TUBGCP6	0.02536986	0.02536986	1.5665E-06	-19.284065
Q9BU61	NDUFAF3	0.17971249	0.17971249	3.0913E-06	-18.303364
Q9BVA0	KATNB1	0.17971249	0.17971249	2.3091E-06	-18.724209
Q9H7Z3	NRDE2	0.17971249	0.17971249	1.9589E-06	-18.961559
Q9H9H4	VPS37B	0.17971249	0.17971249	2.2258E-06	-18.777277
Q9HCM2;Q9UIW2	PLXNA4	0.4237108	0.4237108	4.3518E-05	-14.488016
Q9NP97;Q8TF09	DYNLRB1	0.17971249	0.17971249	7.5763E-06	-17.010076
Q9NQX7	ITM2C	0.4237108	0.4237108	4.112E-05	-14.569784
Q9NRG0	CHRAC1	0.07200566	0.07200566	1.2668E-06	-19.590336

Q9NX04	C1orf109	0.07200566	0.07200566	3.2379E-06	-18.236521
Q9P1Y5	CAMSAP3	0.02536986	0.02536986	4.1828E-07	-21.189014
Q9P275	USP36	0.17971249	0.17971249	6.2199E-06	-17.29468
Q9UDY8	MALT1	0.17971249	0.17971249	8.0158E-07	-20.250655
Q9UGU0	TCF20	0.07200566	0.07200566	2.3786E-06	-18.681432
Q9UI12	ATP6V1H	0.17971249	0.17971249	9.7629E-06	-16.644259
Q9UNN8	PROCR	0.4237108	0.4237108	1.6176E-05	-15.915758
Q9Y450	HBS1L	0.17971249	0.17971249	5.0606E-06	-17.592257

Appendix 8. List of proteins significantly overrepresented in control RNA granules when compared to HD RNA granules. This table presents proteins significantly overrepresented in control RNA granules when compared to HD RNA granules, detailing several key metrics.

Protein.IDs	Gene	p.value	Adj p-value	fc	logfc
O00541	PES1	0.031746	0.031746	0.44214	-1.17743
Q12756;O60333	KIF1A	0.036145	0.036145	0.38078	-1.39297
P16403	HIST1H1C	0.015873	0.015873	0.414302	-1.27125
P49770	EIF2B2	0.031746	0.031746	0.304961	-1.7133
P60709	ACTB	0.009701	0.009701	0.142507	-2.8109
Q71DI3;Q16695;P84243;P68431	HIST2H3A	0.015873	0.015873	0.456069	-1.13267
Q15125	EBP	0.031746	0.031746	0.392313	-1.34992
Q15428	SF3A2	0.007937	0.007937	0.421738	-1.24558
Q8N137	CNTROB	0.034454	0.034454	0.363393	-1.4604
Q8NFH4	NUP37	0.007937	0.007937	0.303621	-1.71965
Q9NVN8	GNL3L	0.031746	0.031746	0.437161	-1.19376
Q9NX20	MRPL16	0.007937	0.007937	0.317709	-1.65422

Appendix 9. List of proteins exclusively present in HD RNA granules. This table presents proteins present in HD RNA granules, detailing several key metrics.

Protein.IDs	Gene	p.value	adj_pvalue	fc	logfc
O00391	QSOX1	0.4237108	0.4237108	63610.8	15.9569841
O00468	AGRN	0.4237108	0.4237108	236260.8	17.8500208
O60518	RANBP6	0.17971249	0.17971249	520998.6	18.99092
O60645	EXOC3	0.07200566	0.07200566	285570.4	18.1234869
O75323	GBAS	0.4237108	0.4237108	1312720.8	20.3241287
O75663	TIPRL	0.17971249	0.17971249	779900.6	19.5729307
O95453	PARN	0.17971249	0.17971249	268612.6	18.0351675
P00533	EGFR	0.02536986	0.02536986	118584.2	16.8555523
P02794	FTH1	0.4237108	0.4237108	312820.8	18.2549769
P06756	ITGAV	0.17971249	0.17971249	151946.6	17.2132049
P07148	FABP1	0.4237108	0.4237108	303460.8	18.2111506
P07858	CTSB	0.17971249	0.17971249	280528.6	18.0977883
P20020;Q16720	ATP2B1	0.02536986	0.02536986	434074.2	18.7275822
P21964	COMT	0.4237108	0.4237108	54382.8	15.7308628
P22413	ENPP1	0.4237108	0.4237108	126684.8	16.9508839

P23229	ITGA6	0.4237108	0.4237108	77776.8	16.2470523
P29144	TPP2	0.4237108	0.4237108	556300.8	19.0855057
P33908	MAN1A1	0.4237108	0.4237108	145174.8	17.1474315
Q8TDQ7;P46926	GNPDA2	0.17971249	0.17971249	457560.6	18.8036033
Q00403	GTF2B	0.17971249	0.17971249	661900.6	19.3362551
Q01650	SLC7A5	0.4237108	0.4237108	20852.8	14.3479535
Q07954	LRP1	0.4237108	0.4237108	306080.8	18.223553
Q12907	LMAN2	0.17971249	0.17971249	280010.6	18.0951219
Q13043	STK4	0.17971249	0.17971249	430440.6	18.7154546
Q13557	CAMK2D	0.17971249	0.17971249	527420.6	19.0085944
Q13610	PWP1	0.4237108	0.4237108	1005200.8	19.9390523
Q14699	RFTN1	0.17971249	0.17971249	441118.6	18.7508071
Q15369	TCEB1	0.17971249	0.17971249	545880.6	19.0582259
Q5VUB5	FAM171A1	0.17971249	0.17971249	137276.6	17.0667262
Q7LBR1	CHMP1B	0.4237108	0.4237108	493840.8	18.9136865
Q8IVM0	CCDC50	0.4237108	0.4237108	237980.8	17.8604857
Q8IWA4	MFN1	0.17971249	0.17971249	1541180.6	20.5556045
Q8IWZ8	SUGP1	0.07200566	0.07200566	251500.4	17.9402012
Q969P0	IGSF8	0.4237108	0.4237108	319220.8	18.2841951
Q96EY5	MVB12A	0.4237108	0.4237108	1866920.8	20.8322293
Q99549	MPHOSPH8	0.17971249	0.17971249	399702.6	18.6085674
Q9BRR8	GPATCH1	0.4237108	0.4237108	168098.8	17.3589499
Q9BY43	CHMP4A	0.17971249	0.17971249	316808.6	18.273252
Q9H269	VPS16	0.17971249	0.17971249	949220.6	19.8563839
Q9HCD5	NCOA5	0.17971249	0.17971249	481220.6	18.8763389
Q9NYB9	ABI2	0.02536986	0.02536986	2259700.2	21.1076999
Q9NYZ3	GTSE1	0.07200566	0.07200566	1190126.4	20.1826834
Q9P1F3	ABRACL	0.17971249	0.17971249	2323020.6	21.1475705
Q9P260	KIAA1468	0.07200566	0.07200566	330090.4	18.3325017
Q9P2P1	NYNRIN	0.07200566	0.07200566	1570954.4	20.5832099
Q9UHI8	ADAMTS1	0.4237108	0.4237108	773760.8	19.5615281
Q9UHY7	ENOPH1	0.17971249	0.17971249	177366.6	17.4363748
Q9UKV8;Q9H9G7	AGO2	0.17971249	0.17971249	358978.6	18.4535383
Q9ULK4	MED23	0.17971249	0.17971249	356062.6	18.4417714
Q9Y3B4	SF3B6	0.07200566	0.07200566	2865140.4	21.4501744
Q9Y467	SALL2	0.4237108	0.4237108	183558.8	17.4858828
Q9Y4C2	TCAF1	0.07200566	0.07200566	599370.4	19.1930883
Q9Y5X3	SNX5	0.17971249	0.17971249	244410.6	17.8989473
Q9Y617	PSAT1	0.17971249	0.17971249	277468.6	18.081965
Q9Y6E0	STK24	0.4237108	0.4237108	87454.8	16.4162499

Appendix 10. List of proteins overrepresented in HD RNA granules when compared to control RNA granules. This table presents proteins significantly overrepresented in HD RNA granules when compared to control RNA granules, detailing several key metrics.

Protein.IDs	Gene	p.value	Adj p-value	fc	logfc
O43837	IDH3B	0.031746	0.031746	2.394738	1.259868
O75083	WDR1	0.021177	0.021177	2.971349	1.571118
O95218	ZRANB2	0.031746	0.031746	2.632144	1.396239
O95433	AHSA1	0.015873	0.015873	2.136761	1.095426
O95714;Q9BVR0	HERC2	0.015873	0.015873	2.050752	1.036153
P19022;P55283	CDH2	0.007937	0.007937	2.610508	1.38433
P25325	MPST	0.015873	0.015873	2.155928	1.108309
P27986;Q92569	PIK3R1	0.015873	0.015873	2.192084	1.132303
P36543	ATP6V1E1	0.034454	0.034454	3.991301	1.996859
P61586;P08134	RHOA	0.031746	0.031746	2.400078	1.263081
Q02218;Q9ULD0	OGDH	0.007937	0.007937	2.085944	1.060701
Q04760	GLO1	0.036145	0.036145	2.749849	1.459352
Q13501	SQSTM1	0.007937	0.007937	2.257046	1.174436
Q15648	MED1	0.044909	0.044909	5.226674	2.385893
Q99536	VAT1	0.034454	0.034454	3.616863	1.854739

Appendix 11. List of HD sEV Proteins Associated with Neurodegenerative Disorders. KEGG analysis of HD sEVs revealed significant hits for multiple neurodegenerative disorders. The table below lists the proteins identified and the corresponding neurodegenerative diseases they are associated with. In the "Neurodegenerative Disorder" column, the "hsa" (Stands for *Homo sapiens* (Species)) followed by a number represents the KEGG pathway identifier for each disease. The number in parentheses, such as (18) in hsa05010 Alzheimer disease - Homo sapiens (human) (18), indicates the number of proteins or genes from the HD sEV dataset that are linked to that particular pathway.

Protein in HD sEVs	Neurodegenerative diseases
NDUFS8	hsa05010 Alzheimer disease - Homo sapiens (human) (18)
	hsa05012 Parkinson disease - Homo sapiens (human) (20)
	hsa05014 Amyotrophic lateral sclerosis - Homo sapiens (human) (23)
	hsa05016 Huntington disease - Homo sapiens (human) (18)
	hsa05020 Prion disease - Homo sapiens (human) (19)
	hsa05022 Pathways of neurodegeneration - multiple diseases - Homo sapiens (human) (21)
PSMD14	hsa05010 Alzheimer disease - Homo sapiens (human) (18)
	hsa05012 Parkinson disease - Homo sapiens (human) (20)
	hsa05014 Amyotrophic lateral sclerosis - Homo sapiens (human) (23)
	hsa05016 Huntington disease - Homo sapiens (human) (18)
	hsa05017 Spinocerebellar ataxia - Homo sapiens (human) (10)
	hsa05020 Prion disease - Homo sapiens (human) (19)
NDUFS4	hsa05010 Alzheimer disease - Homo sapiens (human) (18)

	hsa05012 Parkinson disease - Homo sapiens (human) (20)
	hsa05014 Amyotrophic lateral sclerosis - Homo sapiens (human) (23)
	hsa05016 Huntington disease - Homo sapiens (human) (18)
	hsa05020 Prion disease - Homo sapiens (human) (19)
	hsa05022 Pathways of neurodegeneration - multiple diseases - Homo sapiens (human) (21)
AP2A2	hsa05016 Huntington disease - Homo sapiens (human) (18)
NDUFB8	hsa05010 Alzheimer disease - Homo sapiens (human) (18)
	hsa05012 Parkinson disease - Homo sapiens (human) (20)
	hsa05014 Amyotrophic lateral sclerosis - Homo sapiens (human) (23)
	hsa05016 Huntington disease - Homo sapiens (human) (18)
	hsa05020 Prion disease - Homo sapiens (human) (19)
	hsa05022 Pathways of neurodegeneration - multiple diseases - Homo sapiens (human) (21)
CYC1	hsa05010 Alzheimer disease - Homo sapiens (human) (18)
	hsa05012 Parkinson disease - Homo sapiens (human) (20)
	hsa05014 Amyotrophic lateral sclerosis - Homo sapiens (human) (23)
	hsa05016 Huntington disease - Homo sapiens (human) (18)
	hsa05020 Prion disease - Homo sapiens (human) (19)
	hsa05022 Pathways of neurodegeneration - multiple diseases - Homo sapiens (human) (21)
SLC25A4	hsa05010 Alzheimer disease - Homo sapiens (human) (18)
	hsa05012 Parkinson disease - Homo sapiens (human) (20)
	hsa05016 Huntington disease - Homo sapiens (human) (18)
	hsa05017 Spinocerebellar ataxia - Homo sapiens (human) (10)
	06464 Amyotrophic lateral sclerosis (21)
	hsa05020 Prion disease - Homo sapiens (human) (19)
	hsa05022 Pathways of neurodegeneration - multiple diseases - Homo sapiens (human) (21)
C6	hsa05020 Prion disease - Homo sapiens (human) (19)
NDUFV2	hsa05010 Alzheimer disease - Homo sapiens (human) (18)
	hsa05012 Parkinson disease - Homo sapiens (human) (20)
	hsa05014 Amyotrophic lateral sclerosis - Homo sapiens (human) (23)
	hsa05016 Huntington disease - Homo sapiens (human) (18)
	hsa05020 Prion disease - Homo sapiens (human) (19)
	hsa05022 Pathways of neurodegeneration - multiple diseases - Homo sapiens (human) (21)
COMT	H01450 Obsessive-compulsive disorder (1)
PRKACB	hsa05012 Parkinson disease - Homo sapiens (human) (20)
	hsa05020 Prion disease - Homo sapiens (human) (19)
PSMB6	hsa05010 Alzheimer disease - Homo sapiens (human) (18)
	hsa05012 Parkinson disease - Homo sapiens (human) (20)
	hsa05014 Amyotrophic lateral sclerosis - Homo sapiens (human) (23)
	hsa05016 Huntington disease - Homo sapiens (human) (18)
	hsa05017 Spinocerebellar ataxia - Homo sapiens (human) (10)

	hsa05020 Prion disease - Homo sapiens (human) (19)
	hsa05022 Pathways of neurodegeneration - multiple diseases - Homo sapiens (human) (21)
PSMC2	hsa05010 Alzheimer disease - Homo sapiens (human) (18)
	hsa05012 Parkinson disease - Homo sapiens (human) (20)
	hsa05014 Amyotrophic lateral sclerosis - Homo sapiens (human) (23)
	hsa05016 Huntington disease - Homo sapiens (human) (18)
	hsa05017 Spinocerebellar ataxia - Homo sapiens (human) (10)
	hsa05020 Prion disease - Homo sapiens (human) (19)
	hsa05022 Pathways of neurodegeneration - multiple diseases - Homo sapiens (human) (21)
PSMD8	hsa05010 Alzheimer disease - Homo sapiens (human) (18)
	hsa05012 Parkinson disease - Homo sapiens (human) (20)
	hsa05014 Amyotrophic lateral sclerosis - Homo sapiens (human) (23)
	hsa05016 Huntington disease - Homo sapiens (human) (18)
	hsa05017 Spinocerebellar ataxia - Homo sapiens (human) (10)
	hsa05020 Prion disease - Homo sapiens (human) (19)
	hsa05022 Pathways of neurodegeneration - multiple diseases - Homo sapiens (human) (21)
SEC13	hsa05014 Amyotrophic lateral sclerosis - Homo sapiens (human) (23)
NDUFA6	hsa05010 Alzheimer disease - Homo sapiens (human) (18)
	hsa05012 Parkinson disease - Homo sapiens (human) (20)
	hsa05014 Amyotrophic lateral sclerosis - Homo sapiens (human) (23)
	hsa05016 Huntington disease - Homo sapiens (human) (18)
	hsa05020 Prion disease - Homo sapiens (human) (19)
	hsa05022 Pathways of neurodegeneration - multiple diseases - Homo sapiens (human) (21)
PSMA6	hsa05010 Alzheimer disease - Homo sapiens (human) (18)
	hsa05012 Parkinson disease - Homo sapiens (human) (20)
	hsa05014 Amyotrophic lateral sclerosis - Homo sapiens (human) (23)
	hsa05016 Huntington disease - Homo sapiens (human) (18)
	hsa05017 Spinocerebellar ataxia - Homo sapiens (human) (10)
	hsa05020 Prion disease - Homo sapiens (human) (19)
	hsa05022 Pathways of neurodegeneration - multiple diseases - Homo sapiens (human) (21)
PSMC1	hsa05010 Alzheimer disease - Homo sapiens (human) (18)
	hsa05012 Parkinson disease - Homo sapiens (human) (20)
	hsa05014 Amyotrophic lateral sclerosis - Homo sapiens (human) (23)
	hsa05016 Huntington disease - Homo sapiens (human) (18)
	hsa05017 Spinocerebellar ataxia - Homo sapiens (human) (10)
	hsa05020 Prion disease - Homo sapiens (human) (19)
	hsa05022 Pathways of neurodegeneration - multiple diseases - Homo sapiens (human) (21)
PPP2CA	hsa04730 Long-term depression - Homo sapiens (human) (4)
	H02470 Neurodevelopmental disorder with structural brain abnormalities (2)
	H02632 PP2A-related neurodevelopmental disorder (1)

GNAI1	hsa04730 Long-term depression - Homo sapiens (human) (4)
	hsa05012 Parkinson disease - Homo sapiens (human) (20)
RAE1	hsa05014 Amyotrophic lateral sclerosis - Homo sapiens (human) (23)
GSTO1	06463 Parkinson disease (19)
CDK5	hsa05010 Alzheimer disease - Homo sapiens (human) (18)
	hsa05022 Pathways of neurodegeneration - multiple diseases - Homo sapiens (human) (21)
KLC1	hsa05010 Alzheimer disease - Homo sapiens (human) (18)
	hsa05012 Parkinson disease - Homo sapiens (human) (20)
	hsa05014 Amyotrophic lateral sclerosis - Homo sapiens (human) (23)
	hsa05016 Huntington disease - Homo sapiens (human) (18)
	hsa05020 Prion disease - Homo sapiens (human) (19)
	hsa05022 Pathways of neurodegeneration - multiple diseases - Homo sapiens (human) (21)
SQSTM1	hsa05014 Amyotrophic lateral sclerosis - Homo sapiens (human) (23)
	H02342 Frontotemporal dementia and amyotrophic lateral sclerosis (1)
CAMK2G	hsa05012 Parkinson disease - Homo sapiens (human) (20)
	hsa05022 Pathways of neurodegeneration - multiple diseases - Homo sapiens (human) (21)
	H00773 Autosomal dominant intellectual developmental disorder (6)
DCTN2	hsa05014 Amyotrophic lateral sclerosis - Homo sapiens (human) (23)
	hsa05016 Huntington disease - Homo sapiens (human) (18)
	06463 Parkinson disease (19)
	hsa05022 Pathways of neurodegeneration - multiple diseases - Homo sapiens (human) (21)
ITPR3	hsa04730 Long-term depression - Homo sapiens (human) (4)
	hsa05010 Alzheimer disease - Homo sapiens (human) (18)
	hsa05012 Parkinson disease - Homo sapiens (human) (20)
	hsa05017 Spinocerebellar ataxia - Homo sapiens (human) (10)
	hsa05014 Amyotrophic lateral sclerosis - Homo sapiens (human) (23)
	hsa05020 Prion disease - Homo sapiens (human) (19)
	hsa05022 Pathways of neurodegeneration - multiple diseases - Homo sapiens (human) (21)
ITPR1	hsa04730 Long-term depression - Homo sapiens (human) (4)
	hsa05010 Alzheimer disease - Homo sapiens (human) (18)
	hsa05012 Parkinson disease - Homo sapiens (human) (20)
	hsa05016 Huntington disease - Homo sapiens (human) (18)
	hsa05020 Prion disease - Homo sapiens (human) (19)
	hsa05022 Pathways of neurodegeneration - multiple diseases - Homo sapiens (human) (21)
	06464 Amyotrophic lateral sclerosis (21)
PUM1	hsa05017 Spinocerebellar ataxia - Homo sapiens (human) (10)
ALYREF	hsa05014 Amyotrophic lateral sclerosis - Homo sapiens (human) (23)
NUP43	hsa05014 Amyotrophic lateral sclerosis - Homo sapiens (human) (23)
NUP88	hsa05014 Amyotrophic lateral sclerosis - Homo sapiens (human) (23)

UBQLN2	hsa05014 Amyotrophic lateral sclerosis - Homo sapiens (human) (23)
NDUFB9	hsa05010 Alzheimer disease - Homo sapiens (human) (18)
	hsa05012 Parkinson disease - Homo sapiens (human) (20)
	hsa05014 Amyotrophic lateral sclerosis - Homo sapiens (human) (23)
	hsa05016 Huntington disease - Homo sapiens (human) (18)
	hsa05020 Prion disease - Homo sapiens (human) (19)
	hsa05022 Pathways of neurodegeneration - multiple diseases - Homo sapiens (human) (21)
LAMC1	hsa05020 Prion disease - Homo sapiens (human) (4)
PSMB3	hsa05010 Alzheimer disease - Homo sapiens (human) (4)
	hsa05016 Huntington disease - Homo sapiens (human) (4)
	hsa05012 Parkinson disease - Homo sapiens (human) (4)
	hsa05014 Amyotrophic lateral sclerosis - Homo sapiens (human) (5)
	hsa05017 Spinocerebellar ataxia - Homo sapiens (human) (3)
	hsa05020 Prion disease - Homo sapiens (human) (4)
	hsa05022 Pathways of neurodegeneration - multiple diseases - Homo sapiens (human) (4)
GNAS	hsa05012 Parkinson disease - Homo sapiens (human) (4)
MATR3	hsa05014 Amyotrophic lateral sclerosis - Homo sapiens (human) (5)
TUBA1B	hsa05010 Alzheimer disease - Homo sapiens (human) (4)
	hsa05014 Amyotrophic lateral sclerosis - Homo sapiens (human) (5)
	hsa05016 Huntington disease - Homo sapiens (human) (4)
	hsa05012 Parkinson disease - Homo sapiens (human) (4)
	hsa05020 Prion disease - Homo sapiens (human) (4)
	hsa05022 Pathways of neurodegeneration - multiple diseases - Homo sapiens (human) (4)
MTOR	hsa05010 Alzheimer disease - Homo sapiens (human) (4)
	hsa05017 Spinocerebellar ataxia - Homo sapiens (human) (3)
	hsa05022 Pathways of neurodegeneration - multiple diseases - Homo sapiens (human) (4)
	hsa05016 Huntington disease - Homo sapiens (human) (4)
	hsa05014 Amyotrophic lateral sclerosis - Homo sapiens (human) (5)
PSMD6	hsa05010 Alzheimer disease - Homo sapiens (human) (4)
	hsa05012 Parkinson disease - Homo sapiens (human) (4)
	hsa05014 Amyotrophic lateral sclerosis - Homo sapiens (human) (5)
	hsa05016 Huntington disease - Homo sapiens (human) (4)
	hsa05017 Spinocerebellar ataxia - Homo sapiens (human) (3)
	hsa05020 Prion disease - Homo sapiens (human) (4)
	hsa05022 Pathways of neurodegeneration - multiple diseases - Homo sapiens (human) (4)
SLC9A1	H01891 Autosomal recessive spinocerebellar ataxias (1)
THOC2	H00480 X-linked intellectual developmental disorder (2)
SPATA5	H02470 Neurodevelopmental disorder with structural brain abnormalities (2)
PACS1	H00773 Autosomal dominant intellectual developmental disorder (6)
DARS2	H00871 Leukoencephalopathy with brain stem and spinal cord involvement and lactate elevation (1)

PITRM1	H01891 Autosomal recessive spinocerebellar ataxias (2)
EEF1A2	H00773 Autosomal dominant intellectual developmental disorder (6)
PURA	H00773 Autosomal dominant intellectual developmental disorder (6)
SMARCA4	H00773 Autosomal dominant intellectual developmental disorder (6)
NF2	H01438 Neurofibromatosis type 2 (1)
XRCC1	H01891 Autosomal recessive spinocerebellar ataxias (2)
FTL	H00833 Neurodegeneration with brain iron accumulation (1)
	H01779 Neuroferritinopathy (1)
OGT	H00480 X-linked intellectual developmental disorder (2)
ARID1A	H00773 Autosomal dominant intellectual developmental disorder (6)

Appendix 12. List of HD RNA granules Proteins Associated with Neurodegenerative Disorders. KEGG analysis of HD RNA granules revealed significant hits for multiple neurodegenerative disorders. The table below lists the proteins identified and the corresponding neurodegenerative diseases they are associated with. In the "Neurodegenerative Disorder" column, the "hsa" (Stands for *Homo sapiens* (Species)) followed by a number represents the KEGG pathway identifier for each disease. The number in parentheses, such as (18) in hsa05010 Alzheimer disease - Homo sapiens (human) (18), indicates the number of proteins or genes from the HD RNA granule dataset that are linked to that particular pathway.

Protein in HD RNA granules	Neurodegenerative diseases
COMT	H01450 Obsessive-compulsive disorder (1)
GTF2B	hsa05017 Spinocerebellar ataxia - Homo sapiens (human) (1)
LRP1	hsa05010 Alzheimer disease - Homo sapiens (human) (1)
CAMK2D	hsa05012 Parkinson disease - Homo sapiens (human) (2)
	hsa05022 Pathways of neurodegeneration - multiple diseases - Homo sapiens (human) (2)
MFN1	hsa05012 Parkinson disease - Homo sapiens (human) (2)
	hsa05022 Pathways of neurodegeneration - multiple diseases - Homo sapiens (human) (2)
SQSTM1	hsa05014 Amyotrophic lateral sclerosis - Homo sapiens (human) (1)
	H02342 Frontotemporal dementia and amyotrophic lateral sclerosis (1)
HERC2	H00768 Autosomal recessive intellectual developmental disorder (1)
PIK3R1	hsa05010 Alzheimer disease - Homo sapiens (human) (1)
	hsa05017 Spinocerebellar ataxia - Homo sapiens (human) (1)

Appendix 13. List of control sEV Proteins Associated with Neurodegenerative Disorders. KEGG analysis of control sEVs revealed significant hits for multiple neurodegenerative disorders. The table below lists the proteins identified and the corresponding

neurodegenerative diseases they are associated with. In the "Neurodegenerative Disorder" column, the "hsa" (Stands for *Homo sapiens* (Species)) followed by a number represents the KEGG pathway identifier for each disease. The number in parentheses, such as (18) in hsa05010 Alzheimer disease - *Homo sapiens* (human) (18), indicates the number of proteins or genes from the control sEV dataset that are linked to that particular pathway.

Protein in control sEVs	Diseases
SET	H00773 Autosomal dominant intellectual developmental disorder (1)
DST	H00265 Hereditary sensory and autonomic neuropathy (2)
DNMT1	H00265 Hereditary sensory and autonomic neuropathy (2)
EIF2AK2	H02457 Developmental delay, leukoencephalopathy, and neurologic decompensation (1)
HK1	H02470 Neurodevelopmental disorder with structural brain abnormalities (2)
SHMT2	H02470 Neurodevelopmental disorder with structural brain abnormalities (2)

Appendix 14. Functional enrichment analysis of control RNA granules. The table presents the functional enrichment analysis of control RNA granules. The enriched GO terms are categorized under Biological Process and Cellular Component, along with their corresponding p-values and gene matches. Notably, the analysis did not yield any results for Molecular Function in this dataset. GO terms related to RNA granules are highlighted in red, while those associated with sEVs are marked in blue. The numbers beginning with "GO" refer to specific Gene Ontology identifiers for each term, representing their unique classification in the GO database.

Control RNA granules		
ENRICHED GO terms - genes enriched for GO (biological process)		
GO term	P-value	Gene matches
GO:0036258 - multivesicular body assembly	0.028737	CHMP2A
		IST1
		STAM
		VPS37B
GO:0036257 - multivesicular body organization	0.028737	CHMP2A
		IST1
		STAM
		VPS37B
ENRICHED GO terms - genes enriched for GO (cellular component)		
GO term	P-value	Gene matches
GO:0043232 - intracellular non-membrane-bounded organelle	0.029966	NRDE2
		TUBGCP6
		IST1
		HBS1L

		USP36
		TMSB4X
		BUB1
		DYNLRB1
		CELF1
		C1orf109
		H1-2
		H3C15
		CAMSAP3
		POLR2H
		KIFBP
		PBRM1
		MALT1
		POLR2D
		NUP37
		CNTROB
		KIF1A
		MRPL16
		ACTB
		PES1
		KATNB1
		CHMP2A
GO:0036452 - ESCRT complex	0.044059	STAM
		VPS37B
		CHMP2A

Appendix 15. Functional enrichment analysis of control sEVs. The table displays the functional enrichment analysis of control sEVs, with enriched GO terms classified under Biological Process and Cellular Component, alongside their respective p-values and gene matches. GO terms related to RNA granules are highlighted in red, while those associated with sEVs are indicated in blue. The numbers starting with "GO" represent specific Gene Ontology identifiers, which provide unique classification for each term. Although terms such as "intracellular membrane-bounded organelle" and "membrane-bounded organelle" were found with relatively high p-values, their connections to sEVs were weak and thus excluded from the table for relevance.

Control sEVs		
ENRICHED GO terms - genes enriched for GO (biological process)		
GO term	P-value	Gene matches
GO:0140694 - non-membrane-bounded organelle assembly	0.007953921	EIF5B
		CIRBP
		EIF4ENIF1
		LSM4

Appendix

		STAG2
		RC3H1
		GOLGA2
		TPX2
		CDK5RAP2
		CEP85
		G3BP2
		CEP135
		EIF2S1
		TNKS
GO:0022613 - ribonucleoprotein complex biogenesis	0.04652763	WDR12
		WDR36
		NOC4L
		RIOK1
		KRR1
		NSUN4
		UTP18
		FCF1
		PNO1
		RPL35A
GO:0006913 - nucleocytoplasmic transport	0.07193715	TNPO3
		CASC3
		EIF4ENIF1
		KPNA4
		RBM8A
		NUP35
		TPR
		NDC1
		NUP50
		G3BP2
		TP53
		SET
ENRICHED GO terms - genes enriched for GO (cellular component)		
GO:0043232 - intracellular non-membrane-bounded organelle	2.69E-14	KRI1
		MYO19
		NEFL
		MKI67
		WDR12
		RBM19
		ZNF346
		SMARCC2
		TELO2
		DCP2
		MARCKSL1
		WDR36
		ARPC2

Appendix

		MRPL19
		FAU
		RIOX1
		NES
		RMDN3
		MAP7D3
		SPECC1L
		NOC4L
		INA
		UBAP2
		DYNC1LI1
		ORC3
		TUBB4A
		CASC3
		MRPS22
		CIRBP
		NUSAP1
		EIF4ENIF1
		LSM4
		KRR1
		SAMHD1
		MRPL46
		DFFA
		MAP7D1
		PAWR
		CDH2
		S100A12
		APTX
		CEP170
		PNKP
		NSMCE1
		EIF2AK2
		STAG2
		MPHOSPH9
		STAT1
		PGM1
		CIP2A
		ADD1
		UTP18
		CDK12
		TOP3A
		APOBEC3C
		STMN1
		MRPL48
		RC3H1
		CAMSAP3

Appendix

		METAP1
		PARD3
		KIFBP
		CEP350
		PARN
		GOLGA2
		CDC42EP1
		TPX2
		CDK5RAP2
		SPAG5
		FCF1
		HMOX1
		TPR
		NDC1
		DBN1
		LARP4B
		CEP85
		METTL1
		GRSF1
		ECT2
		RTF1
		RBBP6
		G3BP2
		TTK
		EIF4E2
		SHMT2
		TWINK
		BUB1B
		RPL38
		TP53
		DCP1B
		SET
		CEP290
		PPAN
		SIN3A
		PNO1
		MRPL20
		MRPL37
		ACTR1A
		CEP135
		RPL35A
		SMARCC1
		EIF2S1
		MRPL53
		TBRG4
		TNKS

Appendix

		RPTOR
		ZFR
GO:1990904 - ribonucleoprotein complex	6.53E-12	KRI1
		SART1
		PRPF4
		WDR12
		DHX8
		DCP2
		WDR36
		MRPL19
		FAU
		NOC4L
		RIOK1
		CASC3
		MRPS22
		CIRBP
		LSM4
		KRR1
		NSUN4
		MRPL46
		SF3A2
		UTP18
		CWC27
		MRPL48
		GPATCH1
		RO60
		RBM8A
		HEXIM1
		PRPF3
		FCF1
		GRSF1
		G3BP2
		SNRPA1
		RPL38
PPAN		
PNO1		
MRPL20		
MRPL37		
RPL35A		
EIF2S1		
MRPL53		
ZFR		
GO:0035770 - ribonucleoprotein granule	4.49E-06	DCP2
		INA
		UBAP2
		CASC3

Appendix

		CIRBP
		EIF4ENIF1
		LSM4
		APOBEC3C
		RC3H1
		PARD3
		LARP4B
		GRSF1
		G3BP2
		EIF4E2
		DCP1B
		EIF2S1
		TBRG4
		RPTOR
GO:000932 - P-body	0.001997344	RC3H1
		DCP2
		DCP1B
		EIF4ENIF1
		LSM4
		APOBEC3C
		UBAP2
		EIF4E2
GO:0010494 - cytoplasmic stress granule	0.008252433	EIF2S1
		CIRBP
		RC3H1
		RPTOR
		LARP4B
		CASC3
		G3BP2
GO:0016607 - nuclear speck	0.008389819	CASC3
		PRPF4
		SART1
		PRPF3
		SNRPA1
		RBM10
		ZNF638
		SF3A2
		TIMM50
		RBBP6
		GTF2H4
		EIF4ENIF1
		CDK12
		RBM8A
		RBM19
		PARN

Appendix 16. Functional enrichment analysis of HD sEVs. The table displays the functional enrichment analysis of HD sEVs, with enriched GO terms classified under biological Process, molecular function and cellular Component, alongside their respective p-values and gene matches. GO terms related to RNA granules are highlighted in red, while those associated with sEVs are indicated in blue. The numbers starting with "GO" represent specific Gene Ontology identifiers, which provide unique classification for each term. Although terms such as "intracellular organelle", "ribonucleoprotein granule", "cellular response to stress" and "non-membrane-bounded organelle" were found with relatively high p-values, their connections to RNA granules were there, but were weak and thus excluded from the table for relevance.

HD sEVs		
ENRICHED GO terms - genes enriched for GO (biological process)		
GO term	P-value	Gene matches
GO:0022613 - ribonucleoprotein complex biogenesis	1.16E-05	NOA1
		RCL1
		RPL7
		HEATR3
		PWP1
		SBDS
		WDR3
		MYBBP1A
		SURF6
		NOP14
		MRTO4
		RPS17
		SPATA5
		RPS18
		RPS11
		RPS14
BYSL		
XRCC5		
UTP15		
GO:0061763 - multivesicular body-lysosome fusion	0.0892251	CHMP4B
		CHMP2A
		CHMP4A
GO:0006904 - vesicle docking involved in exocytosis	0.0891057	USO1
		STX18
		VAMP3
		EXOC4
		VPS33A
EXOC1		
ENRICHED GO terms - genes enriched for GO (molecular function)		

Appendix

GO:0043021 - ribonucleoprotein complex binding	0.0083057	SNRPN
		SNRPC
		LTN1
		SRP68
		SBDS
		PRPF31
		NAA10
		RACK1
		PRMT5
		SPATA5
		CSDE1
		MCTS1
		MTOR
		NCLN
ENRICHED GO terms - genes enriched for GO (cellular component)		
GO:1903561 - extracellular vesicle	7.99E-19	DNPB1
		CD2AP
		SQSTM1
		CNP
		PROCR
		NAA50
		KRT6B
		ARL8B
		ATP6V0A1
		YWHAG
		PAFAH1B2
		ALYREF
		CAPN5
		HNRNPC
		ATP6V0C
		STK26
		CBR1
		CPNE3
		CHMP4B
		PDCD5
		ACTBL2
		RPLP2
		RAB35
		COL6A1
		AKR1B1
		SH3BGRL3
		CNDP2
		MAN1A1
FTL		
PRDX5		
MPP5		

Appendix

		CAB39
		ARF4
		UGGT1
		CAPZA2
		PPP2CA
		DUT
		ITM2C
		SRI
		AUP1
		ANXA1
		LAMB1
		ATP1B3
		STX7
		PSMB6
		GDI2
		DNAJA2
		CDK1
		GARS1
		STAMPB
		CRK
		PHPT1
		G6PD
		NAMPT
		GNAS
		DBI
		GNG12
		MVB12B
		ANP32B
		DHX36
		SORD
		RACK1
		SNAP23
		ITGAV
		COMT
		NANS
		GSR
		AP1M1
		ADSS2
		STOM
		PDCD10
		CFL2
		CFL1
		EEF1G
		GNAI1
		LAMC1
		H2BC9

Appendix

		BROX
		ITGA2B
		DCTN2
		LAMA5
		MYO1B
		PSMB3
		C1QTNF3
		TOLLIP
		PRKACB
		STK24
		ACOT7
		PRSS23
		RPS18
		SLC9A1
		SPR
		RPS11
		SPAST
		EIF3I
		IARS1
		RPS14
		SEC13
		HNRNPK
		SPAG9
		TPT1
		PSMA6
		CYRIB
		XPNPEP1
		DLG1
		SEMG1
		CHMP2A
		NUTF2
		WDR1
		RPS20
		APEH
		HNRNPUL1
		RBM17
		MRPL49
		LSM1
		RCL1
		ALYREF
		SNRPN
		HNRNPC
		SNRPC
		SNRPE
		RPL7
		SF3B1
GO:1990904 - ribonucleoprotein complex	1.78E-13	

Appendix

		NRDE2
		RPLP2
		MRPL11
		SRP68
		MRPL1
		PRPF31
		DHX16
		WDR3
		NELFE
		MRPS9
		U2AF1
		SURF6
		RACK1
		UPF1
		TRA2A
		DHX38
		EIF3J
		BCAS2
		MRPL39
		NOP14
		EFTUD2
		MRTO4
		HNRNPLL
		RPS17
		TOP2A
		RPS18
		RPS11
		EIF3I
		RPS14
		PRORP
		MCTS1
		HNRNPK
		BYSL
		DDX42
		MRPL13
		RPL32
		EIF3M
		XRCC5
		UTP15
		SYNCRIP
		RPS20
		WBP11
		CD2AP
		SQSTM1
		TENT4B
		NAA50
GO:0043232 - intracellular non-membrane-bounded organelle	1.21E-10	

Appendix

		SPART
		ACACA
		ARL8B
		MRPL49
		ENAH
		LSM1
		RCL1
		PAFAH1B2
		HNRNPC
		INTS3
		RPL7
		CPNE3
		CHMP4B
		SF3B1
		MAP4
		NRDE2
		ACTBL2
		RPLP2
		MRPL11
		PWP1
		COL6A1
		TWF1
		TUBA1B
		LLPH
		CDK2
		EPB41
		LTN1
		NF2
		MYG1
		SRP68
		MRPL1
		CAPZA2
		PPP2CA
		AUP1
		BUB3
		FNBP1L
		SBDS
		USP36
		HAUS3
		FLII
		GBF1
		HAX1
		WDR3
		NELFE
		CDK1
		BRD3

Appendix

		CRK
		TRIP13
		ITPR3
		MRPS9
		NAA10
		PSMC2
		HIRIP3
		ANP32B
		DHX36
		MYBBP1A
		TOP3B
		SURF6
		BAZ2A
		RACK1
		ANK1
		TFB1M
		KAT7
		UPF1
		PRMT5
		TRA2A
		STOM
		BCAS2
		HPF1
		CFL2
		PUM1
		NEXN
		S100A13
		MRPL39
		CFL1
		EXOC4
		NOP14
		GNAI1
		PELP1
		H2BC9
		CHMP4A
		XRCC1
		CARHSP1
		PRKAA2
		IRAK1
		RCN2
		DCTN2
		YTHDF2
		MRTO4
		RAE1
		MYO1B
		SMARCA4

Appendix

		RPS17
		TOP2A
		STK24
		SPATA5
		RAD50
		RPS18
		RPS11
		CSDE1
		SPAST
		CYB5R3
		PTP4A1
		RPS14
		SEC13
		PRORP
		NUP43
		EGFR
		HNRNPK
		BYSL
		DDX42
		URB1
		PSMA6
		CDK5
		GTF2F2
		CEP72
		RBBP4
		MRPL13
		RPL32
		TRIP6
		CCNB1
		DDX47
		XRCC5
		GPATCH4
		ITPR1
		TERF2IP
		UTP15
		CHMP2A
		MYO18A
		NSDHL
		MMS19
		HELZ
		WDR1
		RPS20
		MBD3
		KLC1
		HAX1
		LSM1
GO:0000932 - P-body	0.0017711	

Appendix

		PSMC2
		PSMA6
		SQSTM1
		PUM1
		UPF1
		CARHSP1
		YTHDF2
		CSDE1
		SRSF10
		SF3B1
		BCAS2
		NAMPT
		PRKAA2
		U2AF1
		RING1
		PUM1
		EFTUD2
		CTR9
		ALYREF
		DDX42
		THOC2
		PRPF31
		ATP6V0A1
		COPS4
		USP36
		BAZ2A
		DHX36
		NRDE2
		NUP43
		SQSTM1
		LSM1
		HAX1
		PSMC2
		DHX36
		UPF1
		PUM1
		CARHSP1
		PRKAA2
		YTHDF2
		CSDE1
		HNRNPK
		PSMA6
		HELZ
		CHMP2A
		CHMP4A
		CHMP4B
GO:0016607 - nuclear speck	0.0104213	
GO:0036464 - cytoplasmic ribonucleoprotein granule	0.0280402	
GO:0000815 - ESCRT III complex	0.0317361	

GO:0015030 - Cajal body	0.0323407	SNRPC
		CDK2
		U2AF1
		EFTUD2
		DDX42
		PRPF31
O:0036452 - ESCRT complex	0.0506182	MVB12B
		CHMP2A
		CHMP4A
		CHMP4B

Appendix 17. Functional enrichment analysis of HD RNA granules. The table displays the functional enrichment analysis of HD RNA granules, with enriched GO terms classified under Biological Process and Cellular Component, alongside their respective p-values and gene matches. GO terms related to RNA granules are highlighted in red, while those associated with sEVs are indicated in blue. The numbers starting with "GO" represent specific Gene Ontology identifiers, which provide unique classification for each term. Although terms such as "intracellular membrane-bounded organelle" and "membrane-bounded organelle" were found with relatively high p-values, their connections to sEVs were weak and thus barred from the table for relevance.

HD RNA granules		
ENRICHED GO terms - genes enriched for GO (biological process)		
GO term	P-value	Gene matches
GO:0007041 - lysosomal transport	0.07789372	CHMP1B
		CHMP4A
		MVB12A
		VPS16
		LRP1
GO:0008333 - endosome to lysosome transport	0.07789372	MVB12A
		VPS16
		CHMP1B
		CHMP4A
GO:0036258 - multivesicular body assembly	0.07789372	CHMP1B
		MVB12A
		CHMP4A
GO:0036257 - multivesicular body organization	0.08182066	CHMP1B
		MVB12A
		CHMP4A
GO:0007032 - endosome organization	0.08413203	CHMP1B
		MVB12A
		CHMP4A
		SQSTM1

ENRICHED GO terms - genes enriched for GO (cellular component)		
GO:0070062 - extracellular exosome	1.70E-05	QSOX1
		AGO2
		MAN1A1
		CHMP1B
		SQSTM1
		CTSB
		IGSF8
		STK24
		FTH1
		SLC7A5
		RFTN1
		COMT
		AHSA1
		AGRN
		ATP2B1
		LMAN2
		FABP1
		ATP6V1E1
		MPST
		ITGAV
		MVB12A
		WDR1
		PSAT1
GLO1		
RHOA		
GO:1903561 - extracellular vesicle	1.70E-05	SQSTM1
		MPST
		AGRN
		RFTN1
		IGSF8
		AGO2
		MAN1A1
		MVB12A
		QSOX1
		AHSA1
		RHOA
		FTH1
		SLC7A5
		ATP2B1
		LMAN2
		ITGAV
		COMT
FABP1		
CHMP1B		
CTSB		

Appendix

		ATP6V1E1
		STK24
		GLO1
		PSAT1
		WDR1
GO:0005768 - endosome	0.026994104	SQSTM1
		RFTN1
		MVB12A
		RELCH
		RHOA
		LRP1
		CHMP1B
		CHMP4A
		ATP6V1E1
		SNX5
		EGFR
		VPS16
		GO:0036452 - ESCRT complex
CHMP1B		
CHMP4A		

